ANALYSIS OF TRICKLE-BED REACTOR FOR ETHANOL PRODUCTION FROM SYNGAS USING *CLOSTRIDIUM RAGSDALEI*

By

MAMATHA DEVARAPALLI

Bachelor of Technology in Chemical Engineering
Jawaharlal Nehru Technological University
Hyderabad, India
2006

Master of Science in Chemical Engineering
Oklahoma State University
Stillwater, Oklahoma
2008

Submitted to the Faculty of the
Graduate College of the
Oklahoma State University
in partial fulfillment of
the requirements for
the Degree of
DOCTOR OF PHILOSOPHY
May, 2014

ANALYSIS OF TRICKLE-BED REACTOR FOR

ETHANOL PRODUCTION FROM SYNGAS

USING *CLOSTRIDIUM RAGSDALEI*

Dissertation Approved:

Dr. Hasan K. Atiyeh

Dissertation Adviser

Dr. Raymond L. Huhnke

Dr. Joshua D. Ramsey

Dr. Mark R. Wilkins

Name: MAMATHA DEVARAPALLI

Date of Degree: MAY, 2014

Title of Study: ANALYSIS OF TRICKLE-BED REACTOR FOR ETHANOL PRODUCTION FROM SYNGAS USING *CLOSTRIDIUM RAGSDALEI*

Major Field: BIOSYSTEMS AND AGRICULTURAL ENGINEERING

Abstract: The conversion of syngas components (CO, CO_2 and H_2) to liquid fuels such as ethanol involves complex biochemical reactions catalyzed by a group of acetogens such as *Clostridium ljungdahlii, Clostridium carboxidivorans* and *Clostridium ragsdalei*. The low ethanol productivity in this process is associated with the low solubility of gaseous substrates CO and H_2 in the fermentation medium. In the present study, a 1-L trickle-bed reactor (TBR) was analyzed to understand its capabilities to improve the mass transfer of syngas in fermentation medium. Further, semi-continuous and continuous syngas fermentations were performed using *C. ragsdalei* to evaluate the ability of the TBR for ethanol production. In the mass transfer studies, using 6-mm glass beads, it was found that the overall mass transfer coefficient (k_La/V_L) increased with the increase in gas flow rate from 5.5 to 130.5 sccm. Further, an increase in the liquid flow rate in the TBR decreased the k_La/V_L due to the increase in liquid hold up volume (V_L) in the packing. The highest k_La/V_L values of 421 h^{-1} and 178 h^{-1} were achieved at a gas flow rate of 130.5 sccm for 6-mm and 3-mm glass beads, respectively. Semi-continuous fermentations were performed with repetitive medium replacement in counter-current and co-current modes. In semi-continuous fermentations with syngas consisting of 38% CO, 5% N_2, 28.5% CO_2 and 28.5% H_2 (by volume), the increase in H_2 conversion (from 18 to 55%) and uptake (from 0.7 to 2.2 mmol/h) were observed. This increase was attributed to more cell attachment in the packing that reduced CO inhibition to hydrogenase along the column length and increased the H_2 uptake. The maximum ethanol produced during counter-current and co-current modes were 3.0 g/L and 5.7 g/L, respectively. In continuous syngas fermentation, the TBR was operated at dilution rates between 0.006 $h^{-1}$and 0.012 h^{-1} and gas flow rates between 1.5 sccm and 18.9 sccm. The highest ethanol concentration of 13 g/L was achieved at dilution and gas flow rates of 0.012 h^{-1} and 18.9 sccm, respectively. The molar ratio of ethanol to acetic acid of 4:1 was obtained during continuous fermentation which was 7.7 times higher than in semi-continuous fermentations. The improvement of the reactor performance in continuous mode gives scope to explore the TBR as a potential bioreactor design for large scale biofuels production.

TABLE OF CONTENTS

Chapter Page

Chapter Page

Chapter Page

LIST OF TABLES

LIST OF FIGURES

Figures Page

Figures Page

Figures Page

CHAPTER I

INTRODUCTION

Total energy consumption in the U.S. is expected to increase by 14% from 2008 to 2035 (EIA, 2010). Although most of the energy consumed in the U.S. comes from fossil fuels, their use is estimated to decrease from 84% in 2008 to 78% in 2035. Further, according to the International Energy Outlook 2011 published by the U.S. EIA, renewables are the fastest growing source of world energy with an increase in their consumption of 2.8% per year (Gruenspecht, 2010). Biofuels have the potential to mitigate climate change and reduce greenhouse gas (GHG) emissions as their production from biomass is considered as carbon neutral. The development of new technologies for biofuel production creates job opportunities, results in economic growth, make the country self-sufficient and reduce dependency on foreign oil (NCOB, 2011). Research on biofuels from biomass came to the forefront in 1980 when the first Energy Security Act was passed by the U.S. Government in 1980 (McCarl and Boadu, 2009). Corn ethanol was the first commercially produced biofuel in the U.S. (Dien et al., 2002). However, corn utilization for fuel raised the debate over its potential interference with the food chain (Daschle, 2007). This gave rise to the use of nonfood feedstocks such as municipal solid waste and lignocellulosic materials for biofuels production.

Biomass to biofuels conversion technologies can be broadly classified into thermochemical and biochemical processes (Ayhan, 2001; McKendry, 2002; Ragauskas et al., 2006). Combustion, pyrolysis and gasification are thermochemical conversion processes which occur in the presence of chemical catalysts at high temperatures and pressures (Goyal et al., 2008). Anaerobic digestion and fermentation are biochemical conversion processes that occur in the presence of biocatalysts at ambient temperatures and pressures (Saxena et al., 2009). The selection of a route for conversion of biomass to energy depends on its economic feasibility, end product requirements and applications (McKendry, 2002). The present study implements the use of gasification-syngas fermentation, a hybrid conversion technology, for the production of ethanol from synthesis gas (syngas). The hybrid conversion technology has the advantage of utilizing the entire biomass components including lignin that is not efficiently utilized in the direct fermentation method (Sierra et al., 2008). In hybrid conversion process, biomass is first gasified to syngas, which is then fermented by anaerobic bacteria to alcohols and organic acids (Wilkins and Atiyeh, 2011).

Gasification is a partial combustion of biomass to produce syngas. CO, CO_2 and H_2 are the major constituents of syngas with traces of contaminants such as N_2O, H_2S and CH_4 (Rajvanshi, 1986). Syngas can be further converted into gaseous fuels such as H_2 and CH_4 or liquid fuels such as ethanol and butanol by chemical or biological routes (Ayhan, 2007; Kumar et al., 2009; Wilkins and Atiyeh, 2011). Various studies were focused on conversion of syngas to ethanol using microbial catalysts such as *Clostridium ljungdahlii, Clostridium autoethanogenum, Clostridium carboxidivorans, Clostridium ragsdalei and Alkalibaculum bacchi* (Abrini et al., 1994; Huhnke et al., 2010; Liou et al.,

2005; Liu et al., 2012; Phillips et al., 1994). As early as 1940, microbiologists started working on describing the pathway followed by bacteria in utilizing CO, CO_2 and H_2 for growth (Wood, 1991). The metabolic pathway followed by CO, CO_2 and H_2 utilizing bacteria have been well presented by Dr. Harland G. Wood and Dr. Lars G. Ljungdahl (Ljungdahl and Wood, 1969; Ragsdale and Pierce, 2008; Wood, 1991). In this pathway, CO or CO_2 can be converted to acetyl-CoA intermediate through the methyl and carbonyl branches. The reducing power required for the formation of acetyl-CoA is provided by either H_2 or CO. Acetyl-CoA is further utilized for formation of cell mass, acetic acid and ethanol. During growth phase, the production of acetic acid is favorable as ATP is produced. Hence this phase is called the acetogenic phase. Once, the cells reach stationary phase, the cells switch to solventogenic phase. In this phase, the reducing power from H_2 and CO is utilized to produce secondary metabolites such as ethanol. Production of ethanol can be improved by changing the redox balance of the electron flow to allow the bacteria to produce more ethanol. An increase in ethanol production can be achieved by adjusting the operating parameters such as pH and addition of reducing agents (Babu et al., 2010; Hu, 2011; Panneerselvam, 2009). However, in addition to controlling these process parameters to increase ethanol production, one must overcome the mass transfer limitation of syngas components (CO and H_2) with low solubility in the fermentation medium.

Gas-liquid mass transfer of CO and H_2 is severely limited as the solubility of these gases is very low in water (Table 1.1). Though CO_2 has high solubility in water; it has been observed that in the presence of CO the microorganisms prefer utilizing CO and generating CO_2 as a byproduct rather than utilizing both CO and CO_2 as the carbon

source (Hu, 2011). The electrons are provided by either CO or H_2. However, utilization of CO as an electron source is thermodynamically more favorable because it has been reported that at any given pH, the Gibb's free energy for the oxidation reaction of CO is more negative than that of H_2 (Hu, 2011). Thus, it is very important to use a reactor, in which CO and H_2 are efficiently transferred into the fermentation medium.

Table 1.1 Solubility of CO, H_2, CO_2 and O_2 in water. Source: (Dean, 1985)

Temperature (°C)	Solubility (g per 100 g)			
	CO	H_2	CO_2	O_2
20	0.0023	0.00016	0.168	0.004
37	0.0017	0.00014	0.110	0.003

Different reactors have been proposed to improve the mass transfer of sparingly soluble gases into the fermentation medium (Bredwell and Worden, 1998; Klasson et al., 1990a). Some reactors that were reported for syngas fermentation include bubble column, air-lift, trickle-bed, hollow fiber membrane and immobilized bioreactors (Kimmel et al., 1991; Klasson et al., 1990b; Rajagopalan et al., 2002). In these reactors, the main aim was to improve the interfacial area between the gas and liquid, which improves mass transfer.

A bioreactor design that can achieve high mass transfer rates and high cell concentrations is desirable for syngas fermentation (Klasson et al., 1991a; Klasson et al., 1992; Vega et al., 1989). TBRs are long columns filled with packing material. In TBRs, liquid flows in the form of a thin film reducing the resistance to mass transfer from gas-liquid interface to the bulk of the liquid. This helps in achieving high rates of mass transfer. Traditionally, TBRs have been used for various processes such as catalytic

hydrogenation, denitrification, desulfurization and oxidation of organic matter (Gianetto and Specchia, 1992).

In syngas fermentation, TBR mass transfer capability for production of acetate using *Peptostreptococcus productus* with 6.4 mm ceramic intalox saddles as the packing material was assessed (Klasson et al., 1990a). Also, TBR was successfully used in the production of methane using a triculture of *Rhodospirillum rubrum, Methanosarcina barkeri and Methanobacterium formicicum* (Kimmel et al., 1991). Additionally, the production of H_2 in a TBR using *R. rubrum, Rubrivivax gelatinosus* photosynthetic bacterium which needs light for growth was reported (Klasson et al., 1993b; Wolfrum and Watt, 2002). Klasson et al. (1990a) compared three reactors namely, the stirred tank reactor (STR), packed bubble column (PBC) and trickle-bed reactor (TBR) for the production of acetate from syngas using *P. productus*. The authors concluded that the CO conversion and mass transfer capability of TBR was higher than for PBC and STR. Based on extensive literature review, no work has been reported on evaluating TBR mass transfer and fermentation capabilities to produce ethanol using syngas. The overall goal of this research project is to characterize the mass transfer ability of the TBR and evaluate its performance during syngas fermentation to produce ethanol using *C. ragsdalei*.

CHAPTER II

LITERATURE REVIEW

2.1 History of Biofuels

Renewable energy can be derived from sunlight, wind, water, geothermal and biomass, which are considered sustainable and environmentally friendly. On the other hand, energy derived from fossil fuels such as coal, oil and natural gas are considered non-renewable and do not regenerate at sustainable rates (Twidell and Weir, 2003). Currently, fossil fuels are used as the main energy source to meet the world energy demand. The Energy Information Administration (EIA) reported that 71% of all oil consumed in the U.S. was used for transportation (EIA, 2012). In 2012, according to EIA statistics around 40% of oil consumed in the U.S. was imported (EIA, 2013). Factors such as high gas prices, rising concerns over national energy security and dependency on foreign oil imports and environmental impacts of high oil usage have led to the focus on research for biofuels (German et al., 2011).

Biofuels are defined as gaseous or liquid fuels produced from biological material such as biomass. Biomass has been used as fuel since man discovered fire. Wood, crops and animal and plant wastes are some examples of biomass (Klass, 2004). Biofuels are classified into first and second generations based solely on the type of biomass used.

Unlike crude oil, biomass is diverse in its composition and thus different conversion technologies have been developed to produce biofuels.

2.2 First Generation Biofuels

First generation biofuels are made from feedstocks such as corn, sugarcane, wheat, rapeseed oil and palm oil. The technology used to convert these feedstocks to fuels such as bioethanol and biodiesel are well established (Sims et al., 2008).

Bioethanol

The steps involved in production of ethanol from sugar and starch crops are shown in Figure 2.1. Sugar crops such as sugar cane, sugar beet and sweet sorghum mostly consist of glucose, fructose and sucrose as their major components (Bai et al., 2008). These fermentable sugars are extracted by grinding or crushing followed by fermentation to ethanol. Further, ethanol is separated from the products stream through a series of distillation and dehydration steps.

Grains such as corn and wheat contain starch as their major component. Starch is a polysaccharide made up of large number of glucose units that are linked through α (1-4) and α (1-6) glycosidic bonds (Pandey, 2010). Starch cannot be directly fermented by yeast. After milling the grains and extracting starch, starch is broken down into monomeric glucose units by hydrolysis with α-amlyase and glucoamylases (Nigam and Singh, 1995). The hydrolyzed starch is then fermented to ethanol. Production of ethanol from starch is done by either the dry grind or wet milling process (Bothast and Schlicher, 2005; Sanchez and Cardona, 2008). The main difference between the two processes is the method of glucose extraction and the co-products formed (Sims et al., 2008). In wet

milling, steeping of corn is followed by separation of germ, fiber and starch. Wet milling produces value added by-products such as corn sweeteners, oil, and corn gluten meal apart from ethanol. In dry grind, the whole corn is milled to produce ethanol along with high protein animal feed called dry distillers' grains with solubles (DDGS). Wet milling requires high capital costs and is less efficient in producing ethanol than the dry grind process (Rausch and Belyea, 2006; Rodríguez et al., 2010). Most of the corn ethanol plants in U.S. are dry grind facilities (USGC, 2012).

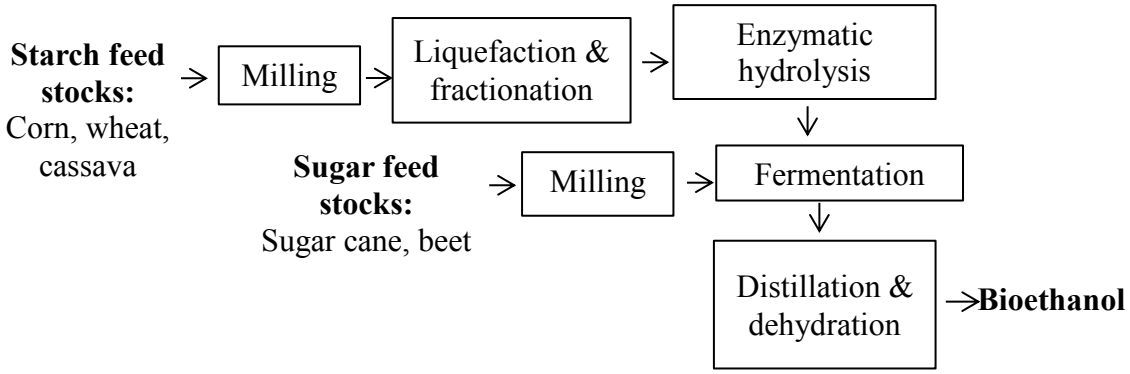

Figure 2.1 Bioethanol production from first generation biomass. Adapted from Sims et al. (2008).

2.3 Second Generation Biofuels

The non-food biomass feedstocks used for the production of second generation biofuels include agricultural and wood residues, organic wastes and dedicated energy crops (Naik et al., 2010). Some examples of agricultural and wood residues are woodchips, cornstover, sugarcane bagasse and sawdust. Municipal solid wastes, recycled cooking oil and animal fat are some examples of organic wastes. Switchgrass and miscanthus are considered dedicated energy crops. Biomass generally referred to as lignocellulosic biomass mainly consists of cellulose, hemicellulose and lignin polymers interlinked in a heterogeneous matrix (Kitani and Hall, 1989). Cellulose is a linear

polysaccharide consisting of several β(1-4) linked D-glucose units. Hemicellulose is a heteropolymer that consists mainly of xylose, mannose, galactose, rhamnose and arabinose. Lignin is a complex polymer made from cross-linked aromatic compounds. Lignin acts as a protective barrier and hinders the depolymerization of cellulose and hemicellulose to fermentable sugars.

In order to produce sustainable biofuel and meet the energy demand, biomass should be available at large scale and low cost. Most of the second generation biomass feedstocks meet this requirement (Carriquiry et al., 2011). Biofuel production from these feedstocks is on the verge of commercialization (Bansal et al., 2013). Unlike conventional fermentation processes used for first generation biofuel production, the process for conversion of biomass to biofuel is complex (Stöcker, 2008; Szczodrak and Fiedurek, 1996).

One of the challenges of second generation biofuels production is the impact of change in land usage (Searchinger et al., 2008). The production of dedicated biomass feedstocks requires vast acreage of land. Land management practices are necessary to reduce any indirect carbon and nitrogen gas emissions that pose a threat to produce harmful greenhouse gases (GHGs) (Tilman et al., 2006). Thermochemical, biochemical and hybrid conversion technologies have been explored for the conversion of lignocellulosic feedstocks to fuels and other products (Figure 2.2). Thermochemical processes include combustion, pyrolysis and gasification. The biochemical route includes fermentation and digestion. The hybrid conversion technology is a gasification-syngas fermentation process which is the focus of this project.

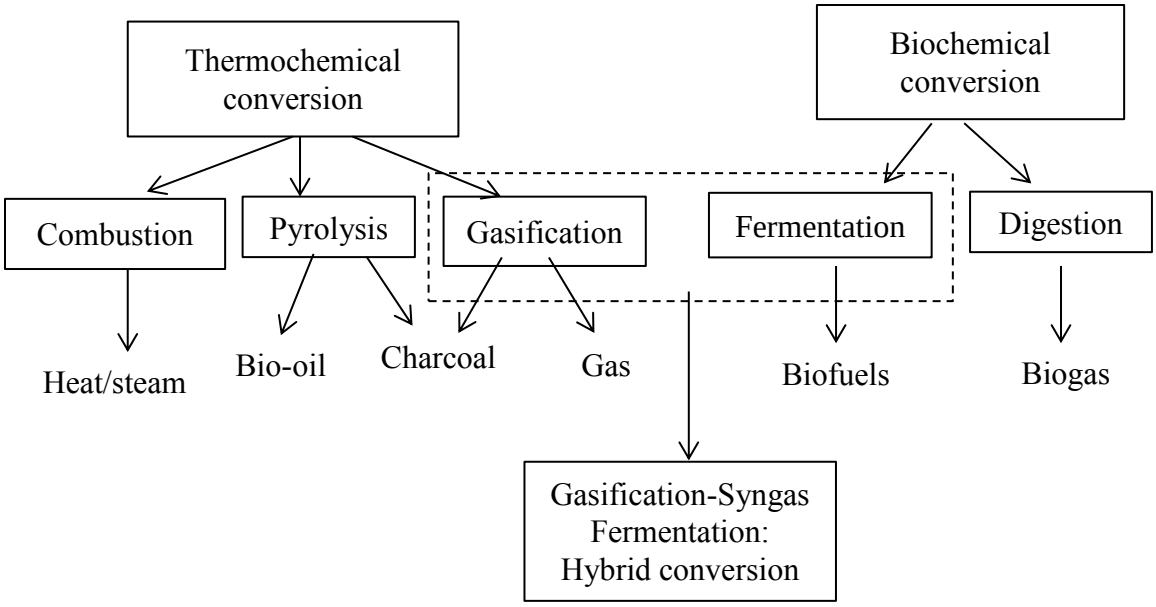

Figure 2.2 Biomass conversion technologies to produce different products. Adapted from Turkenburg (2000).

2.3.1 Gasification-Syngas Fermentation Process

Gasification-syngas fermentation is a hybrid thermochemical-biochemical conversion process. Gasification is partial oxidation of biomass at temperatures between 800 and 900 °C to produce syngas (Saxena et al., 2008). Further, ash, char and tar and traces of CH_4, NH_3 and H_2S are produced during gasification (Bridgwater, 1994). Char and tar are produced due to incomplete conversion of biomass (Kumar et al., 2009).

In direct gasification, oxidizing agents such as air/O_2 are supplied to initiate the exothermic oxidation reactions. The energy released from biomass during this process is used to fuel the endothermic reactions and maintain high temperature in the gasifier (Baskar et al., 2012). On the other hand, the heat required for gasification is entirely supplied through an external heat source during indirect gasification (Phillips and Eggeman, 2007). Use of steam as a heat source increases the H_2 content of the syngas (Belgiorno et al., 2003). When air is used as an oxidizing agent, the gaseous fuel

produced called producer gas, which mainly consists of CO, H_2, CO_2 and N_2. Presence of N_2 reduces the heating value of the producer gas (Belgiorno et al., 2003). Other operating parameters that significantly affect the quality of the gas produced are gasifying agent to biomass ratio and flow rate, temperature and biomass feed rate (Kumar et al., 2009). Further, for effective gas utilization to produce biofuels, impurities such as char, tar and inorganic compounds should be removed in downstream processing by using cyclone separators, wet or dry scrubbing and hot gas condition methods (Huber et al., 2006; Kumar et al., 2009).

Syngas from gasification can be converted to liquid fuels by chemical and biochemical routes. Fischer-Tropsch synthesis is a chemical route in which alkanes from C_1-C_{50} are produced from syngas in the presence of Co, Fe-Ru-based catalysts at 180-250 °C and 20-40 bars (Iglesia et al., 1993; Martínez and López, 2005). However, syngas fermentation is a biochemical route in which biofuels such as ethanol are produced using microbial catalysts.

Syngas produced from biomass gasification is fed into a bioreactor containing acetogenic microorganisms to produce biofuels such as ethanol or higher alcohols. Several studies reported production of higher alcohols such as isopropanol, butanol and hexanol using syngas fermentation (Liu et al., 2014b; Maddipati et al., 2011; Rajagopalan et al., 2002; Ramachandriya et al., 2011; Worden et al., 1991). Under anaerobic conditions, acetogens such as *C. ljungdahlii, C. carboxidivorans, A. bacchi* and *C. ragsdalei* serve as biocatalysts in this fermentation process (Liou et al., 2005; Liu et al., 2012; Phillips et al., 1994; Wilkins and Atiyeh, 2011).

2.3.1.1 Advantages and Disadvantages of Gasification-Syngas Fermentation Hybrid Technology

The main advantage of the gasification process is that any type of biomass can be used as a feedstock for the production of syngas (Kumar et al., 2009). Also, complex biomass component such as lignin which is not fermentable can also be decomposed through gasification (Jenkins et al., 1998; Williams et al., 2003). Additionally, gasification has the benefit of low reaction time compared to biochemical routes (Bridgwater, 2001). However, gasification suffers from the high costs associated with cleaning syngas from undesirable contaminants such as alkali compounds (Kumar et al., 2009). If the syngas from gasification is not cleaned from toxic impurities it will degrade the metal catalysts and reduce their effectiveness in converting syngas to liquid fuel (Sims et al., 2008).

One of the main advantages of syngas fermentation is that it utilizes all the biomass components unlike the saccharification fermentation where lignin cannot be fermented (Lewis et al., 2008; Phillips et al., 1994). Syngas fermentation process is highly specific and can result in high yields (Bredwell et al., 1999; Vega et al., 1989; Worden et al., 1991). Syngas fermentation also occurs at ambient temperatures and pressures unlike Fischer-Tropsch process (Worden et al., 1991). Further, microbial catalysts are not poisoned by trace amount of sulfur gases like metal catalysts during chemical conversion processes (Ahmed and Lewis, 2007). In addition, no xenobiotic products are expected to be formed during syngas fermentation (Worden et al., 1991).

The main disadvantages of syngas-fermentation are (i) low solubility and mass transfer limitations of the CO and H_2 gaseous substrates, (ii) slow reactions resulting in

long residence times and (iii) low metabolic energy is produced when the microorganisms grow on gaseous substrate instead of sugar substrates resulting in slow growth, low cell density and low solvent production (Barik et al., 1988; Vega et al., 1989).

2.3.1.2 Syngas Fermentation

In syngas fermentation, acetogens metabolize CO, CO_2 and H_2 to alcohols and organic acids. The overall biochemical reactions to convert syngas to ethanol and acetic acid are shown below (Klasson et al., 1990a; Vega et al., 1990).

$$6CO + 3H_2O \rightarrow C_2H_5OH + 4CO_2 \quad (2.1)$$

$$2CO_2 + 6H_2 \rightarrow C_2H_5OH + 3H_2O \quad (2.2)$$

$$4CO + 2H_2O \rightarrow CH_3COOH + 2CO_2 \quad (2.3)$$

$$2CO_2 + 4H_2 \rightarrow CH_3COOH + 2H_2O \quad (2.4)$$

In the fermentation process, CO and/or H_2 can supply the electrons used in the enzymatic reactions. Further CO and CO_2 can be used as a carbon source. As per the stoichiometry, if only CO is used as the sole carbon and energy source then the carbon conversion efficient will only be 33%, while, the remaining 67% of the carbon will be lost in the form of CO_2 as per equation 2.1. However, if both CO and H_2 are utilized then equations (2.1) and (2.2) are combined into equation (2.5)

$$3CO + 3H_2 \rightarrow C_2H_5OH + CO_2 \quad (2.5)$$

Therefore, when equimolar concentrations of CO and H_2 are provided, then the maximum carbon conversion efficiency is 67% while 33% of the carbon is lost as CO_2. On the other hand, when the CO and H_2 is utilized solely to produce acetic acid then the carbon conversion efficiency is 100% as indicated in equation (2.6)

$$2CO + 2H_2 \rightarrow CH_3COOH \quad (2.6)$$

However, if only CO is utilized to produce acetic acid then only 50% carbon conversion efficiency can be achieved. The carbon conversion efficiency is high when electrons are supplied by H_2 and CO is utilized as the carbon source. However, H_2 utilization decreases when hydrogenase activity is inhibited by CO (Terrill et al., 2012; Ukpong et al., 2012). This results in CO utilization as both carbon and energy source decreasing the overall conversion efficiency of the process (Ahmed and Lewis, 2007). While the stoichiometry provides an estimate of the maximum theoretical yields of products from the substrates, the actual production rates and yields vary depending on the microorganism, substrate and fermentation conditions (Zeikus, 1980).

2.3.1.3 Syngas Fermentation Biocatalysts

CO can be anaerobically metabolized by photosynthetic, acetogenic, carboxydotrophic and methanogenic microorganisms to hydrogen, methane, acetate, butyrate, ethanol and butanol as end products (Abrini et al., 1994). Microbes that can utilize 1 carbon compounds such as CO, CO_2 and CH_4 as carbon and energy source are called unicarbontrophs (Worden et al., 1991). Among the different anaerobes, acetogens have been of prime interest due to their ability to grow chemolithotrophically (i.e., use inorganic reduced compounds as energy source) and produce ethanol and butanol along with acetate and butyrate from CO, CO_2 and H_2, formate and methanol (Mohammadi et al., 2011).

Clostridium aceticum was the first reported acetogen isolated by Klass Tammo Wieringa in 1936, but was later lost (Drake et al., 2008). In 1942 , the second acetogen , *Moorella thermoacetica* (formerly called *C. thermoaceticum*) was isolated and it was the

most extensively studied acetogen (Fontaine et al., 1942). This microorganism was used to determine the acetyl-CoA pathway enzymology in the laboratories of Harland Goff Wood and Lars Gerhard Ljungdahl (Drake et al., 2008). To date, there are more than 100 acetogenic species isolated from a variety of habitats such as sediments, soils, sludge and intestinal tracts of animals (Drake et al., 2008). Most of the microorganisms currently known to ferment syngas to ethanol are predominantly mesophilic with operating temperatures in the range of 37-40 °C (Munasinghe and Khanal, 2010a). The most widely studied mesophilic microorganisms are *C. aceticum, Acetobacterium woodii, C. ljungdahlii C. carboxidivorans* and *C. ragsdalei* (Huhnke et al., 2010; Phillips et al., 1993; Ukpong et al., 2012; Younesi et al., 2005).

In presence of CO as a reductant, *C. formicaceticum* and *M. thermoacetica* have shown to reduce acids to their corresponding alcohols (Fraisse and Simon, 1988; White et al., 1987). *C. acetobutylicum* is also shown to directly reduce acetate and butyrate to corresponding alcohols (Hartmanis et al., 1984). Recently, it was reported that mono-cultures of *C. ljungdahlii* and *C. ragsdalei* as well as a mixed culture of *A. bacchi* and *C. propionicum* were able to convert added acids such as propionic, butyric and hexanoic acids to their respective alcohols (Liu et al., 2014b; Perez et al., 2013).

C. ljungdahlii is the first microorganism that was reported to produce 48 g/L of ethanol and 3 g/L of acetate in a continuous stirred tank reactor (CSTR) with recycle (Phillips et al., 1993). *C. carboxidivorans* produced 4.86 g/L acetate, 1.06 g/L ethanol and 0.05 g/L butanol when 18 g/L of fructose was provided as a substrate (Liou et al., 2005). However, when equivalent moles of CO (i.e., 16.8 g/L) was provided as a substrate the products shifted to 4.4 g/L ethanol, 0.72 g/L acetate and 1.78 g/L butanol

(Liou et al., 2005). The presence of CO, which acts as an effective electron source, enabled ethanol production rather than acetate production by acetogens (Tanner et al., 2008). The presence of reducing agents and reduction in pH are considered important in the shift of the fermentation products from acetate to ethanol (Babu et al., 2010; Jones and Woods, 1986; Klasson et al., 1992; Maddipati et al., 2011; Panneerselvam et al., 2009; Phillips et al., 1994; Sakai et al., 2004; Worden et al., 1991).

Acetogens metabolize single carbon source compounds via the acetyl-CoA pathway, also called the Wood-Ljungdahl pathway to (i) synthesize acetyl moiety of acetyl-CoA from CO_2, (ii) conserve energy and (iii) assimilate CO_2 to cell carbon (Ljungdhal, 1986; Wood et al., 1986). Acetyl-CoA is a major metabolic intermediate in acetogens and can be utilized to produce acetate, ethanol and cell mass.

2.3.1.4 Wood-Ljungdahl Pathway

The Wood-Ljungdahl pathway is a linear and reductive pathway unlike cyclic CO_2-fixing processes such as the Calvin and tricarboxylic acid cycles (Madigan et al., 2003). Acetogens cannot utilize the Calvin cycle that is employed by photosynthetic and chemosynthetic autotrophs because it lacks ribulose diphosphate carboxylase enzyme (Wood et al., 1986). The Wood-Ljungdahl pathway is considered to occur in both oxidation and reduction directions. Conversion of CO_2 to acetate is a reduction process. However, acetate can be converted back to CO_2 through oxidation (Ragsdale, 1997). Acetogens conserve energy by reduction of CO and/or CO_2, H_2 to acetate. In the Wood-Ljungdahl pathway, synthesis of the acetyl-CoA occurs through two branches, the methyl branch and carbonyl branch. Acetyl-CoA can then be converted to acetate, ethanol and cell mass. The pathway for the conversion of acetyl-CoA to acetate is called acetogenesis

and the conversion of acetyl-CoA to ethanol is called solventogenesis. The electrons necessary for the reduction reactions in the pathway come from oxidation of H_2 by hydrogenase and/or from oxidation of CO by carbon monoxide dehydrogenase (CODH) as shown in equations 2.7 and 2.9.

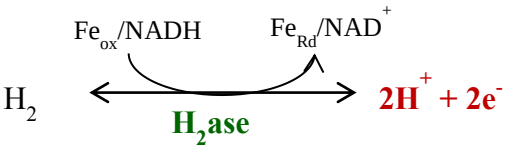

(2.7)

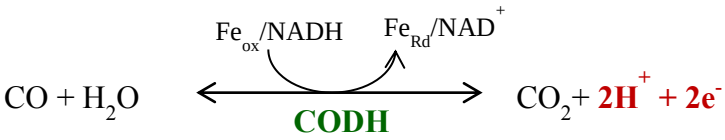

(2.8)

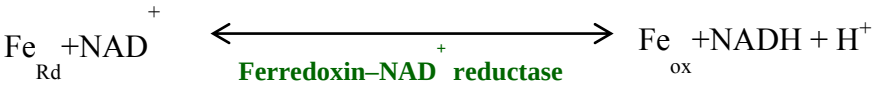

(2.9)

The reducing power donated by H_2 or CO are carried by electron carrier pairs $NADH/NAD^+$, $NADPH/NADP^+$ or ferredoxin (Ljungdhal, 1986) as shown in equations (2.7) through (2.9). While electrons are carried by the electron carrier pairs, adenosine triphosphate (ATP) transports the chemical energy within the cells for metabolism. The hydrolysis of the phosphate bonds releases energy and converts ATP to adenosine diphosphate (ADP). The redox reactions involved in the Wood-Ljungdahl pathway to form ethanol, acetate and cell mass are shown in Figure 2.3.

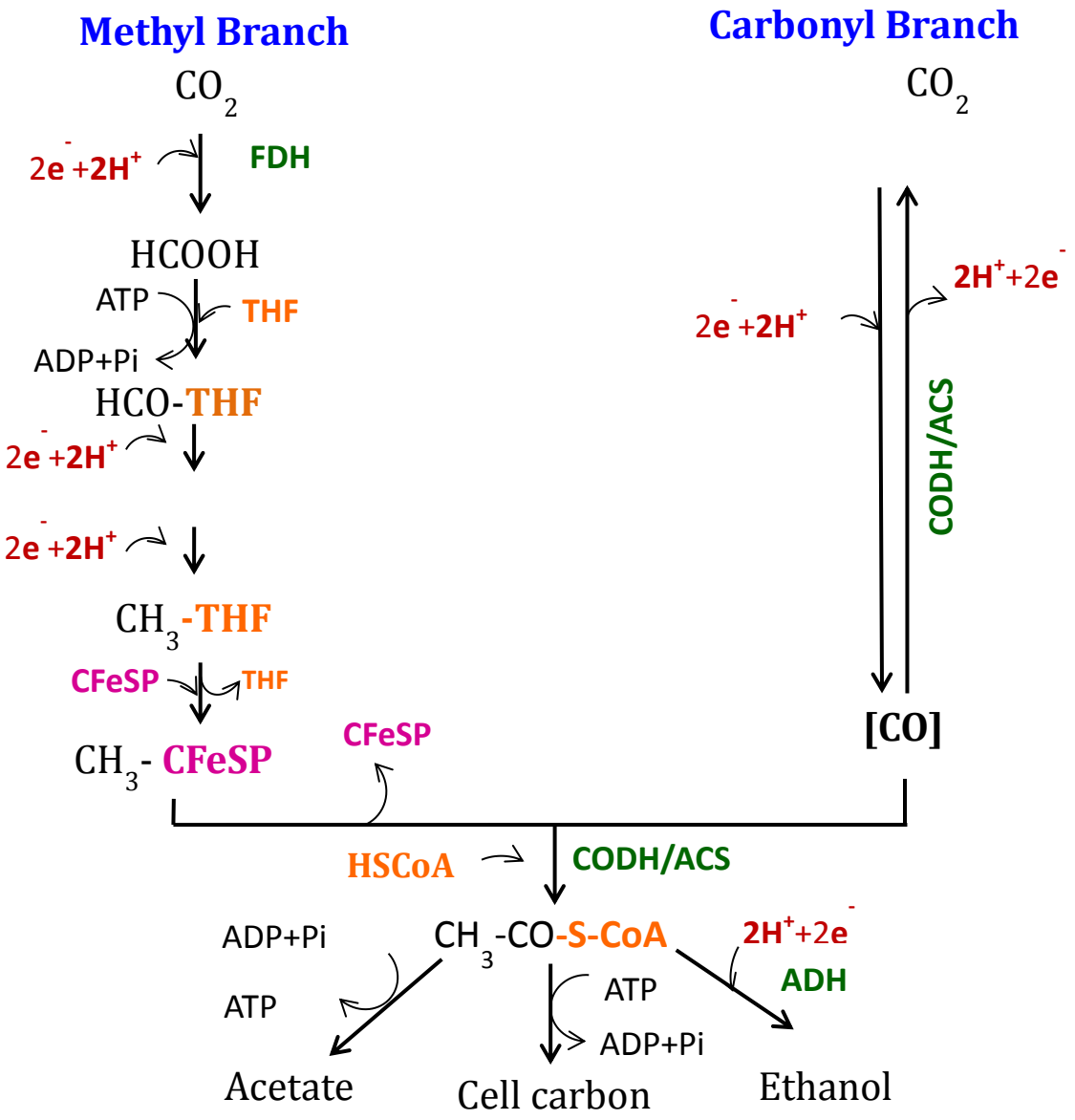

Figure 2.3 Overview of Wood-Ljungdahl pathway. Green text indicates enzymes, orange text indicates coenzymes and pink text indicates co-protein involved in the metabolic pathway. FDH: formate dehydrogenase; CODH/ACS: bifunctional carbon monoxide dehydrogenase/acetyl-CoA synthase; ADH: alcohol dehyrogenase; CFeSP: corrinoid iron(Fe)-sulfur(S) protein; THF: tetrahydrofolate (vitamin B9, folic acid derivative); HSCoA: thiol (SH) functional group Coenzyme A; CH_3-CO-S-CoA: acetyl-Coenzyme A intermediate. Adapted from Drake and Daniel (2004).

Methyl branch

In the methyl branch, CO_2 is reduced to methyl moiety by a series of redox reactions. The reactions (equations 2.10 to 2.15) in the methyl branch are adapted from

Kellum and Drake (1986). CO_2 is converted to formate (HCOOH) by addition of two electrons through NADH/NAD^+ in the presence of formate dehydrogenase (FDH).

$$CO_2 + NADH + H^+ \rightarrow HCOOH + NAD^+ \quad (2.10)$$

Formate combines with tetrahydrofolate (THF or H_4-folate) to form formyl tetrahydrofolate (HCO-THF) at the expense of one ATP molecule. This reaction is catalyzed by formyl tetrahydrofolate synthatase.

$$HCOOH + H_4floate + ATP \rightarrow 10\text{-}HCO\text{-}H_4folate + ADP + Pi \quad (2.11)$$

Formyl tetrahydrofolate is then reduced in a series of reactions (2.12 to 2.14) to methenyl-H_4folate, methylene-H_4folate and methyl-H_4folate in presence of formyl tetrahydrofolate cyclohydrolase, methylene tetrahydrofolate dehydrogenase and methylene tetrahydrofolate reductaseas enzymes, respectively. The process of formyl to methyl reduction happens by addition of 4 electrons through NAD(P)H/$NAD(P)^+$.

$$10\text{-}HCO\text{-}H_4folate + H^+ \rightarrow 5,10\text{-}CH^+\text{=}H_4folate + H_2O \quad (2.12)$$

$$5,10\text{-}CH^+\text{=}H_4folate + NAD(P)H \rightarrow 5,10\text{-}CH_2\text{=}H_4folate + NAD^+ \quad (2.13)$$

$$5,10\text{-}CH_2\text{=}H_4folate + NAD(P)H + H^+ \rightarrow 5\text{-}CH_3\text{-}H_4folate + NAD^+ \quad (2.14)$$

Finally, the methyl group in methyl-H_4folate is transferred to the reduced cobalt in the corrinoid iron-sulfur protein (CFeSP) to form methylated corrinoid iron sulfur protein. This reaction is catalyzed by methyl transferase as shown in equation (2.15).

$$5\text{-}CH_3\text{-}H_4folate + CFeSP \rightarrow CH_3\text{-}CFeSP + H_4folate \quad (2.15)$$

Carbonyl branch

In the carbonyl [CO] branch, nickel containing CODH/ACS catalyzes the reduction of CO_2 to [CO]. Unlike the methyl branch, the carbonyl branch is dominated by the bifunctional CODH/ACS enzyme. This reaction step utilizes two electrons (Ljungdhal, 1986; Wood et al., 1986).

$$CO_2 + 2H^+ + 2e^- \rightarrow [CO] + H_2O \quad (2.16)$$

From Figure 2.3, it can be seen that both the methyl and carbonyl branches start with CO_2. However, when CO is available it will be oxidized to CO_2 as shown in equation (2.8), which can be used as a carbon source in the methyl branch. The utilization of CO as an electron source reduces the overall carbon conversion efficiency of the process as discussed earlier. On the other hand, in the carbonyl branch CO can directly bind to the CODH/ACS enzyme.

CODH/ACS is a bifunctional enzyme that also catalyzes the acetyl-CoA synthesis step. Hence, it is also called acetyl-CoA synthase (ACS). In presence of ACS, the methyl group ($-CH_3$) and the carbonyl group [CO] are assembled with free CoA enzyme (HSCoA) to form the intermediate compound acetyl-CoA (CH_3CO-S-CoA) (Ljungdhal, 1986; Wood et al., 1986).

$$CH_3\text{-CFeSP} + [CO] + HSCoA \rightarrow CH_3CO\text{-SCoA} + CFeSP \quad (2.17)$$

Acetyl-CoA is an important metabolic intermediate, which serves as a precursor for both anabolic and catabolic pathways. It can be used either (i) as a building block for cell carbon; (ii) for generation of ATP through acetate production or (iii) for production of liquid biofuels such as ethanol. In anabolic pathway, acetyl-CoA is converted to

phosphoenolpyruvate, which forms cellular material (Diekert and Wohlfarth, 1994). In catabolic pathway, acetate is formed from acetyl-CoA with release of energy in the form of ATP. Cell growth is usually associated with acetate formation as it produces ATP, which is essential for cell production. Acetic acid production from acetyl-CoA is a two-step process. Phosphotransacetylase catalyzes the acetyl-phosphate production reaction. Phosphate replaces the CoA enzyme resulting in the release of the HSCoA enzyme as shown in equation 2.18 (Ljungdhal, 1986; Wood et al., 1986).

$$CH_3CO\text{-}S\text{-}CoA + Pi \rightarrow CH_3CO\text{-}S\text{-}Pi + HSCoA \quad (2.18)$$

Acetyl-phosphate reacts further with adenosine diphosphate (ADP) resulting in phosphorylation of ADP to ATP and production of acetic acid. This reaction is catalyzed by acetate kinase(Ljungdhal, 1986; Wood et al., 1986).

$$CH_3CO\text{-}S\text{-}Pi + ADP \rightarrow CH_3COOH + ATP \quad (2.19)$$

Acetic acid production is favorable during the growth phase as ATP, which is an essential molecule for cell growth, is generated in this process. However, since a molecule of ATP is consumed in equation (2.11) and a molecule of ATP is produced in equation (2.19), the net ATP produced in the production of acetic acid is considered to be zero. Hence, additional ATP must be produced for cell growth. ATP is reported to be generated via chemiosmosis or electron transport (ET) coupled phosphorylation (Das and Ljungdahl, 2003). In this process, the reduction of terminal electron acceptors such as metal ions, nitrogen and sulfur by the ET chain results in the generation of trans-membrane gradient of H^+. This is consequently used by membrane bound ATP synthase to produce ATP from Pi and ADP (Senior, 1988). Thus, the electrons produced in equations (2.7) and (2.8) from H_2 and CO can be utilized in ATP production. Further,

since these electrons are not consumed during ATP production, they can also be used in the production of acetic acid and ethanol. Apart from cell carbon and acetic acid production, acetyl-CoA can also be converted to ethanol. Acetaldehyde dehydrogenase catalyzes the reduction of acetyl-CoA to acetaldehyde as shown in equation (2.20) (Reeves, 2011). Acetaldehyde can also be produced from acetic acid. Aldehyde ferredoxin oxidoreductase catalyzes the acetic acid to acetaldehyde reaction as shown in equation (2.21) (Reeves, 2011). Acetaldehyde is reduced to ethanol via alcohol dehydrogenase. Ethanol production is electron intensive process. The electrons are produced from the oxidation of H_2 and/or CO and carried by $NADH/NAD^+$ or Fd_{Rd}/Fd_{OX} carrier pairs.

$$CH_3CO\text{-}S\text{-}CoA + NADH + H^+ \rightarrow CH_3CHO + NAD^+ + HS\text{-}CoA \quad (2.20)$$

$$CH_3COOH + Fe_{Rd} \rightarrow CH_3CHO + Fe_{OX} \quad (2.21)$$

$$CH_3CHO + NADH + H^+ \rightarrow CH_3COOH + NAD^+ \quad (2.22)$$

Apart from ethanol, higher alcohols such as butanol can also be produced through the Wood-Ljungdahl pathway. Two molecules of acetyl-CoA combine to form acetoacetyl-CoA. This compound can be further utilized to produce butyrate and butanol. The detailed discussion of the metabolic pathway is outside the scope of this research. However, it can be found in Grethlein et al. (1991).

2.3.1.5 Factors Affecting the Syngas Fermentation

Temperature, pH, gas composition, gas partial pressures, medium components, reducing agents and gas-liquid mass transfer affect the cell growth and product distribution during syngas fermentation (Abrini et al., 1994; Hurst and Lewis, 2010; Munasinghe and Khanal, 2010a). The ability to predict and control the onset of

solventogenesis is important for improving ethanol yields and productivity. Even though the effect of some of the above operating parameters on the ethanol yield and productivity using different clostridia species were studied; there are opportunities for further optimization of these parameters to make ethanol production from syngas an economical process.

Temperature

Fermentation temperature impacts the cell growth, enzyme activities and gas solubility. Acetogenic species such as *C. ljungdahlii, C. ragsdalei, C. carboxidivorans* and *A. bacchi* used in syngas fermentation are mesophiles with an optimum temperature between 37 and 40°C (Gaddy and Clausen, 1992; Huhnke et al., 2010; Liou et al., 2005). However, thermophiles such as *Carboxydocella sporoproducens, Moorella thermoacetica, M. thermoautotrophica* have an optimum temperature between 50 and 80°C (Daniel et al., 1990; Henstra et al., 2007; Savage et al., 1987; Slepova et al., 2006). Thermophilic conditions usually result in reduction of gas solubility, however the rate of gas transfer is considered to increase due to low viscosity of the medium (Munasinghe and Khanal, 2010a).

pH

Fermentative bacteria maintain a pH gradient across the membrane and regulate the internal pH which is essential for stability and functioning of metabolic enzymes (Gutierrez, 1989) . Studies with *C. acetobutylicum* reported that when acetate and butyrate production decrease external pH, acids accumulate inside cells and lower their internal pH to maintain a constant pH gradient (Gottwald and Gottschalk, 1985). However, accumulation of high concentrations of undissociated acid inside the cells

stresses them and decreases the pH gradient. Thus, the cells counteract by producing solvents (Ahmed, 2006; Gottschal and Morris, 1981; Gottwald and Gottschalk, 1985). In syngas fermentation, the external pH in the fermentation medium is a widely studied physiological parameter to optimize cell growth and solvent production. The optimum external pH range for cell growth of most of the syngas fermenting microbes usually varies from 5.5 to 6.5 (Abrini et al., 1994; Liou et al., 2005; Tanner et al., 1993). The optimum external pH for solvent production was reported to be around 4.5 to 4.8 (Ahmed et al., 2006; Sakai et al., 2004; Worden et al., 1991). Recently a moderately alkaliphilic bacterium called *A. bacchi* has shown capabilities to grow on syngas at an optimum pH between 8 and 8.5 and produce ethanol at pH range between 6.5 and 7 (Allen et al., 2010; Liu et al., 2012). In syngas fermentation studies, the changes in external pH were correlated with the substrate metabolism and release of metabolic by-products (Devi et al., 2010; Hu, 2011; Kundiyana et al., 2011b; Liu et al., 2014a). However, future studies on understanding the internal pH changes and the pH gradient during the fermentation would be beneficial to improve solvent production in syngas fermentation.

Gas partial pressure

The concentration of CO in syngas has a significant impact on the overall process efficiency and utilization of other syngas components (namely CO_2 and H_2). Hu (2011) reported that electron production from CO is thermodynamically favorable compared to H_2 independent of pH, ionic strength and gas partial pressure. In a syngas fermentation using *C. carboxidivorans*, the increase of CO partial pressure from 35.5 to 70.9 kPa and from 35.5 to 202.7 kPa was reported to decrease hydrogenase activity by 84% and 97 %, respectively (Hurst, 2005). In addition, CO partial pressure of 8.5 kPa was reported to

inhibit hydrogenase activity of *C. ragsdalei* by 90% (Skidmore, 2010). The decrease in hydrogenase activity and H_2 utilization results in a decrease in overall gas conversion efficiency of the process. However, a study on effect of CO partial pressure using CO:CO_2 (molar ratios of 1.7 to 4) gas mix without H_2 reported that *C. carboxidivorans* switched from non-growth related to growth related ethanol production and grew 440% more when the partial pressure of CO was increased from 35.5 to 202.79 kPa (Hurst and Lewis, 2010).

It should be noted that syngas produced during gasification contains H_2 along with CO and CO_2. Thus ideally, for high product yields and efficient gas utilization, CO and CO_2 should be used as carbon source and H_2 should be used as the sole electron source (Hu et al., 2011; Skidmore, 2010). In a batch culture with *C. ljungdahlii*, when the total pressure of syngas was varied from 81.1 to 182.4 kPa, the ethanol to acetate molar ratio of 5:1 was achieved at total syngas pressure of 162.1 and 182.4 kPa (Najafpour and Younesi, 2006; Younesi et al., 2005). Further, Younesi et al. (2005) reported that H_2 and CO_2 consumption occurred after CO was exhausted indicating CO as a preferred substrate for cell growth.

Medium components

Fermentation medium components such as vitamins, minerals and metals act as cofactors or coenzymes that are necessary for enzymes to catalyze biochemical reactions (Zabriskie and Mill, 1988). Additionally, syngas fermentation medium is often supplemented with yeast extract (YE) to provide the amino acids and nitrogenous compounds necessary for cell synthesis and with buffer solutions (such as 2-(N-morpholino) ethanesulfonic acid and [N-tris(hydroxymethyl)methyl]-3-

aminopropanesulfonic acid) to maintain the medium pH (Liu et al., 2012; Saxena, 2008; Tanner et al., 1993). While the addition of YE results in an undefined medium; addition of YE and buffer solution would be expensive and uneconomical for commercial syngas fermentation (Gao et al., 2013). Several studies were reported on the optimization of the nutrients for ethanol production using syngas fermentation. Studies with *C. ljungdahlii* showed that reducing or completely removing YE from fermentation medium increased ethanol concentration from 1 g/L to 48 g/L (Phillips et al., 1993; Vega et al., 1989). The increase in the concentrations of Ni^{2+}, Zn^{2+}, SeO_4^- and WO_4^- from 0.84 µM, 6.96 µM, 1.06 µM and 0.68 µM to 8.4 µM, 34.8 µM, 5.3 µM and 6.8 µM, respectively, improved ethanol production by *C. ragsdalei* by fourfold (Saxena and Tanner, 2011). In another study with *C. ragsdalei*, limiting calcium pantothenate, vitamin B_{12} and cobalt chloride in two-stage continuous bioreactor resulted in 15 g ethanol/g cell compared to 2.5 g ethanol/g cell in a single-stage bioreactor (Kundiyana et al., 2011a). In other studies, standard YE medium was replaced with defined minimal medium, cotton seed extract (CSE) and corn steep liquor (CSL) to reduce medium cost and improve ethanol production (Gao et al., 2013; Kundiyana et al., 2010; Maddipati et al., 2011). CSL medium, which is rich in vitamins, minerals and amino acids was shown to produce 40% more ethanol using *C. ragsdalei* (Maddipati et al., 2011). Also, the use of a completely defined minimal medium was shown to result in 36% higher ethanol yield than in standard YE medium at 5% of the cost of the YE medium (Gao et al., 2013).

Reducing agents

Reducing agents are artificial electron carriers that alter $NADH/NAD^+$ ratio. Reducing agents significantly decrease the redox potential of the fermentation medium

(Frankman, 2009). Redox potential is a fermentation parameter that defines the ability of the solution to undergo oxidation reduction reaction (IFIS, 2009). In syngas fermentation using *C. ragsdalei*, a decreasing trend of redox potential during cell growth and increasing trend of redox potential during ethanol production was reported (Kundiyana et al., 2010; Maddipati et al., 2011). Solventogenesis is an electron intensive process that requires high levels of NADH (Rao et al., 1987). Addition of reducing agents was reported to increase the NADH levels in cells and direct electron flow towards ethanol production (Babu et al., 2010; Panneerselvam et al., 2009; Sim and Kamaruddin, 2008). Reducing agents such as neutral red were also reported to increase the activity of aldehyde dehydrogenase and alcohol dehydrogenase enzymes, which catalyze the aldehyde and ethanol production from acetyl-CoA intermediate (Girbal et al., 1995). It was reported that the addition of methyl viologen to the fermentation medium of *Thermoanaerobacter ethanolicus* and *C. acetobutylicum* resulted in the onset of ethanol production from glucose (Rao and Mutharasan, 1986; Rao et al., 1987). In syngas fermentation studies with *C. carboxidivorans*, addition of neutral red was reported to increase alcohol dehydrogenase activity and ethanol production (Ahmed et al., 2006). The addition of methyl viologen and dithiothreitol to fermentation medium with *C. ragsdalei* also showed enhancement in ethanol production (Babu et al., 2010; Panneerselvam et al., 2009).

Gas-liquid mass transfer

A major engineering challenge in the commercialization of syngas fermentation is the transfer of gaseous substrates into the fermentation medium at high rate to increase productivity (Bredwell et al., 1999; Munasinghe and Khanal, 2010a). Gas-liquid mass

transfer is considered as one of the rate limiting steps in syngas fermentation due to the low solubility of CO and H_2 in fermentation medium (Bredwell et al., 1999). Low solubility of CO and H_2 in fermentation medium would result in low gas uptake rate and productivity. The rate of mass transfer (*dn/dt*) is given as follows(Sherwood et al., 1975):

$$\frac{1}{V} \cdot \frac{dn}{dt} = -\frac{k_L a}{V} \cdot (C_i - C_L) \quad (2.23)$$

where, *dn/dt* is the rate of mass transfer (*mmol/h*); $k_L a/V$ is the overall mass transfer coefficient (h^{-1}); C_i is the concentration of the gas in gas liquid interface (*mmol/L*); C_L is the concentration of gas in the bulk liquid (*mmol/L*) and *V* is the liquid volume in the reactor (*L*). The rate of gas transfer can be increased by either increasing the mass transfer coefficient ($k_L a/V$) or by increasing the driving force (C_i-C_L). The driving force can be increased by operating the reactor at high CO partial pressures that will increase CO solubility (Klasson et al., 1993b). However, high concentrations of CO could be inhibitory to the microorganisms (Munasinghe and Khanal, 2010a). The mass transfer limiting conditions occur when the concentration of CO in the liquid is zero, at which the reaction rate is a function of the gas transfer rate.

Mass transfer characteristics of various reactor configurations have been studied and compared by many researchers (Bredwell and Worden, 1998; Cowger et al., 1992; Jones, 2007; Klasson et al., 1990b; Klasson et al., 1991a; Klasson et al., 1993a; Munasinghe and Khanal, 2010b; Riggs and Heindel, 2006). In an STR, the mass transfer coefficient can be increased by increasing the agitation speed or the gas flow rate. Using high gas flow rates decreases the gas conversion efficiencies unless the gas is recycled. The increase in agitation speed has been widely used to increase the $k_L a$ in STRs. The hydrodynamic shear generated by the impeller reduces the bubble size and increases the

interfacial area for mass transfer (Bredwell et al., 1999). However, the commercial feasibility of using high agitation speeds to increase mass transfer is questioned due to the high costs associated with the power requirement for large reactors. In a study by Ungerman and Heindel (2007), it was reported that a dual impeller scheme with axial flow impeller at the top and lower concave impeller has a similar k_La with less power requirement than Rushton impellers. In a study by Bredwell and Worden (1998), a micro bubble sparger was shown to be energy efficient and increase the k_La by six fold over conventional gas sparging with a stainless steel frit. In the case of a air lift reactor, the use of a 20 μm bulb diffuser was reported to provide higher mass transfer coefficient (91 h^{-1}) than air lift reactor configurations with column diffusers, gas spargers and gas spargers with mechanical mixing (Munasinghe and Khanal, 2010b). Also, it was claimed that due to the simple reactor configuration and low energy requirements, the scale up of air lift reactors with a 20 μm bulb diffuser will be easy and cheap compared to a conventional STR (Munasinghe and Khanal, 2010b).

In some syngas fermentation studies for the production of hydrogen and methane with a mixed culture *of R. rubrum, M. formicicum* and *M. barkeri*, performances of different reactors were compared (Klasson et al., 1990b; Klasson et al., 1991a; Klasson et al., 1992). The TBR was reported to have better CH_4 productivity, CO gas conversion and mass transfer capabilities than the packed bubble column reactor (PBR). The mass transfer coefficients of 3.5 h^{-1} and 780 h^{-1} were reported for PBR and TBR, respectively (Klasson et al., 1990b). The TBR showed better mass transfer capabilities than PBR and CSTR in the production of acetate by *P. productus* from syngas. Also, for the same mass transfer coefficient, higher specific rates of CO conversion efficiencies were reported for

a PBR than in a CSTR (Klasson et al., 1990a). Further, in another mass transfer study, comparison between CSTR, TBR and HFR reported that HFR with polydimethylsiloxane (PDMS) provided better gas liquid mass transfer followed by TBR with 6-mm glass beads packing (421 h^{-1}) and CSTR (114 h^{-1}) (Orgill et al., 2013). In general, the mass transfer capabilities of a bioreactor can be manipulated to match the cell kinetics by adjusting the operating parameters such as agitation speeds, gas and liquid flow rates. However, care must be taken while doing so as increasing gas flow rate would compromise the gas utilization while increasing agitation speeds and liquid flow rates would have detrimental effects on the cell viability and costs associated with power in large scale production.

Bioreactor Designs for Syngas Fermentation

A bioreactor should provide a controlled environment to enhance cell growth, substrate conversion and productivity of the biological process, and minimize the overall cost of production of desired products (Wilkins and Atiyeh, 2012). Continuous stirred tank reactors, bubble columns, packed columns, air-lift, trickle beds and hollow fiber reactors are some of the bioreactor configurations studied for alcohol production using syngas fermentation (Datar et al., 2004; Hickey et al., 2011; Kimmel et al., 1991; Kundiyana et al., 2010). Further, these reactors can be operated in different fermentation modes such as batch, fed-batch, continuous with and without cell recycle (Ahmed et al., 2006; Cotter et al., 2009; Grethlein et al., 1991; Lewis et al., 2007; Maddipati et al., 2011; Phillips et al., 1993; Ramachandriya et al., 2011). In a study by Klasson et al. (1990a), when two STRs in series were employed a 30 fold increase in ethanol productivity was reported for syngas fermentation using *C. ljungdahlii*. In another study by Bredwell and

Worden (1998), the use of microsparger in a conventional STR for production of acetate, ethanol and butyrate by *Butyribacterium methylotrophicum* was reported to increase the mass transfer by six times with one half the flow rate used without a microsparger. The highest ethanol concentration of 48 g/L was reported to be produced in a CSTR with cell recycle system indicating that continuous mode is the best way to increase the ethanol productivity (Phillips et al., 1993).

The key parameters that define an efficient syngas fermentation bioreactor design are its ability to (i) provide gas-liquid mass transfer that balances the cells kinetic requirement without inhibiting the cells metabolic activity, (ii) insure the viability of the biocatalyst, (iii) reduce the operation and maintenance cost (iv) sustain high cell concentrations and (v) scale up easily. The ability to maintain high cell concentrations and high gas transfer rates in the reactor can greatly enhance the productivity and reduce the reactor size resulting in lower operation and maintenance costs.

2.3.1.6 Commercialization of Gasification-Syngas Fermentation Hybrid Technology

LanzaTech, Coskata, and INEOS Bio are among the companies that are currently pursuing commercialization of syngas fermentation technology for biofuels production (Liew et al., 2013). Coskata's licensed strains *C. ragsdalei* and *C. carboxidivorans* from Oklahoma State University and University of Oklahoma for further development (Huhnke et al., 2010; Lewis et al., 2007). The company fully integrated demonstration facility in Madison, Pennsylvania, and recently isolated and patented a new strain *C. coskatii* (Zahn and Saxena, 2012). The company is focusing on fermentation of syngas produced from natural gas reforming or gasification of wood and coal (Coskata, 2011).

INEOS Bio has operated the first commercial cellulosic ethanol and power generation facility using syngas fermentation technology in Vero Beach, Florida since July 2013 (INEOS, 2013). The company utilizes patented bacteria to produce ethanol and generate power from vegetative and woody waste. The company was projected to produce 8 million gallons of ethanol per year and generate 6 MW of renewable electricity (INEOS, 2013).

LanzaTech is a New Zealand based company that utilizes CO-rich flue gases from steel making industries to produce ethanol and 2, 3-butanediol using its proprietary *Clostridial* biocatalyst. It has a pilot plant facility in Glenbrook, New Zealand and a demonstration facility in Shanghai, China that has an operating capacity of 100,000 gallons ethanol per year. In 2013, LanzaTech announced building a commercial facility with a capacity of 50 million gallons of ethanol per year in Shanghai, China (Liew et al., 2013).

For the biofuels industry to thrive, the coexistence of different technologies to produce different types of biofuels is necessary. There is need for further research with focus on reducing the costs of biofuels production through optimization of existing and development of new technologies. The hybrid gasification-syngas fermentation process upon further development is expected to be a sustainable technology for feasible biofuels production.

CHAPTER III

OBJECTIVES

The overall goal of this study is to determine the mass transfer of the trickle-bed reactor (TBR) and its suitability for ethanol production using syngas fermentation. The three main objectives of this project are:

- **Objective I**: Determine the mass transfer characteristics of the TBR at various gas and liquid flow rates with 3- and 6-mm glass beads using air-water system.
- **Objective II**: Investigate semi-continuous syngas fermentations and evaluate the effects of gas and liquid flow rates on ethanol production and syngas utilization in the TBR using *Clostridium ragsdalei*.
- **Objective III**: Examine continuous syngas fermentation and evaluate the effects of gas flow rate and dilution rate on ethanol production and syngas utilization in the TBR using *C. ragsdalei*.

To evaluate the suitability of TBR for ethanol production using syngas fermentation, the first step is to understand the effects of liquid and gas flow rates, and size of packing material on mass transfer of the sparingly soluble syngas components (CO and H_2) in the fermentation medium. Understanding the effect of these key parameters is important to control the mass transfer to match the kinetic requirement of

C. ragsdalei during fermentation. Additionally, examining semi-continuous and continuous syngas fermentations in the TBR will provide guidance into which fermentation scheme is easier to operate and can result in higher ethanol production. While operating in semi-continuous and continuous modes, biofilm formation of *C. ragsdalei* cells on the glass beads will also be explored. In continuous fermentation mode, there is a loss of cell mass from the reactor with the product effluent stream. Hence, the effect of dilution rate on cell washout and ethanol production will be investigated.

CHAPTER IV

ANALYSIS OF MASS TRANSFER CHARACTERISTICS OF TRICKLE BED REACTOR FOR SYNGAS FERMENTATION

ABSTRACT

Mass transfer capabilities of the reactor should be balanced with the kinetic capacity of the microorganism used for efficient alcohol production via syngas fermentation. In this study, the mass transfer characteristics of a 1-L trickle bed reactor (TBR) were examined with different bead sizes, gas and liquid flow rates. The boundary layer theory was used to estimate CO and H_2 mass transfer coefficients from experimental data obtained using O_2 from air as the transferred species. Two different mass transfer coefficients, the overall mass transfer coefficient (k_La/V_S) and the mass transfer coefficient (k_La/V_L) in the reactive volume (V_L) also called the dynamic liquid holdup volume, were determined. The ratio of the predicted k_La/V_S to experimental k_La/V_S was 1.02 with an R^2=0.95 indicating that the model predictions were in good agreement with the experimental data. Assuming mass transfer limiting conditions, the k_La/V_L was used to predict the amounts of CO and H_2 that can be provided in the TBR compared to the kinetic capacity of *Clostridium ragsdalei* during syngas

fermentation. This allows balancing CO and H_2 mass transfer with *C. ragsdalei* uptake rates to ensure efficient fermentation with high gas conversion efficiencies.

***Keywords*:** Gas fermentation reactors; mass transfer; liquid hold up; trickle-bed reactor (TBR).

4.1 Introduction

In the 2011 International Energy Outlook of the U.S. Energy Information Administration, it was reported that renewables are the fastest growing source of world energy with an increase in their consumption of 2.8% per year (Conti, 2011). Factors such as environmental concerns related to greenhouse gas (GHG) emissions combined with the high fuel prices recorded from 2003 to 2008 lead to the development of energy from renewable sources. The U.S. being the largest producer of corn successfully commercialized the production of corn ethanol (Dien et al., 2002). However, use of corn for fuel raised the debate over its potential interference with the food chain (Tenenbaum, 2008). This gave rise to the use of biomass feedstocks such as dedicated energy crops, agricultural and forest residues and municipal solid wastes for the production of biofuels.

Biomass can be converted to biofuels by direct and indirect fermentation. Hydrolysis-fermentation (Gomez et al., 2008) is a direct process; whereas, gasification-syngas fermentation is an indirect process. Gasification-syngas fermentation of biomass to ethanol has the advantage of utilizing the entire biomass components including lignin, which is not efficiently utilized in the direct fermentation method (Sierra et al., 2008). In gasification-syngas fermentation, the biomass is first converted to syngas, which is then fermented by anaerobic bacteria to organic acids and alcohols. Gasification is a partial combustion of biomass that produces CO, CO_2 and H_2 as the major constituents of syngas

with traces of contaminants such as N_2O, H_2S and CH_4. Syngas fermentation involves conversion of syngas components to biofuels using microbial catalysts such as *Clostridium ljungdahlii, Clostridium autoethanogenum, Clostridium carboxidivorans* and *Clostridium ragsdalei* (Abrini et al., 1994; Liou et al., 2005; Phillips et al., 1994; Tanner et al., 2008). Mass transfer limitation is considered to be one of the major bottlenecks for syngas fermentation.

Mass transfer of CO and H_2 is severely limited because of their low solubility in water. Bubble column, packed bed reactors, air lift, trickle bed, hollow fiber membrane and immobilized bioreactors have been proposed to improve the mass transfer of CO and H_2 into the fermentation medium (Bredwell and Worden, 1998; Kimmel et al., 1991; Klasson et al., 1990b; Rajagopalan et al., 2002). This paper evaluates and compares the mass transfer characteristics of a 1-L TBR for the syngas fermentation with data reported in the literature. Traditionally, TBRs have been used for processes such as catalytic hydrogenation, denitrification, desulfurization and oxidation of organic matter on metal or biological catalysts (Gianetto and Specchia, 1992).

To evaluate the TBR's capabilities, it is important to understand the effects of operating parameters such as liquid and gas flow rates and packing size on the mass transfer of CO and H_2. This will help in defining the key parameters for controlling mass transfer in the TBR to match the microorganism's kinetic requirements during syngas fermentation.

The mass transfer in the TBR was previously assessed during fermentation by keeping the cell density of photosynthetic bacteria (*Rhodospirillum rubrum* and *Rubrivivax gelatinous*) constant (Kimmel et al., 1991; Klasson et al., 1990b; Wolfrum

and Watt, 2002; Wolfrum and Weaver, 2002). These microorganisms produce H_2 from CO by the water-gas shift reaction and their cell concentration was regulated by varying the light intensity. This technique for mass transfer and kinetic analysis is not applicable to all fermentations. For example, in syngas fermentation *C. ragsdalei* grows on CO and a limited cell concentration can be achieved due to nutrient limitations.

Recently, a technique of using myoglobin for measuring CO concentrations in water was developed (Riggs and Heindel, 2006). This technique was used to directly assess CO mass transfer in a non-reacting system (i.e., without cells) (Munasinghe and Khanal, 2010b; Ungerman and Heindel, 2007). There are many disadvantages to this technique, such as dilution, sampling and bubbles in the syringe, that reduce the measurement accuracy of CO concentration (Riggs and Heindel, 2006). Considering the errors associated with this new technique, the mass transfer characteristics of the TBR in the present study were assessed by performing aeration experiments using air as the transferred species. Unlike for CO and H_2, probes can be used to measure dissolved O_2 concentration in the liquid. CO and H_2 mass transfer coefficients can be assessed from the O_2 data using boundary layer theory (Sherwood et al., 1975).

The mass transfer analysis of TBR is typically based on the overall mass transfer coefficient (k_La/V_S) which considers the total liquid volume (V_S) in the TBR system (Cowger et al., 1992; Kimmel et al., 1991). However, during syngas fermentation in TBR, the mass transfer happens between the gas and liquid present in the dynamic liquid holdup volume between the packing material (V_L), which is also called the reactive volume. Thus, the mass transfer coefficient in the reactive volume (k_La/V_L) becomes an important parameter in determining the reactor's characteristics. The novelty of the

present study is in the detailed mass transfer analysis of the TBR and determination of both the overall mass transfer coefficient (k_La/V_S) and the mass transfer coefficient in the reactive volume (k_La/V_L). In addition, the determined overall mass transfer coefficient (k_La/V_S) was compared with the values predicted using mass transfer model proposed in the literature (Fukushima and Kusaka, 1977). Further, under mass transfer limited condition, theoretical analysis was done to assess and compare the CO and H_2 provided in the TBR at a given operating condition with the kinetic requirement of *C. ragsdalei*.

4.2 Materials and Methods

4.2.1 Mass Transfer Procedure

The 1-L TBR was made of a borosilicate glass column with a 51 cm inner diameter and 61 cm length. The reactor was operated in counter-current mode with liquid flowing from the top to bottom and gas flowing from the bottom to top. The bottom of the reactor was used as a liquid sump to hold 200 ml of DI water and a peristaltic pump (7523-20, Cole-Parmer, Vernon, IL, USA) was used to recirculate the liquid from the sump to the top of the reactor. Air was used as a mass transfer agent to assess the reactor's mass transfer characteristics. The dissolved oxygen (DO) was stripped from the DI water by purging the column with N_2 until the % DO reached zero and then the liquid was aerated. The N_2 and air gas flow rates were controlled using a rotameter. The N_2 and air inlets were connected to the rotameter using a T-connector. The flow of gas in the rotameter was changed from air to N_2 by switching the ball valves in the gas lines. The changes in % DO concentration with time were recorded using Biocommand software (New Brunswick, Edison, NJ, USA). The experimental mass transfer set up and detailed procedure were previously described in Orgill et al. (2013) and can also be found in

Appendix A. The experiments were performed in duplicates. The overall mass transfer coefficient of O_2 (k_La/V_s) in the TBR at a given gas and liquid flow rate was calculated according to Eq 4.1 (Garcia-Ochoa and Gomez, 2009):

$$\frac{k_L a}{V_S} = -\frac{ln\left(1-\frac{C_L}{C_S}\right)}{t} \tag{4.1}$$

where, k_L is the mass transfer coefficient (m/h), a is the mass transfer area (m^2), V_L is the dynamic liquid holdup volume in the TBR (m^3), V_S is the total volume of the system including sump and circulation loop (m^3), C_L is the bulk DO concentration in the liquid (mol/m^3), C_S is the saturated DO concentration (mol/m^3), and t is the time (h).
Since C_L/C_S is a ratio, % DO in the bulk liquid was used in place of C_L and saturated % DO was used in place of C_S.

The experimental overall mass transfer coefficient (k_La/V_S) for O_2 was used to estimate the overall mass transfer coefficients for CO and H_2 using boundary layer theory. The aim of this mass transfer analysis was to determine the effect of bead size, liquid and gas flow rates on the overall mass transfer coefficient (k_La/V_S) and on mass transfer coefficient in the reactive volume (k_La/V_L) for CO and H_2 in the TBR. The analysis was done at various flow rates of gas (5.5 sccm to 130.9 sccm) and liquid (50 ml/min to 1000 ml/min) with 3 and 6-mm glass beads as the packing material. The mass transfer experiments were performed at 37 °C, which is the operating temperature during fermentation. The four basic flow regimes; namely trickle flow, pulse flow, spray and bubble flow regimes, are defined for a TBR based on the way gas and liquid contact in the reactor (Gunjal et al., 2005; Ramachandran and Chaudhari, 1983; Ranade et al., 2011a; Sie and Krishna, 2011). The gas –liquid interfacial area varies significantly depending on the type of f1ow regime encountered in the reactor. This in turn affects the

mass transfer of sparingly soluble gaseous components into the liquid. Hence, the above mentioned wide range of gas and liquid flow rates were used to assess their effect on the mass transfer capabilities of the TBR.

4.2.2 Determination of dynamic liquid holdup and void fraction of the bed

Dynamic liquid holdup

The dynamic liquid holdup *(h_d)* is the ratio of the liquid holdup volume to the total bed volume. The total bed volume was 772 ml. The dynamic liquid holdup volume is defined as the volume of liquid held between the beads at a certain liquid and gas flow rate. Before measuring the dynamic holdup volume, the beads were completely wetted to negate the static holdup effects on the measurement. The dynamic liquid holdup volume (V_L) in the packing was experimentally determined by recirculating the liquid at a desired flow rate. After the system reached steady state, the volume of liquid in the sump was noted. The difference in the initial and final volumes of liquid in the sump after reaching steady state is the dynamic holdup volume that is held up in the voids between the beads. The dynamic holdup volume at various liquid flow rates for 3 and 6-mm beads is reported in Appendix A, Table A1. The dynamic liquid holdup volume (V_L) divided by the total volume of the bed gave the dynamic liquid holdup (h_d). This was repeated for all the liquid and gas flow rates used in the mass transfer studies.

Fractional void volume

The experimental fractional void volumes (ε) in the TBR for 3 and 6-mm beads were estimated as the ratio of the void volume to the actual volume of the TBR without beads. A measured volume of water was added into the TBR until all beads were fully covered with water. The volume of water up to the bottom of the packing bed was

subtracted from the measured total volume that fully covered the TBR bottom and beads to determine the void volume of the TBR.

4.2.3 Determination of CO and H_2 mass transfer coefficient

According to the boundary layer theory (Sherwood et al., 1975), the mass transfer coefficient and diffusivities of two different chemical species under identical hydrodynamic conditions can be correlated by

$$\frac{\left({k_L a}/{V_S}\right)_i}{\left({k_L a}/{V_S}\right)_j} = \left(\frac{D_i}{D_j}\right)^{1/2} \tag{4.2}$$

Where, $(k_L a/V_S)_i$ and $(k_L a/V_S)_j$ are the mass transfer coefficients of the *i* and *j* gases respectively, and D_i and D_j are diffusivities for the *i* and *j* gases, respectively. The diffusivities of O_2, CO and H_2 at 37 °C are 3.05 x10^{-9} m^2/s, 3.26x10^{-9} m^2/s and 6.48x10^{-9} m^2/s, respectively (Verhallen et al., 1984; Wise and Houghton, 1968). Using these diffusivity values, the mass transfer coefficients of CO and H_2 were determined from the experimental $k_L a/V_S$ of O_2. Further, the $k_L a/V_L$ was estimated by multiplying $k_L a/V_S$ by V_S/V_L. The V_L is the dynamic liquid holdup volume within the packing at a given flow rate and *Vs* is the total liquid volume in the TBR system.

4.3 Results and Discussion

The overall mass transfer coefficient ($k_L a/V_S$) and the liquid hold up (h_d) data of the 3 and 6-mm beads were predicted using mathematical models defined in the literature and compared to the data obtained in the present study. The mass transfer coefficient in the reactive volume ($k_L a/V_L$) on the other hand is important in syngas fermentation during mass transfer limiting conditions. Under the mass transfer limited condition, the gas transferred into the liquid is immediately consumed by the cells present between the

beads in the TBR. Thus, at any given time the concentration of the gas in the liquid is approximately zero. In this scenario, the mass transfer characteristic of the TBR is better described by k_La/V_L. Further during mass transfer limited condition, a theoretical analysis was performed using the TBR k_La/V_L and *C. ragsdalei* batch fermentation kinetic data to balance the kinetic capacity of the microorganism with the mass transfer provided by the TBR. A detailed discussion and analysis of both the mass transfer parameters k_La/V_S and k_La/V_L is given in the following sections.

4.3.1 Overall mass transfer coefficient

The mass transfer characteristics of the TBR can be defined by the overall mass transfer coefficient (k_La/V_S), which is based on the total liquid volume in the reactor (V_S) and by the mass transfer coefficient in the reactive volume (k_La/V_L), which is based on dynamic liquid holdup volume (V_L). The k_La/V_S of O_2 obtained experimentally at 37 °C varied from 1 to 30 h^{-1} (Appendix A). The predicted k_La/V_S values for CO and H_2 using Eq 4.2 varied from 1 to 30 h^{-1} and 1 to 45 h^{-1}, respectively (Figures 4.1 and 4.2). The k_La/V_S profiles of CO and H_2 are very similar to the O_2 profile obtained experimentally at various gas and liquid flow rates.

A summary of the mass transfer coefficients ($k_{L,i}\,a/V_S$) obtained in different reactors during syngas fermentations for producing methane, hydrogen, ethanol, and acetate is shown in Table 4.1. The gas flow rates used in previous studies were from 0 to 50 ml/min and the liquid flow rates were from 100 to 300 ml/min (Cowger et al., 1992; Klasson et al., 1990b; Klasson et al., 1991a). $k_{L,CO}\,a/V_S$ values in the range of 8.7 h^{-1} to 53 h^{-1} were reported during syngas fermentation in a TBR for the production of H_2, methane and acetate (Cowger et al., 1992; Klasson et al., 1990b; Klasson et al., 1991a). All these

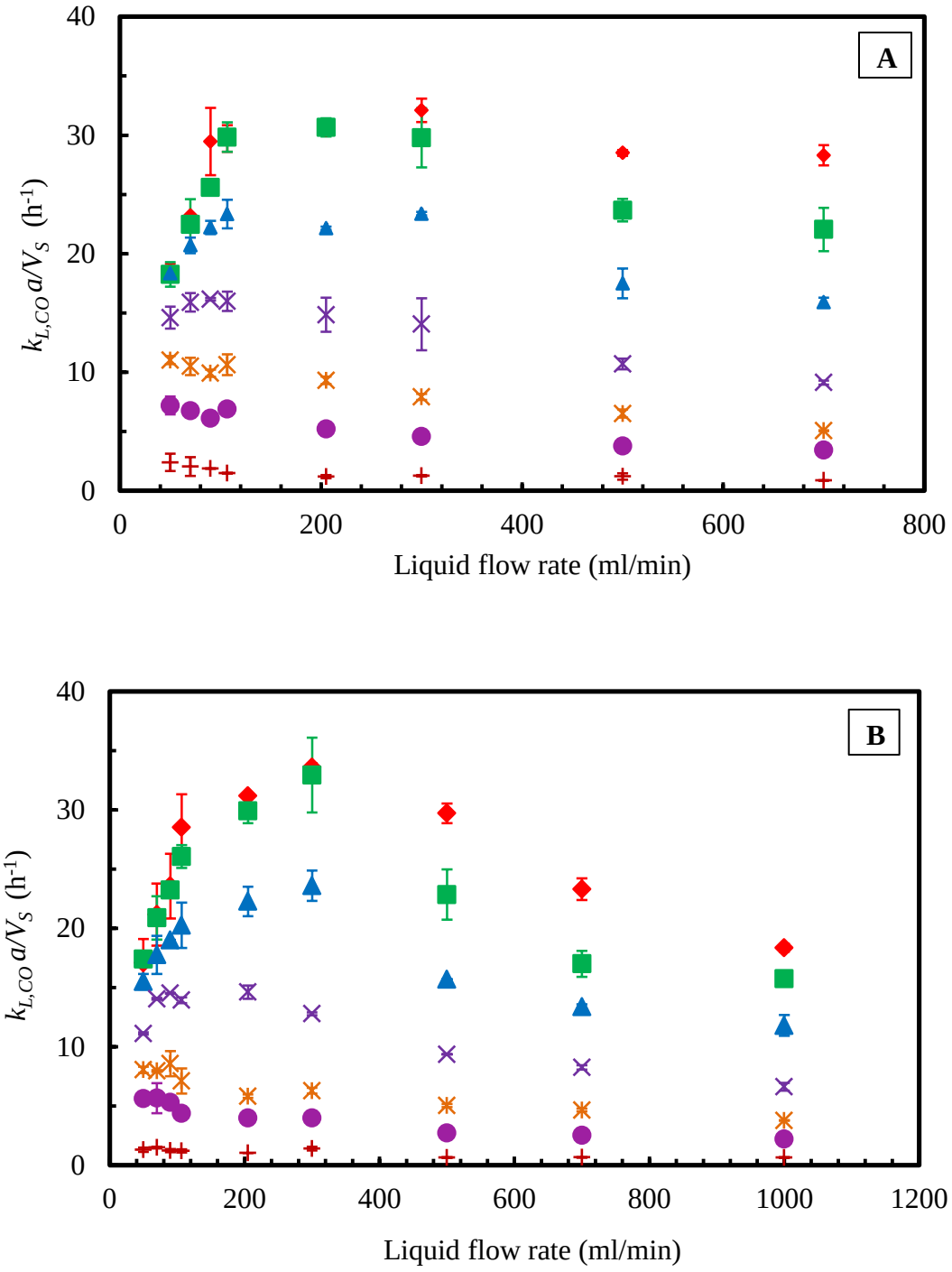

Figure 4.1 $k_{L,CO}\,a/V_S$ at 37 °C for (A) 3-mm beads (B) 6-mm beads and at different gas flow rates.
(+) 5.5 sccm (●) 18.4 sccm (*) 28.2 sccm (×) 46.4 sccm (▲) 72.8 sccm (■) 106.4 sccm (♦) 130.9 sccm. Error bars represent ± 1 standard deviation (n=2).

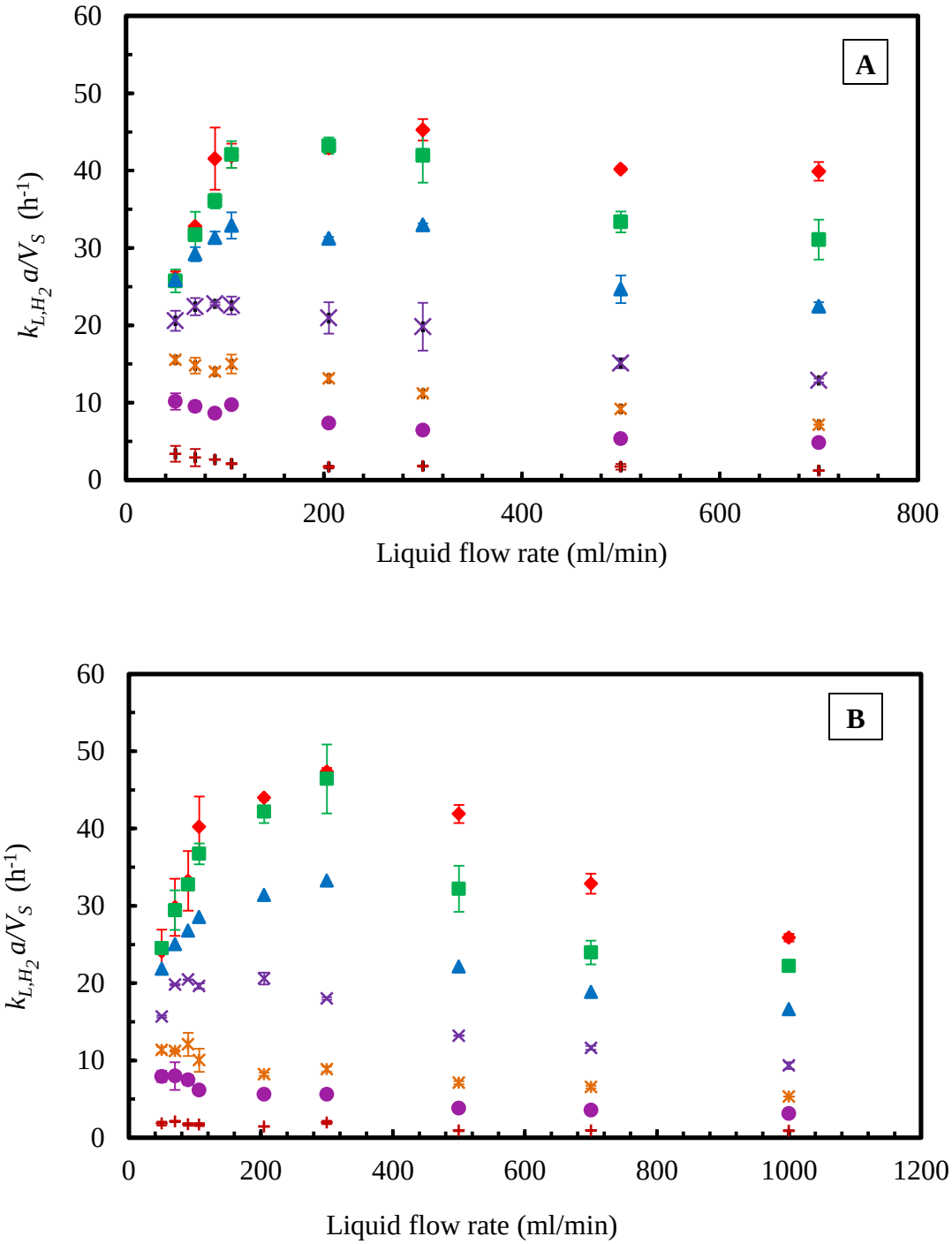

Figure 4.2 $k_{L,H2}a/V_S$ at 37 °C for (A) 3-mm beads (B) 6-mm beads and at different gas flow rates.
(+) 5.5 sccm (●) 18.4 sccm (*) 28.2 sccm (×) 46.4 sccm (▲) 72.8 sccm (■) 106.4 sccm (♦) 130.9 sccm. Error bars represent ± 1 standard deviation (n=2).

Table 4.1 Overall mass transfer coefficient, productivity and conversion data of syngas fermentation from literature for different reactors

Reactor[a]	Working volume (L)	Microorganism	$k_{L,CO}\,a/V_S$ (h^{-1})	Flow rates[b] (ml/min)		Products (g/L day)		% CO conversion	References
STR-convention sparger	1.5	*B. methylotrophicum*	14.2	G (13-40)	-	CH_3COOH	3.84		(Bredwell and Worden, 1998)
STR-micro sparger	1.5	*B. methylotrophicum*	90.6	G (5-10)	-	CH_3COOH	3.84		
STR	0.35	*P. productus*	31.0	G (3-15)	-	CH_3COOH		40-80	
PBC	0.86	*P. productus*	14.0	G (1.5-20)		CH_3COOH		40-90	
TBR	1.1	*P. productus*	31.2	G (5-30)	L-395	CH_3COOH		50-100	(Klasson et al., 1990a)
			16.8		L-308			40-100	
			9.0		L-125			35-70	
Single STR	0.35	*C. ljungdahlii*	-	-	-	C_2H_5OH	0.11		
Two STRs in series	0.35	*C. ljungdahlii*	-	-	-	C_2H_5OH	2.88	100% (Reactor A)	
TBR	0.95	*R. gelatinosus*	25.2	G (5-50)	L-200	H_2	1.21-2.14	15-70	(Wolfrum and Watt, 2002)
	1.1	*R. gelatinosus*	11.4	G (5-50)	L-200	H_2	0.99-2.14	15-60	
	5	*R. gelatinosus*	11.4	G (25 – 250)	L-500			15-60	
TBR	1.1	*R. rubrum, M. barkeri* and *Methanobacterium*	53.0	G (0-33)	L-125, 229, 278	CH_4	0.77	40-100	(Kimmel et al., 1991)

[a] STR: Stirred tank reactor; PBC: Packed bed column; TBR: Trickle bed reactor
[b] L and G : Liquid and gas flow rates

studies reported an increase in the $k_{L,CO}\,a/V_S$ with an increase in liquid flow rate (Table 4.1) unlike in the present study where liquid flow rate effect was negligible between 100 to 300 ml/min for all the gas flow rate range tested from 5.5 to 130.9 sccm (Figures 4.1 and 4.2). This is because the flow regimes encountered in the TBR in the present study could be different from previous studies. Another reason for the difference is the dissimilarities in the bed height and the type of packing material used. The bed height used in the present study was 38 cm while the bed height previously reported was about 51 cm (Cowger et al., 1992; Klasson et al., 1990b; Klasson et al., 1991a). Also the packing materials used in the previous studies were 6.4 mm intalox saddles; whereas the packing materials used in the present study were 3 and 6-mm glass beads.

In a review article on bioreactors for syngas fermentation by Bredwell et al. (1999), trickle beds were described as a liquid continuous and gas continuous type of reactor. In a gas continuous reactor, the mass transfer coefficient and interfacial area are relatively unaffected by the gas flow rate for sparingly soluble gases because the gas side mass transfer resistance is low. However, in liquid continuous reactors, the interfacial area is strongly dependent on the gas flow rate and an increase in gas flow rate increases k_La/V_S. In the present study, the k_La/V_S values for CO and H_2 changed more by the gas flow rate indicating that the flow regime in the TBR was liquid continuous for most of the flow conditions used in this study (Figures 4.1 and 4.2). Especially when the gas flow rates were between 5.5 and 46.4 sccm and liquid flow rates were between 50 and 300 ml/min, the gas was more in the form of a discontinuous phase (i.e., transition or pulses or

bubbles flow) and so the interfacial area for the mass transfer of O_2, CO and H_2 was more affected by the gas flow rate. For both 3 and 6-mm beads at gas flow rates above 46.4 sccm, the TBR was gas continuous and at liquid flow rates between 50 and 90 ml/min, the beads were converted from partially wetted to completely wetted, which increased the interfacial area between the gas and liquid, thus the k_La/V_S increased. Once the liquid flow rate was increased from 106 to 1000 ml/min, the thickness of the liquid film increased thus restricted the continuous gas flow. This changed the gas-liquid boundary layer from the surface of the liquid film on the beads to the surface of the gas bubble but did not further increase the interfacial area. Thus, no increase in the k_La/V_S was observed beyond 106 ml/min of liquid flow rate and 46.4 sccm gas flow rate.

4.3.2 Mass transfer in the reactive volume

The fermentation biochemical reactions involving sparingly soluble gases can proceed appreciably only when the gases are transferred into the liquid. In column reactors such as TBRs, the gas-liquid interaction solely happens within the packed bed. Further, the scale-up of the reactor will be based on the packed bed portion of the reactor where gas and liquid interacts. Thus, k_La/V_L is of significance as it defines the mass transfer characteristics in the packed bed. Also, under mass transfer limited conditions the gas is assumed to be consumed as soon as it is transferred into the V_L (i.e., C_L~0). Hence, under these conditions, the mass transfer is based on V_L, which more accurately defines the mass transfer characteristics of the TBR.

The mass transfer coefficients based of the dynamic liquid holdup volume (i.e., reactive volume) namely $k_{L,CO}\,a/V_L$ and $k_{L,H2}\,a/V_L$ at various gas and liquid flow rate are shown in Figures 4.3 and 4.4. It was observed that as the gas flow rate increased, the $k_{L,CO}\,a/V_L$ and $k_{L,H2}a/V_L$ increased similar to $k_{L,CO}\,a/V_S$ and $k_{L,H2}\,a/V_S$. On the other hand, $k_{L,CO}\,a/V_L$ and $k_{L,H2}\,a/V_L$ decreased considerably with increasing liquid flow rate due to the increase in liquid holdup (Figure 4.5), which was also described in Orgill et al. (2013). While gas flow rate in the range tested had no effect on the holdup volume, the increasing liquid flow rate displaced the gas, which resulted in increased liquid holdup. The increase in the liquid holdup volume resulted in flow of gas in the form of bubbles and the gas-liquid interfacial area was a function of the surface area of the bubbles and no longer a function of the surface area provided by the beads. Further, the void fraction was the same about 0.38 for 3 and 6-mm beads, while the liquid retention time and holdup volume were higher in 3-mm than in the 6-mm beads because the 3-mm beads specific surface area was 50% higher. Thus, the $k_{L,CO}\,a/V_L$ and $k_{L,H2}\,a/V_L$ with the 3-mm beads was lower than the 6-mm beads by the same percentage. The maximum $k_{L,CO}\,a/V_L$ and $k_{L,H2}\,a/V_L$ values for 6-mm beads were 435 h^{-1} and 613 h^{-1}, respectively. However, the maximum $k_{L,CO}\,a/V_L$ and $k_{L,H2}\,a/V_L$ values for 3-mm beads were 184 h^{-1} and 260 h^{-1}, respectively.

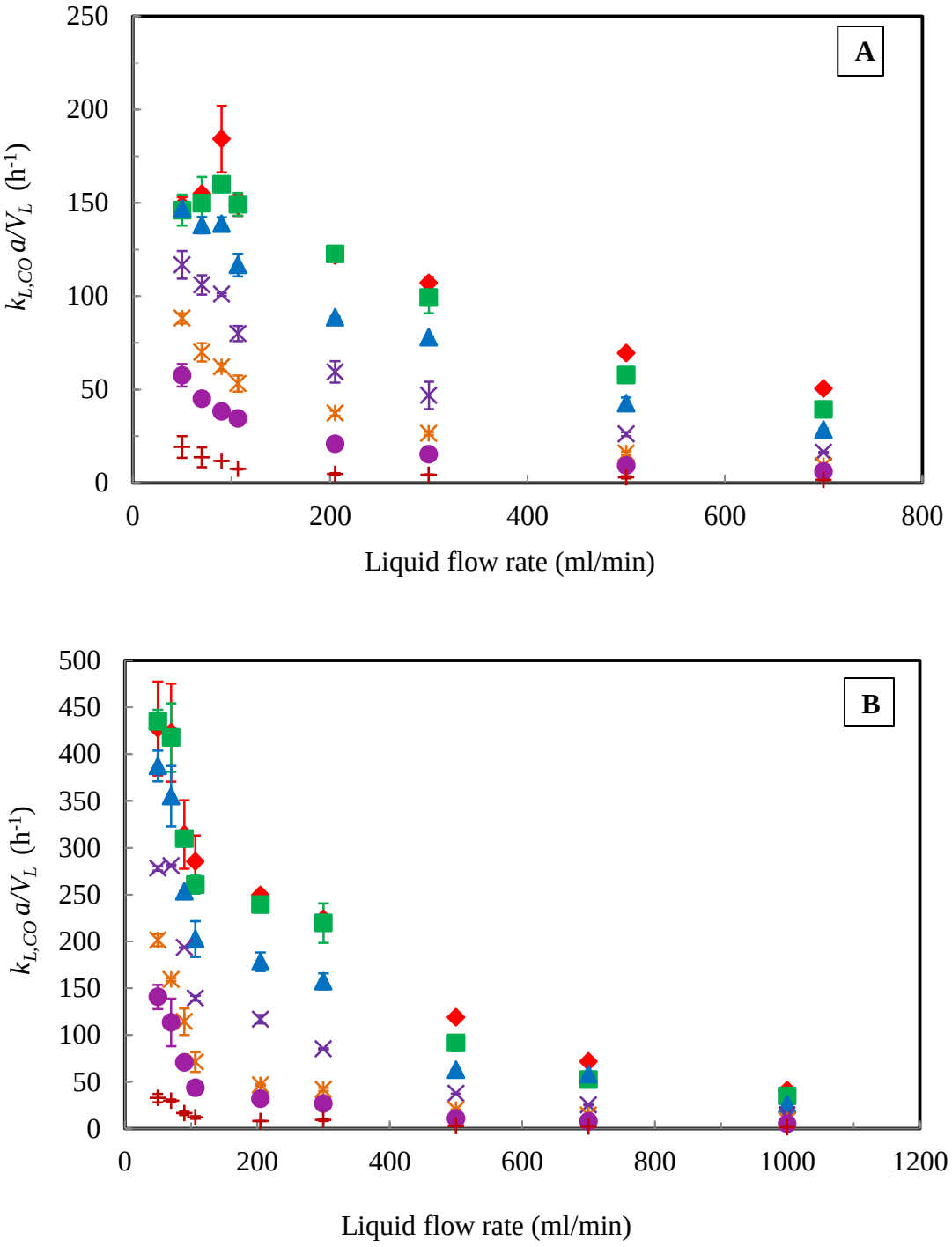

Figure 4.3 $k_{L,CO}\,a/V_L$ at 37 °C for (A) 3-mm beads (B) 6-mm beads and at different gas flow rates.
(+) 5.5 sccm (●) 18.4 sccm (*) 28.2 sccm (×) 46.4 sccm (▲) 72.8 sccm (■) 106.4 sccm (♦) 130.9 sccm. Error bars represent ± 1 standard deviation (n=2).

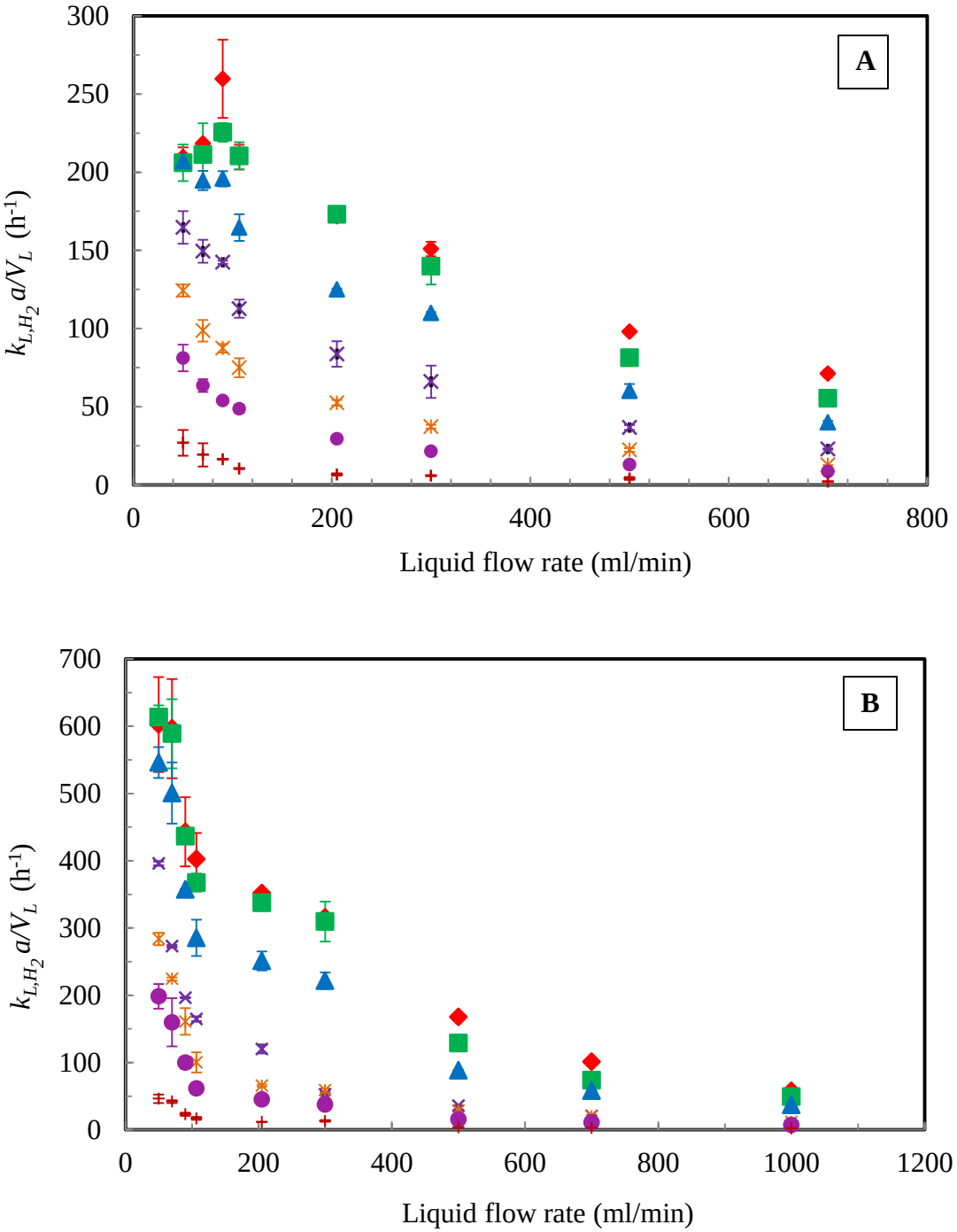

Figure 4.4 $k_{L,H2}\,a/V_L$ at 37 °C for (A) 3-mm beads (B) 6-mm beads and at different gas flow rates.
(+) 5.5 sccm (●) 18.4 sccm (*) 28.2 sccm (×) 46.4 sccm (▲) 72.8 sccm (■) 106.4 sccm (♦) 130.9 sccm Error bars represent ± 1 standard deviation (n=2).

4.3.3 Liquid holdup

From the liquid holdup experiments, it was observed that for the gas and liquid flow rates tested, the gas flow rate did not affect the liquid holdup volume in the TBR; whereas, the change in liquid flow rate largely affected the holdup volume (Appendix A, Table A1). In Figure 4.5, the experimental dynamic liquid holdup values for 3 and 6-mm beads were compared to predicted values from the Otake and Okada correlation for spheres (Goto and Smith, 1975). The Otake and Okada liquid holdup correlation for spherical packing and for Reynolds number between 10 and 2000 is given as:

$$h_d = 1.25\, Re_L^{0.676} Ga^{-0.44} a_t d_p \qquad (4.3)$$

where h_d is the dynamic holdup (dimensionless), Re_L is the Liquid Reynolds number ($u_L d_p \rho_L / \mu_L$), Ga is Galileo number ($d_p^3 \rho_L^2 g / \mu_L^2$), a_t is total external surface area of particle ($6(1-\varepsilon)/d_p$, m^2/m^3), d_p is the diameter of particle (m), ρ_L is the density of liquid, (kg/m^3), μ_L is the dynamic viscosity of water (Pa·s), ε is the fractional void volume of the bed (dimensionless) and u_L is the liquid velocity (m/s).

This correlation was derived from liquid holdup experimental data obtained using non-porous spherical particles ranging from 10 to 50 mm (Goto and Smith, 1975). The % error between the experimental and predicted holdup values for 6-mm beads varied from 3% to 24%. However, the deviations were much higher (7% to 60%) when Eq. 4.3 was used with the 3-mm beads.

In order to better fit the liquid holdup data with 3-mm beads using the Otake and Okada correlation, new constants were obtained by performing

regression analysis on the experimental liquid holdup data obtained from the present study with both 3 and 6-mm beads. The Otake and Okada correlation with the new constants is given as:

$$h_d = 10.613\, Re_L^{0.651} Ga^{-0.576} a_t d_p \qquad (4.4)$$

Using the new correlation Eq 4.4, the % error between the experimental and predicted holdup values for 6-mm beads varied from 4% to 26%, while, the difference in the experimental and predicted holdup values for 3-mm beads were from 3% to 20%.

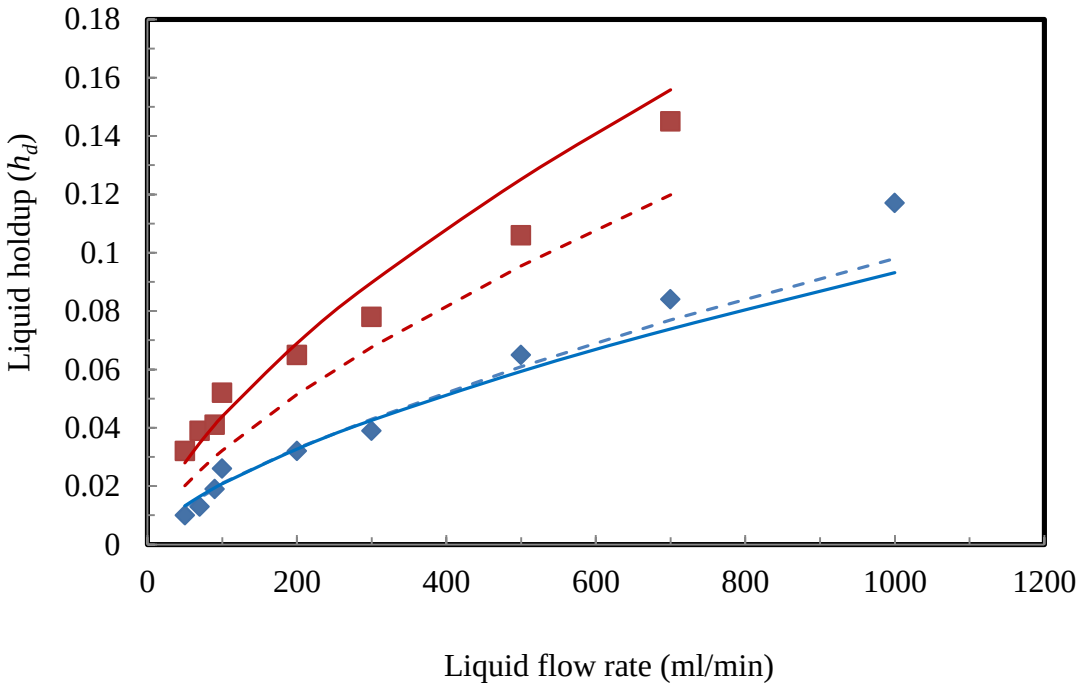

Figure 4.5 Experimental and predicted liquid holdup at various liquid flow rates. (■) 3-mm beads, (♦) 6-mm beads, experimental. Dashed lines indicate the predicted data from Otake and Okada correlation Eq. 4.3. Solid lines are the predicted holdup data using Eq. 4.4 with new constants to fit 3 mm beads data. Blue represents 6-mm beads and red represents 3 mm beads

A change in the slope of the liquid holdup indicates a transition between flow regimes (Ranade et al., 2011a). From Figure 4.5, for both bead sizes a

change in the slope of the liquid holdup is observed with change in liquid flow rates from 50 to 100 ml/min and from 100 to 1000 ml/min. A visual inspection of the flow patterns in the TBR indicated that when the liquid flow rate was 50 to 100 ml/min, the gas flow was continuous and no gas bubbles were observed. However, for both bead sizes when the liquid flow rate was increased from 100 to 1000 ml/min, gas bubbles were observed in the TBR. This indicated that the flow regime transitioned from gas continuous (from 50 to 100 ml/min) to bubble flow regime (from 100 to 1000 ml/min) as the liquid flow rate was increased.

4.3.4 Comparison of $k_{L,i}a/V_S$ from experimental data and mass transfer model

The overall gas-liquid mass transfer resistance for transfer of gas into the liquid in the TBR can be described according to the two film theory (Herskowitz and Smith, 1983). The two film theory assumes that only resistances for diffusion of solute are those residing in the fluids themselves and there is no resistance to solute transfer across the interface separating the phases. Thus, the overall gas-liquid mass transfer resistance is described by Eq 4.4

$$\frac{1}{K_L a_i} = \frac{1}{H \cdot k_G a_i} + \frac{1}{k_L a_i} \tag{4.4}$$

where $K_L a_i$ is the overall mass transfer coefficient (h^{-1}), $k_L a_i$ is liquid side mass transfer coefficient (h^{-1}), $k_G a_i$ is the gas side mass transfer coefficient (h^{-1}) and H is the Henry's law constant (dimensionless). For sparingly soluble gases such as O_2, CO and H_2, the liquid side resistance is higher than the gas side resistance and hence the above equation can be approximated as

$$\frac{1}{K_L a_i} \sim \frac{1}{k_L a_i} \tag{4.5}$$

or $$K_L a_i \sim k_L a_i \tag{4.6}$$

where a_i is the interfacial area defined as a/V_S (m^2/m^3), a is mass transfer area (m^2) and Vs is the total liquid volume (m^3). Many empirical mass transfer models have been proposed for the prediction of the liquid side mass transfer coefficient (Fukushima and Kusaka, 1977; Gianetto and Specchia, 1992; Goto et al., 1977; Herskowitz and Smith, 1983; Mahajani and Sharma, 1979; Reiss, 1967; Sylvester and Pitayagulsarn, 1975; Ufford and Perona, 1973). Most of the proposed models are very specific to the size and type of packing, liquid and gas flow rates, and type of fluid (foaming, non-foaming liquids or organic solutions). There are a few models that defined the mass transfer coefficient to be solely a function of liquid flow rate (Mahajani and Sharma, 1979; Turek and Lange, 1981). These models accurately predict the mass transfer coefficient for gas continuous regime where the mass transfer coefficient is only a function of liquid flow rates. Further, other models propose the mass transfer coefficient to be a function of both gas and liquid flow rates (Fukushima and Kusaka, 1977; Sato et al., 1972; Sylvester and Pitayagulsarn, 1975). The empirical model given by Fukushima and Kusaka (1977) describes the mass transfer coefficient as a function of liquid and gas Reynolds numbers and the Schmidt number as follows:

$$\frac{k_L a_i d_p^2}{D_L(1-h_e)} = \beta_1 S_p^{\beta 2} Re_L^{\beta 3} Re_G^{\beta 4} Sc^{1/2} \left(\frac{d_p}{d_t}\right)^{\beta 5} \tag{4.7}$$

where, h_e is the external liquid holdup, ($h_e = h_d + h_{es}$, dimensionless), Re_L is Reynolds number for liquid stream ($u_L d_p \rho_L / \mu_L$, dimensionless), Re_G is Reynolds number for the gas stream ($u_G d_p \rho_G / \mu_G$, dimensionless), S_p is a shape factor (S_x/d_p^2,

dimensionless), S_x is the external particle surface ($4\pi\ (d_p/2)^2$, m^2), u_G is the gas velocity (m/s), d_p is diameter of the beads (m), μ_G is air dynamic viscosity (Pa·s), h_{es} is the external static holdup (dimensionless) and β_1 to β_5 are the correlation parameters for Eq 4.7. The values of these correlation parameters for different flow regimes are given in Table 4.2.

Table 4.2 Correlation parameters for Eq 4.7 (Herskowitz and Smith, 1983).

Flow regime	β1	β2	β3	β4	β5
Gas continuous	2	0.2	0.73	0.2	0.2
Pulsing	0.11	0	1	0.4	-0.3
Spray	0.037	0	0.48	0.9	-0.3
Dispersed bubble	6.1×10^{-5}	-0.6	2.1	0.2	-1.5

From Figure 4.6, it can be observed that the ratio of the predicted and the experimental $k_{L,i}\,a/V_S$ (i.e., slope of the trend line) is 1.02 with a coefficient of determination (R^2) of 0.95. An R^2 of 0.95 indicates that the $k_{L,i}\,a/V_S$ model predictions and the $k_{L,i}\,a/V_S$ experimental data for the 6-mm beads are a good fit. The predicted $k_{L,i}\,a/V_S$ values were within 25% of the experimental values (Figure 4.6). The deviation can be explained because Eq 4.7 was based on the experiments performed for O_2 absorption into sodium sulfite solution using 12.7 mm ceramic spheres and 9.5 mm raschig rings as the packing material (Fukushima and Kusaka, 1977) and not smaller beads. This correlation could not predict the $k_{L,i}\,a/V_S$ values in the TBR obtained with 3-mm beads in the present study. The standard deviations were as high as $\pm$ 14 h^{-1} and $\pm$ 23 h^{-1} for CO and H_2, respectively (data not shown). The high standard deviation in the empirical correlation was because Eq 4.7 was derived using packing sizes above 9.5 mm, which is much larger than the 3-mm packing size used in the present study.

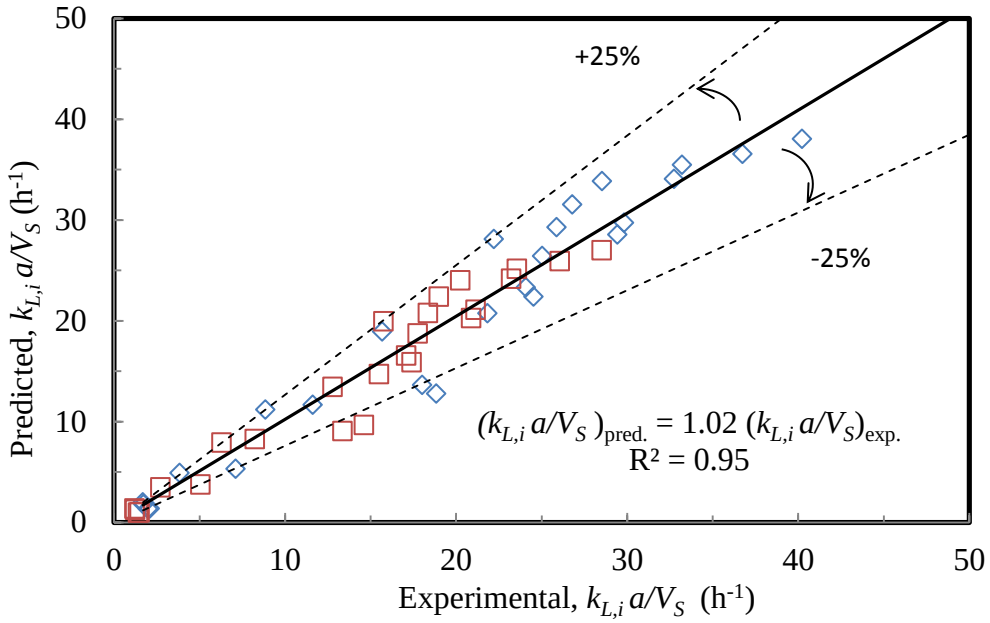

Figure 4.6 Comparison between experimental and predicted k_La/V_S for 6-mm beads using Eq 4.7 (◇) H_2 (□) CO. Dotted lines indicate ± 25% error.

4.3.5 Kinetic and mass transfer limitations

In this section, a prediction of the mass transfer capability of the TBR was compared with the gas uptake requirements of *C. ragsdalei* during syngas fermentation. The specific growth rate (μ = 0.06 h^{-1}), the maximum cell mass concentration (X_m = 0.25 g/L) and specific gas uptake rates (q_{CO} = 14 mmol/g cells·h and q_{H2}= 10 mmol/g cells·h) of *C. ragsdalei* were obtained from fermentation data reported by Maddipati (2010). The cells were assumed to be growing exponentially until reaching a maximum concentration of 0.25 g/L. The cell mass concentration was calculated using an exponential growth correlation.

$$X = X_0 e^{\mu t} \tag{4.8}$$

where, X_0 is the initial cell mass concentration at time zero (g cells/L) and μ is the specific growth rate of cells (h^{-1}). During the growth phase, as the cells concentration (X) increases with time, the molar CO and H_2 uptake (q_iX) by *C. ragsdalei* increase proportionally. The CO and H_2 molar uptake (q_iX) of *C. ragsdalei* and the molar transfer rate of CO and H_2 are calculated from the equation below:

$$-\frac{1}{V_L}\cdot\frac{dn_i}{dt}=\frac{k_{L,i}\,a}{V_L}\left(C_i^*-C_{L,i}\right)=q_iX \qquad (4.9)$$

where, dn_i/dt is the gas transfer rate (mol/h) for component i , V_L is the dynamic liquid holdup volume (L), $k_{L,i}\,a/V_L$ is the mass transfer coefficient of gas component i in the reactive volume (h^{-1}), C_i^* is the saturation concentration of the gas component i (mol/L), $C_{L,i}$ is the concentration of gas component i in the liquid at time t (mol/h), q_i is the specific uptake rate of the gas component i (mol/g cells·h), X is the cell mass concentration at time t (g cells /L) and i represents either CO or H_2 gas components.

During syngas fermentation under mass transfer limiting conditions, it was assumed that the gas transferred to the liquid in the reaction zone (i.e., dynamic liquid holdup volume, V_L) was immediately consumed and C_L was zero (i.e., the concentrations of H_2 and CO in the liquid phase were zero). Comparison between the uptake rates of CO and H_2 by *C. ragsdalei* and the molar transfer rates of CO and H_2 in the TBR with 3 and 6-mm beads at four different operating conditions (Table 4.3) are shown in Figure 4.7 and 4.8.

Figures 4.7 and 4.8 show that *C. ragsdalei* reached its maximum kinetic capacity at 30 h regardless of the gas and liquid flow rates examined. The

Table 4.3 k_La/V_L for CO and H_2 in the TBR at 37 °C.

		3-mm beads		6-mm beads	
L[a]	G[b]	$k_{L,CO}\,a/V_L$	$k_{L,H2}\,a/V_L$	$k_{L,CO}\,a/V_L$	$k_{L,H2}\,a/V_L$
ml/min	sccm	h^{-1}	h^{-1}	h^{-1}	h^{-1}
200	5.5	4.76	6.70	8.20	11.57
200	18.4	20.88	29.44	31.93	45.01
500	5.5	2.95	4.16	2.61	3.67
500	18.4	9.22	12.99	10.88	15.33

[a]Liquid flow rate; [b]Gas flow rate

predicted uptake rate of CO by *C. ragsdalei* at gas and liquid flow rates of 5.5 sccm and 200 ml/min, respectively, exceeded the TBR gas transfer rates at 19 h and 28 h for 3-mm and 6-mm beads, respectively (Figure 4.7). This indicates that fermentation became mass transfer limited 9 h faster in 3-mm beads than in 6-mm beads because the $k_{L,CO}\,a/V_L$ in 3-mm beads was around 40% lower than the $k_{L,CO}\,a/V_L$ in 6-mm beads (Table 4.3). Further, when the liquid flow rate was increased to 500 ml/min with the gas flow rate at 5.5 sccm, the predicted gas uptake rate by *C. ragsdalei* exceeded the TBR gas transfer rate earlier (about 10 h) than at liquid flow rate of 200 ml/min for both bead sizes. This is because the $k_{L,CO}\,a/V_L$ decreased with the increase in the liquid flow rate resulting in lower gas transfer (Figure 4.7). However, for both 3 mm beads, the CO transfer rate in the TBR exceeded *C. ragsdalei* uptake rate at 18.4 sccm in the first 30 h (Figure 4.7a). After 30 h, the predicted mass transfer rate was about equal to the uptake rate. The mass transfer ability of the TBR with 3 mm beads at gas and liquid flow rates of 18.4 sccm and 200 ml/min, respectively, exceeded the uptake rate by *C. ragsdalei* (Figure 4.7b). A higher mass transfer rate of the TBR with 6-mm beads

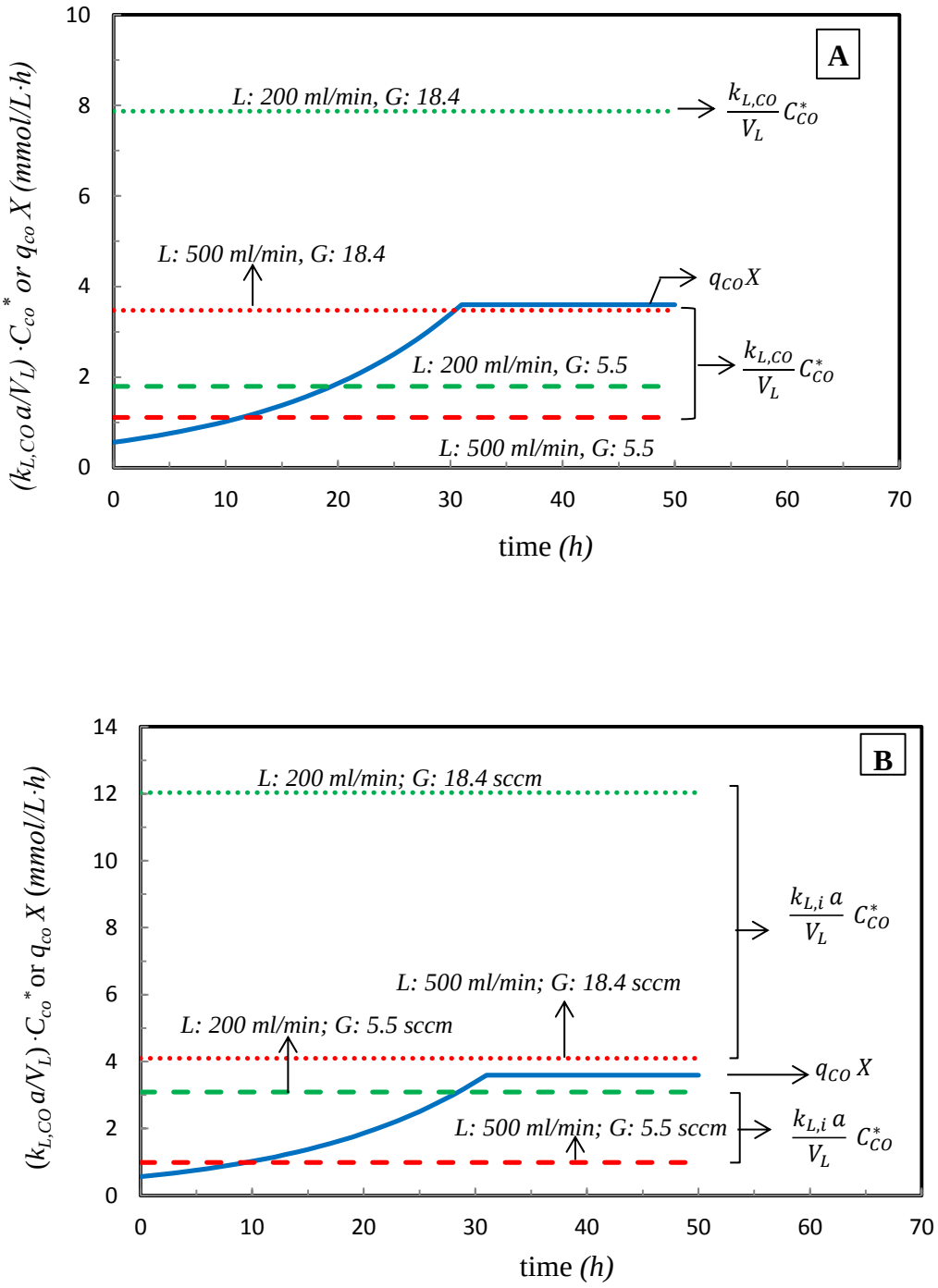

Figure 4.7 Molar CO transfer rate in the TBR and *C. ragsdalei* CO uptake rate (A) 3-mm beads (B) 6-mm beads. (—) CO uptake rate, $q_{co}\,X$,(– –) Molar transfer rate $(k_{L,CO}\,a/V_L)\cdot C_{co}^{\,*}$ at 5.5 sccm (·····) Molar transfer rate $(k_{L,CO}\,a/V_L)\cdot C_{co}^{\,*}$ at 18.4 sccm. Green color indicates 200 ml/min of liquid flow rate and red color indicates 500 ml/min of liquid flow rate.

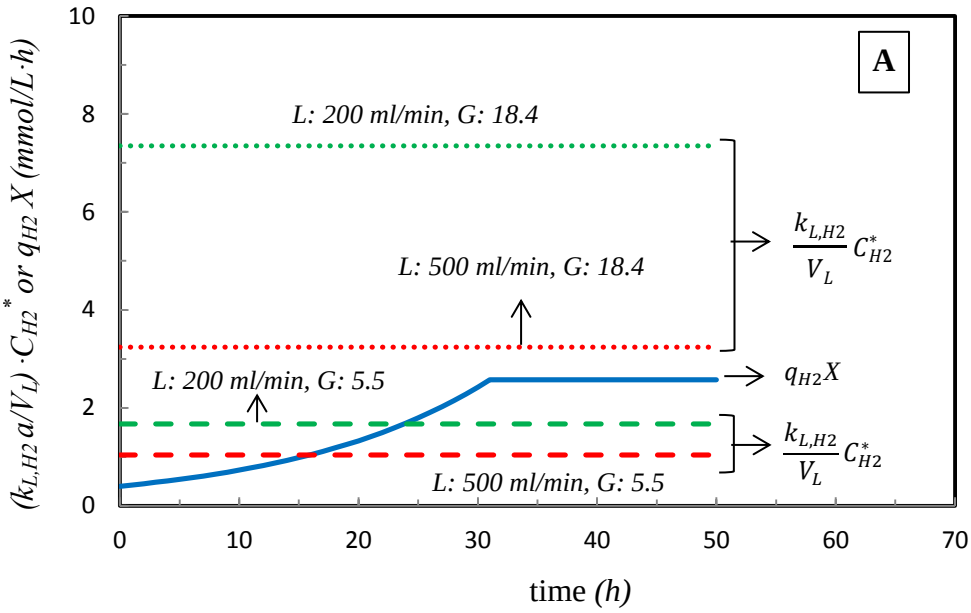

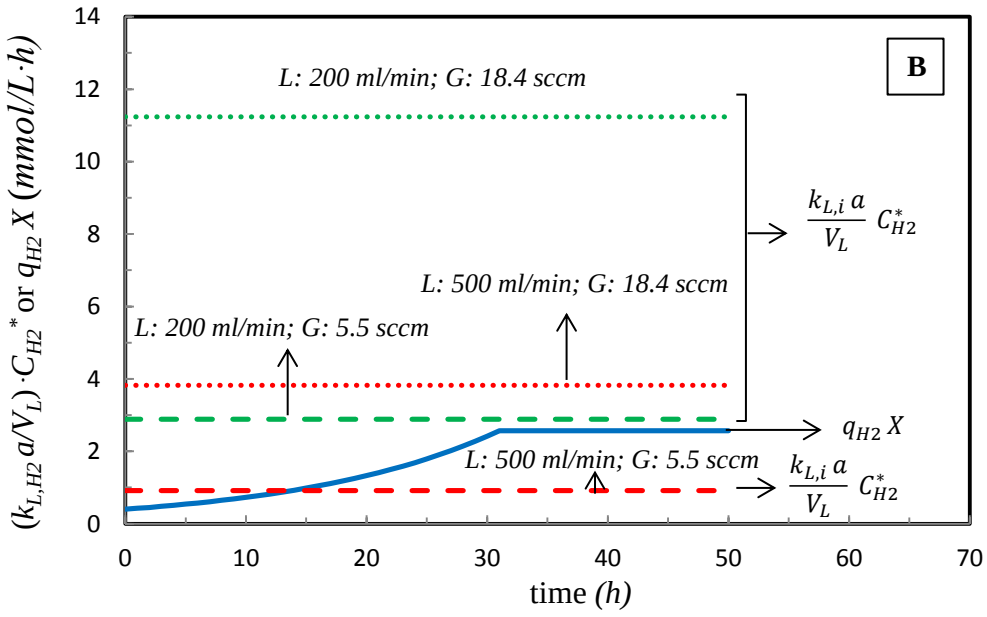

Figure 4.8 Molar H_2 transfer rate in the TBR and *C. ragsdalei* H_2 uptake rate (A) 3-mm beads (B) 6-mm beads. (—) H_2 uptake rate, $q_{H2}\,X$, (– –) Molar transfer rate $(k_{L,H2}\,a/V_L)\cdot C_{H2}^{\ *}$ at 5.5 sccm (·····) Molar transfer rate $(k_{L,H2}\,a/V_L)\cdot C_{H2}^{\ *}$ at 18.4 sccm. Green color indicates 200 ml/min of liquid flow rate and red color indicates 500 ml/min of liquid flow rate.

compared to the uptake rate was also predicted at both liquid flow rates with 18.4 sccm of gas flow rate.

Additionally, from Figure 4.8, it can be observed that the H_2 transfer rate in the TBR always exceeded the H_2 uptake rate by *C. ragsdalei* at 18.4 sccm and both flow rates tested. This was also the case for 200 ml/min liquid flow rate and 5.5 sccm gas flow rate for 6-mm beads (Figure 4.8b). However, for the TBR with 3-mm beads at the same operating condition, the fermentation reached H_2 mass transfer limitation at 23 h. Further, when the liquid flow rate was increased to 500 ml/min with gas flow rate of 5.5 sccm, H_2 gas uptake rate exceeded the TBR gas transfer rate at 15 h for both 3-mm and 6-mm beads. In general, from the above analysis it can be observed that the gas transfer rates in the TBR increased with increasing the gas flow rate and decreasing the liquid flow rate. Thus, to perform efficient syngas fermentation in a TBR, the gas transfer rate should be balanced with the cells kinetic capacity such that the gas conversion efficiencies are not compromised.

4.4 Conclusions

Unlike the stirred tank reactor, mass transfer in the TBR is defined by two mass transfer coefficients, namely the overall mass transfer coefficient (k_La/V_S) and the mass transfer coefficient in the reactive volume (k_La/V_L). The k_La/V_S and k_La/V_L in the TBR increased with increasing gas flow rate from 5.5 to 130.9 sccm. The k_La/V_L decreased with increasing liquid flow rate due to an increase in the liquid holdup volume. The highest $k_{L,CO}\,a/V_L$ and $k_{L,H2}\,a/V_L$ values with 6-mm beads were 435 h^{-1} and 613 h^{-1}, respectively. The maximum $k_{L,CO}\,a/V_L$ and $k_{L,H2}$

a/V_L values for 3-mm beads were 184 h^{-1} and 260 h^{-1}, respectively. For syngas fermentation, k_La/V_L should be considered in estimating the gas transfer rate. Also, using high gas flow rates to satisfy the cells' gas uptake rate can negatively affect gas conversion efficiency. Therefore, the operating condition should be selected to balance between the gas transfer rate and the cells' gas uptake rate without compromising the gas conversion efficiencies or productivity.

Acknowledgments

This research was supported by a grant from the Sun Grant Initiative through the U.S. Department of Transportation and Oklahoma Agricultural Experiment Station.

CHAPTER V

SEMI-CONTINUOUS FERMENTATION IN A TRICKLE BED REACTOR USING *CLOSTRIDIUM RAGSDALEI* FOR ETHANOL PRODUCTION

ABSTRACT

An efficient syngas fermentation bioreactor should provide a mass transfer capability that matches the kinetics of the microorganism in order to obtain high gas conversion efficiency and productivity. Mass transfer and gas utilization efficiencies of a trickle bed reactor (TBR) during syngas fermentation by *Clostridium ragsdalei* were evaluated at various gas and liquid flow rates. Fermentations were performed at 37 ^{o}C using a syngas mixture of 38% CO, 28.5% CO_2, 28.5% H_2 and 5% N_2 by volume. Results showed that increasing the gas flow rate from 2.3 to 4.6 sccm increased the CO uptake rate by 80% and decreased the H_2 uptake rate by 50%. However, due to the formation of the biofilm, cell activity increased, resulting in over fourfold increase in H_2 uptake rate at 4.6 sccm. In semi-continuous fermentation, fresh medium was added intermittently to avoid nutrient limitation. Replenishment of the nutrients provided conditions that supported cell growth resulting in more acetic acid production than ethanol. At 1632 h, the final amount of ethanol and acetic acid produced were 5.7 and 12.3 g/L, respectively, at 200 ml/min of

liquid flow rate and 4.6 sccm gas flow rate. Co-current operation helped overcome flooding and gas bypass issues encountered in counter-current mode of operation.

Keywords: Semi-continuous syngas fermentation, *Clostridium ragsdalei*, Ethanol, Trickle bed reactor, mass transfer

5.1 Introduction

Syngas fermentation is a biochemical conversion of synthesis gas (a mixture of CO, H_2 and CO_2) into alcohols and organic acids. *Clostridium ljungdahlii, Clostridium carboxidivorans, Alkalibaculum bacchi* have been used in syngas fermentation (Liu et al., 2012; Phillips et al., 1994; Ukpong et al., 2012). The microorganisms undergo a set of enzyme catalyzed reactions through the Wood-ljungdahl pathway to metabolize CO, H_2 and CO_2 into cell mass, ethanol and acetic acid (Wood et al., 1986). The overall stoichiometry for ethanol and acetic acid production from syngas is given as (Ljungdhal, 1986; Vega et al., 1989):

$$6CO + 3H_2O \rightarrow C_2H_5OH + 4CO_2 \quad (5.1)$$

$$4CO + 2H_2O \rightarrow CH_3COOH + 2CO_2 \quad (5.2)$$

$$6H_2 + 2CO_2 \rightarrow C_2H_5OH + 3H_2O \quad (5.3)$$

$$4H_2 + 2CO_2 \rightarrow CH_3COOH + 2H_2O \quad (5.4)$$

Syngas fermentation is a hybrid conversions technology that has many advantages such as ambient fermentation temperature and pressure, flexibility in using any type of feedstock (such as lignocellulosic and municipal solid wastes) and utilization of all the lignocellulosic biomass components including lignin). Despite these advantages, syngas fermentation suffers from low productivity associated with low cell density, enzyme inhibition and mass transfer limitations. The mass transfer limitation is a major challenge,

which is attributed to the low solubility of syngas components (namely CO and H_2) in the fermentation medium.

Bioreactor designs such as continuously stirred tank reactors (CSTRs) with microspargers, packed columns, bubble columns, trickle beds and hollow fiber reactors have been employed to improve the mass transfer of gases into liquid medium (Bredwell and Worden, 1998; Klasson et al., 1991b; Orgill et al., 2013; Vega et al., 1990; Wolfrum and Watt, 2002). In a traditional CSTR, increasing the agitation speed and gas flow rate will increase the gas-liquid mass transfer (Orgill et al., 2013). However, in commercial scale syngas fermentations, the high power to volume ratio requirements for large reactors may not be economical (Bredwell et al., 1999). Further, increasing the gas flow rate typically decreases the gas conversion efficiency during syngas fermentation if not enough cells are available in the bioreactor. The use of a microsparger has been suggested to be an energy efficient method to increase gas liquid mass transfer in a CSTR (Bredwell and Worden, 1998). In a study by Ismail et al. (2008), when ring sparger was replaced by a microsparger, the H_2 production efficiency of the water-gas shift reaction by *Rhodospirillum rubrum* was increased by 15-40%. Unlike CSTRs, column reactors have no moving parts and thus have a low power requirement. In some fermentation studies, it was reported that trickle bed reactors (TBR) had better mass transfer characteristics, productivity and gas conversions than packed bubble columns and CSTR (Cowger et al., 1992; Klasson et al., 1990a).

TBRs are long columns filled with packing material, which are widely used in chemical and biochemical processes when gas-liquid interactions occur in presence of a solid catalyst (Saroha and Nigam, 1996). The gas and liquid flow to the TBR can either

be co-current or counter-current (Gianetto and Specchia, 1992). The liquid trickles down the packing in the form of a thin film and reduces the resistance to gas-liquid mass transfer. In syngas fermentation studies, a TBR was successfully used to produce (i) H_2 using photosynthetic bacterium such as *R. rubrum* and *Rubrivivax gelatinosus* (Cowger et al., 1992); (ii) CH_4 using tricultures of *R. rubrum, Methanobacterium formicum* and *Methanosarcina barkeri* (Kimmel et al., 1991; Klasson et al., 1990b) and (iii) acetate using *Peptostreptococcus productus* (Klasson et al., 1990a). However, based on extensive literature review no studies were reported on syngas fermentation using a TBR for ethanol production. The present research focuses on characterizing a 1-L TBR for ethanol production from syngas using *Clostridium ragsdalei*. In this study, semi- continuous fermentations were performed in the TBR with 6-mm glass beads. Further, the effect of gas and liquid flow rates on gas conversion efficiency, ethanol productivity and apparent mass transfer were assessed.

5.2 Materials and Methods

5.2.1 Microorganism and Medium preparation

Clostridium ragsdalei (ATCC-PTA-7826) a strict anaerobic bacterium was kindly provided by Dr. Ralph Tanner, University of Oklahoma. It is a rod shaped gram-positive bacterium that grows at an optimum temperature of 37°C and pH of 5.8 (Huhnke et al., 2010). *C. ragsdalei* was maintained and grown on a standard yeast extract medium that consisted mainly of 0.5 g/L yeast extract (YE), 10 g/L 2-(N-morpholino)ethanesulfonic acid (MES) buffer, 25 ml/L mineral solution, 10 ml/L vitamin solution and 10 ml/L metal solution. The chemical components and their concentrations in the mineral, metal and vitamin solutions were previously reported by Saxena (2008) and can be found in

Appendix G. Also, 0.1% rezasurin as an O_2 indicator and 10 ml/L of 4% cysteine sulfide as a reducing agent were added.

5.2.2 Inoculum preparation

To reduce the lag phase, C. *ragsdalei* stock culture was passaged three times prior to inoculating the reactor. The inoculum was prepared in 250-ml serum bottles with 100 ml of medium. A 10% (v/v) of inoculum was used to prepare the passages. The bottles were pressurized to 239 kPa with 40% CO, 30% CO_2 and 30% H_2 syngas mixture by volume. The cells were transferred from one passage to another after reaching an cell optical density (OD_{660}) of about 0.5. The third passage was used as the inoculum for the TBR. A 60% (v/v) inoculum was used to inoculate the TBR. From preliminary fermentations (Appendix B), it was observed that the culture took around 15-20 days to grow with low inoculum. This was attributed to the high mass transfer in the TBR which resulted in high availability of CO to relatively low inventory of cells during startup resulting in CO inhibition. Increasing the inoculum size and using a low gas flow rate (2.3 standard cubic centimeters per minute (sccm), i.e., 0.005 volume of gas provided per volume of liquid per minute, vvm) started the fermentation in the TBR with 48 h.

5.2.3 TBR experimental set up

The schematic for the TBR used in syngas fermentation is shown in Figure 5.1. The TBR was designed in house and is made of a 51 mm diameter borosilicate glass column 610 mm in length. The TBR design limitation was attributed to the size of the autoclave used to sterilize the TBR set up. Additionally, for comparison purposes the TBR design in the present study was similar to the TBR design reported in the literature (Wolfrum and Watt, 2002). The 6-mm soda lime glass beads (#26396-621, VWR,

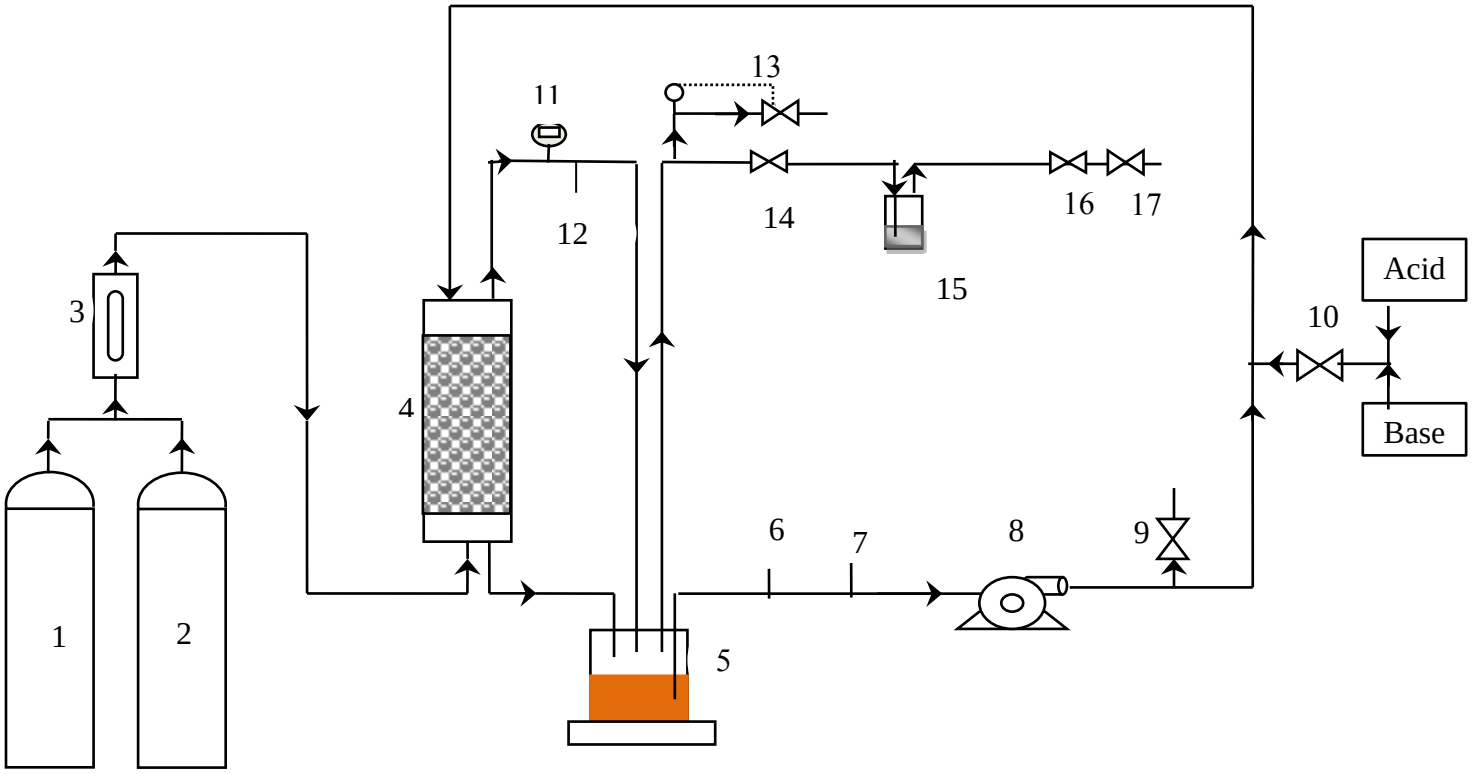

Figure 5.1 TBR Semi-continuous fermentation set up.

(1) Nitrogen cylinder (2) Syngas cylinder (3) Rotameter (4) Trickle bed reactor (5) Medium sump (6) ORP probe (7) pH probe (8) Masterflex pump (9) Liquid sampling port (10) acid/base addition (11) Pressure gauge (12) Gas sampling port (13) By pass line with solenoid valve and pressure switch (14) Back pressure regulator (15) Gas bubbler (16) 108 kPa check valve (17) Ball valve

Atlanta, GA) were used as the packing material because they provided higher mass transfer (k_La/V_L) than the 3-mm beads during mass transfer studies. A metal mesh with openings smaller than 3 mm was placed 9 cm from the bottom of the TBR to hold the glass beads in the reactor. A perforated circular liquid distributor with 3.2 mm holes was placed 11 cm below the reactor lid. The three reactor sections where held together with horseshoe clamps. The liquid outlet line from the TBR was connected to a 500 ml pyrex glass bottle. This bottle was used as a sump to hold 500 ml of medium. The TBR was initially operated in counter-current mode. To ensure no gas bypass from the bottom of the TBR liquid outlet to the sump headspace, a liquid head was maintained at the bottom of the TBR. A peristaltic pump (7523-20, Cole-Parmer, Vernon,IL, USA) circulated the liquid at a desired flow rate. The pH probe (EW 05662-45, Cole-Parmer, Vernon Hills, IL) and ORP probe (00238GG, Cole-Parmer, Vernon Hills, IL) were placed in line in the recirculation loop before the peristaltic pump. In addition, a liquid sample and acid/base addition ports were placed inline in the recirculation loop after the peristaltic pump. The gas exit line from the TBR was connected to the sump gas inlet. A back pressure regulator was connected to the sump gas exit line to control the pressure in the TBR at 115 kPa. A pressure gauge was connected at the TBR gas exit line to check the pressure in the reactor. The gas exit line was further connected to a safety exhaust line with a pressure switch and a solenoid valve to vent excess pressure in the reactor. A bubbler was placed at the outlet of the pressure regulator to trap any product loss as a vapor with the exhaust stream

5.2.4 Experimental Procedure

The sterilization of the TBR set up was done in an autoclave (Primus Sterilizer Co. Inc., Omaha, NE) at 121^{o} C for 20 min. After sterilization, the TBR was purged with N_2 for 6 h. In the meanwhile, 200 ml of fresh medium was prepared and transferred into a 500 ml serum bottle. The medium was then boiled and purged with N_2 for about 3 to 5 min to remove O_2 and sealed with impermeable butyl rubber stoppers and aluminum crimp seals. The medium was then sterilized in the autoclave. The bottle was pressurized to 239 kPa with N_2 so that the medium can be transferred to the TBR with the pressure difference. A sterile Teflon tubing of 3.2 mm size with 22G 38 mm needles on both ends was used to transfer the medium from the serum bottle into the reactor through the liquid sample port (Figure 5.1). Isopropanol (70% solution) was used for sterilization of the sampling port.

After addition of 200 ml of fresh medium into the TBR, the TBR was purged with N_2 for at least 8 h. Then, the inlet gas line to the TBR was switched to the syngas mixture of 38% CO, 5% N_2, 28.5% CO_2 and 28.5% H_2 by volume (Stillwater Steel and Supply Company, Stillwater, OK). This gas mixture was similar to coal derived syngas (Klasson et al., 1993b). A 60% (v/v) inoculum was added into the reactor through the liquid sample port in the same way as the 200 ml fresh medium. The temperature in the TBR and sump was maintained at 37 ^{o}C using silicone heating tape and a surface thermocouple connected to a temperature controller (Omega CN 370 series, Stamford, CT).

Gas and liquid samples were taken periodically for product analysis. For TBR startup, a 200 ml/min liquid flow rate and 2.3 sccm gas flow rate were used. Preliminary experiments were performed to establish a startup procedure for TBR (Appendix B). It

was found that medium replacement was important for semi-continuous fermentation to maintain cell activity and avoid nutrient limitations (Appendix B). Hence in this study, multiple runs with an addition of fresh medium were performed to maintain the cell metabolic activity and build the biofilm in the TBR. After each run, the spent medium in the TBR was replaced with 400 ml of fresh medium when the CO conversion efficiency dropped between 35 and 40%. Two gas (2.3 and 4.6 sccm) and three liquid flow rates (200, 500 and 700 ml/min) were tested. Runs R1 and R2 were performed at a liquid and gas flow rates of 200 ml/min and 2.3 sccm, respectively (Table 5.1). Runs R3 to R10 were performed at 200 ml/min of liquid flow rate and 4.6 sccm gas flow rate. For runs R11 to R15, the gas flow rate was 4.6 sccm while the liquid flow rates varied between 200 and 700 ml/min. All the runs from R1 to R15 were performed in counter-current mode. Runs R17 to R19 were in co-current flow mode. The switch to co-current mode was also done to avoid the operational difficulties with gas bypass and foam formation at high liquid recirculation rates (500 and 700 ml/min).

Table 5.1 Operating conditions used in semi-continuous fermentation runs in TBR

Run no.	Liquid flow rate	Gas flow rate
	ml/min	sccm
R1, R2	200	2.3
R3 to R10, R12, R19	200	4.6
R11, R13, R17	500	4.6
R14, R15, R18	700	4.6

R1-R15: counter-current flow; R16: TBR run unsuccessful due to leaks and yielded no data; R17- R19: Co-current flow.

5.2.5 Sample Analysis

Cell optical density measurement

The cell concentration was measured using a UV spectrophotometers (Coleparmer, Vernon Hills, IL) at 660 nm. Liquid samples were centrifuged in a benchtop microcentrifuge (Accuspin Micro, Fischer scientific, Pittsburgh, PA) at 13,000 rpm for 10 min and the supernatant was collected and stored for solvent analysis. At the end of all runs, the total cell optical density in the medium and attached to the packing was measured. The beads were collected in a clean tub and washed four times each with 500 ml of DI water. Duplicate liquid samples were collected from each wash and measured at 660 nm. The TBR wall was also washed to measure the concentration of cells attached to it. The summation of cell concentrations from the washes and the TBR wall provided the total cell optical density in the reactive volume in the packing.

Solvent analysis

The liquid samples were analyzed for solvent concentrations (mainly ethanol and acetic acid) using DB-FFAP capillary column gas chromatography (GC) with flame ionization detector (FID) (Agilent Technologies, Wilmington, DE). H_2 was used as carrier gas with an initial flow rate of 2.3 ml/min for 1.5 min. It was then ramped at 1 ml/min^2 until the flow reached 4 ml/min. The inlet port temperature was set at 200 °C with a split ratio of 50:1. The FID was set at 250 °C with H_2 and air flow rate of 40 ml/min and 450 ml/min, respectively. The initial oven temperature was 40 °C with a holding time of 1.5 min. Then it was ramped at 25 °C/min until the temperature reached 60 °C. Further, the temperature was increased from 60 °C to 235 °C at a ramping rate of 40 °C/min.

Gas analysis

The gas samples were analyzed using a Carboxen 1010 PLOT capillary column (Supelco, Bellefonte, PA, USA) in a 6890N GC with a thermal conductivity detector (TCD) (Agilent Technologies, Wilmington, DE). A 100 µl gas sample was injected using Hamilton gas tight syringe (Hamilton Co., Reno, NV). Argon was used as carrier gas with initial flow rate of 2 ml/min for 3.5 min, then it was increased to 2.5 ml/min at a ramping rate of 0.1 ml/min^2. The inlet port temperature was set at 200 °C with 30:1 split ratio and TCD temperature was set at 230 °C. The oven temperature was set to 80 °C for 3.5 min, then it was ramped to 235 °C at 40 °C/min. The gas and liquid data analysis was done using Chemstation software (Agilent Technologies, Wilmington, DE).

pH measurement

The readings from an inline pH probe (Figure 5.1) connected to the Bioflo 110 controller (New Brunswick Scientific Co., Edison, NJ) were logged into the computer using Biocommand software. The ORP measurements were recorded periodically from a digital ORP meter (# ORCN37, Omega Engineering, Stamford, CT).

5.3 Results and Discussion

5.3.1 Cell growth and pH

The cell optical density (OD_{660}) profiles of all fermentation runs at different operating conditions (Table 5.1) are shown in Figure 5.2. The cell OD_{660} in run R1 reached a maximum of 0.5 and then decreased as the nutrients in the medium were depleted. Replacing the medium increased the cell OD_{660} in run R2. However, the cell OD_{660} dropped again due to nutrient limitation. This trend was similar for all fermentation runs. It can be observed that irrespective of the final cell OD_{660} in the previous run, the

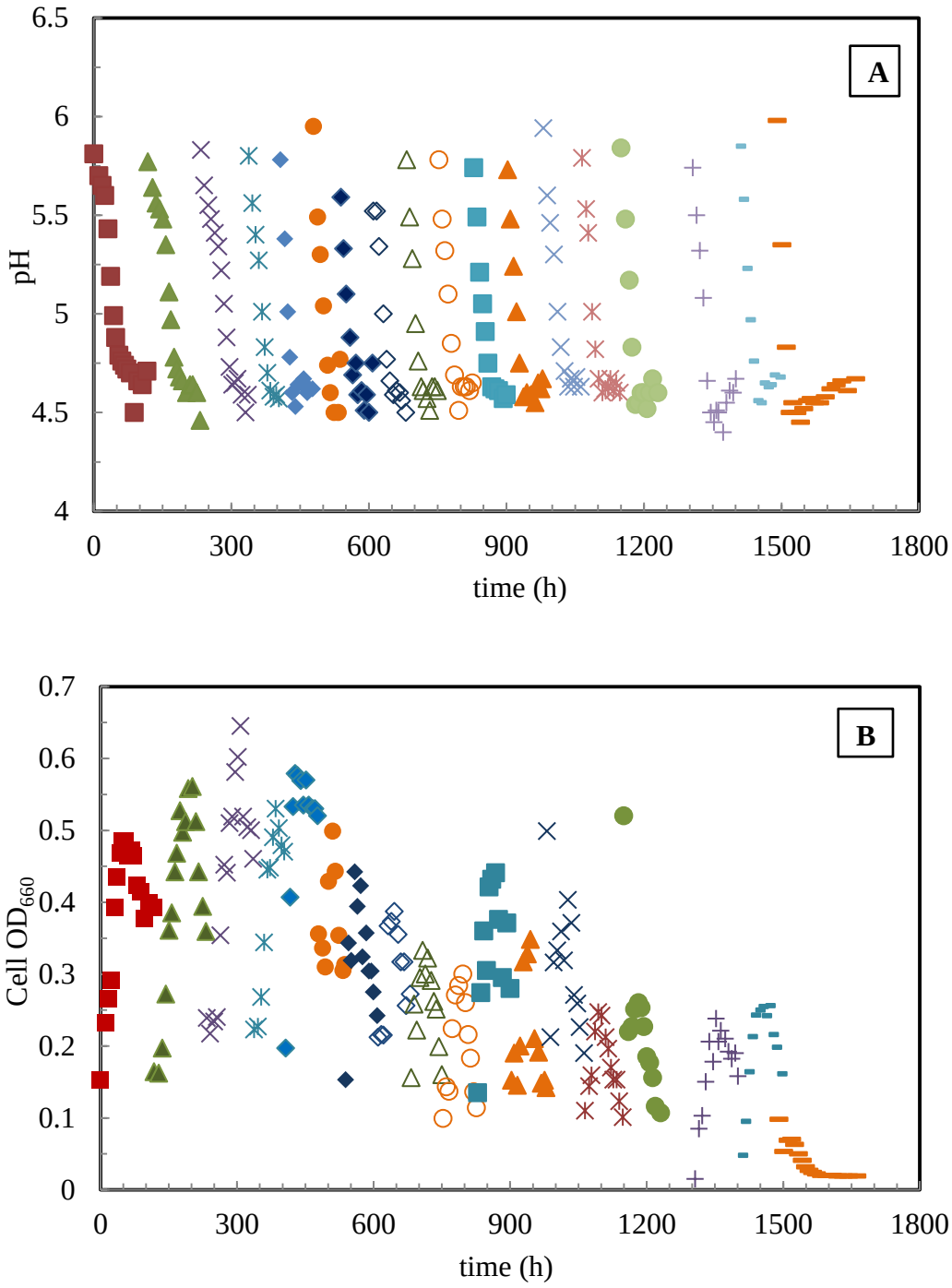

Figure 5.2 (A) pH (B) Cell OD_{660} profile of *C. ragsdalei* during semi-continuous syngas fermentation in TBR.

(■) R1 (▲) R2 (×) R3 (✳) R4 (◆) R5 (●) R6 (◆) R7 (◇) R8 (△) R9 (○) R10 (■) R11 (▲) R12 (×) R13 (✳) R14 (●) R15 (+) R17 (-) R18 (—) R19; R1, R2: L = 200 ml/min, G = 2.3 sccm; R4-R9, R19: L = 200 ml/min, G = 4.6 sccm; R11, R17: L = 500 ml/min, G =4.6 sccm; R14, R15, R18: L = 700 ml/min, G = 4.6 sccm. R1-R15: Counter-current mode; R17-R19: Co-current mode.

initial measured cell OD_{660} in the medium was about the same from R7 to R15 (Figure 5.2). This indicates a possible cells resuspension from biofilm into the medium after medium replacement and starting the liquid recirculation. However, in the co-current flow operation from 1307 h to 1734 h, a maximum cell OD_{660} of 0.2 was measured in the medium and the cell OD_{660} dropped to 0.02 from 1573 to 1662 h. The maximum cell OD_{660} in the medium in the runs from R3 to R19 decreased (Figure 5.2). For the first 336 h of fermentation time, the maximum cell OD_{660} observed in the liquid medium increased from 0.485 in run R1 to 0.645 in run R3. Further, from 336 to 826 h, the maximum cell OD_{660} in the liquid medium decreased from 0.53 in run R4 to 0.3 in run R10. The decrease of the cell OD_{660} in the liquid medium is attributed to the biofilm formation on the beads in the reactive volume of the TBR. Regardless of the decrease in the cell OD_{660} in the medium (Figure 5.2), high CO and H_2 gas conversions efficiencies (Figure 5.4) were observed for runs R3 to R10 indicating high activity of cells in the packing.. The biofilm formation on the packing material was not reported in any earlier syngas fermentation studies in TBR to produce H_2, CH_4 and acetate by photosynthetic and methanogenic bacteria (Kimmel et al., 1991; Klasson et al., 1990b; Klasson et al., 1993b; Wolfrum and Watt, 2002).

At the end of fermentation, the beads were collected in a tub and washed four times with 500 ml DI water. The cell OD_{660} in the wash1, wash2, wash3 and wash4 were 1.91, 0.54, 0.13, and 0.052, respectively. A cell OD_{660} of 0.097 was obtained in the 500 ml of DI water used to wash the column. The overall cell OD_{660} in the TBR after 1662 h (R19) was calculated to be 2.59 based on 500 ml medium. Pictures showing the biofilm in the TBR and cells in the wash samples from beads are presented in Appendix E.

Based on the cell mass concentration measured in the medium, the specific growth rate (μ) was between 0.04 h^{-1} to 0.06 h^{-1} for all runs except for runs R14, R15, R18 and R19. The specific growth rates were 0.09 h^{-1}, 0.02 h^{-1}, 0.06 h^{-1} and 0.09 h^{-1} for runs R14, R15, R17 and R18, respectively. Further, for run R19 a decreasing profile of the cell optical density was observed indicating less cell growth in the medium.

The specific growth rate of *C. ragsdalei* in standard yeast extract medium with 1 g/L of YE in batch bottles and CSTR fermentations was reported to be 0.06 h^{-1} (Maddipati et al., 2011). The specific growth rates obtained in the TBR for runs R1 to R10 were comparable to the values reported in the literature. However, the specific growth rate calculated from the cell mass concentration in the medium alone for all TBR runs (especially from R14 to R19) is not accurate because cells were mostly in the biofilm.

The pH of the medium dropped during fermentation due to acetic acid production (Figure. 5.2). In the initial runs (R1 and R2) at 2.3 sccm gas flow rate and 200 ml/min of liquid recirculation rate, it took 106 h for the pH to drop from 5.8 to 4.6. However, at a gas flow rate of 4.6 sccm and liquid flow rate of 200

ml/min, the drop in the pH from 5.8 to 4.6 happened in 89 h and 47 h in R3 and R4, respectively. The increase in the rate of pH drop in the subsequent runs (Figure 5.2) was attributed to the increase in the rate of acetic acid production (Figure 5.6). During counter-current operation at 4.6 sccm gas flow rate and 200, 500 and 700 ml/min liquid recirculation rates, the pH drop happened in 38 h in runs R4 to R10 and R12), 46 h for R11 and 13) and 38.5 h for R14 and 15, respectively. During co-current operation, at 200, 500 and 700 ml/min liquid recirculation rates and 4.6 sccm gas flow rate, the pH drop

happened in 28 h for R19), 39 h for R17 and 38 h for R18, respectively. The pH drop from 5.8 to 4.6 occurred in an average of 39 h irrespective of the operating conditions.

5.3.2 Product profiles

The acetic acid and ethanol profiles for all runs are shown in Figure 5.3. The ethanol and acetic acid concentrations had an increasing trend in all the fermentation runs. Because the fermentation time is not the same in all the runs, the comparison between runs was made at 61±2 h^{-1} after the start of each run because it was the minimum time each run was performed. In runs R1 and R2 when the liquid recirculation rate was 200 ml/min and gas flow rate was 2.3 sccm, the average amount of ethanol and acetic acid produced were 1.19 g/L and 3.78 g/L, respectively. In R3 and R4, doubling the gas flow rate resulted in a 75% increase in ethanol production and only a 6% increase in acetic acid concentration (Table 5.2). However, in the subsequent runs R5 and R6, the ethanol concentration dropped by 15% and 43% , respectively, compared to R4 (Figure 5.3). On the other hand, the acetic acid concentrations increased by 50% and 40% in R5 and R6, respectively, compared to R4.

For runs R7 to R10, the average ethanol concentration was 1.19 g/L and similar to R6. However, the average acetic acid concentration was 4.58 g/L and decreased by 20% compared to R6 (about 4.58 g/L). This difference in the ethanol and acetic acid produced from R3 to R10 is attributed to the biofilm development in the packing. In a syngas fermentation study by Liu et al. (2014a), accumulation of high cell concentration in the bioreactor was reported to favor acetic acid production for ATP generation as high amount of energy is required for cell maintenance. In the present study, the formation of biofilm in the TBR increased the total cell concentration attached to the packing material.

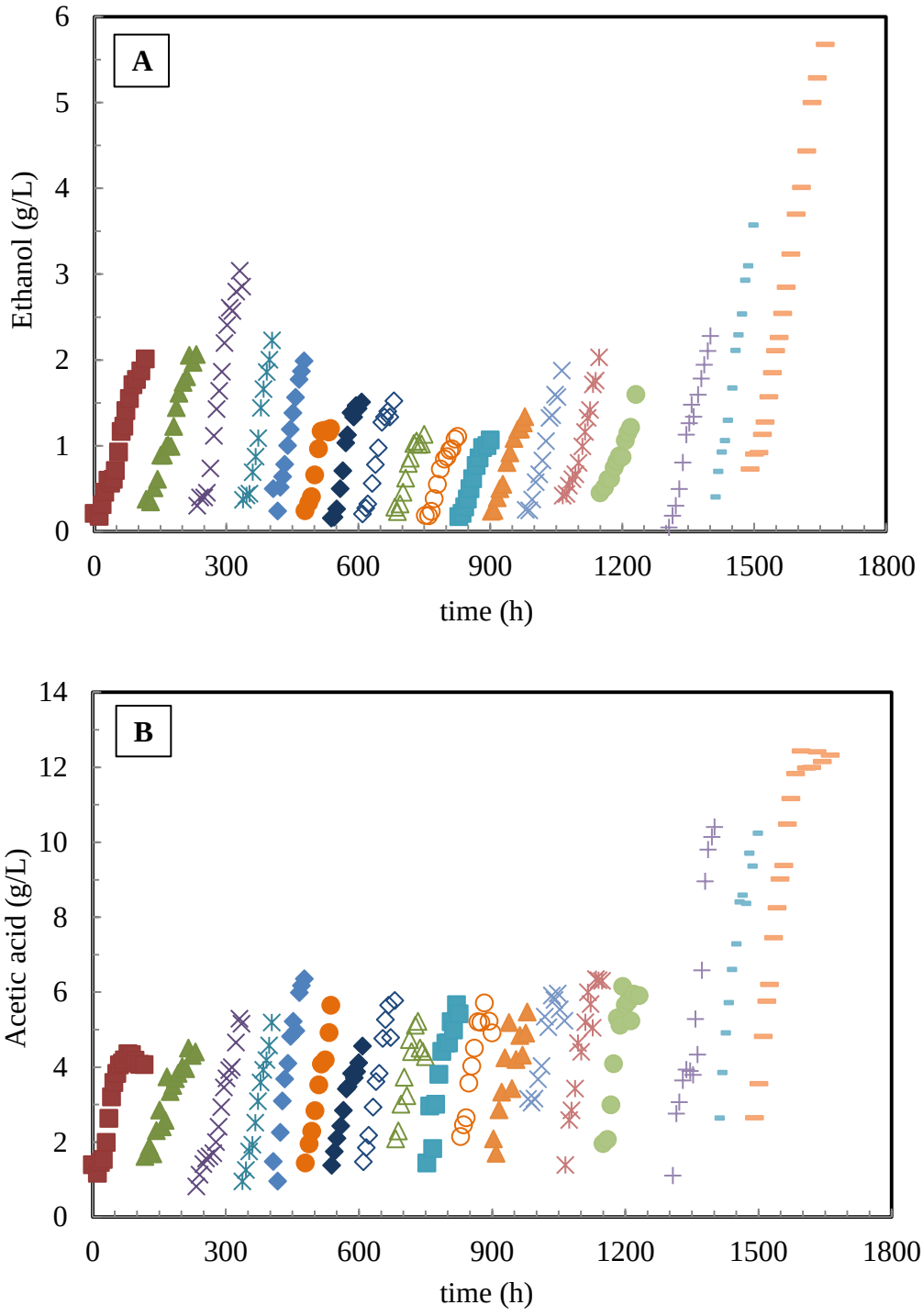

Figure 5.3 Product concentration profiles during semi-continuous syngas fermentation in TBR (A) Ethanol (B) Acetic acid.
( ) R1 ( ) R2 ( ) R3 ( ) R4 ( ) R5 ( ) R6 ( ) R7 ( ) R8 ( ) R9 ( ) R10 ( ) R11 ( ) R12 ( ) R13 ( ) R14 ( ) R15 ( ) R17 ( ) R18 ( ) R19; R1, R2: L = 200 ml/min, G = 2.3 sccm; R4-R9, R19: L = 200 ml/min, G = 4.6 sccm; R11, R17: L = 500 ml/min, G =4.6 sccm; R14, R15, R18: L = 700 ml/min, G = 4.6 sccm. R1-R15: Counter-current mode; R17-R19: Co-current mode.

Table 5.2 Product concentrations, yields and gas conversion efficiencies for runs R1 to R19 in the TBR

			Products at 61±2 h		Gas conversion efficiencies		Product yield[c] at 61±2 h	
R[a]	Time	Liquid-Gas Flow rate	Ethanol	Acetic acid	$CO_{max.}$	$H_{2,max.}$	Ethanol	Acetic acid
	h	ml/min-sccm	g/L	g/L	%	%	%	%
1	0-116	200-2.3	1.16	4.06	90.97	67.99	57.54	83.74
2	118-232	200-2.3	1.22	3.51	83.15	55.7	59.54	69.25
3	234-336	200-4.6	2.19	3.45	64.61	21.83	90.10	65.36
4	338-404	200-4.6	2.00	4.58	69.25	17.54	66.46	77.19
5	407-477	200-4.6	1.77	5.98	66.54	18.68	49.63	91.70
6	479-537	200-4.6	1.20	5.65	66.46	19.66	47.05	108.00
7	539-608	200-4.6	1.43	4.11	73.89	26.65	48.64	54.32
8	610-681	200-4.6	1.33	4.79	79.27	37.73	39.73	60.74
9	683-750	200-4.6	1.02	4.41	81.21	40.91	25.73	42.46
10	753-826	200-4.6	0.96	4.99	78.2	41.36	27.97	66.64
11	829-900	500-4.6	1.00	5.23	69.32	49.06	30.77	59.73
12	903-979	200-4.6	1.19	4.84	76.95	46.81	30.43	45.72
13	981-1063	500-4.6	1.35	5.79	66.69	48.13	41.95	52.46
14	1065-1148	700-4.6	1.41	5.04	66.59	49.89	37.16	70.84
15	1150-1231	700-4.6	1.15	5.23	69.92	53.66	24.67	60.13
17[b]	1307-1401	500-4.6	1.34	4.33	77.26	52.17	64.17	83.73
18[b]	1403-1489	700-4.6	2.53	8.37	79.53	54.6	81.78	114.58
19[b]	1491-1662	200-4.6	2.10	9.02	70.6	52.68	50.59	122.06

[a] R1-R15 were in counter-current mode and R16 had leak issues and resulted in no data
[b]Co-current mode
[c]Yields were calculated based on CO consumed in Eqns. 5.5. and 5.6

This in turn could have increased the energy required for cell maintenance. Hence, from run R5 to R10, the cells produced more acetic acid which resulted in a 50% decrease in ethanol concentration compared to R3 and R4 at the same operating conditions.

When gas conversion efficiencies and product concentrations did not change at the same operating conditions (R8 to R10, Figure 5.3) the TBR was considered to be at quasi-steady state. At this point, the liquid recirculation rate was changed to 500 ml/min (R11 and R13) and 700 ml/min (R14 and R15) to observe the effect of liquid recirculation rate on fermentation. The variation in the amount of ethanol and acetic acid produced at different liquid flow rates in counter-current mode was between 5 to 10% (Table 5.2). This indicates that the liquid flow rate had no effect on the amount of products produced. At low gas flow rates and high liquid flow rates the gas-liquid interaction in the TBR is in bubble flow regime (Ranade et al., 2011a). As discussed in Section 4.3.3, during counter-current operation the TBR was operated in bubble flow regime (i.e., continuous liquid phase and gas flows as bubbles) at the gas and liquid flow rates shown in Table 5.1. Therefore, the gas-liquid interfacial area which affects the gas-liquid mass transfer is a function of the gas flow rate rather than the liquid flow rate. Hence, the liquid flow rate in the range used had no effect on the fermentation. Further, in co-current operation, it was observed that 89% and 57% more ethanol was produced in run R18 and run R19, respectively, than in run R17. Also, 93% and 108% more acetic acid was produced in run R18 and run R19 than in R17. In co-current mode, up to 98% more ethanol was produced than in counter-current mode. Further, the acetic acid produced in co-current mode was up to 83% higher than in counter-current mode.

Overall, syngas fermentation in the TBR with co-current mode was easier to operate and produced more ethanol and acetic acid than in counter-current mode. Unlike counter-current flow, the capacity of co-current operation is not limited by flooding over a wider range of gas and liquid flow rates (Bredwell et al., 1999; Charpentier, 1981; Klasson et al., 1992). Better gas liquid interaction and no operational hindrances such as gas bypass, flooding and foaming are attributed to higher ethanol and acetic acid production in co-current operation. The final ethanol and acetic acid concentrations in the TBR with co-current flow at 1662 h were 5.67 g/L and 12.32 g/L, respectively. In semi-continuous fermentations, nutrients were replenished in a new run when the CO conversion efficiency dropped to 40%. Replenishing nutrients resulted in conditions that favored cell growth and biofilm establishment in the packing. Acetic acid production is also favored with nutrient replenishments because it is associated with ATP generation required for cell growth and maintenance.

5.3.3 Gas conversions

The CO and H_2 conversion efficiencies for all runs are shown in Figure 5.4. The CO conversion efficiency increased in run R1, reached a maximum of 90% and then of started decreasing due to reduced cell activity with nutrient limitation. In run R2, replacing the medium resulted in an increase in CO conversion efficiency. However, the conversion efficiency started to decline due to nutrient limitation. This trend was similar for both CO and H_2 conversion efficiencies for all runs (Figure 5.4). In the initial runs (R1 and R2), maximum conversion efficiencies of 87.06 % CO and 61.84% H_2 were achieved with the liquid recirculation rate of 200 ml/min and gas flow rate of 2.3 sccm. When the gas flow rate was doubled to 4.6 sccm, the maximum gas conversion

efficiencies decreased to 66.71% CO and 19.43% H_2 for runs R3 to R6. For runs R7-R10 and R12, the maximum CO conversion efficiency increased and was stable at 77.90%. However, the maximum H_2 conversion efficiency in run R7 increased from 26.65% to 46.81% in run R12. There was sustained increase in the maximum H_2 conversion for runs R3 to R10. This increase is attributed to biofilm formation. As the biofilm establishes, the kinetic capacity increases due to the increase of the cell biomass in the packing. In the subsequent runs (from R3 to R10) at the same operating conditions (Table 5.1), an increase in the CO and H_2 conversion efficiencies was observed (Figure 5.4). The lower conversion efficiencies of H_2 compared to CO is attributed to CO inhibition of hydrogenase. The hydrogenase activity of *C. ragsdalei* was inhibited by 90% when the CO partial pressure was 8.5 kPa (Skidmore, 2010). The decrease in hydrogenase activity decreases H_2 utilization and conversion efficiency. H_2 was reported to be utilized after CO has been depleted during syngas fermentation in batch bottle with *C. ljungdahlii* (Younesi et al., 2005). In the present study, the partial pressure of CO at the inlet of the TBR was 43.18 kPa (absolute). The availability of high concentrations of CO initially inhibited the H_2 uptake and resulted in low H_2 conversion efficiency. However, cells in the biofilm consume CO as the syngas flows from the bottom to the top of the TBR. This causes CO concentrations to drop along the length of the TBR and reduces its inhibition on hydrogenase. This resulted in an increase in the H_2 conversion efficiency for R3 to R10 (Figure 5.5). The H_2 conversion efficiency for runs R3 to R8 increased, which indicated an increase in the cell activity in the biofilm. However, the H_2 conversion efficiency was similar for runs R8 to R10, indicating that the biofilm reached a quasi-steady state. This phenomenon of increase in H_2 conversion due to biofilm was not

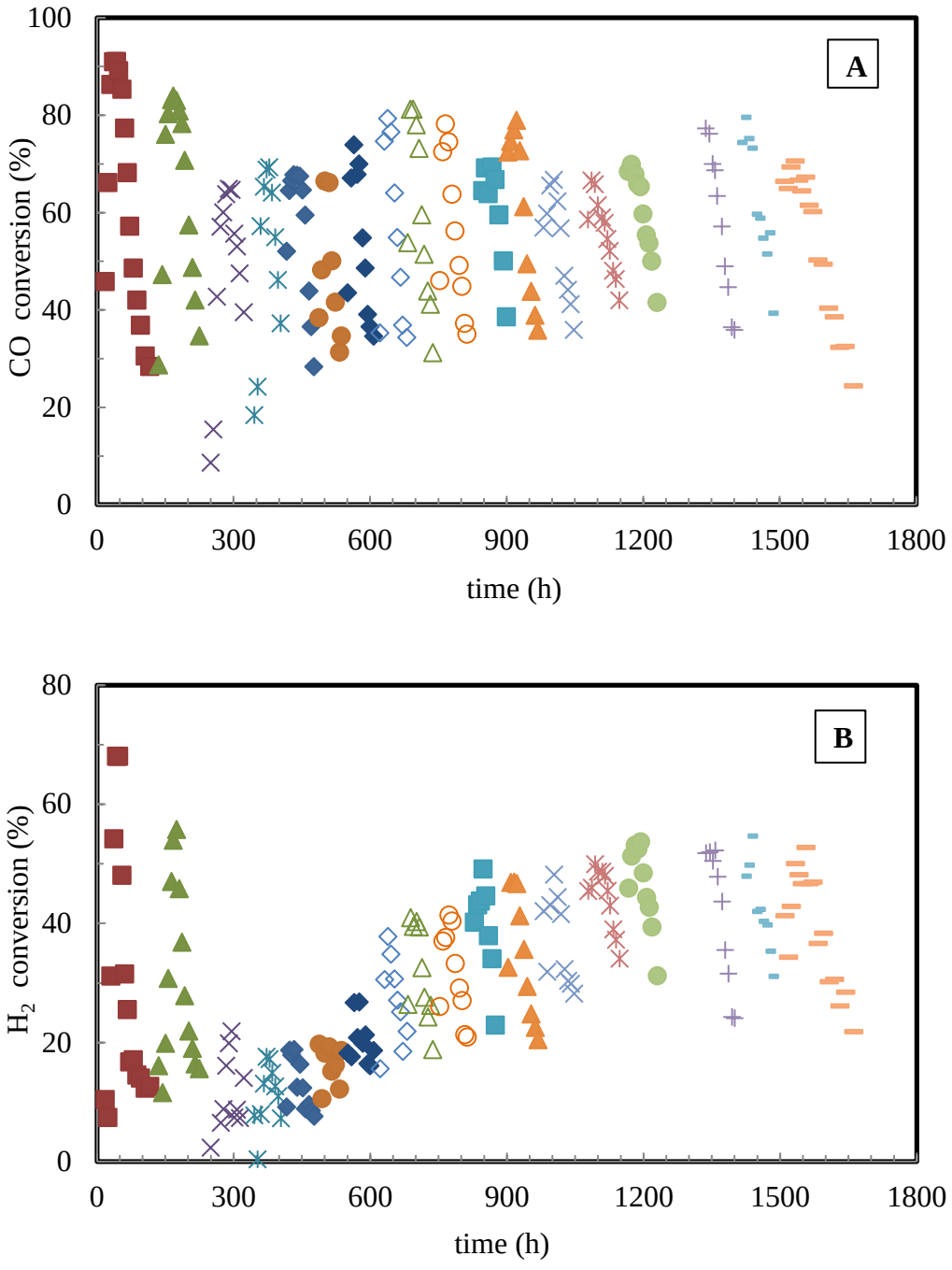

Figure 5.4 Gas conversion efficiencies for all runs in semi-continuous TBR fermentation. (A) CO (B) H_2.

( ) R1 ( ) R2 ( ) R3 ( ) R4 ( ) R5 ( ) R6 ( ) R7 ( ) R8 ( ) R9 ( ) R10 ( ) R11 ( ) R12 ( ) R13 ( ) R14 ( ) R15 ( ) R17 ( ) R18 ( ) R19; R1, R2: L = 200 ml/min, G = 2.3 sccm; R4-R9, R19: L = 200 ml/min, G = 4.6 sccm; R11, R17: L = 500 ml/min, G =4.6 sccm; R14, R15, R18: L = 700 ml/min, G = 4.6 sccm. R1-R15: Counter-current mode; R17-R19: Co-current mode.

discussed in the literature because no biofilm formation was reported in earlier TBR syngas fermentation studies (Kimmel et al., 1991; Klasson et al., 1993b; Wolfrum and Watt, 2002).

After the TBR reached quasi-steady state, the liquid flow rate was changed from runs R10 to R15 (Table 5.1). The variations in the maximum CO and H_2 conversion efficiencies at different liquid flow rate were below 15%. Additionally, in the co-current mode from runs R17 to R19, the variations in the maximum gas conversion efficiencies at different liquid flow rates were below 11% (Table 5.2). This indicates that the liquid flow rate had small effect on the CO and H_2 conversion efficiencies in the counter-current and co-current modes.

5.3.4 Cumulative gas uptake profiles

The CO and H_2 cumulative uptake profiles are shown in Figure 5.5. The cumulative CO and H_2 uptake increased in all the runs. Similar to the product profiles, the comparison between runs was made at 61±2 h^{-1} from the beginning of each run. In the initial runs R1 and R2, the cumulative gas uptake was 99 mmol of CO and 36 mmol of H_2. When the gas flow rate was increased from 2.3 to 4.6 sccm in run R3, the cumulative CO uptake increased by 36% while the cumulative H_2 uptake decreased by 50% compared to R2. While the cumulative CO uptake rate was similar for run R3 to R10, the cumulative H_2 uptake increased by 212% in run R10 compared to run R3 at the same operation condition. This was due to biofilm formation as discussed earlier. The results showed that the liquid flow rate had a minor effect on the cumulative gas uptake in both counter-current and co-current mode of operation.

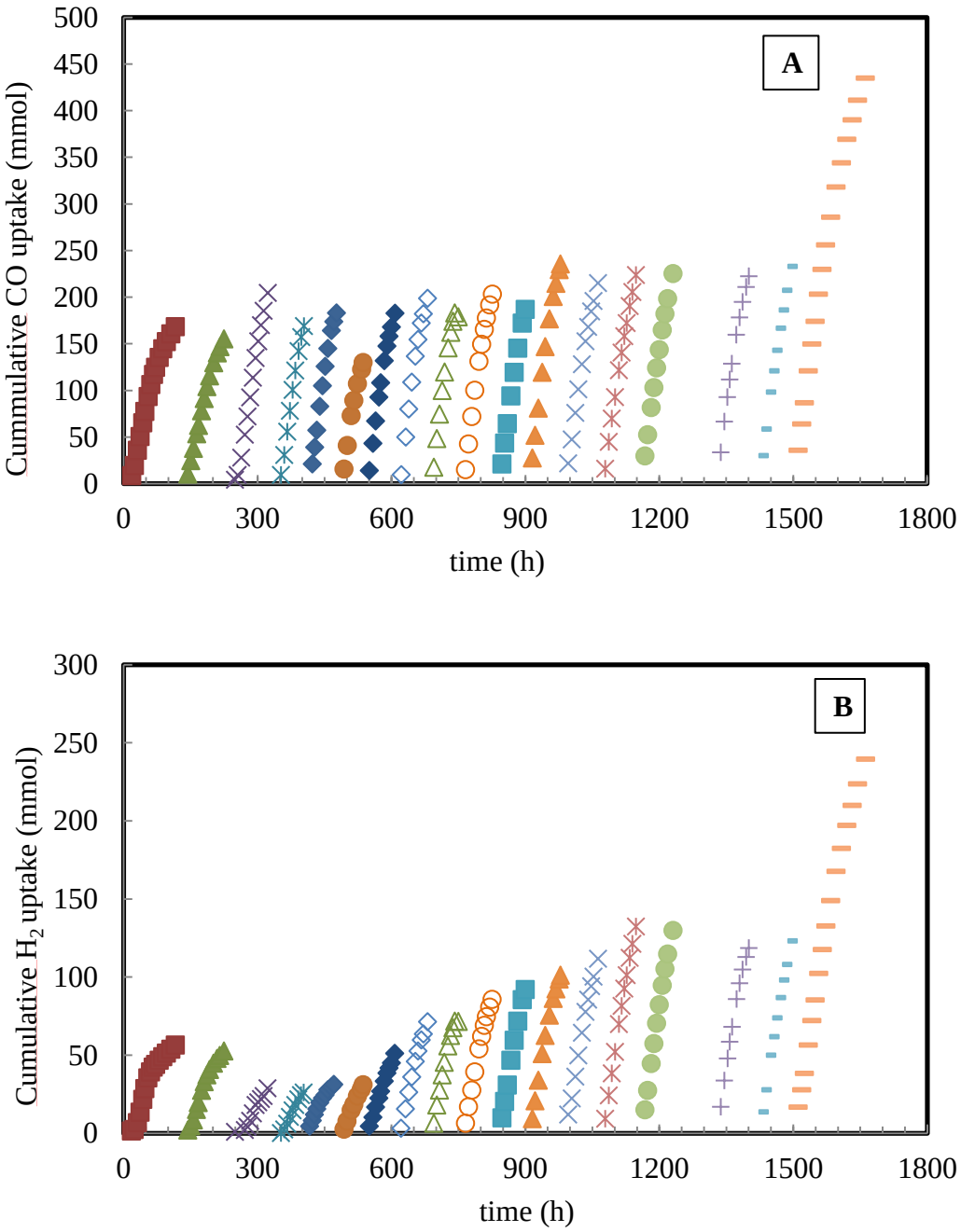

Figure 5.5 Cumulative gas uptake profiles for all runs in semi-continuous TBR fermentation. (A) CO (B) H_2

(■) R1 (▲) R2 (×) R3 (✳) R4 (◆) R5 (●) R6 (◆) R7 (◇) R8 (△) R9 (○) R10 (■) R11 (▲) R12 (×) R13 (✳) R14 (●) R15 (+) R17 (-) R18 (—) R19; R1, R2: L = 200 ml/min, G = 2.3 sccm; R4-R9, R19: L = 200 ml/min, G = 4.6 sccm; R11, R17: L = 500 ml/min, G =4.6 sccm; R14, R15, R18: L = 700 ml/min, G = 4.6 sccm. R1-R15: Counter-current mode; R17-R19: Co-current mode.

5.3.5 Rates of gas uptake and product formation

The rates of CO and H_2 uptake are shown in Figure 5.6. They were estimated from the linear slope of the experimental cumulative gas uptake in the first 61±2 h of fermentation for each run. The averages CO and H_2 uptake rate by *C. ragsdalei* for runs R1 and R2 were 2.17 mmol/h and 0.94 mmol/h, respectively. In R3, when the gas flow rate was increased to 4.6 sccm, the rate of CO uptake increased by 42% and rate of H_2 uptake decreased by 48%. In the subsequent runs (from R4 to R9) at the same operating conditions, the rate of CO uptake increased further by 10% in R4 and 30% in R9 compared to R3. However, the rate of H_2 uptake increased by 12% in R4 and 184% in R9 compared to R3. The increase in the rates of CO and H_2 uptake in the subsequent runs is an indication of increased cell activity due to the biofilm formation. It can also be observed from Figure 5.6 that the rate of CO uptake was similar for runs R4 to R19. However, there was a steady increase in the H_2 uptake rate from R4 to R8 followed by a similar uptake rates for runs R9 and R10. The biofilm was considered to be established under quasi-steady state conditions when the variation in rates of CO and H_2 uptake were below 10% in run R10 compared to runs R8 and R9.

The product formation rates for each run (Figure 5.6) were calculated from the linear slope of the ethanol and acetic acid concentration profiles in the first 61±2 h of fermentation (Figure 5.3). In runs R1 and R2, the average ethanol and acetic acid production rates were 0.38 mmol/L·h and 0.68 mmol/L·h, respectively. When the gas flow rate was doubled, ethanol production rate increased by 43% in R3 and R4 compared to R2. The acetic acid production rates increased by 13% in R3 and 59% in R4 compared

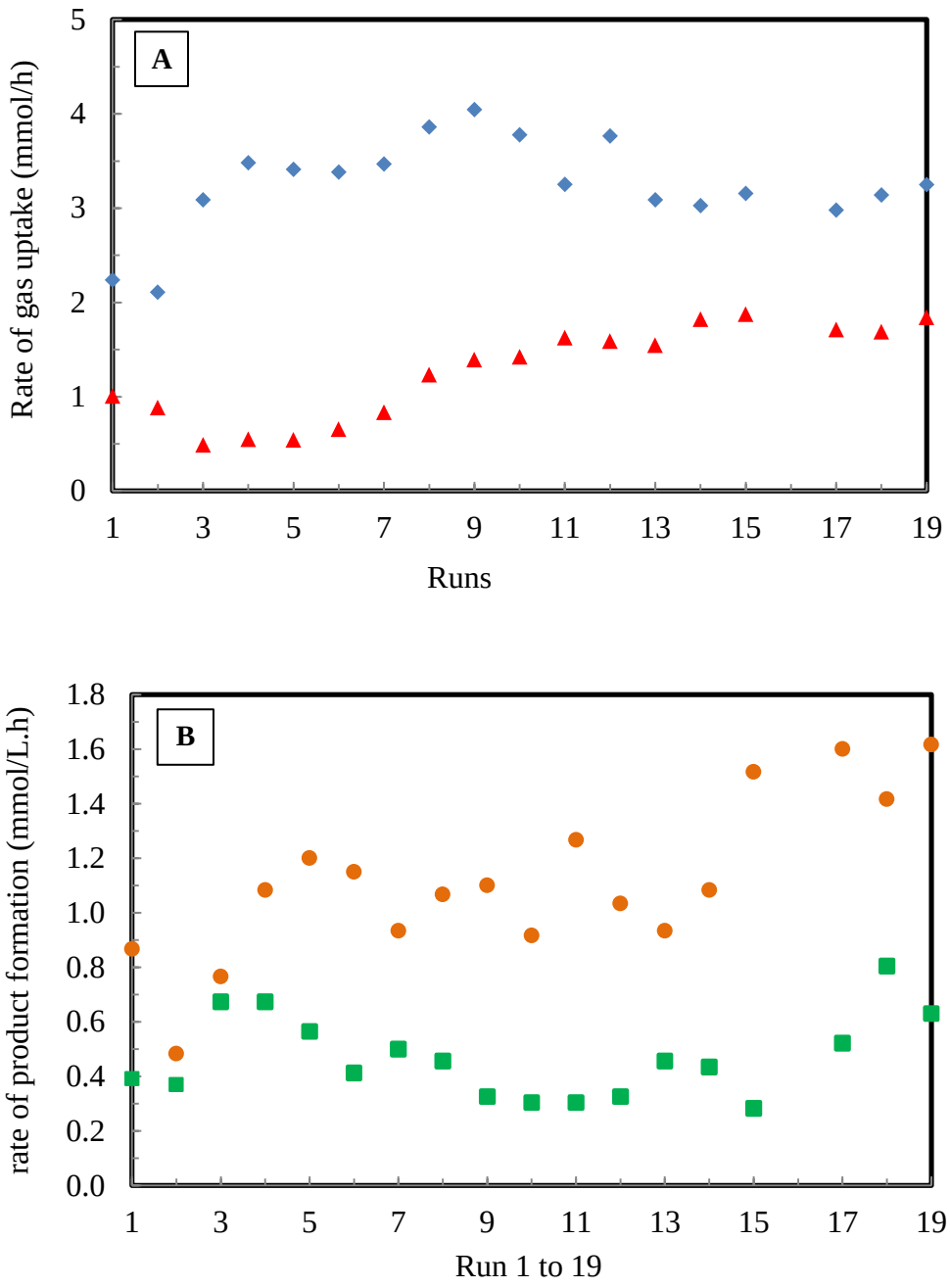

Figure 5.6 (A) Gas uptake and (B) product formation rates for runs R1-R19 during semi-continuous fermentation in TBR. (◆) CO (▲) H_2 (■) Ethanol (●) Acetic acid.

to R2. The ethanol production rate decreased by 15% in run R5 and 51% in run R9 compared to R4. While the acetic acid production rate slightly increased up to 11% from

runs R5 to R9compared to R4 . It can be observed from Figure 5.6B that ethanol production rates were decreasing for runs R3 to R10 even though the operating conditions were the same (Table 5.1). On the other hand, the acetic acid production rate slightly increased and remained stable. The decrease in the ethanol production rate was attributed to the increase in cell maintenance due to biofilm formation. When the liquid recirculation rates was varied from runs R10 to R15, small changes ethanol and acetic acid production rates were observed. However, higher ethanol and acetic acid production rates were obtained in the co-current mode from runs R17 to R19 indicating a better gas liquid interaction.

5.3.6 Product yields, reductant and carbon balance

Ethanol and acetic acid yields (Table 5.2) were calculated as follows (Liu et al., 2012) :

$$\text{Ethanol yield} = \frac{\frac{\text{Total moles of ethanol produced}}{\text{Total moles of CO consumed}}}{\frac{\text{1 mole of ethanol produced}}{\text{6 moles of CO consumed}}} \times 100\% \quad (5.5)$$

$$\text{Acetic acid yield} = \frac{\frac{\text{Total moles of acetic acid produced}}{\text{Total moles of CO consumed}}}{\frac{\text{1 mole of acetic acid produced}}{\text{4 moles of CO consumed}}} \times 100\% \quad (5.6)$$

The average ethanol and acetic acid yields for R1 and R2 were 58.54% and 76.50%, respectively (Table 5.2). When the gas flow rate was doubled from 2.3 to 4.6 sccm in run R3, the ethanol yield increased to 90.10 % and acetic acid yield was at 65.36%.

However, from run R4 to R6 the ethanol yield decreased by 29% and acetic acid yield increased by 40%. The increase in acetic acid yields from R4 to R6 is attributed to the initiation of the biofilm development as ATP energy is produced during this process.

As fermentation progressed (R7-R10), most of the gas was consumed for assimilation of cell biomass and maintenance resulting in decrease of both ethanol and acetic acid yields. From R7 to R9, ethanol yields further decreased from 48.64% in R7 to 27.97% in R9, while the acetic acid yields slightly increased from 54.32% in R7 to 66.64% in R9. The variations in the ethanol and acetic acid yields at different liquid recirculation rates were below 23%. The ethanol and acetic acid yields in the TBR with co-current mode for runs R17 to R19 were at least 50% higher than in counter-current operation for runs R10 to R15.

Based on the stoichiometry from Eq 5.1 to 5.4, 6 electrons and 4 electrons are required for production of ethanol and acetic acid, respectively. The electrons are generated from the oxidation of CO and H_2 during fermentation. The ratio of total number of electrons in the products (ethanol and acetic acid) to the total number of electrons generated by the oxidation of CO and H_2 should equal 1 for a balanced reductant. Additionally the ratio of total carbon in products (ethanol and acetic acid) to the total carbon consumed provided the carbon balance for the fermentation at each run. The reductant and the carbon balances for runs R1 to R19 were calculated from the Eq 5.7 and Eq 5.8 below:

$$\text{Reductant balance} = \frac{\text{total reductants in products}}{\text{consumed CO and } H_2} = \frac{6 \cdot n_{EtOH} + 4 \cdot n_{AA}}{n_{CO} + n_{H2}} \times 100\% \quad (5.7)$$

$$\text{Carbon balance} = \frac{\text{total carbon in products}}{\text{total carbon consumed}} = \frac{2 \cdot n_{EtOH} + 2 \cdot n_{AA} + 1 \cdot n_{CO2}}{1 \cdot n_{CO}} \times 100\% \quad (5.8)$$

where, n_{EtOH} is the total moles of ethanol produced at the end of each run (mmol), n_{AA} is the total moles of acetic acid produced at the end of each run (mmol), n_{CO} and n_{H2} are the

total moles of CO and H_2 consumed at the end of each run (mmol), respectively, and n_{CO2} is the net moles of CO_2 produced (mmol).

The reductant, carbon balance and molar ratio of CO_2 produced to CO consumed for runs R1 to R19 is shown in Figure 5.7. If CO was solely utilized to produce acetic acid as per Eq 5.2, then theoretically 0.5 moles of CO_2 should be produced from 1 mole of CO (i.e, molar ratio of CO_2 produced to CO consumed is 0.5). However, when CO is solely utilized to produce ethanol as per Eq 5.1, then the molar ratio of CO_2 produced to CO consumed is 0.67. For runs R3, R4 and R5, CO was mostly consumed with low H_2 uptake (Figures 5.6) the molar ratio of CO_2 produced to CO consumed was about 0.56

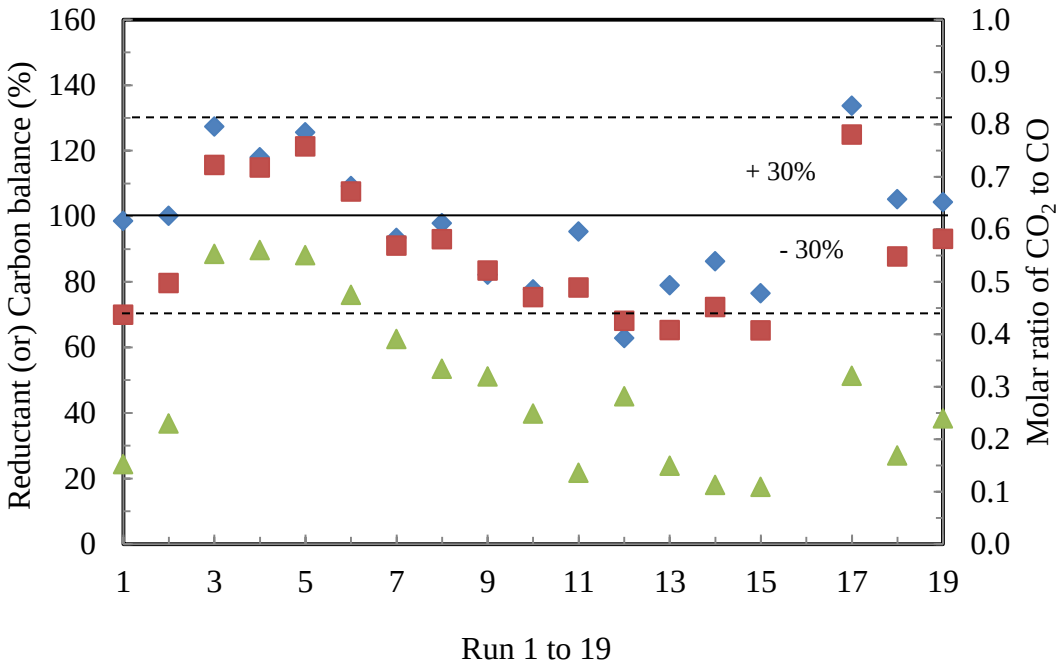

Figure 5.7 Carbon and Reductant balance for Run 1 to Run 19 (◆) Reductant balance (■) Carbon balance (▲) molar ratio of CO_2 produced to CO consumed.

(Figure 5.7). However, if H_2 is solely consumed to produce ethanol and acetic acid as per Eq 5.3 and 5.4, the molar ratio of CO_2 produced to CO consumed should be zero. From

Figure 5.7, it can also be observed that for runs R6 to R11 the molar ratio of CO_2 produced to CO consumed decreased from 0.55 to 0.14 as the H_2 uptake increased (Figure 5.6). Additionally, from run R11 to R19 as the H_2 uptake reached steady state (Figure 5.6), the molar ratio of CO_2 to CO remained low and averaged to 0.19 (Figure 5.7).

From R1 to R19, the reductant and carbon balance closed to 100±30%. The error in these balances could be associated with the gas analysis. Because of the low molar gas flow rates used (0.12 mmol/min and 0.24 mmol/min) a small error in the gas composition analysis at the TBR exit could result in an overall higher % error in the carbon and reductant balances. Also, operational issues such as gas bypass and flooding issues encountered during counter-current operation especially at high liquid recirculation rates (runs R11 to R15) could also have contributed to the error in the carbon and reductant balances.

5.3.7 Apparent mass transfer

The apparent mass transfer coefficients $k_{L,CO}\,a/V_L$ and $k_{L,H2}\,a/V_L$ were calculated using the equation below (Orgill et al., 2013; Sherwood et al., 1975).

$$\frac{k_{L,i}a}{V_L} = \frac{-\frac{1}{V_L}\frac{dn_i}{dt}}{\left[\frac{C_{out,i}-C_{in,i}}{\ln\left(C_{out,i}/C_{in,i}\right)}\right]} \qquad (5.9)$$

where, dn_i/dt is the molar rate of gas component i transferred into the medium (mmol/h), V_L is the dynamic liquid holdup volume in the TBR (L), $k_{L,i}\,a/V_L$ is the mass transfer coefficient of gas (h^{-1}) and i represents either CO or H_2, $C_{in,i}$ is the inlet concentration of

gas component *i* at the TBR inlet (mmol/L) and $C_{out,i}$ is the outlet concentration of gas component *i* at the TBR exit (mmol/L).

During fermentation, the driving force will be very high under mass transfer limiting conditions because the cells consume dissolved gases and the concentration of the gases will be zero in the medium. Further, the gas will be in plug flow along the column length and the variation in the inlet and outlet gas concentrations will be very high. Thus, when gas phase analysis is used to calculate the mass transfer coefficient, the driving force can be approximated to the logarithmic average value between the inlet and outlet gas streams (Garcia-Ochoa and Gomez, 2009).

From Figure 5.8, it can be observed that the apparent $k_{L,CO}\,a/V_L$ and $k_{L,H2}\,a/V_L$ increased with increase in the gas uptake, reached a maximum and then started to decrease due to decrease in the cell activity as the nutrients were depleted in the medium. This trend is similar to all the fermentation runs R1 to R19. The maximum apparent $k_{L,CO}\,a/V_L$ and $k_{L,H2}\,a/V_L$ were 544 h^{-1} and 260 h^{-1}, respectively for runs R1 and R2. However, when the gas flow rate was doubled the maximum apparent $k_{L,CO}\,a/V_L$ increased by 24% and $k_{L,H2}\,a/V_L$ decreased by 46% for runs R3 to R5. Further, for runs R7to R10 the maximum apparent $k_{L,CO}\,a/V_L$ increased up to 50% and the maximum apparent $k_{L,H2}\,a/V_L$ increased up to 103% compared to R3 at the same operating condition due to biofilm formation. This increase in the apparent mass transfer of CO and H_2 (Figure 5.8) at the same operating condition in the subsequent runs from R3 to R10 is associated with increase in the gas uptake of the cells (Figure 5.6). When the liquid recirculation rate was increased from 200 ml/min (R10 and R12) to 500 ml/min (R11 and R13) the maximum apparent $k_{L,CO}\,a/V_L$ and $k_{L,H2}a/V_L$ decreased by 68% and 49%, respectively. Additionally,

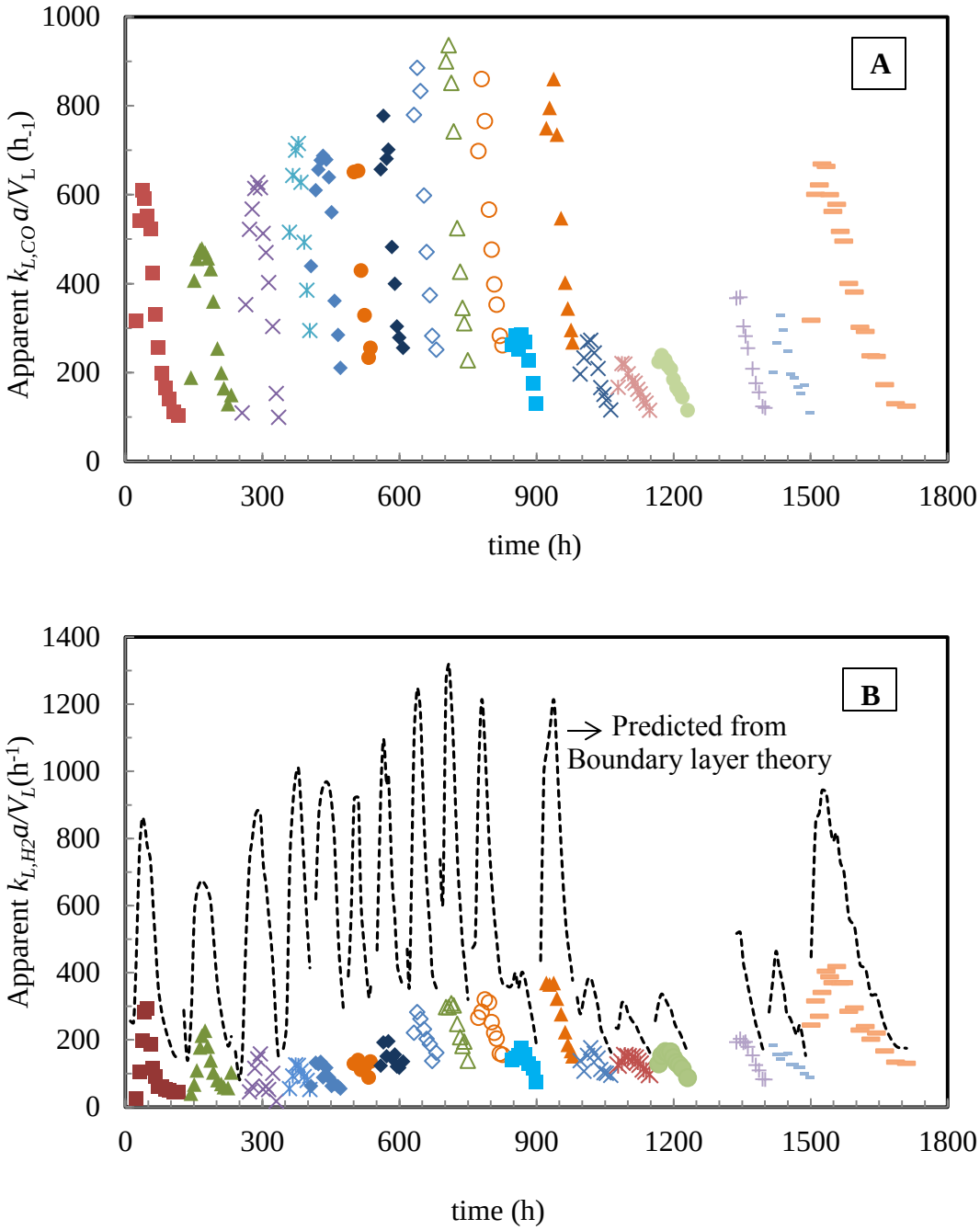

Figure 5.8 (A) Apparent $k_{L,CO}\,a/V_L$ (B) Apparent $k_{L,H2}a/V_L$ during semi-continuous syngas fermentation in TBR.
(■) R1 (▲) R2 (×) R3 (✳) R4 (◆) R5 (●) R6 (◆) R7 (◇) R8 (△) R9 (○) R10 (■) R11 (▲) R12 (×) R13 (✳) R14 (●) R15 (+) R17 (-) R18 (—) R19; R1, R2: L = 200 ml/min, G = 2.3 sccm; R4-R9, R19: L = 200 ml/min, G = 4.6 sccm; R11, R17: L = 500 ml/min, G =4.6 sccm; R14, R15, R18: L = 700 ml/min, G = 4.6 sccm. R1-R15: Counter-current mode; R17-R19: Co-current mode. (---) Predicted $k_{L,H2}a/V_L$ using boundary layer theory.

at 700 ml/min of liquid recirculation rate (R14 and R15), the maximum apparent $k_{L,CO}$ a/V_L and $k_{L,H2}a/V_L$ decreased by 73% and 54%, respectively compared to runs R9 and R10 at 200 ml/min. As discussed in Section 4.3.2, the increase in the liquid recirculation rate increased the liquid holdup volume (see Appendix A, Table A1), which resulted in a decrease in the $k_{L,i}\,a/V_L$ values for both CO and H_2.

The $k_{L,H2}a/V_L$ was also predicted from the apparent $k_{L,CO}\,a/V_L$ using boundary layer theory (Figure 5.8B). According to this theory (Sherwood et al., 1975), the mass transfer coefficient and diffusivities of two different chemical species under identical hydrodynamic conditions can be correlated by

$$\frac{\left({}^{k_{L,i}a}/_{V_L}\right)_i}{\left({}^{k_{L,i}a}/_{V_L}\right)_j} = \left(\frac{D_i}{D_j}\right)^{1/2} \tag{5.10}$$

where, $(k_{L,i}\,a/V_L)_{\,i}$ and $(k_{L,i}\,a/V_L)_{\,j}$ are the mass transfer coefficients of the *i* and *j* gases, respectively, and D_i and D_j are diffusivities for the *i* and *j* gases, respectively. The diffusivities of CO and H_2 at 37 °C are $3.26\text{x}10^{-9}$ m^2/s and $6.48\text{x}10^{-9}$ m^2/s, respectively (Verhallen et al., 1984; Wise and Houghton, 1968). Figure 5.8 shows the predicted $k_{L,H2}a/V_L$ (dashed lines) using the boundary layer theory based on CO data, which were much higher than the apparent $k_{L,H2}a/V_L$ calculated from the experimental H_2 consumption data. This clearly indicates that the capability of the TBR to transfer H_2 into the medium were not fully utilized due to the cells' kinetic limitation mostly associated with inhibition of hydrogenase activity by CO (Hurst, 2005; Skidmore, 2010). The apparent $k_{L,i}\,a/V_L$ has a decreasing trend with increasing liquid flow rate as shown in pure mass transfer experiments (Orgill et al., 2013). However, the apparent $k_{L,i}\,a/V_L$ obtained

in fermentation experiments are at least tenfold higher than that observed in the pure mass transfer experiments with air-water system (Orgill et al., 2013).

5.4 Conclusions

Repetitive semi-continuous fermentation runs with medium replenishment in the TBR resulted in a total cell OD_{660} of 2.5 after 1662 h. Maximum gas conversion efficiencies of around 87% CO and 62% H_2 were achieved at 2.3 sccm gas flow rate, while maximum of 81% CO and 55% H_2 conversion efficiencies were achieved at 4.6 sccm. The establishment of the biofilm in the TBR reduced CO inhibition and improved H_2 conversion and uptake by 1.9 times at 4.6 sccm of gas flow and 200 ml/min of liquid recirculation rate. At the end of the experiment at 1662 h, 12.3 g/L of acetic acid and 5.7 g/L of ethanol were produced. Acetic acid is a growth associated product. Hence, its production rates were higher than ethanol due to the repeated replenishment of nutrients which provided growth supporting environment. Operating the TBR in co-current mode reduced the gas bypass and TBR flooding issues that were encountered in counter-current mode of operation.

Acknowledgments

This research was supported by a grant from the Sun Grant Initiative through the U.S. Department of Transportation and Oklahoma Agricultural Experiment Station.

CHAPTER VI

CONTINUOUS SYNGAS FERMENTATION IN A TRICKLE BED REACTOR USING *CLOSTRIDIUM RAGSDALEI*

ABSTRACT

A trickle-bed reactor (TBR) can minimize the liquid resistance to mass transfer because a very thin liquid film is in contact with the gas, which improves the mass transfer. In the present study, continuous syngas fermentation was performed in a 1-L TBR for ethanol production by *C. ragsdalei*. The effects of dilution and gas flow rates on product formation, productivity, gas uptakes and conversion efficiencies were examined. The results showed that CO and H_2 conversion efficiencies reached over 90% when the gas flow rate was maintained between 1.50 and 2.79 sccm at a dilution rate of 0.0088 h^{-1}. A 4:1 molar ratio of ethanol to acetic acid was achieved in co-current continuous mode at dilution rates of 0.0088 h^{-1} and 0.012 h^{-1}, and gas flow rates from 10.10 to 12.22 sccm and 15.91 to 18.93 sccm, respectively. This is higher than the 1:2 molar ratio achieved in co-current semi- continuous fermentation at a gas flow rate of 4.60 sccm.

Keywords: Continuous syngas fermentation, *Clostridium ragsdalei* P11, Ethanol, Trickle bed reactor.

6.1 Introduction

Syngas fermentation process is part of the hybrid conversion technology for the conversion for renewable feedstocks to biofuels and chemicals. Microorganisms such as *Clostridium ljungdahlii, Clostridium carboxidivorans, Clostridium ragsdalei, Alkalibaculum bacchi* metabolize syngas components (CO, CO_2 and H_2) via reductive acetyl-CoA pathway to produce ethanol, acetic acid and cell carbon (Liu et al., 2014a; Phillips et al., 1994; Ukpong et al., 2012; Wilkins and Atiyeh, 2011). One major advantage of the hybrid conversion process is the ability to utilize feedstocks such as municipal solid wastes, industrial fuel gases and biomass (Belgiorno et al., 2003; Datar et al., 2004; Simpson et al., 2013). However, challenges for this technology include mass transfer limitations, enzyme inhibition, low cell concentration and low ethanol productivity.

Ethanol has been reported to be a non-growth associated product in *Clostridia sp*. (Cotter et al., 2009; Datar et al., 2004; Klasson et al., 1992). Many researchers focused on improving ethanol productivity by optimizing media components, adding reducing agents, adjusting pH and optimizing bioreactor design to improve mass transfer of CO and H_2 in fermentation medium (Babu et al., 2010; Gao et al., 2013; Guo et al., 2010; Hu, 2011; Klasson et al., 1991b; Panneerselvam et al., 2009; Saxena and Tanner, 2011; Worden et al., 1991). *C. ljungdahlii* is the most extensively studied microorganism for ethanol production using syngas fermentation. A tenfold (from 5g/L to 48 g/L) and over three fold (from 0.4 g/L to 1.5 g/L) increases in ethanol and cell mass concentrations, respectively, were achieved in a continuous stirred tank reactor (CSTR) with cell recycle

using *C. ljungdahlii* by designing a defined production medium and controlling pH at 4.5 (Phillips et al., 1993).

In studies using *C. ragsdalei,* pH of 5.8 to 6 was shown to be optimum for cell growth (Huhnke et al., 2010; Kundiyana et al., 2011b) while maintaining a pH of 4.5 during solventogenic phase was shown to favor ethanol production (Hu, 2011). In batch bottle fermentations using *C. ragsdalei*, the addition of methyl viologen and dithiothreitol reducing agents were shown to enhance ethanol production by 2.5 fold (0.51 g/L to 1.3 g/L) and a 5 fold (0.52 g/L to 2.7 g/L), respectively (Babu et al., 2010; Panneerselvam et al., 2009). Ethanol production can also be enhanced by optimizing the bioreactor design to increase the mass transfer of low soluble syngas components (CO and H_2).

Bioreactor designs such as air-lift reactors, CSTR and hollow fiber membrane (HFM) reactors have been extensively studied to understand their capabilities to improve CO mass transfer into fermentation medium (Lee et al., 2012; Munasinghe and Khanal, 2010b; Ungerman and Heindel, 2007). Further, improved ethanol production over batch bottle fermentations was reported when fermentations were performed in bubble columns using *C. carboxidivorans*, two stage CSTR with cell recycle using *C. ljungdahlii*, two stage CSTR with partial cell recycle using *C.ragsdalei,* CSTR with cell recycle using *A. bacchi* and HFR using *C. ljungdahlii* (Kundiyana et al., 2011a; Lee, 2010; Liu et al., 2014a; Rajagopalan et al., 2002; Richter et al., 2013).

In a study by Orgill et al. (2013), the trickle bed reactor (TBR) was reported to provide higher mass transfer capabilities than a CSTR. Further, in semi-continuous fermentation, formation of biofilm in the TBR improved the H_2 uptake by reducing the CO inhibition as the gas moves up along the column length (Section 5.3.4). However,

higher acetic acid production was observed in the semi- continuous fermentations due to repetitive medium replacement that provided growth supporting environment (Section 5.3.2). During batch and semi-continuous fermentations, cells undergo lysis as the nutrients levels deplete; causing the fermentation to cease. Production of ethanol in batch process is time and labor intensive due to the long doubling times of syngas fermenting microbes (Richter et al., 2013). During continuous fermentation, high cell concentrations can be maintained and the cells are viable for a longer period (Shuler and Kargi, 2002). Further, continuous supply of fresh medium would enable to maintain the cell activity and adapt the cells in the biofilm to the produce more solvent by controlling the fermentation parameters such as dilution rate, pH and gas flow rate. The focus of the present study is to improve ethanol production in the TBR during continuous operation. The supply of nutrients to the TBR was controlled by altering the dilution rate. Further, once the pH dropped from 5.8 to 4.5 due to cell growth and acetic acid production the pH was maintained at 4.5 throughout the fermentation. The effect of dilution rate and gas flow rate on gas conversions, gas uptakes, product concentrations, yields and productivities in both counter-current and co-current modes of operation were studied.

6.2 Materials and Methods

6.2.1 Microorganism and Medium preparation

Clostridium ragsdalei (ATCC-PTA-7826) is a rod shaped, gram-positive, strict anaerobic bacterium obtained from an anaerobic enrichment inoculated using fresh water sediment from a duck pond at the University of Oklahoma by Dr. Ralph Tanner (Huhnke et al., 2010). It is a mesophilic bacterium that grows at an optimum temperature of 37°C and pH of 5.8 (Huhnke et al., 2010). *C. ragsdalei* was maintained and grown on standard

yeast extract medium. The medium composition and inoculum preparation procedure has been reported previously (section 5.2.1 and 5.2.2).

6.2.2 Fermentation experimental set up

The schematic for continuous syngas fermentation in a TBR is shown in Figure 6.1. The TBR was designed in house, which is made of borosilicate glass column of 5.1 cm diameter and 61 cm long. The detailed reactor design was reported earlier (section 5.2.3). The 6-mm soda lime glass beads (#26396-621, VWR, Atlanta, GA) were used as the packing material because they provided higher mass transfer (k_La/V_L) than the 3-mm beads. The TBR liquid outlet was connected to a 500 ml Pyrex glass bottle, which was used as a sump to hold 500 ml of medium. The TBR was operated both in counter-current and co-current modes. A peristaltic pump (7523-20, Cole-Parmer, Vernon, IL, USA) circulated the liquid at a desired flow rate. The pH probe (EW 05662-45, Cole-Parmer, Vernon Hills, IL) and ORP probe (00238GG, Cole-Parmer, Vernon Hills, IL) were placed in line in the recirculation loop before the peristaltic pump. A liquid sample port along with the product stream outlet was also connected in the recirculation loop. A 6.4 mm T-connector with a port to add fresh medium into the reactor was placed in the recirculation loop before the medium enters the top of the reactor. The fresh medium from the feed tank was pumped to the reactor using a Bioflo pump on the Bioflo 110 controller (New Brunswick Scientific Co., Edison, NJ). The product stream was connected to another Bioflo pump that pumped out the product to a tank. An addition port for acid and base was added in the recirculation loop after the sampling port and was connected to the Bioflo controller for pH control. N_2 was purged continuously through the feed and product tanks at 20 sccm to maintain anaerobic conditions. A one-way valve

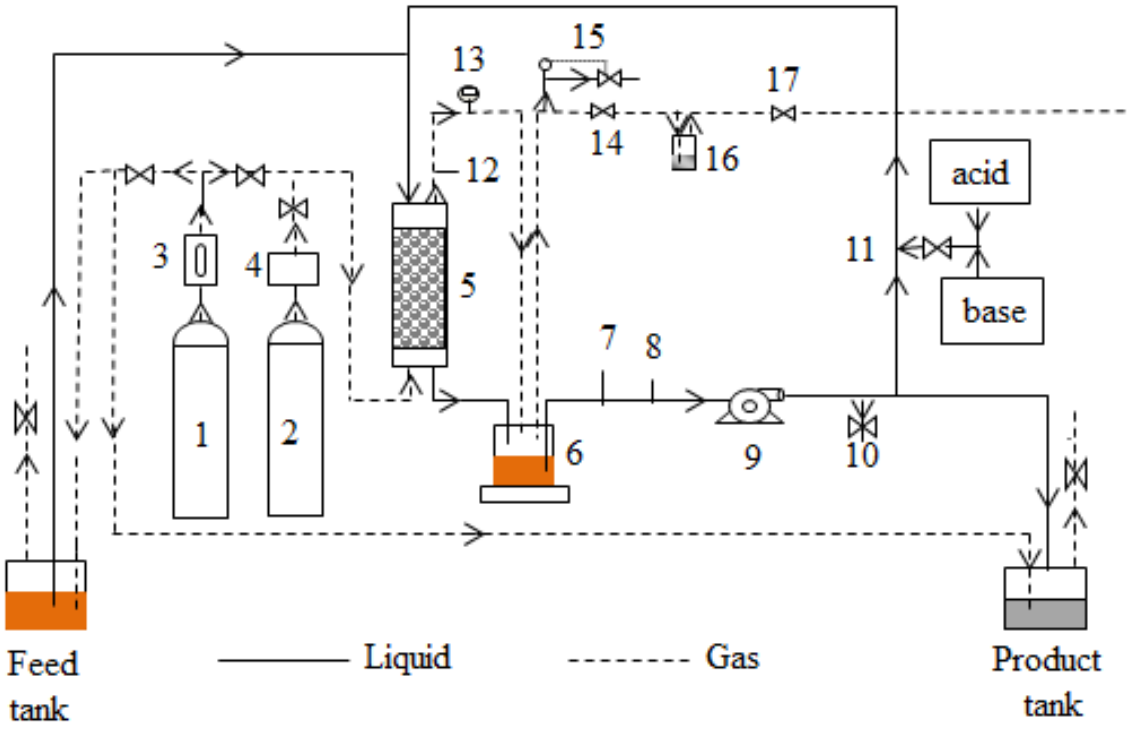

Figure 6.1 TBR continuous syngas fermentation set up.

(1) Nitrogen cylinder (2) Syngas cylinder (3) Rotameter (4) mass flow controller (5) Trickle bed reactor (6) Sump to hold medium (7) ORP probe (8) pH probe (9) Masterflex pump (10) Liquid sample port (11) Acid/base addition (12) TBR Gas sample port (13) Pressure gauge (14) Back pressure regulator (15) By pass safety line with solenoid valve and pressure switch (16) Gas bubbler (17) Ball valve. Dashed lines indicate gas lines and solid lines indicate liquid lines.

was connected at the gas outlet of both tanks to make sure the gas flows out and air does not flow back into the tanks. In counter-current mode of operation, the gas entered at the bottom of the TBR. The exhaust gas from TBR was fed into the sump headspace and then out to the sump gas exit line. In co-current operation, both the gas and liquid entered the TBR at the top and exited through the same exit line to the sump. The sump acted as a gas-liquid separator. Further, a back pressure regulator was connected to the sump gas exit line to ensure that a 115 kPa pressure was maintained in the TBR. A pressure gauge was connected at the TBR gas exit line to measure the pressure in the TBR. An additional

gas exit line was connected to the sump as a safety exhaust line with a pressure switch and a solenoid valve to vent the excess pressure in the TBR. A bubbler was placed after the pressure regulator to minimize losses of products exiting with the gas.

6.2.3 Continuous Fermentation

The sterilization of the TBR was done in an autoclave (Primus Sterilizer Co. Inc, Omaha, NE) at 121^{o} C for 20 min. After sterilization, the reactor was purged with N_2 for 5 h. First, 200 ml of fresh sterile medium was added into the TBR and purged with N_2 for 8 h. Then, the gas was switched to syngas with 38% CO, 5% N_2, 28.5% CO_2 and 28.5% H_2 (by volume) (Stillwater Steel and Supply Company, Stillwater, OK), which is similar to the composition of coal derived syngas (Klasson et al., 1993b). A 60% (v/v) inoculum was added into the TBR through the liquid sample port. The temperature of the TBR was maintained at 37 ^{o}C using silicone heating tape and a surface thermocouple connected to a temperature controller (Omega CN 370 series, Stamford, CT). The liquid recirculation rate was set at 200 ml/min. At the beginning of the fermentation, the gas flow rate was set at 1.5 sccm. Initially, the TBR was operated in semi-continuous mode. After the CO and H_2 conversion efficiencies reached about 90%, the TBR was switched to continuous mode by turning on the fresh medium and product pumps at a desired flow rate. The effects of three dilution rates of 0.006 h^{-1}, 0.0088 h^{-1} and 0.012 h^{-1} on product formation and gas conversion efficiency were examined. At each dilution rate, the effect of gas flow rate was examined. The gas flow rate was increased in the TBR until the CO conversion efficiency dropped below 40% at each dilution rate. Then, the gas flow rate was decreased and a new dilution rate was used. Gas and liquid samples were withdrawn from the TBR periodically. To avoid flooding of the TBR by cell debris, the recirculation rate

was increased from 200 to 500 ml/min for about 10 min at every sampling time to clear the TBR from cell debris.

6.2.4. Sample Analysis

Cell mass, pH and ORP measurement

The cell optical density was measured at 660 nm using UV spectrophotometers (Cole Parmer, Vernon Hills, IL). The total cell optical density of the attached cells was measured at the end of the fermentation as described in Section 5.2.5. The readings from the pH probe connected to the Bioflo 110 controller (New Brunswick Scientific Co., Edison, NJ) were logged into a computer using Biocommand software. The ORP measurements were recorded manually using a digital ORP meter (# ORCN37, Omega Engineering, Stamford, CT).

Product and gas analysis

Acidified liquid samples for product analysis were prepared by addition of 500 µl of 0.1 N HCl to 500 µl of liquid sample. The acidified samples were analyzed using DB-FFAP capillary column gas chromatography with a flame ionization detector (FID) (Agilent Technologies, Wilmington, DE). H_2 was used as the carrier gas. The gas samples were analyzed using a Carboxen 1010 PLOT capillary column (Supelco, Bellefonte, PA, USA) in a 6890N gas chromatography with a thermal conductivity detector (TDC) (Agilent Technologies, Wilmington, DE). A 100-µl sample from the TBR gas exit line was injected using a Hamilton gas tight syringe (Hamilton Co., Reno, NV). Argon was used as the carrier gas. The gas and liquid data analysis was done using Chemstation software (Agilent Technologies, Wilmington, DE). More details of the method used to analyze gas and liquid samples were described in Section 5.2.5.

6.3 Results and Discussion

6.3.1 Cell growth and pH

The cell OD_{660} and pH profiles in the TBR for syngas fermentation in counter-current and co-current modes are shown in Figure 6.2. The TBR was operated in semi-continuous mode in the first 197 h and then was switched to continuous operation. The TBR was operated in a counter-current mode until 1700 h. The flow mode was then changed to co-current to avoid flooding and gas bypass issues encountered in the counter-current operation. After 174 h of lag phase, the cells started to grow. The cell OD_{660} increased from 0.17 to 0.35 at 197 h. At 197 h the TBR was switch to continuous operation with a dilution rate set at 0.012 h^{-1} corresponding to a medium feed flow rate of 0.1 ml/min. This dilution rate corresponds to a liquid retention time of 83 h. The gas flow rate was 1.88 sccm. The cell OD_{660} increased to 0.53 at 207 h and remained constant until 224 h. The cell OD_{660} started decreasing slowly to 0.17 at 319 h. There was no positive effect on the cell OD_{660} when the gas flow rate was increased from 1.88 to 2.3 sccm at 261 h. A cell washout was observed at a dilution rate of 0.012 h^{-1}. Therefore, the medium feed flow rate was reduced to 0.05 ml/min at 305 h (i.e., dilution rate of 0.006 h^{-1} and a liquid retention time of 167 h). The decrease in the dilution rate resulted in an increase in a cell OD_{660} to 0.295 by 357 h.

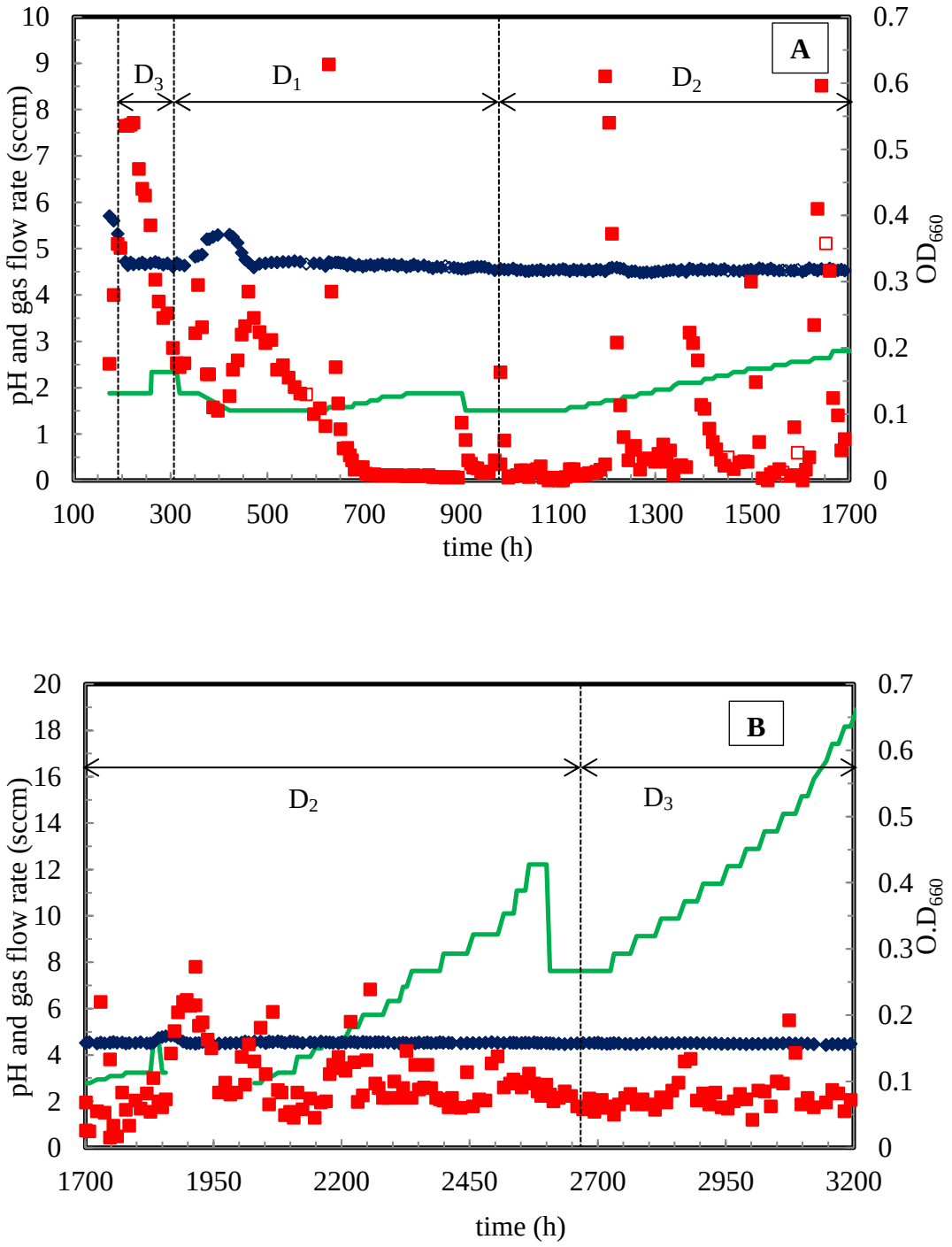

Figure 6.2 pH and Cell OD_{660} profiles during continuous syngas fermentation in (A) Counter-current (B) Co-current at various dilution rates (D_1, D_2 and D_3 of 0.006 h^{-1}, 0.0088 h^{-1} and 0.012 h^{-1}, respectively); (◆) pH (■) Cell $O.D_{660}$ (—) Gas flow rate. Open symbols indicate flooded TBR.0 h to 174 h: lag phase resulted in no data.

The fermentation was interrupted by a power shutdown, which resulted in no gas flow between 329 h to 351 h. This caused a decrease in cell activity (i.e., a decrease in CO and H_2 gas uptakes) up to 398 h. The cell OD_{660} dropped from 0.295 at 357 h to 0.1 at 398 h. The fermentation slowly recovered when the gas flow rate was decreased to 1.5 sccm at 375 h. The cell OD_{660} increased from 0.1 at 398 h to 0.285 at 461 h with a specific growth rate of 0.016 h^{-1} at 0.006 h^{-1} of dilution rate. The cell OD_{660} in the liquid medium dropped to approximately zero around 700 h. The TBR was flooded during counter-current flow mode at 627, 901, 909 and 981 h. Cells from the biofilm were resuspended into the medium when the pressure was released to clear the flooded medium between the beads. This resulted in a sudden increase of the measured cell OD_{660} in the medium. The flooding was initially observed at the top of the TBR at 627 h. Then, as more cells formed between the beads in the TBR, flooding was observed across the whole length of the TBR at 981 h. To avoid flooding issues caused by cell debris and clogging of void spaces in the TBR, the liquid recirculation rate was increased from 200 to 500 ml/min for 10 min intermittently at 1197, 1371, 1498, 1628, 1643 and 1652 h during the counter-current mode. In co-current mode from 1700 to 3200 h, the liquid recirculation was increased at every sampling time for 10 min because it had a positive effect on the ethanol production. The cell OD_{660} resuspended into the medium was less than 0.2 from 1700 h to 3200 h during co-current operation.

The TBR and glass beads were washed with DI water to calculate the total amount of cells attached to the beads in the TBR after 5 months of continuous fermentation (Table 6.1). The dry weight of cells accumulated in the TBR was 4.24 g.

The pictures of the cells attached to the TBR wall, beads and in product tank are shown in Appendix F.

Table 6.1 Cell mass balance from beads and TBR column wash with DI Water

samples description	OD_{660}			Cell mass[a]
	Sample 1	Sample 2	Average	g
1st wash of beads with 2 L DI water	4.68	4.17	4.43	3.40
2nd wash of beads with 1 L DI water	0.42	0.41	0.41	0.11
3rd wash of beads with 500 ml of DI water	0.15	0.11	0.13	0.00
column wash without beads in 1 L DI water	1.91	2.02	1.97	0.73
Total cell mass after 3700 h				4.24

a: cell dry weight in (g/L) = 0.396 x OD_{660} - 0.0521(Panneerselvam, 2009); Multiplying cell dry weight (g/L) with the volume of DI water with which the cells were washed equals the cell mass.

The pH of the medium decreased from 5.7 at 174 h to 4.7 at 207 h during the cell growth phase. The pH in the fermentation medium was maintained at 4.6 by the addition between 0.5 and 1 ml of 2 N KOH after every sampling time. During the recovery of fermentation activity after the power interruption between 375 h to 422 h, the pH slightly increased to 5.2 after addition of 1.75 ml of 2 N KOH to maintain pH slightly favorable to cell growth conditions. The pH dropped from 5.3 to 4.7 as cell OD_{660} increased between 422 h to 461 h. After 461 h, the pH was maintained between 4.5-4.6 by adding 0.5 to 1 ml of 2 N KOH at every sampling time.

6.3.2 Gas conversions

The CO and H_2 gas conversion profiles counter-current and co-current modes are shown in Figure 6.3. The CO and H_2 conversion efficiencies were 92% and 72%,

respectively, when the fermentation was switched from semi-continuous to continuous mode at 197 h. In counter-current mode, the TBR was operated at dilution rates of 0.012 h^{-1}, 0.0088 h^{-1} and 0.006 h^{-1} from 197 to 305 h, 305 to 989 h and 989 to 1700 h, respectively. At 0.012 h^{-1} and 1.88 sccm of gas flow rate, 93% CO and 74% H_2 conversion efficiencies were achieved. However, when the gas flow rate was increased to 2.34 sccm, the CO and H_2 conversion efficiencies slightly dropped to 88% and 71%, respectively. At 305 h, when the dilution rate was decreased to 0.006 h^{-1}, the CO and H_2 conversions continued to decrease and reached 81% CO and 60% H_2, respectively, at 2.34 sccm of gas flow rate.

At 319 h, the gas flow rate was reduced to 1.88 sccm and the conversion efficiencies increased to 88% CO and 74% H_2, respectively. However, the conversion efficiencies decreased when the fermentation was hindered from 329 to 422 h due to power shutdown and no gas flow between 329 h to 351 h. At 351 h and 1.88 sccm, the conversion efficiencies dropped to 40% CO and 31 % H_2. However, the fermentation slowly recovered when the gas flow rate was decreased to 1.5 sccm at 375 h, reaching conversion efficiencies of 92% CO and 86 % H_2 at 620 h. As the gas flow rate was increased from 1.51 to 1.88 sccm, the liquid medium flooded the TBR at 627 h, which resulted in a sharp decrease in gas conversion efficiencies, from 92 % CO and 86% H_2 at 620 h to 81% CO and 75% H_2 at 627 h (Figure 6.3). This decrease in the gas conversion efficiencies was attributed to the decrease in the cell activity. The TBR flooding caused the gas to bypass from the bottom of the TBR to the sump headspace and decreased the availability of syngas to the cells in the biofilm.

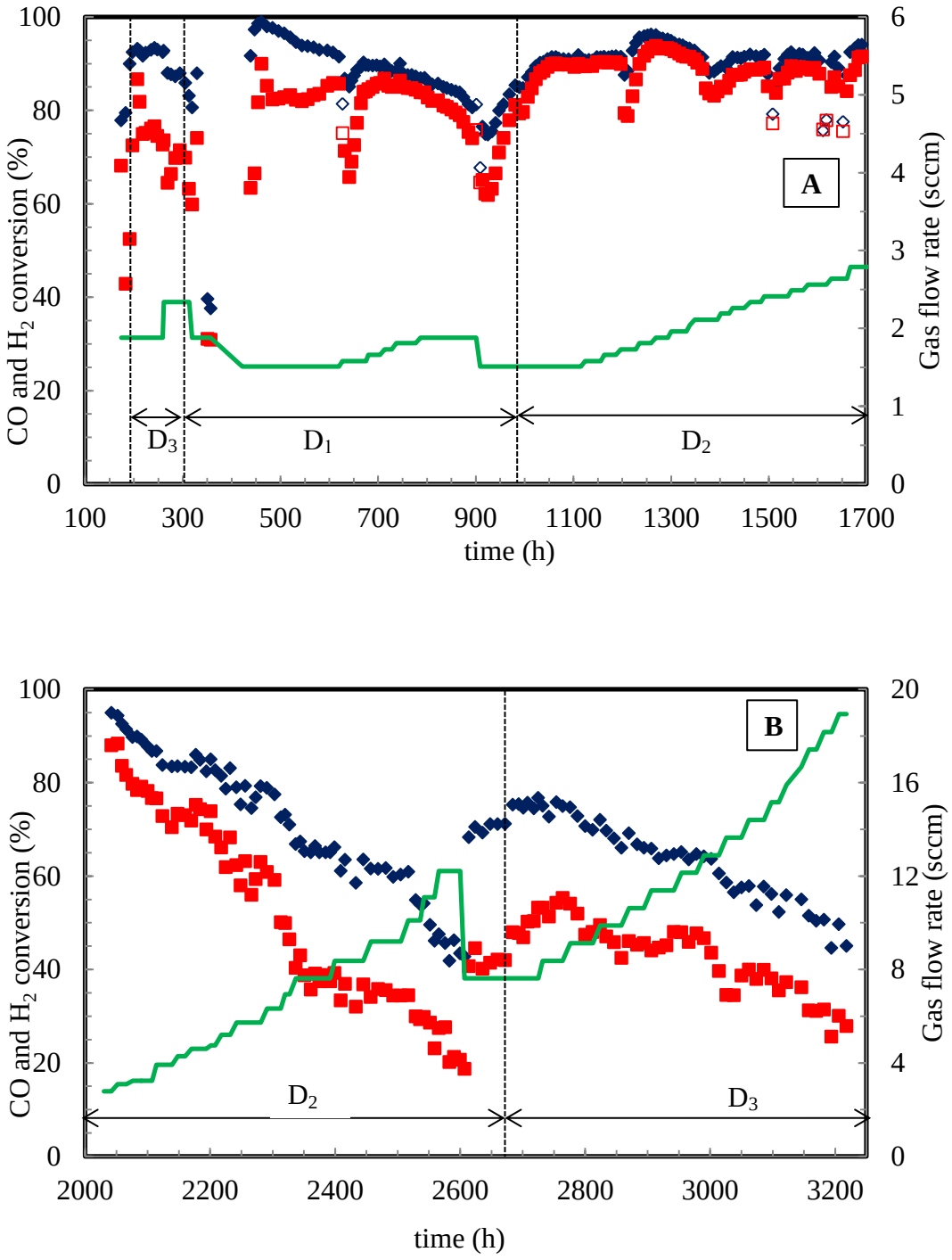

Figure 6.3 Gas conversions during continuous syngas fermentation in TBR (A) Counter-current (B) Co-current at various dilution rates (D_1, D_2 and D_3 are 0.006 h^{-1}, 0.0088 h^{-1} and 0.012 h^{-1}, respectively); (◆) % CO conversion (■) % H_2 conversion (—) Gas flow rate in sccm. Open symbols are points were reactor flooded. 0 h to 174 h: lag phase resulted in no data; 1700 h to 2042 h: gas leaks resulted in no gas analysis data.

Because of flooding at 901 h and 909 h with 1.88 sccm, the conversion efficiencies decreased to 68% CO and 65% H_2. The gas flow rate was then reduced to 1.5 sccm to avoid flooding and increase the gas conversion efficiencies. At 0.006 h^{-1} dilution rate, 981 h and 1.5 sccm, the gas conversion recovered to 85% CO and 81% H_2.The dilution rate was increased to 0.0088 h^{-1} at 989 h. Steady gas conversion efficiencies of 91 % CO and 90% H_2 were achieved from 989 to 1115 h. While the CO conversion efficiency was about the same at both 0.006 h^{-1} and 0.0088 h^{-1}, the H_2 conversion efficiency was 5% higher at 0.0088 h^{-1} than at 0.006 h^{-1} for the same gas flow rate. This increase in gas uptake could be due to increase in the rate of nutrients provided at higher dilution rate, which increased the cell optical density and cell activity. From 989 h to 1700 h, a sharp decrease in the CO and H_2 conversion efficiencies was observed at 1197, 1371, 1498, 1628, 1643 and 1652 h when the liquid recirculation rate was increased for 10 min to clear the cell debris in the TBR. Overall, from 989 to 1700 h at 0.0088 h^{-1} of dilution rate, the gas flow rate was increase from 1.51 sccm to 2.79 sccm resulting in about 91% CO and 89% H_2 conversion efficiencies.

In co-current mode, 0.0088 h^{-1} and 0.012 h^{-1} dilution rates were tested from 1700 to 2672 h and from 2672 to 3200 h. The fermentation was successfully performed without operational issues at gas flow rates as high as 12.22 and 18.93 sccm at dilution rates of 0.0088 h^{-1} and 0.012 h^{-1}, respectively. However, from 1700 to 2042 h, TBR gas inlet line leaked which resulted in inaccurate gas flow rate measurements and no gas analysis data was obtained during this time period. Hence, all the co-current results are discussed from 2042 h. From Figure 6.2 it can be observed that at 0.0088 h^{-1}, increasing the gas flow rate from 2.79 sccm at 2042 h to 12.22 sccm at 2607 h resulted in a decrease

in gas conversion efficiencies from 95% CO and 88% H_2 at 2042 h to 43% CO and 19% H_2 at 2607 h.

When the gas flow rate was decreased to 7.62 sccm at 2607 h at 0.0088 h^{-1}, the gas conversion efficiencies increased quickly to 71% CO and 42% H_2. These conversions efficiencies were slightly higher than the 65% CO and 38% H_2 conversion efficiencies observed at the same operating conditions at 2375 h. From Figure 6.2, it can also be observed that at low gas flow rates (2.79 to 7.62 sccm) the CO and H_2 conversion efficiencies only differed by 7% at 2042 h. However, when the gas flow rate was increased above 7.62 sccm, the H_2 conversion efficiencies decreased at a faster rate than when the gas flow rate was below 7.62 sccm. Further, the H_2 conversion efficiencies were 40% lower than the CO conversions at 2337 h.

In co-current mode, at 2672 h and 7.62 sccm when the dilution rate was increased to 0.012 h^{-1}, the CO and H_2 conversion efficiencies slightly increased and reached 77% CO and 53% H_2 at 2725 h. At the same gas flow, these conversions at 0.012 h^{-1} were 8% higher for CO and 21% higher for H_2 than at 0.0088 h^{-1}. Further, when the gas flow rate was increased from 8.37 sccm at 2732 h to 18.93 sccm at 3218 h, the CO and H_2 conversion efficiencies slowly dropped from 75% CO and 53% H_2 at 2732 h to 45% CO and 28% H_2, respectively. Also, the difference between CO and H_2 conversion efficiencies increased from 29% at 2732 h and 8.37 sccm to 38% at 3218 h. The difference between CO and H_2 conversion efficiencies at 0.012 h^{-1} of dilution rate is lower than the difference observed at 0.0088 h^{-1} indicating an increase in gas uptake at higher dilution rates. It can also be observed from Figure 6.3 that the decrease in CO and H_2 gas conversion efficiencies were slower at 0.012 h^{-1} than at 0.0088 h^{-1} indicating

higher gas uptakes at 0.012 h^{-1} than at 0.0088 h^{-1}. In a two stage CSTR continuous syngas fermentation, the increase in the dilution rate from 0.01 h^{-1} to 0.016 h^{-1} was reported to increase the cell OD_{600} from 9.9 to 17.8 due to supply of more nutrients (Richter et al., 2013). Additionally, the high cell concentration in the reactor would increase the rate of gas consumption (Klasson et al., 1991a). Because of increasing dilution rate and supplying nutrients, the gas conversion efficiency and uptake increased indicating more cell activity and mass in the biofilm.

6.3.3 Gas uptake profiles

The gas uptake profiles are shown in Figure 6.4 for counter-current and co-current operation. The specific gas uptake rates in mmol/gcell·h were not calculated because the cell mass in the biofilm varies and was not known at every time point. The calculations of specific uptake rate using the cell mass in the biofilm obtained at the end of the fermentation will result in inaccurate estimations as the cell mass could have varied with changing dilution rate. Hence, the gas uptakes are described only in terms of mmol/h.

The reactor was changed from semi-continuous to continuous operation at 197 h; the gas uptake rates at this time were 2 mmol/h of CO and 1.2 mmol/h of H_2 at 1.88 sccm. At 261 h when the gas flow rate was increased to 2.34 sccm, the uptake rates slightly increased to 2.5 mmol/h of CO and 1.5 mmol/h of H_2 at 294 h. At 305 h when the dilution rate was decreased to 0.006 h^{-1}, the gas uptake rates started decreasing and reached to 1.8 mmol/h of CO and 1 mmol/h of H_2 at 319 h. To recover the gas uptake rates, the gas flow rate was reduced to 1.88 sccm at 319 h. At 329 h, the uptake rates of CO and H_2 recovered back to 2 mmol/h and 1.2 mmol/h, respectively. However, when the fermentation was interrupted by a power failure the cell activity decreased and the gas

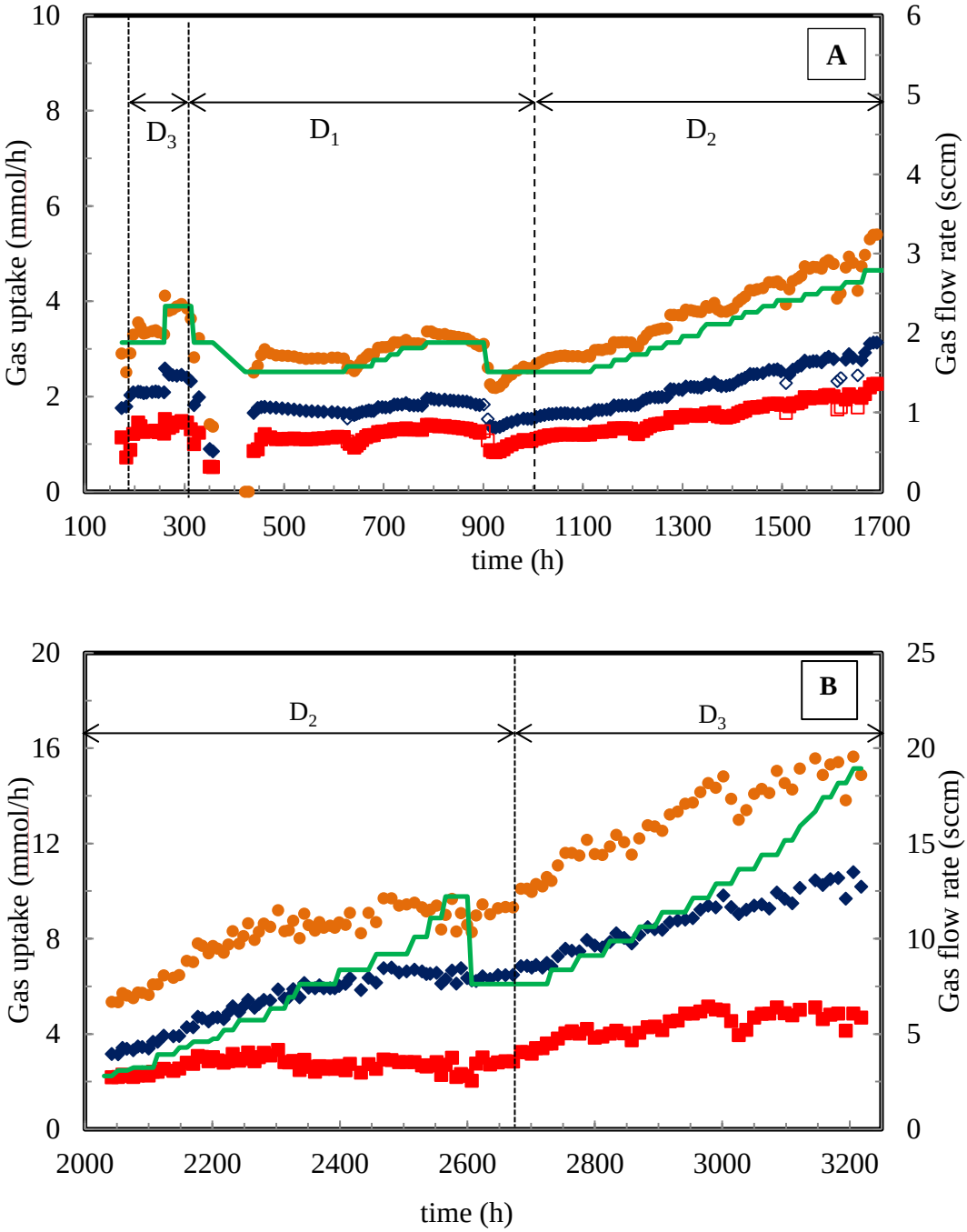

Figure 6.4 Gas uptake during continuous syngas fermentation in TBR (A) Counter-current (B) Co-current at various dilution rates (D_1, D_2 and D_3 are 0.006 h^{-1}, 0.0088 h^{-1} and 0.012 h^{-1}, respectively); (◆) CO uptake (■) H_2 uptake (●) $CO+H_2$ uptake (—) Gas flow rate D_1, D_2 and D_3 are 0.006 h^{-1}, 0.0088 h^{-1} and 0.012 h^{-1} dilution rates respectively. Open symbols are points were reactor flooded.0 h to 174 h: lag phase resulted in no data; 1700 h to 2042 h: gas leaks resulted in no gas analysis data.

flow rate was reduced to 1.51 sccm at 375 h to recover the fermentation. The gas flow rate was kept constant at 1.5 sccm and the dilution rate was maintained at 0.006 h^{-1} from 375 h to 620 h. At 620 h, the gas uptake rates were observed to be 1.7 mmol/h of CO and 1.1 mmol/h of H_2. From 620 h to 787 h, the gas flow rate was increased from 1.5 to 1.88 sccm. This resulted in a slight increase in CO and H_2 uptake rates to 2 mmol/h and 1.4 mmol/h at 787 h, respectively. These gas uptakes were maintained up to 900 h. However, flooding at 901 h and 909 h resulted in a decline of CO and H_2 uptake to 1.5 mmol/h and 1 mmol/h, respectively. Hence, the gas flow rate was decreased to 1.5 sccm at 909 h and was maintained at this flow rate until 981 h. At 981 h, the CO and H_2 uptake rates were still the same. However, since the same uptake rates were achieved at a lower gas flow rate the gas conversion efficiencies achieved increased as discussed in Section 6.3.2. From 989 to 1700 h, the dilution rate was maintained at 0.0088 h^{-1} during counter-current operation. A step increment of gas flow rate by 5-10 % from 1.5 sccm at 989 h to 2.79 sccm at 1700 h resulted in an increase of gas uptake rate to 3.1 mmol/h of CO and 2.1 mmol/h of H_2.

The gas flow rate was increased from 2.79 to 6.33 sccm in co-current mode from 1700 h to 2313 h at 0.0088 h^{-1}, which increased the gas uptake rates to 5.9 mmol/h CO and 3.3 mmol/h H_2 by 2313 h. Further increasing the gas flow rate from 6.33 to 12.22 sccm from 2313 to 2672 h resulted in a decrease of H_2 uptake rate to between 2.4 and 3.0 mmol/h, while the CO uptake rate increased between 6.0 and 6.7 mmol/h. The average CO and H_2 gas uptake rate from 2313 to 2672 h was 8.5 mmol/h. It can be observed that the increase in the dilution rate and gas flow rate increased the overall CO and H_2 uptake rates (Figure 6.4). In co-current flow, it was observed that increasing the dilution rate by

36% (0.0088 h^{-1} to 0.012 h^{-1}) resulted in an increase in total gas uptake of 47%. The gas uptake rates in co-current mode were 2.5 fold higher than in counter-current mode. This was attributed to the ability to operate the TBR in co-current mode at higher gas flow rates.

6.3.4 Product profiles

The ethanol and acetic acid profiles are shown in Figure 6.5. The ethanol and acetic acid concentrations were 0.59 g/L and 2.36 g/L, respectively, when continuous fermentation started at 197 h. Ethanol and acetic acid concentrations increased to 1.98 g/L and 4.98 g/L, respectively, from 197 to 305 h. From 329 h to 422 h, the ethanol and acetic acid concentrations decreased. This decrease was associated with the brief interruption in gas flow that ceased the fermentation for around 100 h and caused products wash out. At 422 h, the fermentation was recovered and the product concentrations started to increase. From 429 to 627 h, when the TBR was operated at 1.5 sccm and 0.006 h^{-1} the concentrations of ethanol and acetic acid at 627 h increased to 3.19 g/L and 6.15 g/L, respectively. From 627 to 787 h, when the gas flow rate was increased by 20% from 1.5sccm, the ethanol concentration increased by 20 % while the acetic acid concentration decreased by 20%. From 787 h to 909 h and at 1.88 sccm, the ethanol concentration slowly increased to 4.29 g/L while acetic acid concentration remained at 4.95 g/L. Due to flooding at 901 h and 909 h, the gas flow rate was reduced to 1.5 sccm and the TBR was allowed to recover back. At 989 h, the dilution rate was increased by 50% to 0.0088 h^{-1} and kept constant until 1700 h. A 50% increase in the dilution rate increased the product removal rate from the TBR, which decreased the

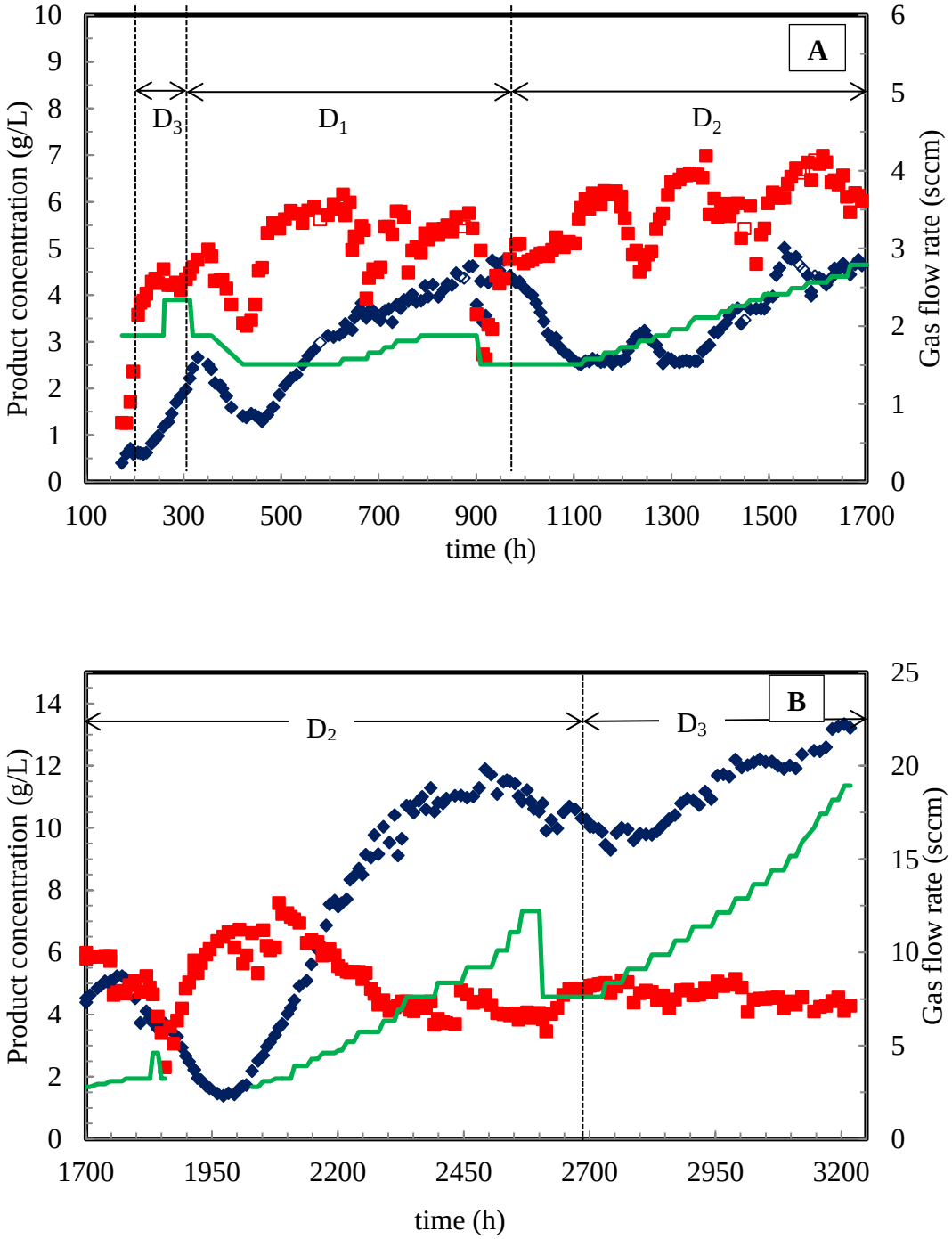

Figure 6.5 Product concentrations during continuous syngas fermentation in TBR. (A) Counter-current (B) Co-current at various dilution rates (D_1, D_2 and D_3 are 0.006 h^{-1}, 0.0088 h^{-1} and 0.012 h^{-1}, respectively); (◆) Ethanol in g/L (■) Acetic acid in g/L (—) Gas flow rate in sccm. D_1, D_2 and D_3 are 0.006 h^{-1}, 0.0088 h^{-1} and 0.012 h^{-1} dilution rates respectively. Open symbols are points were reactor flooded. 0 h to 174 h: lag phase resulted in no data.

ethanol concentration by about 40% to 2.51 g/L at 1115 h. However, the acetic acid concentration increased by 15% to around 5.86 g/L at 1115 h. This increase in acetic acid concentration could be due to an increase in rate of acetic acid production at higher dilution rate. As discussed in Section 6.3.2, the cell activity and concentration in the biofilm could have increased at higher dilution rate. The increase in cell concentration is associated with acetic acid production and ATP generation as high amount of energy is required for cell maintenance (Liu et al., 2014a).

From 1115 h to 1700 h, the gas flow rate was increased from 1.5 to 2.79 sccm in a step increment of 5% every 24 to 36 h. When the gas flow rate was increased from 1.51 to 1.73 sccm from 1115 to 1197 h, the ethanol and acetic acid concentrations were stable at 2.5 g/L and 6.2 g/L, respectively. Increasing the gas flow rate did not increase the ethanol or acetic acid produced. However, at 1197 h when the liquid recirculation rate was increased to 500 ml/min for 10 min to clear the cell debris, the ethanol concentration slowly increased and reached 3.24 g/L and acetic acid concentration slowly decreased to 4.66 g/L at 1245 h (Figure 6.5). This intermittent increase of liquid recirculation rate could have cleared the cell debris from the packing and had a positive effect on ethanol production.

From 1245 to 1324 h as the cell OD_{660} in the medium decreased from 0.61 to 0.03, the ethanol concentration started to decrease reaching a concentration of 2.58 g/L and the acetic acid concentration increased to 6.56 g/L by 1324 h and 1.96 sccm. The decrease in ethanol concentration occurred along with the decrease in cell OD_{660} in the medium. To test the positive effect of the intermittent increase of liquid recirculation rate on ethanol production, the liquid flow rate was again increased to 500 ml/min for 10 min

at 1371 h. The ethanol slowly increased and reached to 3.71 g/L while acetic acid slightly decreased to 4.66 g/L at 1474 h. Since, increasing the liquid recirculation rate intermittently had a positive effect on ethanol production, it was performed when the cell OD_{660} decreased to zero. This intermittent increase in liquid recirculation rate along with increasing gas flow rate resulted in 5.01 g/L of ethanol and 6.09 g/L of acetic acid at 1532 h and 2.41 sscm. From 1532 h to 1700 h, the gas flow rate was increased to 2.79 sccm. At 1700 h, 4.39 g/L of ethanol and 5.79 g/L of acetic acid were produced. Frequent flooding and gas bypass issues were encountered in counter-current operation that hindered the ability to increase the gas flow rate beyond 2.79 sccm. Hence, the operation was changed to co-current mode from 1700 h to 3200 h.

In co-current mode, gas flow rates were increased to as high as 18.93 sccm without operational issues. A step increment of gas flow rate by 5 to 10% every 24 to 36 h along with increase of the liquid recirculation rate to 500 ml/min for 10 min at every sampling time resulted in increased ethanol production. At 2052 h and 3.09 sccm, 2.69 g/L of ethanol and 6.71 g/L of acetic acid were produced (Figure 6.5). An increasing trend in ethanol production and a decreasing trend in acetic acid production were observed as the gas flow rate was increased from 3.09 sccm to 9.2 sccm. At 2493 h and 9.2 sccm, 11.88 g/L of ethanol and 4.63 g/L of acetic acid were produced. An increase in gas flow rate by 197% resulted in a 340% increase in ethanol production and a 30% decrease in acetic acid production.

Further increasing the gas flow rate from 9.2 to 11.09 sccm at 2542 h did not increase ethanol production. At 2542 h, the ethanol and acetic acid concentrations were 11.49 g/L and 3.96 g/L, respectively. Additionally, increasing the gas flow rate from

11.09 to 12.22 sccm slightly decrease the ethanol concentration to 10.53 g/L while the acetic acid concentration was stable at 4.05 g/L. This indicates that beyond a gas flow rate of 9.2 sccm, the cells reached a kinetic limitation and were not able to process more gas even when more gas was provided. Further when the gas flow rate was decreased from 12.2 sccm to 7.62 sccm at 2607 h, the ethanol and acetic acid concentrations were stable at 10.79 g/L and 3.84 g/L, respectively, and remained at these values until 2672 h. When the dilution rate was increased from 0.0088 h^{-1} to 0.012 h^{-1} at 2510 h, the ethanol concentration dropped slowly to 9.87 g/L. However the acetic acid concentration slightly increased to 4.98 g/L at 2551 h and 7.62 sccm. Further increase in the gas flow rate from 7.62 sccm to 18.93 sccm resulted in 13.21 g/L ethanol and 4.28 g/L acetic acid at 3218 h. The increase in the dilution rate from 0.0088 h^{-1} to 0.012 h^{-1}, decreased ethanol concentration by 16% while the acetic acid concentration was stable. However, more gas was processed by the cells at 0.012 h^{-1}, which resulted in 18% more ethanol production at 18.93 sccm and 0.012 h^{-1} than at 9.2 sccm and 0.0088h^{-1}.

Syngas fermentation bioreactors must maximize gas liquid mass transfer, while achieving high cell densities to promote fast reaction Klasson et al. (1991a). . As discussed in Section 6.3.2, high dilution rates supported high cell concentration in the TBR, which increased the cell activity. Also, the increase in the gas flow rate increased CO and H_2 transfer rates into the medium, which supported ethanol production.

6.3.5 Productivity and yields

The productivity and yields of ethanol and acetic acid are shown in Figure 6.6 . Ethanol and acetic acid yields and productivities were calculated using the following equations (Liu et al., 2012; Shuler and Kargi, 2002):

$$\text{Ethanol Yield} = \frac{\frac{\text{moles ethanol produced}}{\text{moles of CO consumed}}}{\frac{\text{1 mole ethanol produced}}{\text{6 moles CO consumed}}} \times 100\% \quad (6.1)$$

$$\text{Acetic acid Yield} = \frac{\frac{\text{moles Acetic acid produced}}{\text{moles CO consumed}}}{\frac{\text{1 mole acetic acid produced}}{\text{4 moles CO consumed}}} \times 100\% \quad (6.2)$$

$$P_i = D \cdot C_i \quad (6.3)$$

where, i is the product (ethanol or acetic acid) ; P_i is the productivity, g/L·h; D is the dilution rate, h^{-1}; C_i is product concentration , g/L.

The ethanol and acetic acid productivities were 0.014 g/L·h and 0.055 g/L·h, respectively, at 259 h, 0.012 h^{-1} and 1.88 sccm (Figure 6.6). At 261 h when the gas flow rate was increased to 2.34 sccm, ethanol productivity increased to 0.022 g/L·h while the acetic acid productivity decreased to 0.049 g/L·h by 294 h. At 0.006 h^{-1} dilution rate and 1.5 sccm, ethanol and acetic acid productivities at 620 h increased to 0.019 g/L·h and 0.035 g/L·h, respectively. Further increasing the gas flow rate and at a dilution rate of 0.006 h^{-1} ethanol productivity increased to 0.029 g/L·h with no changes to acetic acid productivity. As the gas flow rate was increased in slow increments to 2.79 sccm, the ethanol and acetic acid productivity increased to 0.041 g/L·h and 0.053 g/L·h, respectively, by 1691 h. During counter-current mode, it can be observed that the acetic acid productivity was always higher than the ethanol productivity.

From Figure 6.6 it can be observed that at 2005 h, acetic acid productivity was 0.059 g/L·h, which is about 76% higher than the ethanol productivity. After 2005 h, acetic acid productivity was slowly decreasing while ethanol productivity increased. At 2170 h, 4.6 sccm and 0.0088h^{-1}, the ethanol productivity increased to 0.054 g/L·h and acetic acid

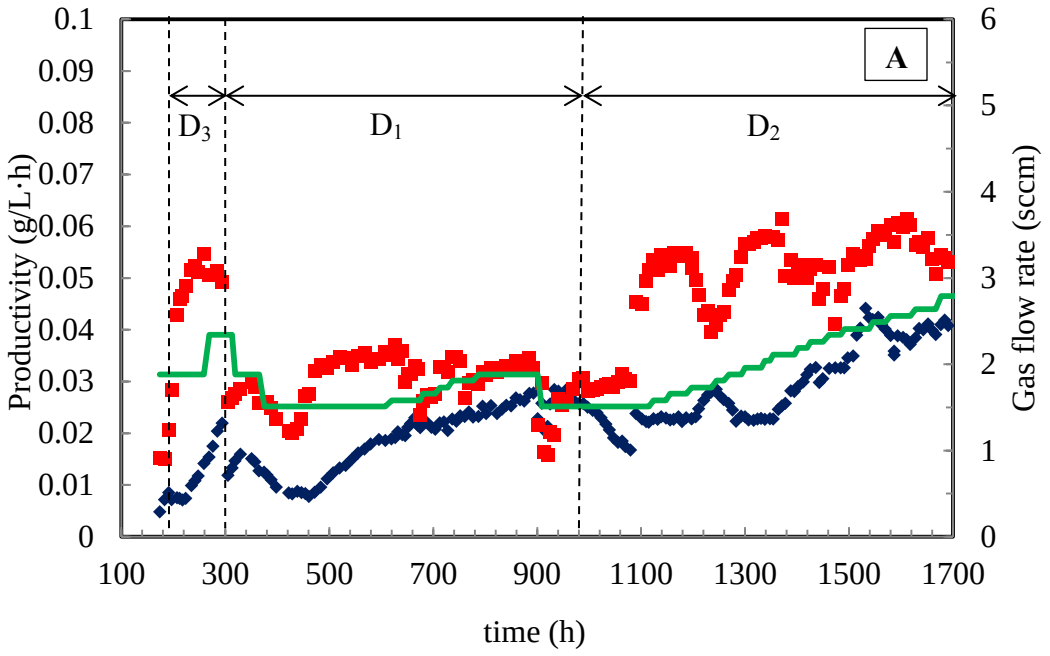
A
D3
D1
D2
Productivity (g/L·h)
Gas flow rate (sccm)
time (h)
0.1
0.09
0.08
0.07
0.06
0.05
0.04
0.03
0.02
0.01
0
6
5
4
3
2
1
0
100
300
500
700
900
1100
1300
1500
1700

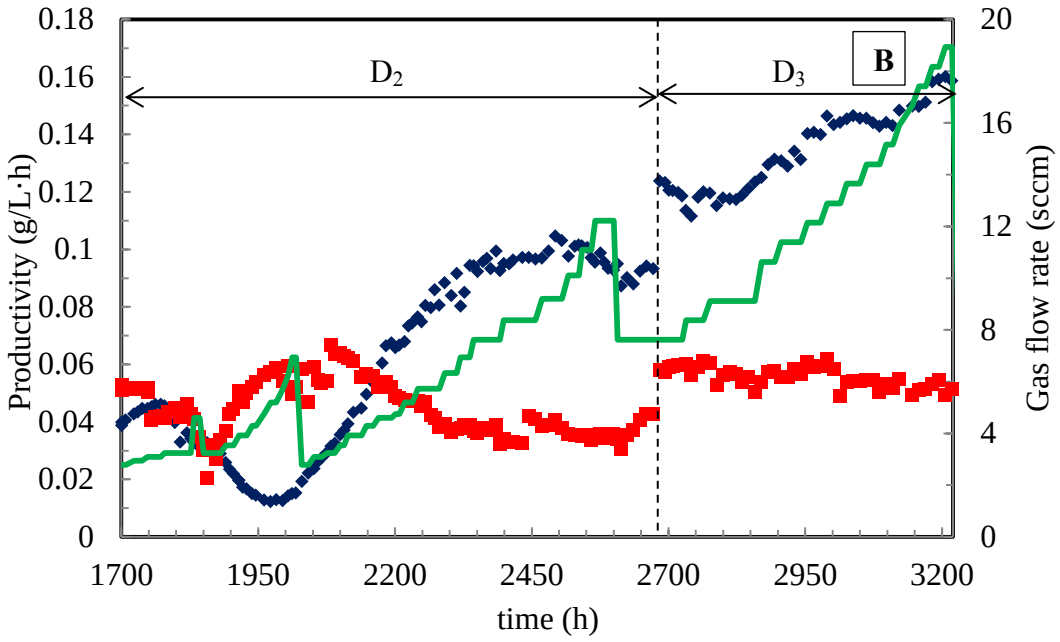
B
D2
D3
Productivity (g/L·h)
Gas flow rate (sccm)
time (h)
0.18
0.16
0.14
0.12
0.1
0.08
0.06
0.04
0.02
0
20
16
12
8
4
0
1700
1950
2200
2450
2700
2950
3200

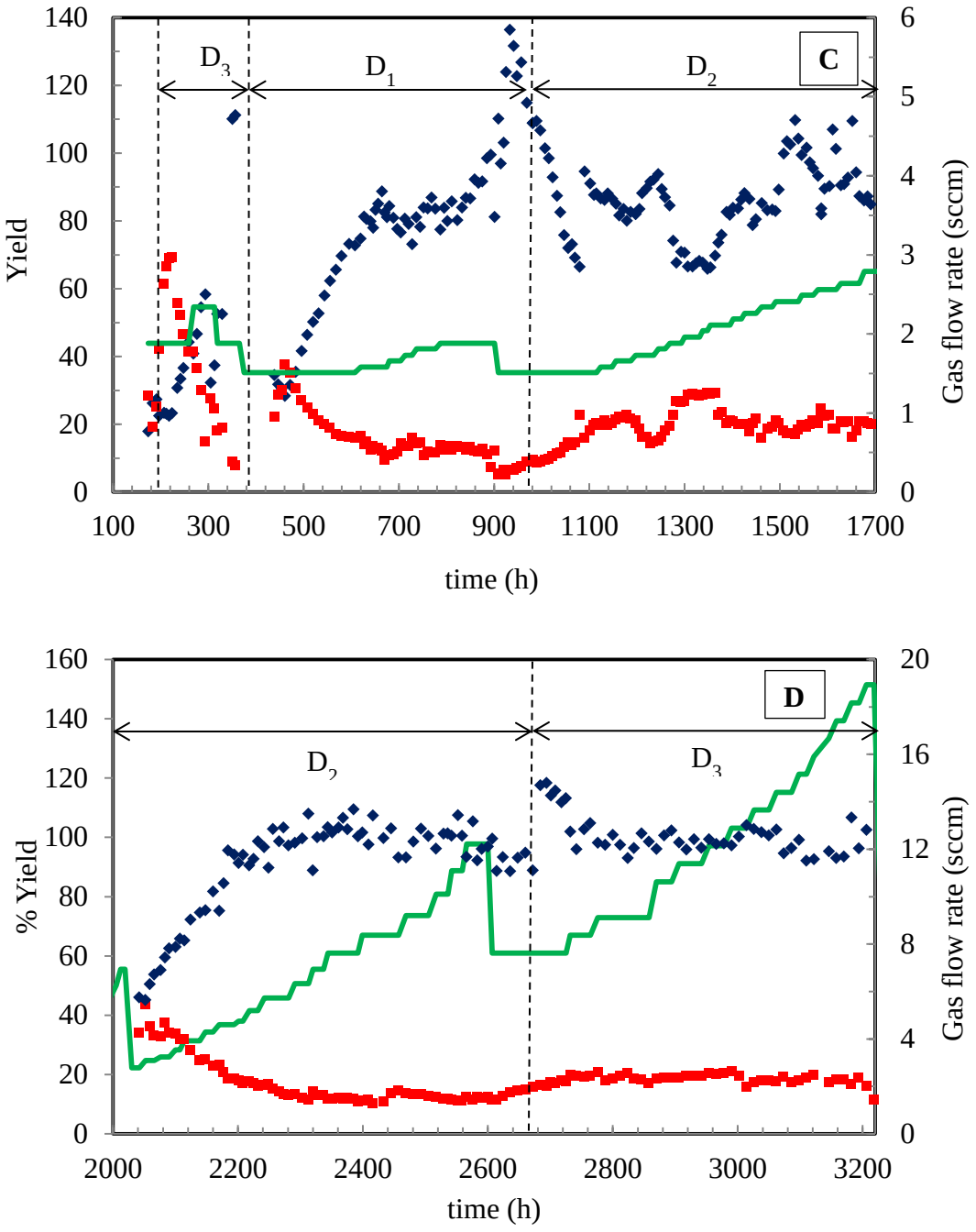

Figure 6.6 Productivity and product yield during continuous syngas fermentation in TBR

(A) Productivity, counter-current (B) Productivity, co-current (C) Yield, counter-current (D) Yield, in co-current at various dilution rates (D_1, D_2 and D_3 are 0.006 h^{-1}, 0.0088 h^{-1} and 0.012 h^{-1}, respectively.) (◆) Ethanol (■) Acetic acid (—) Gas flow rate in sccm. 0 h to 174 h: lag phase resulted in no data. 1700 h to 2042 h: gas leaks resulted in no gas analysis data.

productivity decreased to 0.052 g/L·h. From 2170 to 2672 h, at 0.0088h^{-1} with 10% increments increase in gas flow rate every 24-36 h, ethanol and acetic acid productivities reached maximum of 0.10 g/L·h and 0.041 g/L·h, respectively, at 2493 h and 9.2 sccm. When the gas flow rate was decreased to 7.62 sccm at 2607 h, the ethanol productivity slightly decreased to 0.093 g/L·h and the acetic acid productivity was stable at 0.042 g/L·h by 2672 h. At 2684 h, 7.62 sccm and 0.012 h^{-1}, the ethanol and acetic acid productivities were about 0.12 g/L·h and 0.058 g/L·h, respectively. At 7.62 sccm gas flow rate, the ethanol and acetic acid productivities were 0.124 g/L·h and 0.058 g/L·h, respectively, at 0.012 h^{-1} and up to 35% higher than at 0.0088 h^{-1}. Further at 0.012 h^{-1} dilution rate, when the gas flow rate was increased from 7.62 sccm to 18.93 sccm with 10% gas flow rate increments every 24 to 36 h, ethanol productivity increased to 0.16 g/L·h while acetic acid productivity was steady at 0.051 g/L·h by 3218 h.

The maximum ethanol productivity achieved in co-current mode was 4 times higher than that achieved during counter-current mode (Figure 6.6). Further, the maximum ethanol productivity achieved at a dilution rate of 0.012 h^{-1} was around 1.6 times higher than at 0.0088 h^{-1} during co-current operation. The TBR was operated at higher gas flow rates in co-current mode, which increased CO and H_2 transfer rates into the medium and resulted in higher ethanol productivity than in counter-current mode.

The maximum ethanol productivity achieved in the present study was 0.16 g/L·h at 18.93 sccm, 0.012 h^{-1} (Figure 6.6). This is higher than ethanol productivity of 0.11 g/L·h reported for *C. ljungdahlii* in CSTR without cell recycle or for *A. bacchi* in a CSTR (0.07 g/L·h) (Liu et al., 2014a; Mohammadi et al., 2012). However, the ethanol productivity in the present study was lower than the 0.37 g/L·h ethanol productivity

reported for *C. ljungdahlii* in a two stage CSTR with cell recycle (Richter et al., 2013). The highest ethanol productivity of 1.6-15 g/L·h was claimed for *C. ljungdahlii* when fermentation was performed using a syngas with high H_2:CO molar ratio (from 1.8:1 to 5:1) in a CSTR at 608 kPa (Gaddy et al., 2007).

The TBR should be optimized by employing better packing material that reduces the time for biofilm formation. Additionally, there is a need to recycle the exhaust gas or operate two TBRs in series to increase the syngas utilization and the overall gas conversion efficiency. The improvement in TBR performance is expected by utilizing better packing material for immobilization of cells and increasing the H_2:CO ratio in the syngas. Glass beads used in this study have a void fraction of 0.38, which is lower than the void fraction provided by other packing materials such as intalox saddles (0.6 to 0.9) and pall rings (0.9) (Coulson et al., 1999). Low void fraction reduces the availability of free space for gas-liquid mass transfer and decreases the reactive holdup volume. Further, use of cell immobilization techniques (Klein and Ziehr, 1990; Núñez and Lema, 1987) such as covalent coupling using cross linking agents, entrapment, and adsorption on packing with rough surfaces can reduce the time of the biofilm formation and improve the TBR performance.

Ethanol and acetic acid yields were calculated from Eqs 6.1 and 6.2. During counter-current mode, ethanol yield was 22% while the acetic acid yield was 42% at 197 h and 1.88 sccm (Figure 6.6). However, the acetic acid yield slowly dropped to 15% while the ethanol yield increased to 58% at 294 h. At dilution rate of 0.006 h^{-1} from 305 h to 989 h, the ethanol yield increased from 28% at 461 h to 85% at 850 h, while the acetic acid yield decreased from 38% at 461 h to 13% at 850 h. At dilution rate of 0.0088 h^{-1}

between 989 h and 1700 h, the average ethanol yield was 85% while the average acetic acid yield was 20%. As the gas flow rate was increased and the pH was maintained at 4.5, ethanol yields increased due to the availability of more reductant and favored solvent production conditions. In co-current operation from 1700 to 2672 h and at 0.0088 h^{-1}, the ethanol yield increased from 40% at 2042 h and reached to a maximum yield of 100% at 2232 h and remained close to 100% from 2232 to 2672 h with the increase in gas flow rate from 5.2 to 12.22 sccm. However, the acetic acid yield decreased from 49% at 2042 h to 16% at 2232 h and remained close to 13% from 2232 to 2672 h. Ethanol yield was about 100% and acetic acid yield was about 16% when the gas flow rate was increased from 7.62 to 18.93 sccm between 2672 to 3200 h and at 0.012 h^{-1}. In co-current operation, cells were able to process more gas and achieved high ethanol yield.

In semi-continuous fermentation in the TBR discussed in Chapter 5, the maximum CO and H_2 conversion efficiencies achieved at gas flow of 4.6 sccm rate in co-current mode were 82% (CO uptake rate of 4.4 mmol/h) and 55% (H_2 uptake rate of 2.2 mmol/h), respectively (Sections 5.3.3 and 5.3.4). In continuous fermentation during co-current mode, gas conversion efficiencies of 82% CO (CO uptake rate of 4.4 mmol/h uptake) and 72% H_2 (H_2 uptake rate of 2.74 mmol/h) were achieved at a gas flow rate of 4.6 sccm and dilution rate of 0.0088 h^{-1}.

In the semi-continuous fermentations, the medium was in batch mode and gas was fed continuously into the TBR with repetitive medium replacement to maintain cell activity. However, in continuous fermentation, both the medium and gas were fed continuously into the TBR. Further, at 4.6 sccm in semi-continuous fermentation a maximum ethanol productivity of 0.040 g/L·h was achieved while 0.054 g/L·h of ethanol

productivity was achieved during continuous fermentation. This clearly showed the advantage of continuous fermentation on gas uptake and ethanol productivity. Further, during continuous fermentation the gas uptake rates were increased by operating at high gas flow rates, i.e., 18.93 sccm, without any inhibition issues that were encountered during semi-continuous fermentations.

The maximum gas uptake rates of 10.2 mmol CO/h and 4.7 mmol H_2/h were achieved in continuous fermentation at a dilution rate of 0.012 h^{-1} and 18.93 sccm (Figure 6.4). These gas uptakes were twofold higher than in semi-continuous fermentation. In addition, the molar ratio of ethanol to acetic acid produced during continuous fermentation was 4:1 (at 0.012 h^{-1} and 18.93 sccm) which was higher than in semi-continuous fermentation (1:2 ratio produced). In semi-continuous fermentation, as the nutrients were depleted from the medium, the gas conversion efficiencies and uptake rates decreased. Replacement of the medium in semi-continuous fermentations resulted in a nutrient rich environment at pH 5.8 that promoted cell growth and thus more acetic acid production. However, during continuous fermentation the nutrients levels were maintained by altering the dilution rate and the pH was maintained at 4.5 that favored ethanol production.

6.4 Conclusion

The highest ethanol concentration, ethanol productivity and ethanol to acetic acid molar ratio of 13.2 g/L, 0.16 g/L·h and 4:1, respectively, were obtained during co-current continuous syngas fermentation at a dilution rate of 0.012 h^{-1} and gas flow rate of 18.93 sccm. Additionally, the maximum gas uptake rates of 10.2 mmol CO /h and 4.7 mmol H_2/h were achieved at the same conditions. Clearing the voids in the TBR from cell

debris increased ethanol production due to better contact between active cells and the gas in the medium. In co-current operation, the gas uptake rates doubled and ethanol productivity increased up to fivefold with the increase in the gas flow rate from 2.79 sccm to 18.93 sccm and dilution rate from 0.0088 h^{-1} to 0.012 h^{-1}. The overall TBR performance related to product formation and gas uptake in co-current mode was better and up to threefold higher than in counter-current mode because of processing more gas without flooding of the TBR.

Acknowledgments

This research was supported by a grant from the Sun Grant Initiative through the U.S. Department of Transportation and Oklahoma Agricultural Experiment Station.

CHAPTER VII

CONCLUSIONS AND RECOMMENDATIONS

7.1 Conclusions

Below are the key conclusions drawn from this research:

- The mass transfer coefficient in the reactive volume (k_La/V_L) in the trickle-bed reactor (TBR) with bead sizes of 3- and 6-mm increased with an increase in the gas flow rate from 5.5 to 130.9 sccm.
- The k_La/V_L decreased with an increase in the liquid flow rate due to the increase in the liquid holdup volume (V_L). The thickness of the liquid film on the beads and mass transfer resistance increased with V_L.
- The highest $k_{L,O2}\,a/V_L$ values obtained with 3- and 6-mm beads were 178 h^{-1} and 421 h^{-1}, respectively.
- The $k_{L,O2}a/V_L$ for the TBR (421 h^{-1}) was higher than k_La/V_L obtained from previously reported data for a stirred tank reactor (114 h^{-1}).

- The highest $k_{L,CO}\,a/V_L$ and $k_{L,H2}a/V_L$ values in the TBR with 6-mm beads were 435 h^{-1} and 613 h^{-1}, respectively. The maximum $k_{L,CO}\,a/V_L$ and $k_{L,H2}\,a/V_L$ values for 3-mm beads were 184 h^{-1} and 260 h^{-1}, respectively.
- In the semi-continuous fermentations, replenishing nutrients by replacing 80% of the exhausted medium with fresh medium resulted in formation of biofilm in the packing. A cell OD_{660} of about 2.5 was measured on the packing at the end of fermentation. Protein analysis of the washed beads showed no firm attachment of cells on the beads.
- At 4.6 sccm gas flow rate in semi-continuous fermentation, H_2 conversion efficiencies and uptake rates were about 18% and 0.71 mmol H_2/h, respectively, at 400 h. As the fermentation progressed and the biofilm was established on the beads, the H_2 conversion efficiencies and uptake rates increased by threefold at 800 h.
- At the end of the last semi-continuous fermentation, 12.3 g/L of acetic acid and 5.7 g/L of ethanol were produced. Acetic acid, a growth associated product, was produced in higher concentrations than ethanol due to the repetitive replenishment of nutrients by medium replacement that created growth supporting environment.
- A molar ratio of ethanol to acetic acid of 1:2 was produced during semi-continuous fermentations.
- During continuous syngas fermentation in the TBR, maximum CO and H_2 gas conversion efficiencies of up to 90 % was obtained when the gas flow rate was maintained between 1.5 to 2.79 sccm.
- Both CO and H_2 uptake rates increased with an increase in the gas flow rates (up to 9.2 sccm at dilution rate of 0.0088 h^{-1} and at 15.16 sccm with a dilution rate of 0.012

h^{-1}). The increase in the gas flow rate from 9.2 to 12.22 sccm at 0.0088 h^{-1} and from 15.16 to 18.93 sccm at 0.012 h^{-1}resulted in no further increase in gas uptake rates, which indicates a cell kinetic limitation at these conditions.

- During continuous syngas fermentation, CO and H_2 conversion efficiencies decreased by up to 60% and 80%, respectively, with an increase in the gas flow rate from 2.79 to 18.93 sccm irrespective of the increase in the gas uptake rates.
- Gas uptake rate, ethanol concentration and productivity increased by up to two fold with the increase in the dilution rate from 0.0088 h^{-1} to 0.012 h^{-1} in co-current mode.
- In continuous syngas fermentation when the TBR was operated in co-current mode, 13.2 g/L of ethanol was produced while acetic acid remained constant at 4.5 g/L at a dilution rate of 0.012 h^{-1}. The maximum ethanol productivity of 0.16 g/L·h was achieved at 0.012 h^{-1}. Further at 0.012 h^{-1}, the maximum gas uptakes of CO and H_2 obtained were 10.2 and 4.7 mmol/h, respectively.
- A molar ratio of ethanol to acetic acid of 4:1 was produced during continuous fermentation.
- Overall ability to operate the TBR at high gas flow rates resulted in better reactor performance in co-current mode than in counter-current operation in both semi-continuous and continuous fermentations.

7.2 Future Work

- The void fraction (ε) in the trickle-bed reactor provided by the glass beads is about 0.38, which is very low compared to the intalox saddles ($0.6 < \varepsilon < 0.9$) and Pall rings ($\varepsilon \approx 0.9$) that have better packing characteristics. Using a superior packing material

that provides more contact area and high void volume for gas and liquid contact should be explored.

- Efficient methods for cell immobilization on the packing should be studied. Better cell immobilization through adsorption can be achieved by using packing materials with rough surfaces. Covalent coupling of the cells by treating the packing material with a cross-linking agent should also be explored.
- Medium optimization through medium design to achieve high cell concentrations in a shorter time would drastically reduce the immobilization time.
- Continuous fermentation should be performed by replacing the standard yeast extract medium with a defined medium or minimum nutrient medium that supports ethanol production.
- Examination of different microorganisms such as *C. ljungdahlii, A. bacchi* or mixed cultures to produce ethanol or higher alcohols in the TBR can provide a better understanding of the TBR performance and capability compared to other reactors.

REFERENCES

Abrini, J., Naveau, H., Nyns, E.-J. 1994. *Clostridium autoethanogenum*, sp. Nov., an anaerobic bacterium that produces ethanol from carbon monoxide. *Archives of Microbiology*, 161(4), 345-351.

Ahmed, A. 2006. Effects of biomass-generated syngas on cell-growth, product distribution and enzyme activities of *Clostridium carboxidivorans* $P7^T$, Ph.D. Dissertation, Oklahoma State University, pp. 229.

Ahmed, A., Cateni, B.G., Huhnke, R.L., Lewis, R.S. 2006. Effects of biomass-generated producer gas constituents on cell growth, product distribution and hydrogenase activity of *Clostridium carboxidivorans* $P7^T$. *Biomass and Bioenergy*, 30(7), 665-672.

Ahmed, A., Lewis, R.S. 2007. Fermentation of biomass-generated synthesis gas: Effects of nitric oxide. *Biotechnology and Bioengineering*, 97(5), 1080-1086.

Allen, T.D., Caldwell, M.E., Lawson, P.A., Huhnke, R.L., Tanner, R.S. 2010. *Alkalibaculum bacchi* gen. Nov., sp. Nov., a co-oxidizing, ethanol-producing acetogen isolated from livestock-impacted soil. *International Journal of Systematic and Evolutionary Microbiology*, 60(10), 2483-2489.

Ayhan, D. 2001. Biomass resource facilities and biomass conversion processing for fuels and chemicals. *Energy Conversion and Management*, 42(11), 1357-1378.

Ayhan, D. 2007. Progress and recent trends in biofuels. *Progress in Energy and Combustion Science*, 33(1), 1-18.

Babu, B.K., Atiyeh, H., Wilkins, M., Huhnke, R. 2010. Effect of the reducing agent dithiothreitol on ethanol and acetic acid production by *Clostridium* strain P11 using simulated biomass-based syngas. *Biological Engineering*, 3(1), 19-35.

Bai, F., Anderson, W., Moo-Young, M. 2008. Ethanol fermentation technologies from sugar and starch feedstocks. *Biotechnology Advances*, 26(1), 89-105.

Bansal, A., Illukpitiya, P., Singh, S.P., Tegegne, F. 2013. Economic competitiveness of ethanol production from cellulosic feedstock in tennessee. *Renewable Energy*, 59(0), 53-57.

Barik, S., Prieto, S., Harrison, S., Clausen, E., Gaddy, J. 1988. Biological production of alcohols from coal through indirect liquefaction. *Applied Biochemistry and Biotechnology*, 18(1), 363-378.

Baskar, C., Baskar, S., Dhillon, R.S. 2012. *Biomass conversion: The interface of biotechnology, chemistry and materials science*. Springer-Verlag Berlin Heidelberg, New York, pp.450.

Belgiorno, V., De Feo, G., Della Rocca, C., Napoli, R.M.A. 2003. Energy from gasification of solid wastes. *Waste Management*, 23(1), 1-15.

Bothast, R., Schlicher, M. 2005. Biotechnological processes for conversion of corn into ethanol. *Applied Microbiology and Biotechnology*, 67(1), 19-25.

Bredwell, M.D., Worden, R.M. 1998. Mass-transfer properties of microbubbles. 1. Experimental studies. *Biotechnology Progress*, 14(1), 31-38.

Bredwell, M.D., Srivastava, P., Worden, R.M. 1999. Reactor design issues for synthesis-gas fermentations. *Biotechnology Progress*, 15(5), 834-844.

Bridgwater, A. 1994. Catalysis in thermal biomass conversion. *Applied Catalysis A: General*, 116(1), 5-47.

Bridgwater, A. 2001. Thermal conversion of biomass and waste: The status, Bio-Energy Research Group, Aston University. Birmingham. Accessed March 18th, 2014. http://www.scribd.com/doc/87343858/Thermal-Conversion-of-Biomass-and-Waste-The-Status.

Carriquiry, M.A., Du, X., Timilsina, G.R. 2011. Second generation biofuels: Economics and policies. *Energy Policy*, 39(7), 4222-4234.

Charpentier, J.-C. 1981. Mass-transfer rates in gas-liquid absorbers and reactors. in: *Advances in chemical engineering*, (Eds.) G.R.C.J.W.H. Thomas B. Drew, V. Theodore, Vol. Volume 11, Academic Press, pp. 1-133.

Conti, J., Holtberg, P., Doman, L. E., Smith, K. A., Sullivan, J. O., Vincent, K. R., Murphy, E. B. T. . 2011. International energy outlook 2011. in: *Washington: Independent Statistics and Analysis of US Energy Information Administration*. Accessed March 18th, 2014. http://large.stanford.edu/courses/2010/ph240/riley2/docs/EIA-0484-2010.pdf.

Coskata. 2011. Semi-commercial facility demonstrates two years of successful operation, Coskata, Inc.'s. Madison, PA. Accessed March 18th, 2014. http://www.coskata.com/company/media.asp?story=504B571C-0916-474E-BFFA-ACB326EFDB68.

Cotter, J.L., Chinn, M.S., Grunden, A.M. 2009. Ethanol and acetate production by *Clostridium ljungdahlii* and *Clostridium autoethanogenum* using resting cells. *Bioprocess and Biosystems Engineering*, 32(3), 369-380.

Coulson, J., Richardson, J., Sinnot, R. 1999. *Chemical engineering. An introduction to chemical engineering design. Vol. 6*. Pergamon Press, New York, USA, pp. 838.

Cowger, J.P., Klasson, K.T., Ackerson, M.D., Clausen, E., Caddy, J.L. 1992. Mass-transfer and kinetic aspects in continuous bioreactors using *Rhodospirillum rubrum*. *Applied Biochemistry and Biotechnology*, 34-35(1), 613-624.

Daniel, S.L., Hsu, T., Dean, S., Drake, H. 1990. Characterization of the H_2-and CO-dependent chemolithotrophic potentials of the acetogens *Clostridium thermoaceticum* and *Acetogenium kivui*. *Journal of Bacteriology*, 172(8), 4464-4471.

Das, A., Ljungdahl, L.G. 2003. Electron-transport system in acetogens. in: *Biochemistry and physiology of anaerobic bacteria*, Springer, pp. 191-204.

Daschle, T. 2007. Food for fuel-debating the tradeoffs of corn-based ethanol. *Foreign Affairs*, 86, 157.

Datar, R.P., Shenkman, R.M., Cateni, B.G., Huhnke, R.L., Lewis, R.S. 2004. Fermentation of biomass-generated producer gas to ethanol. *Biotechnology and Bioengineering*, 86(5), 587-594.

Dean, J.A. 1985. Physical properties. in: *Lange's handbook of chemistry*, Vol. 1, McGraw-Hill. New York, pp. 5.

Devi, M.P., Mohan, S.V., Mohanakrishna, G., Sarma, P. 2010. Regulatory influence of CO_2 supplementation on fermentative hydrogen production process. *International Journal of Hydrogen Energy*, 35(19), 10701-10709.

Diekert, G., Wohlfarth, G. 1994. Metabolism of homoacetogens. *Antonie Van Leeuwenhoek*, 66(1-3), 209-221.

Dien, B.S., Bothast, R.J., Nichols, N.N., Cotta, M.A. 2002. The us corn ethanol industry: An overview of current technology and future prospects. *International Sugar Journal*, 104(1241), 204-211.

Drake, H.L., Daniel, S.L. 2004. Physiology of the thermophilic acetogen *Moorella thermoacetica*. *Research in Microbiology*, 155(10), 869-883.

Drake, H.L., Gößner, A.S., Daniel, S.L. 2008. Old acetogens, new light. *Annals of the New York Academy of Sciences*, 1125(1), 100-128.

EIA. 2010. Annual energy outlook, (Ed.) D.o. Energy, U.S Energy Information Administration. Washington, D.C. Accessed March 18th, 2014. http://www.eia.gov/oiaf/aeo/pdf/0383(2010).pdf.

EIA. 2012. Petroleum statistics, Energy Information Administration. Washington, D.C. Accessed March 18th, 2014. http://www.eia.gov/energyexplained/index.cfm?page=oil_home#tab2.

EIA. 2013. This week in petroleum, U.S Energy Information Administration. Washington, D.C. Accessed March 18th, 2014. http://www.eia.gov/energy_in_brief/article/foreign_oil_dependence.cfm.

Fond, O., Jansen, N., Tsao, G. 1985. A model of acetic acid and 2, 3-butanediol inhibition of the growth and metabolism of *Klebsiella oxytoca*. *Biotechnology Letters*, 7(10), 727-732.

Fontaine, F., Peterson, W., McCoy, E., Johnson, M.J., Ritter, G.J. 1942. A new type of glucose fermentation by *Clostridium thermoaceticum*. *Journal of Bacteriology*, 43(6), 701-715.

Fraisse, L., Simon, H. 1988. Observations on the reduction of non-activated carboxylates by *Clostridium formicoaceticum* with carbon monoxide or formate and the influence of various viologens. *Archives of Microbiology*, 150(4), 381-386.

Frankman, A.W. 2009. Redox, pressure and mass transfer effects on syngas fermentation. in: *Department of Chemical Engineering*, MS Thesis, Brigham Young University, pp. 106.

Fukushima, S., Kusaka, K. 1977. Liquid-phase volumetric and mass-transfer coefficient, and boundary of hydrodynamic flow region in packed column with cocurrent downward flow. *Journal of Chemical Engineering of Japan*, 10(6), 468-474.

Gaddy, J.L., Clausen, E.C. 1992. *Clostridiumm ljungdahlii*, an anaerobic ethanol and acetate producing microorganism, U.S. Patent No. 5,173,429.

Gaddy, J.L., Arora, D.K., Ko, C.-W., Phillips, J.R., Basu, R., Wikstrom, C.V., Clausen, E.C. 2007. Methods for increasing the production of ethanol from microbial fermentation, U.S. Patent No. 7,285,402.

Gao, J., Atiyeh, H.K., Phillips, J.R., Wilkins, M.R., Huhnke, R.L. 2013. Development of low cost medium for ethanol production from syngas by *Clostridium ragsdalei*. *Bioresource Technology*, 147, 508-515.

Garcia-Ochoa, F., Gomez, E. 2009. Bioreactor scale-up and oxygen transfer rate in microbial processes: An overview. *Biotechnology Advances*, 27(2), 153-176.

German, L., Schoneveld, G.C., Pacheco, P. 2011. The social and environmental impacts of biofuel feedstock cultivation: Evidence from multi-site research in the forest frontier. *Ecology and Society*, 16(3), 24.

Gianetto, A., Specchia, V. 1992. Trickle-bed reactors: State of art and perspectives. *Chemical Engineering Science*, 47(13), 3197-3213.

Girbal, L., Croux, C., Vasconcelos, I., Soucaille, P. 1995. Regulation of metabolic shifts in *Clostridium acetobutylicum* atcc 824. *FEMS microbiology reviews*, 17(3), 287-297.

Gomez, L.D., Steele-King, C.G., McQueen-Mason, S.J. 2008. Sustainable liquid biofuels from biomass: The writing's on the walls. *New Phytologist*, 178(3), 473-485.

Goto, S., Smith, J. 1975. Trickle-bed reactor performance. Part I. Holdup and mass transfer effects. *AIChE Journal*, 21(4), 706-713.

Goto, S., Levec, J., Smith, J. 1977. Trickle-bed oxidation reactors. *Catalysis Reviews Science and Engineering*, 15(1), 187-247.

Gottschal, J., Morris, J. 1981. The induction of acetone and butanol production in cultures of *Clostridium acetobutylicum* by elevated concentrations of acetate and butyrate. *FEMS Microbiology Letters*, 12(4), 385-389.

Gottwald, M., Gottschalk, G. 1985. The internal pH of *Clostridium acetobutylicum* and its effect on the shift from acid to solvent formation. *Archives of Microbiology*, 143(1), 42-46.

Goyal, H., Seal, D., Saxena, R. 2008. Bio-fuels from thermochemical conversion of renewable resources: A review. *Renewable and Sustainable Energy Reviews*, 12(2), 504-517.

Grethlein, A.J., Worden, R.M., Jain, M.K., Datta, R. 1991. Evidence for production of *n*-butanol from carbon monoxide by *Butyribacterium methylotrophicum*. *Journal of Fermentation and Bioengineering*, 72(1), 58-60.

Gruenspecht, H. 2010. International energy outlook 2011. in: *Center for Strategic and International Studies*, U.S. Energy Information Administration. Washington, DC, pp. 21. Accessed March 18th, 2014. http://livebettermagazine.com/eng/reports_studies/pdf/International_Energy_Outlook_2010.pdf.

Gunjal, P.R., Kashid, M.N., Ranade, V.V., Chaudhari, R.V. 2005. Hydrodynamics of trickle-bed reactors: Experiments and cfd modeling. *Industrial & Engineering Chemistry Research*, 44(16), 6278-6294.

Guo, Y., Xu, J., Zhang, Y., Xu, H., Yuan, Z., Li, D. 2010. Medium optimization for ethanol production with *Clostridium autoethanogenum* with carbon monoxide as sole carbon source. *Bioresource Technology*, 101(22), 8784-8789.

Gutierrez, N.A. 1989. Role of motility and chemotaxis in solvent production by *Clostridium acetobutylicum* in: *Biotechnology*, Ph.D. Dissertation, Massey University, pp. 482.

Hartmanis, M.N., Klason, T., Gatenbeck, S. 1984. Uptake and activation of acetate and butyrate in *Clostridium acetobutylicum*. *Applied Microbiology and Biotechnology*, 20(1), 66-71.

Henstra, A.M., Sipma, J., Rinzema, A., Stams, A.J.M. 2007. Microbiology of synthesis gas fermentation for biofuel production. *Current Opinion in Biotechnology*, 18(3), 200-206.

Herskowitz, M., Smith, J.M. 1983. Trickle-bed reactors: A review. *AIChE Journal*, 29(1), 1-18.

Hickey, R., Basu, R., Datta, R., Tsai, S.-P. 2011. Method of conversion of syngas using microorganism on hydrophilic membrane, U.S. Patent 7,923,227.

Hu, P. 2011. Thermodynamic, sulfide, redox potential and pH effects on syngas fermentation. in: *Chemical Engineering*, Ph.D. Dissertation, Bringham Young University, pp. 206.

Hu, P., Bowen, S.H., Lewis, R.S. 2011. A thermodynamic analysis of electron production during syngas fermentation. *Bioresource Technology*, 102(17), 8071-8076.

Huber, G.W., Iborra, S., Corma, A. 2006. Synthesis of transportation fuels from biomass: Chemistry, catalysts, and engineering. *Chemical Reviews*, 106(9), 4044-4098.

Huhnke, R., Lewis, R.S., Tanner, R.S. 2010. Isolation and characterization of novel clostridial species, U.S. Patent no. 7,704,723.

Hurst, K.M. 2005. Effect of carbon monoxide and yeast extract on growth, hydrogenase activity and product formation of *Clostridium carboxidivorans* $P7^T$. in: *Chemical Engineering*, Master of Science, Oklahoma State University, pp. 160.

Hurst, K.M., Lewis, R.S. 2010. Carbon monoxide partial pressure effects on the metabolic process of syngas fermentation. *Biochemical Engineering Journal*, 48(2), 159-165.

IFIS. 2009. Dictionary of food science and technology. 2 ed, (Ed.) I.F.I. Service, Wiley-Blackwell. Singapore, pp. 488.

Iglesia, E., Reyes, S.C., Madon, R.J., Soled, S.L. 1993. *Selectivity control and catalyst design in the fischer-tropsch*. Academic Press, Inc., Iselin, New Jersey, pp.221.

INEOS. 2013. Ineos bio produces cellulosic ethanol at commercial scale, INEOS Bio. Vero Beach, FL. Accessed March 18th, 2014. http://www.ineos.com/en/businesses/INEOS-Bio/News/INEOS-Bio-Produces-Cellulosic-Ethanol/?business=INEOS+Bio.

Ismail, K.S.K., Najafpour, G., Younesi, H., Mohamed, A.R., Kamaruddin, A.H. 2008. Biological hydrogen production from co: Bioreactor performance. *Biochemical Engineering Journal*, 39(3), 468-477.

Jenkins, B., Baxter, L., Miles Jr, T., Miles, T. 1998. Combustion properties of biomass. *Fuel Processing Technology*, 54(1), 17-46.

Jones, D.T., Woods, D.R. 1986. Acetone-butanol fermentation revisited. *Microbiological Reviews*, 50(4), 484.

Jones, S.T. 2007. Gas-liquid mass transfer in an external airlift loop reactor for syngas fermentation. in: *Chemical Engineering*, Ph.D. Dissertation, Iowa State University, pp. 378.

Kellum, R., Drake, H.L. 1986. Effects of carbon monoxide on one-carbon enzymes and energetics of *Clostridium thermoaceticum*. *FEMS Microbiology Letters*, 34(1), 41-45.

Kimmel, D.E., Klasson, K.T., Clausen, E.C., Gaddy, J.L. 1991. Performance of trickle-bed bioreactors for converting synthesis gas to methane. *Applied Biochemistry and Biotechnology*, 28-29(1), 457-469.

Kitani, O., Hall, C.W. 1989. *Biomass handbook*. Gordon and Breach Science Publishers, New York, pp.963.

Klass, D.L. 2004. Biomass for renewable energy and fuels. in: *Encyclopedia of energy*, (Ed.) C.J. Cleveland, Elsevier. New York, pp. 193-212.

Klasson, K., Elmore, B., Vega, J., Ackerson, M., Clausen, E., Gaddy, J. 1990a. Biological production of liquid and gaseous fuels from synthesis gas. *Applied Biochemistry and Biotechnology*, 24(1), 857-873.

Klasson, K., Cowger, J., Ko, C., Vega, J., Clausen, E., Gaddy, J. 1990b. Methane production from synthesis gas using a mixed culture of *R. fubrum, M. barkeri,* and *M. formicicum*. *Applied Biochemistry and Biotechnology*, 24(1), 317-328.

Klasson, K., Ackerson, M., Clausen, E., Gaddy, J. 1991a. Bioreactor design for synthesis gas fermentations. *Fuel*, 70(5), 605-614.

Klasson, K., Ackerson, M., Clausen, E., Gaddy, J. 1991b. Bioreactors for synthesis gas fermentations. *Resources, Conservation and Recycling*, 5(2), 145-165.

Klasson, K., Gupta, A., Clausen, E., Gaddy, J. 1993a. Evaluation of mass-transfer and kinetic parameters for *Rhodospirillum rubrum* in a continuous stirred tank reactor. *Applied Biochemistry and Biotechnology*, 39(1), 549-557.

Klasson, K.T., Ackerson, M.D., Clausen, E.C., Gaddy, J.L. 1992. Bioconversion of synthesis gas into liquid or gaseous fuels. *Enzyme and Microbial Technology*, 14(8), 602-608.

Klasson, T.K., Ackerson, M.D., Clausen, E.C., Gaddy, J.L. 1993b. Biological conversion of coal and coal-derived synthesis gas. *Fuel*, 72(12), 1673-1678.

Klein, J., Ziehr, H. 1990. Immobilization of microbial cells by adsorption. *Journal of Biotechnology*, 16(1), 1-15.

Kumar, A., Jones, D.D., Hanna, M.A. 2009. Thermochemical biomass gasification: A review of the current status of the technology. *Energies*, 2(3), 556-581.

Kundiyana, D.K., Huhnke, R.L., Maddipati, P., Atiyeh, H.K., Wilkins, M.R. 2010. Feasibility of incorporating cotton seed extract in *Clostridium* strain P11 fermentation medium during synthesis gas fermentation. *Bioresource Technology*, 101(24), 9673-9680.

Kundiyana, D.K., Huhnke, R.L., Wilkins, M.R. 2011a. Effect of nutrient limitation and two-stage continuous fermentor design on productivities during "*Clostridium ragsdalei*" syngas fermentation. *Bioresource Technology*, 102(10), 6058-6064.

Kundiyana, D.K., Wilkins, M.R., Maddipati, P., Huhnke, R.L. 2011b. Effect of temperature, pH and buffer presence on ethanol production from synthesis gas by "*Clostridium ragsdalei*". *Bioresource Technology*, 102(10), 5794-5799.

Lee, P.-H. 2010. Syngas fermentation to ethanol using innovative hollow fiber membrane. in: *Civil, Construction and Environmental Engineering*, Ph.D. Dissertation, Iowa State University, pp. 157.

Lee, P.-H., Ni, S.-Q., Chang, S.-Y., Sung, S., Kim, S.-H. 2012. Enhancement of carbon monoxide mass transfer using an innovative external hollow fiber membrane (hfm) diffuser for syngas fermentation: Experimental studies and model development. *Chemical Engineering Journal*, 184, 268-277.

Lewis, R.S., Tanner, R.S., Huhnke, R.L. 2007. Indirect or direct fermentation of biomass to fuel alcohol, U.S. Patent no. 11/441,392.

Lewis, R.S., Frankman, A., Tanner, R.S., Ahmed, A., Huhnke, R.L. 2008. Ethanol via biomass-generated syngas. *International Sugar Journal*, 110(1311), 150-155.

Liew, F.M., Köpke, M., Simpson, S.a.D. 2013. Gas fermentation for commercial biofuels production, (Ed.) P.Z. Fang, IntechOpen. Rijeka, Croatia, pp. 125-173.

Liou, J.S.-C., Balkwill, D.L., Drake, G.R., Tanner, R.S. 2005. *Clostridium carboxidivorans* sp. Nov., a solvent-producing *Clostridium* isolated from an agricultural settling lagoon, and reclassification of the acetogen *Clostridium scatologenes* strain sl1 as *Clostridium drakei* sp. Nov. *International Journal of Systematic and Evolutionary Microbiology*, 55(5), 2085-2091.

Liu, K., Atiyeh, H.K., Tanner, R.S., Wilkins, M.R., Huhnke, R.L. 2012. Fermentative production of ethanol from syngas using novel moderately alkaliphilic strains of *Alkalibaculum bacchi*. *Bioresource Technology*, 104(0), 336-341.

Liu, K., Atiyeh, H.K., Stevenson, B.S., Tanner, R.S., Wilkins, M.R., Huhnke, R.L. 2014a. Continuous syngas fermentation for the production of ethanol, n-propanol and n-butanol. *Bioresource Technology*, 151(0), 69-77.

Liu, K., Atiyeh, H.K., Stevenson, B.S., Tanner, R.S., Wilkins, M.R., Huhnke, R.L. 2014b. Mixed culture syngas fermentation and conversion of carboxylic acids into alcohols. *Bioresource Technology*, 152(0), 337-346.

Ljungdahl, L., Wood, H. 1969. Total synthesis of acetate from CO_2 by heterotrophic bacteria. *Annual Reviews in Microbiology*, 23(1), 515-538.

Ljungdhal, L. 1986. The autotrophic pathway of acetate synthesis in acetogenic bacteria. *Annual Reviews in Microbiology*, 40(1), 415-450.

Maddipati, P. 2010. Ethanol production from syngas by *Clostridium* strain P11 using corn steep liquor as a nutrient replacement. in: *Biosystems Engineering*, M.S. Thesis, Oklahoma State University, pp. 164.

Maddipati, P., Atiyeh, H.K., Bellmer, D.D., Huhnke, R.L. 2011. Ethanol production from syngas by *Clostridium* strain P11 using corn steep liquor as a nutrient replacement to yeast extract. *Bioresource Technology*, 102(11), 6494-6501.

Madigan, M., Martinko, J., Parker, J. 2003. *Brock biology of microorganisms*. Prentice Hall, New Jersey, pp. 1019.

Mahajani, V., Sharma, M. 1979. Effective interfacial area and liquid side mass transfer coefficient in trikle bed reactors. *Chemical Engineering Science*, 34(12), 1425-1428.

Martínez, A., López, C. 2005. The influence of zsm-5 zeolite composition and crystal size on the in situ conversion of fischer–tropsch products over hybrid catalysts. *Applied Catalysis A: General*, 294(2), 251-259.

McCarl, B.A., Boadu, F.O. 2009. Bioenergy and us renewable fuels standards: Law, economic, policy/climate change and implementation concerns. *Drake Journal of Agricultural Law*, 14, 43.

McKendry, P. 2002. Energy production from biomass (part 2): Conversion technologies. *Bioresource Technology*, 83(1), 47-54.

Mohammadi, M., Najafpour, G.D., Younesi, H., Lahijani, P., Uzir, M.H., Mohamed, A.R. 2011. Bioconversion of synthesis gas to second generation biofuels: A review. *Renewable and Sustainable Energy Reviews*, 15(9), 4255-4273.

Mohammadi, M., Younesi, H., Najafpour, G., Mohamed, A.R. 2012. Sustainable ethanol fermentation from synthesis gas by C*lostridium ljungdahlii* in a continuous stirred tank bioreactor. *Journal of Chemical Technology & Biotechnology*, 87(6), 837-843.

Munasinghe, P.C., Khanal, S.K. 2010a. Biomass-derived syngas fermentation into biofuels: Opportunities and challenges. *Bioresource Technology*, 101(13), 5013-5022.

Munasinghe, P.C., Khanal, S.K. 2010b. Syngas fermentation to biofuel: Evaluation of carbon monoxide mass transfer coefficient (kla) in different reactor configurations. *Biotechnology Progress*, 26(6), 1616-1621.

Naik, S., Goud, V.V., Rout, P.K., Dalai, A.K. 2010. Production of first and second generation biofuels: A comprehensive review. *Renewable and Sustainable Energy Reviews*, 14(2), 578-597.

Najafpour, G., Younesi, H. 2006. Ethanol and acetate synthesis from waste gas using batch culture of *Clostridium ljungdahlii*. *Enzyme and Microbial Technology*, 38(1–2), 223-228.

NCOB. 2011. Biofuels: Ethical issues, Nuffield Councl on Bioethics. London, pp. 226. Accessed March 18th, 2014. http://nuffieldbioethics.org/biofuels-0.

Nigam, P., Singh, D. 1995. Enzyme and microbial systems involved in starch processing. *Enzyme and Microbial Technology*, 17(9), 770-778.

Núñez, M., Lema, J. 1987. Cell immobilization: Application to alcohol production. *Enzyme and Microbial Technology*, 9(11), 642-651.

Orgill, J.J., Atiyeh, H.K., Devarapalli, M., Phillips, J.R., Lewis, R.S., Huhnke, R.L. 2013. A comparison of mass transfer coefficients between trickle-bed, hollow fiber membrane and stirred tank reactors. *Bioresource Technology*, 133, 340-346.

Pandey, A. 2010. *Handbook of plant-based biofuels*. CRC Press, Boca Raton, FL, pp.312.

Panneerselvam, A., Wilkins, M., DeLorme, M., Atiyeh, H., Huhnke, R. 2009. Effects of various reducing agents on syngas fermentation by "*Clostridium ragsdalei*". *Biological Engineering*, 2(3), 135-144.

Panneerselvam, A. 2009. Effect of glucose and reducing agents on syngas fermentation by *Clostridia* species P11. in: *Biosystems Engineering*, M.S. Thesis, Oklahoma State University, pp. 91.

Perez, J.M., Richter, H., Loftus, S.E., Angenent, L.T. 2013. Biocatalytic reduction of short-chain carboxylic acids into their corresponding alcohols with syngas fermentation. *Biotechnology and Bioengineering*, 110(4), 1066-1077.

Phillips, J.R., Klasson, T.K., Clausen, E.C., Gaddy, J.L. 1993. Biological production of ethanol from coal synthesis gas. *Applied Biochemistry and Biotechnology*, 39-40(1), 559-571.

Phillips, J.R., Clausen, E.C., Gaddy, J.L. 1994. Synthesis gas as substrate for the biological production of fuels and chemicals. *Applied Biochemistry and Biotechnology*, 45(1), 145-157.

Phillips, S., Eggeman, T.J. 2007. Thermochemical ethanol via indirect gasification and mixed alcohol synthesis of lignocellulosic biomass. National Renewable Energy Laboratory, Golden, Colorado, pp.125.

Po, H.N., Senozan, N. 2001. The Henderson-Hasselbalch equation: Its history and limitations. *Journal of Chemical Education*, 78(11), 1499.

Ragauskas, A.J., Williams, C.K., Davison, B.H., Britovsek, G., Cairney, J., Eckert, C.A., Frederick, W.J., Hallett, J.P., Leak, D.J., Liotta, C.L., Mielenz, J.R., Murphy, R., Templer, R., Tschaplinski, T. 2006. The path forward for biofuels and biomaterials. *Science*, 311(5760), 484-489.

Ragsdale, S.W. 1997. The eastern and western branches of the wood/ljungdahl pathway: How the east and west were won. *Biofactors*, 6(1), 3-11.

Ragsdale, S.W., Pierce, E. 2008. Acetogenesis and the wood–ljungdahl pathway of CO_2 fixation. *Biochimica et Biophysica Acta (BBA)-Proteins and Proteomics*, 1784(12), 1873-1898.

Rajagopalan, S., P. Datar, R., Lewis, R.S. 2002. Formation of ethanol from carbon monoxide via a new microbial catalyst. *Biomass and Bioenergy*, 23(6), 487-493.

Rajvanshi, A.K. 1986. Biomass gasification. *Alternative Energy in Agriculture*, 2, 83-102.

Ramachandran, P., Chaudhari, R. 1983. *Three-phase catalytic reactors*. Gordon and Breach Science Publishers, New York, pp.427.

Ramachandriya, K.D., Wilkins, M.R., Delorme, M.J., Zhu, X., Kundiyana, D.K., Atiyeh, H.K., Huhnke, R.L. 2011. Reduction of acetone to isopropanol using producer gas fermenting microbes. *Biotechnology and Bioengineering*, 108(10), 2330-2338.

Ranade, V.V., Chaudhari, R., Gunjal, P.R. 2011a. *Trickle bed reactors: Reactor engineering & applications*. *1st ed*. Elsevier Science Limited, Kidlington, Oxford, pp.284.

Ranade, V.V., Chaudhari, R., Gunjal, P.R. 2011b. *Trickle bed reactors: Reactor engineering & applications*. Elsevier, UK.

Rao, G., Mutharasan, R. 1986. Alcohol production by C*lostridium acetobutylicum* induced by methyl viologen. *Biotechnology Letters*, 8(12), 893-896.

Rao, G., Ward, P., Mutharasan, R. 1987. Manipulation of end-product distribution in strict anaerobes. *Annals of the New York Academy of Sciences*, 506(1), 76-83.

Rausch, K., Belyea, R. 2006. The future of coproducts from corn processing. *Applied Biochemistry and Biotechnology*, 128(1), 47-86.

Reeves, A. 2011. Recombinant microorganisms having modified production of alcohols and acids, U.S. Patent No. 8,039,239.

Reiss, L. 1967. Cocurrent gas-liquid contacting in packed columns. *Industrial & Engineering Chemistry Process Design and Development*, 6(4), 486-499.

Richter, H., Martin, M., Angenent, L. 2013. A two-stage continuous fermentation system for conversion of syngas into ethanol. *Energies*, 6(8), 3987-4000.

Riggs, S.S., Heindel, T.J. 2006. Measuring carbon monoxide gas—liquid mass transfer in a stirred tank reactor for syngas fermentation. *Biotechnology Progress*, 22(3), 903-906.

Rodríguez, L.F., Li, C., Khanna, M., Spaulding, A.D., Lin, T., Eckhoff, S.R. 2010. An engineering and economic evaluation of quick germ–quick fiber process for dry-grind ethanol facilities: Analysis. *Bioresource Technology*, 101(14), 5282-5289.

Sakai, S., Nakashimada, Y., Yoshimoto, H., Watanabe, S., Okada, H., Nishio, N. 2004. Ethanol production from h_2 and co_2 by a newly isolated thermophilic bacterium, *Moorella sp.* Huc22-1. *Biotechnology Letters*, 26(20), 1607-1612.

Sanchez, O.J., Cardona, C.A. 2008. Trends in biotechnological production of fuel ethanol from different feedstocks. *Bioresource Technology*, 99(13), 5270-5295.

Saroha, A., Nigam, K. 1996. Trickle bed reactors. *Reviews in Chemical Engineering*, 12(3-4), 207-347.

Sato, Y., Hirose, T., Takahashi, F., Toda, M. 1972. Performance of fixed-bed catalytic reactor with co-current gas− liquid flow. *Pacific Chemical Engineering Congress*, 8-3.

Savage, M.D., Wu, Z., Daniel, S.L., Lundie, J., Leon, L., Drake, H.L. 1987. Carbon monoxide-dependent chemolithotrophic growth of *Clostridium thermoautotrophicum*. *Applied and Environmental Microbiology*, 53, 1902-1906.

Saxena, J. 2008. Development of an optimized and cost-effective medium for ethanol production by *Clostridium* strain P11. in: *Department of Botany and Microbiology*, Ph.D. Dissertation, University of Oklahoma. Ann Arbor, pp. 131.

Saxena, J., Tanner, R.S. 2011. Effect of trace metals on ethanol production from synthesis gas by the ethanologenic acetogen, *Clostridium ragsdalei*. *Journal of Industrial Microbiology & Biotechnology*, 38(4), 513-521.

Saxena, R., Adhikari, D., Goyal, H. 2009. Biomass-based energy fuel through biochemical routes: A review. *Renewable and Sustainable Energy Reviews*, 13(1), 167-178.

Saxena, R.C., Seal, D., Kumar, S., Goyal, H.B. 2008. Thermo-chemical routes for hydrogen rich gas from biomass: A review. *Renewable and Sustainable Energy Reviews*, 12(7), 1909-1927.

Searchinger, T., Heimlich, R., Houghton, R.A., Dong, F., Elobeid, A., Fabiosa, J., Tokgoz, S., Hayes, D., Yu, T.-H. 2008. Use of us croplands for biofuels increases greenhouse gases through emissions from land-use change. *Science*, 319(5867), 1238-1240.

Senior, A. 1988. Atp synthesis by oxidative phosphorylation. *Physiological Reviews*, 68(1), 177-231.

Sherwood, T.K., Pigford, R.L., Wilke, C.R. 1975. *Mass transfer*. McGraw-Hill Inc., New York, pp.512.

Shuler, M.L., Kargi, F. 2002. *Bioprocess engineering*. Prentice Hall New York, pp.576.

Sie, S., Krishna, R. 2011. Process development and scale up: III. Scale-up and scale-down of trickle bed processes. *Reviews in Chemical Engineering*, 14(3), 203-252.

Sierra, R., Smith, A., Granda, C., Holtzapple, M.T. 2008. Producing fuels and chemicals from lignocellulosic biomass. *Chemical Engineering Progress*, 104(8), 10.

Sim, J.H., Kamaruddin, A.H. 2008. Optimization of acetic acid production from synthesis gas by chemolithotrophic bacterium– *Clostridium aceticum* using statistical approach. *Bioresource Technology*, 99(8), 2724-2735.

Simpson, S.D., Collet, C., Cockrem, M., Oakley, S.D., Koepke, M. 2013. Carbon capture in fermentation, US Patent no. 8376736

Sims, R., Taylor, M., Saddler, J., Mabee, W. 2008. From 1st-to 2nd-generation biofuel technologies: *An overview of current industry and rd&d activities*, International

Energy Agency. Paris, France, pp. 120. http://environmentportal.in/files/2nd_Biofuel_Gen.pdf.

Skidmore, B.E. 2010. Syngas fermentation: Quantification of assay technoques, reaction kinetics and pressure dependencies of the *Clostridium* P11 hydrogenase. in: *Department of Chemical Engineering*, M.S. Thesis, Bringham Young University, pp. 136.

Slepova, T.V., Sokolova, T.G., Lysenko, A.M., Tourova, T.P., Kolganova, T.V., Kamzolkina, O.V., Karpov, G.A., Bonch-Osmolovskaya, E.A. 2006. *Carboxydocella sporoproducens* sp. Nov., a novel anaerobic CO-utilizing/H_2-producing thermophilic bacterium from a kamchatka hot spring. *International Journal of Systematic and Evolutionary Microbiology*, 56(4), 797-800.

Stöcker, M. 2008. Biofuels and biomass-to-liquid fuels in the biorefinery: Catalytic conversion of lignocellulosic biomass using porous materials. *Angewandte Chemie International Edition*, 47(48), 9200-9211.

Sylvester, N.D., Pitayagulsarn, P. 1975. Mass transfer for two-phase cocurrent downflow in a packed bed. *Industrial & Engineering Chemistry Process Design and Development*, 14(4), 421-426.

Szczodrak, J., Fiedurek, J. 1996. Technology for conversion of lignocellulosic biomass to ethanol. *Biomass and Bioenergy*, 10(5), 367-375.

Tang, I., Okos, M.R., Yang, S.T. 1989. Effects of pH and acetic acid on homoacetic fermentation of lactate by *Clostridium formicoaceticum*. *Biotechnology and bioengineering*, 34(8), 1063-1074.

Tanner, R.S., Miller, L.M., Yang, D. 1993. *Clostridium ljungdahlii* sp. Nov., an acetogenic species in clostridial rrna homology group i. *International Journal of Systematic Bacteriology*, 43(2), 232-236.

Tanner, R.S., Wall, J., Harwood, C., Demain, A. 2008. Production of ethanol from synthesis gas. *Bioenergy*. ASM Press. pp. 147-151.

Tenenbaum, D.J. 2008. Food *vs*. Fuel: Diversion of crops could cause more hunger. *Environmental Health Perspectives*, 116(6), A254.

Terrill, J., Wilkins, M., DeLorme, M., Atiyeh, H., Lewis, R. 2012. Effect of energetic gas composition on hydrogenase activity and ethanol production in syngas fermentation by *Clostridium ragsdalei*. . *Biological Engineering Transactions*, 8, 87-96.

Tilman, D., Hill, J., Lehman, C. 2006. Carbon-negative biofuels from low-input high-diversity grassland biomass. *Science*, 314(5805), 1598-1600.

Turek, F., Lange, R. 1981. Mass transfer in trickle-bed reactors at low reynolds number. *Chemical Engineering Science*, 36(3), 569-579.

Turkenburg, W.C. 2000. Renewable energy technologies. UNDP/UNDESA/WEC: Energy and the Challenge of Sustainability. World Energy Assessment. New York: UNDP, 219-272.

Twidell, J., Weir, T. 2003. *Renewable energy resources*. Taylor & Francis Group, New York, pp.601.

Ufford, R.C., Perona, J.J. 1973. Liquid phase mass transfer with concurrent flow through packed towers. *AIChE Journal*, 19(6), 1223-1226.

Ukpong, M.N., Atiyeh, H.K., De Lorme, M.J., Liu, K., Zhu, X., Tanner, R.S., Wilkins, M.R., Stevenson, B.S. 2012. Physiological response of *Clostridium carboxidivorans* during conversion of synthesis gas to solvents in a gas-fed bioreactor. *Biotechnology and Bioengineering*, 109(11), 2720-2728.

Ungerman, A.J., Heindel, T.J. 2007. Carbon monoxide mass transfer for syngas fermentation in a stirred tank reactor with dual impeller configurations. *Biotechnology progress*, 23(3), 613-620.

USGC. 2012. Ddgs user handbook, US Grains Council. Washington, DC, pp. 406. http://www.ethanolrfa.org/page/-/rfa-association-site/studies/2012_DDGS_Handbook.pdf?nocdn=1.

Vega, J.L., Prieto, S., Elmore, B.B., Clausen, E.C., Gaddy, J.L. 1989. The biological production of ethanol from synthesis gas. *Applied Biochemistry and Biotechnology*, 20-21(1), 781-797.

Vega, J.L., Clausen, E.C., Gaddy, J.L. 1990. Design of bioreactors for coal synthesis gas fermentations. *Resources, Conservation and Recycling*, 3(2–3), 149-160.

Verhallen, P., Oomen, L., Elsen, A., Kruger, J., Fortuin, J. 1984. The diffusion coefficients of helium, hydrogen, oxygen and nitrogen in water determined from the permeability of a stagnant liquid layer in the quasi-s. *Chemical Engineering Science*, 39(11), 1535-1541.

Wang, G., Wang, D.I.C. 1984. Elucidation of growth inhibition and acetic acid production by *Clostridium thermoaceticum*. *Applied and environmental microbiology*, 47(2), 294-298.

White, H., Lebertz, H., Thanos, I., Simon, H. 1987. *Clostridium thermoaceticum* forms methanol from carbon monoxide in the presence of viologen dyes. *FEMS Microbiology Letters*, 43(2), 173-176.

Wilkins, M.R., Atiyeh, H.K. 2011. Microbial production of ethanol from carbon monoxide. *Current Opinion in Biotechnology*, 22(3), 326-330.

Wilkins, M.R., Atiyeh, H. 2012. Fermentation. in: *Food and industrial bioproducts and bioprocessing*, (Ed.) N.T. Dunford, John Wiley & Sons, Inc. Ames, Iowa, pp. 185.

Williams, R., Jenkins, B., Nguyen, D. 2003. Solid waste conversion: A review and database of current and emerging technologies. Department of Biological and Agricultural Engineering, University of California. Davis, California. Accessed March 18th, 2014. http://energy.ucdavis.edu/files/05-06-2013-2003-solid-waste-conversion-review-and-assessment.pdf.

Wise, D., Houghton, G. 1968. Diffusion coefficients of neon, krypton, xenon, carbon monoxide and nitric oxide in water at 10–60 °C. *Chemical Engineering Science*, 23(10), 1211-1216.

Wolfrum, E.J., Watt, A.S. 2002. Bioreactor design studies for a hydrogen-producing bacterium. *Applied Biochemistry and Biotechnology*, 98(1), 611-625.

Wolfrum, E.J., Weaver, P. 2002. Bioreactor development for biological hydrogen production. in: *Proceedings of the 2002 U.S. DOE Hydrogen Program Review*, National Renewable Energy Laboratory. Golden, CO, pp. 10. Accessed March 18th, 2014. http://www1.eere.energy.gov/hydrogenandfuelcells/pdfs/32405a2.pdf.

Wood, H. 1991. Life with CO or CO_2 and H_2 as a source of carbon and energy. *The FASEB Journal*, 5(2), 156-163.

Wood, H.G., Ragsdale, S.W., Pezacka, E. 1986. The acetyl-coa pathway of autotrophic growth. *FEMS Microbiology Letters*, 39(4), 345-362.

Worden, R.M., Grethlein, A.J., Jain, M.K., Datta, R. 1991. Production of butanol and ethanol from synthesis gas via fermentation. *Fuel*, 70(5), 615-619.

Younesi, H., Najafpour, G., Mohamed, A.R. 2005. Ethanol and acetate production from synthesis gas via fermentation processes using anaerobic bacterium, *Clostridium ljungdahlii*. *Biochemical Engineering Journal*, 27(2), 110-119.

Zabriskie, D.W., Mill, T.O. 1988. *Traders guide to fermentation media formulation*. Traders Protein, pp.60.

Zahn, J.A., Saxena, J. 2012. Ethanologenic clostridium species, *Clostridium coskatii*, U.S. Patent no. 8,143,037.

Zeikus, J. 1980. Chemical and fuel production by anaerobic bacteria. *Annual Reviews in Microbiology*, 34(1), 423-464.

Zeng, A.-P., Biebl, H., Deckwer, W.-D. 1990. Effect of pH and acetic acid on growth and 2, 3-butanediol production of *Enterobacter aerogenes* in continuous culture. *Applied Microbiology and Biotechnology*, 33(5), 485-489.

Zeng, A.P., Ross, A., Biebl, H., Tag, C., Günzel, B., Deckwer, W.D. 1994. Multiple product inhibition and growth modeling of *Clostridium butyricum* and *Klebsiella pneumoniae* in glycerol fermentation. *Biotechnology and Bioengineering*, 44(8), 902-911.

APPENDICES

A EXPERIMENTAL DATA OF OXYGEN FROM THE MASS TRANSFER ANALYSIS OF TBR

This appendix contains results published in a part of journal article in Bioresource Technology and appears in this dissertation with the journal's permission.

Orgill, J.J., Atiyeh, H.K., Devarapalli, M., Phillips, J.R., Lewis, R.S., Huhnke, R.L. 2013. A comparison of mass transfer coefficients between trickle-bed, hollow fiber membrane and stirred tank reactors. *Bioresource Technology*, 133, 340-346.

This appendix contains of the O_2 mass transfer and the liquid holdup volume data that were not included in Chapter 4. Mass transfer analysis of the TBR was performed using air-water system at various gas (5.5 to 130.9 sccm) and liquid (50 to 100 ml/min) flow rates for both 3- and 6-mm glass beads.

A1 Materials and Methods

The TBR setup is shown in Figure A1. The TBR was made of borosilicate glass 51 cm inner diameter and 61.0 cm length. Soda lime glass beads of size 3-mm (# 26396-508, VWR, Atlanta, GA) and 6-mm (#26396-621, VWR, Atlanta, GA) were used as the packing material. A metal mesh with openings smaller than 3-mm was placed 10 cm from the bottom of the TBR to hold the glass beads in the reactor. A perforated circular liquid distributor with 3.2 mm holes was placed 5.1 cm above the beads. Stainless-steel tubes with 3.2 mm and 6.4 mm diameter were used for liquid and gas, respectively. The

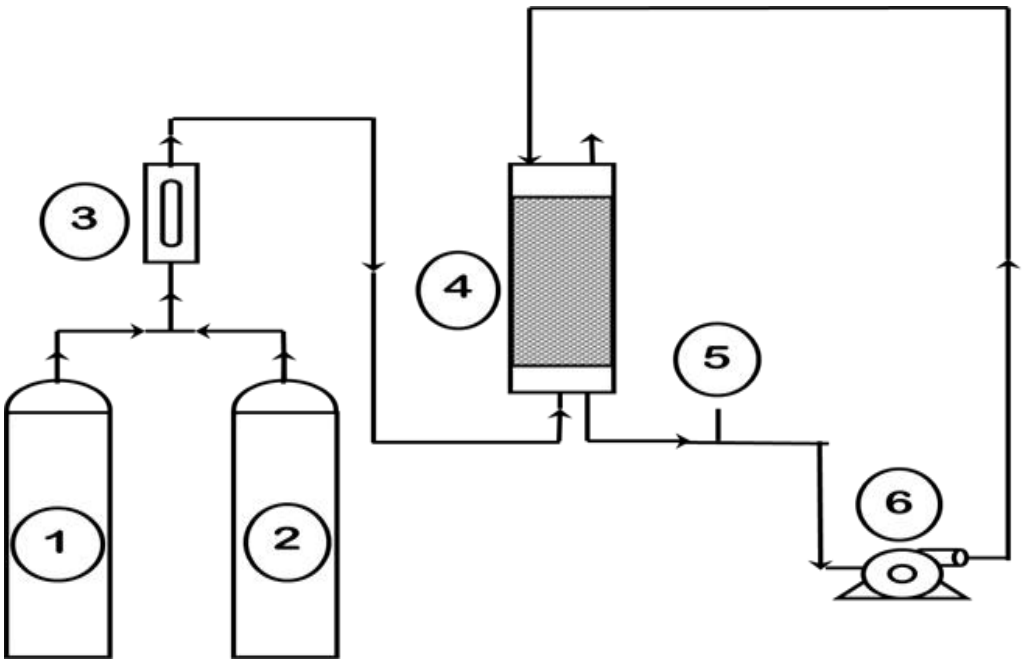

Figure A1 TBR mass transfer experimental setup. (1) nitrogen gas, (2) zero grade air, (3) rotameter, (4) TBR, (5) DO probe, and (6) pump.

bottom of the TBR acted as a sump, which was initially filled with 200 mL of DI water. The TBR was operated in counter-current mode. A peristaltic pump (7523-20, Cole-Parmer, Vernon, IL) circulated the liquid at a desired flow rate. Various gas (5.5 to 130.9 standard cubic centimeters per minute, sccm) and liquid (50 to 1000 mL/min) flow rates were tested. A dissolved oxygen (DO) probe (P0720-6580, New Brunswick, Edison, NJ) was placed in line in the recirculation loop and connected to a Bioflo110 control unit (New Brunswick, Edison, NJ) for data acquisition. The TBR was first purged with N_2 at a set gas flow rate (33 sccm) using a rotameter until the % DO in water reached close to 0%. Then, the gas was switched from N_2 to air (Stillwater Steel Suppliers, Oklahoma City, OK). The % DO in water with time was recorded using the Biocommand software (New Brunswick, Edison, NJ) for further analysis. Runs were performed in duplicate. The overall mass transfer coefficient of O_2 ($k_{L,O2}a/V_L$) in the TBR at a given gas and liquid flow rate was calculated according to Eq A.1(Garcia-Ochoa and Gomez, 2009).

$$\frac{k_{L,O2}a}{V_L} = -\frac{\ln\left(1-\frac{C_L}{C_S}\right)}{t}\cdot\frac{V_S}{V_L} \qquad \text{(A.1)}$$

where, k_L is the mass transfer coefficient (m/h), a is the mass transfer area (m^2), V_L is the volume of liquid within the TBR (m^3), V_S is the total volume of the system including sump and circulation loop (m^3), C_L is the bulk DO concentration in the liquid (mol/m^3), C_S is the saturated DO concentration (mol/m^3), and t is the time (h). Since C_L/C_S is a ratio, % DO in the bulk liquid was used in place of C_L and saturated % DO was used in place of C_S. After the circulation loop and sump were filled, V_L was calculated by measuring the difference between the initial and final liquid volumes in the TBR sump at a given gas and liquid flow rate.

A2 Results and Discussion

A2.1 Overall mass transfer coefficient of oxygen

The overall mass transfer coefficient of oxygen ($k_{L,O2}a/V_S$) increased with increase in the gas flow rate (Figure A2). However, liquid flow rate had no effect up to 46.4 sccm of gas flow rate. Above 46.4 sccm, increasing the liquid flow rate from 50 ml/min to 100 ml/min increased the $k_{L,O2}a/V_S$ and further increasing the liquid flow rate from 100 ml/min to 1000 ml/min had no effect on the $k_{L,O2}a/V_S$. The $k_{L,O2}a/V_S$ for both 3- and 6-mm beads was between 1 to 30 h^{-1}. The $k_{L,O2}a/V_S$ profile is similar to the $k_{L,CO}a/V_S$ and $k_{L,H2}a/V_S$ profiles discussed in Section 4.3.1.

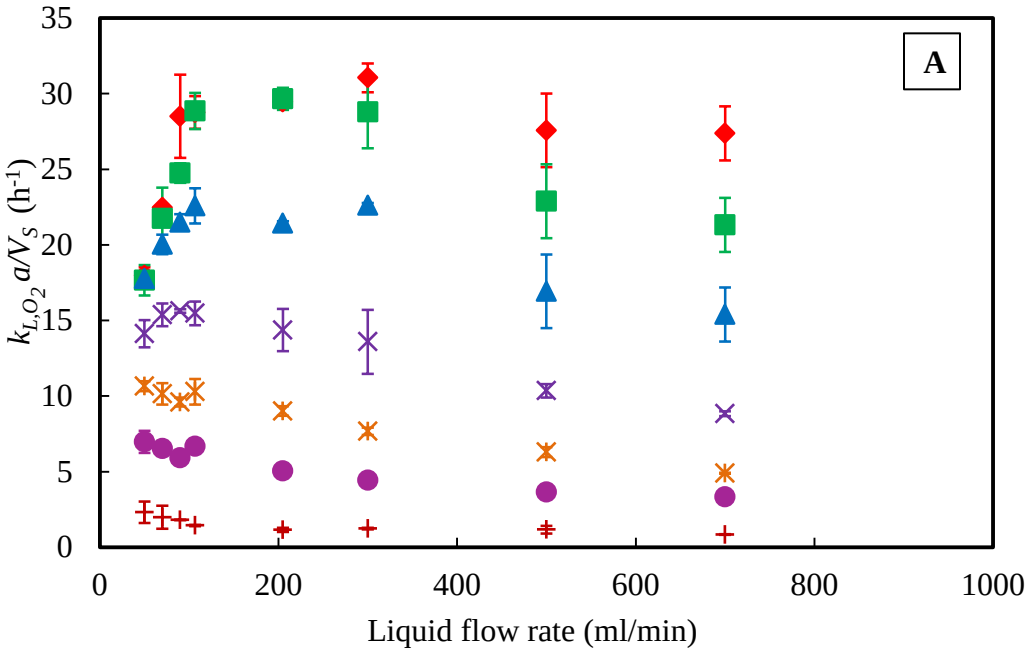

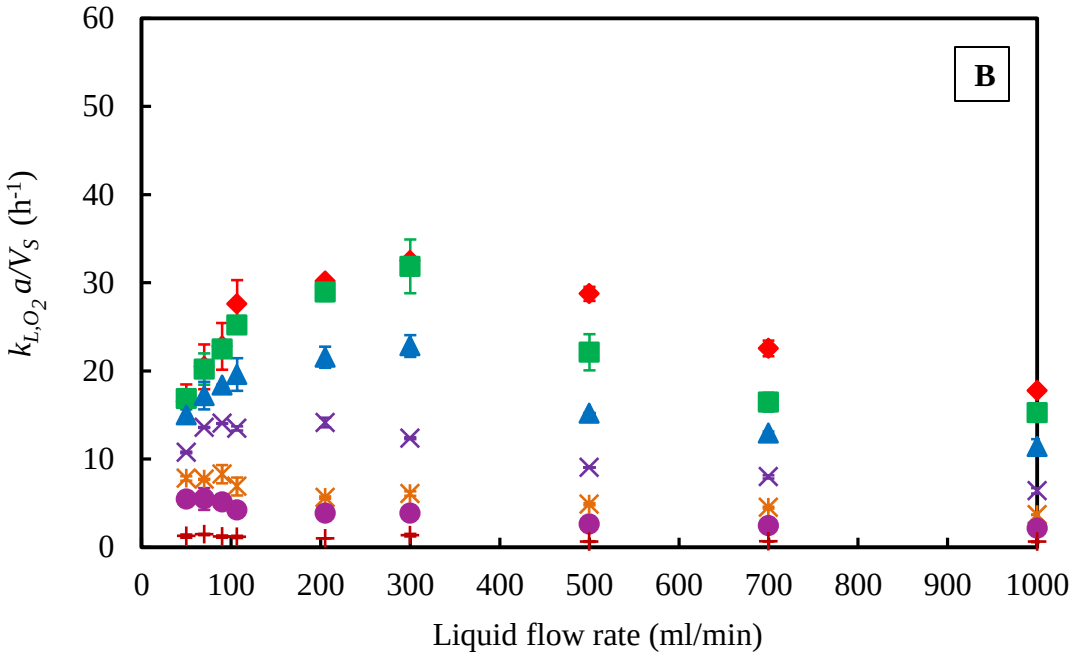

Figure A2 $k_{L,O2}\,a/V_S$ at 37 °C for (A) 3-mm beads (B) 6-mm beads and at different gas flow rates.

(+) 5.5 sccm (●) 18.4 sccm (*) 28.2 sccm (×) 46.4 sccm (▲) 72.8 sccm (■) 106.4 sccm (♦) 130.9 sccm. Error bars represent ± 1 standard deviation (n=2).

A2.2 Mass transfer coefficient of oxygen in reactive volume

The effects of bead size and various liquid and gas flow rates on the mass transfer coefficients ($k_{L,O2}a/V_L$) in the TBR for 3-mm and 6-mm beads are shown in Figure A3. The $k_{L,O2}a/V_L$ increased with an increase in the gas flow rate from 5.5 sccm to 130.9 sccm. However, $k_{L,O2}a/V_L$ values decreased with an increased liquid flow rate for a given gas flow rate. This is due to an increase in the liquid holdup with increasing liquid flow rate (Table A1). The gas flow rate had no effect on the liquid holdup in the TBR. However, increasing the liquid flow rate will displace the gas phase thus increasing the liquid holdup (Ranade et al., 2011b). For the range of liquid flow rates from 50 mL/min to 1000 mL/min used in this study, the liquid holdup within the 3-mm beads was 30% to

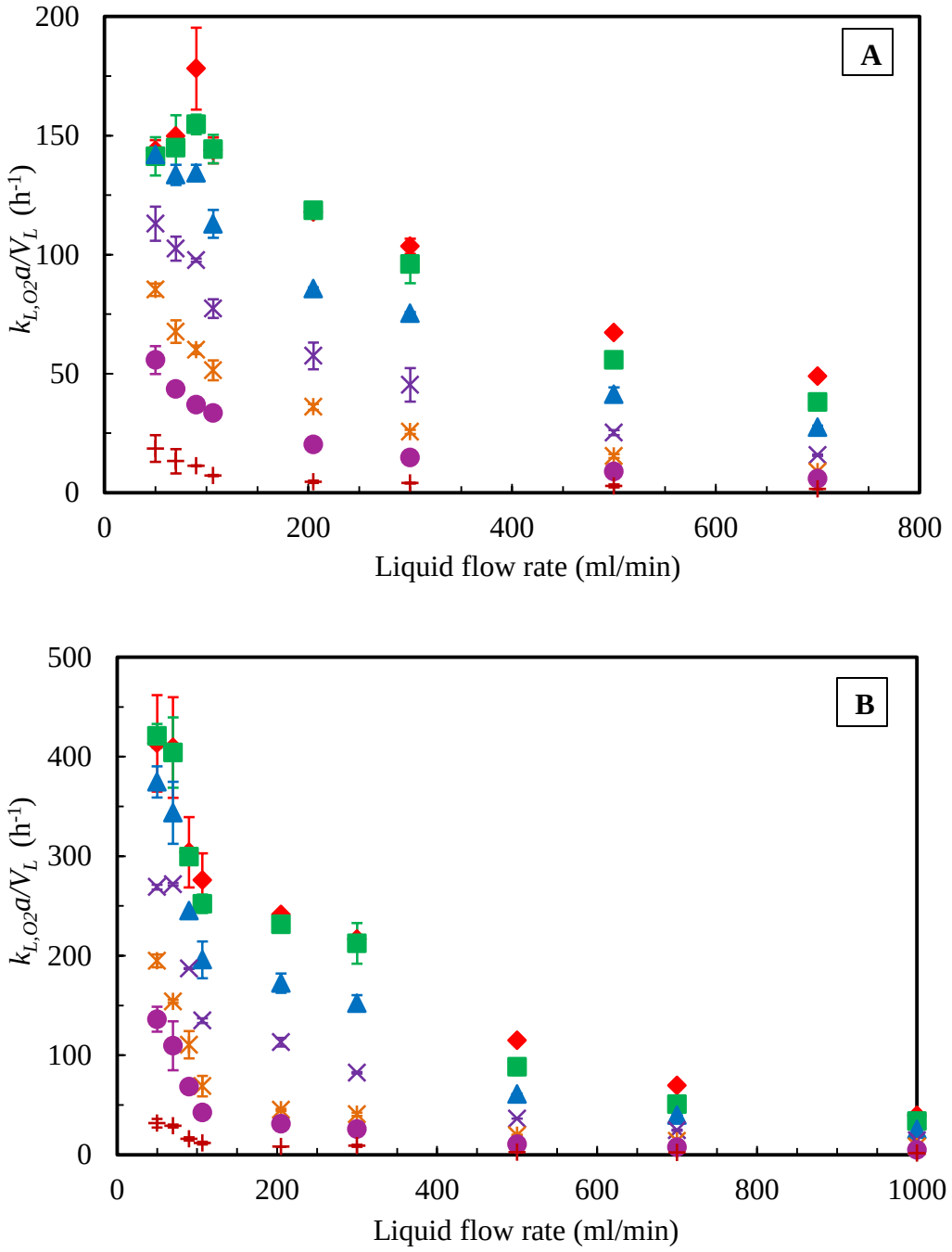

Figure A3 $k_{L,O2}\,a/V_L$ at 37 °C for (A) 3-mm beads (B) 6-mm beads and at different gas flow rates. (+) 5.5, (●) 18.2, (*) 28.2, (×) 46.4, (▲) 72.8, (■) 106.4, (♦) 130.9 sccm. Error bars represent ± 1 standard deviation (n=2).

60% higher than with the 6-mm beads (Table A1). The specific surface area, defined as the surface area of the particle divided by its volume, was 50% higher for the 3-mm beads as compared to the 6-mm beads. This resulted in an increase of the liquid retention time and holdup. Thus, the $k_{L,O2}a/V_L$ value in the TBR with 3-mm beads was lower by the same percentage compared to 6-mm beads. The highest $k_{L,O2}a/V_L$ values in the TBR with 3-mm and 6-mm beads were 178 h^{-1} and 421 h^{-1}, respectively (Figure A3).

Table A1 Liquid holdup (V_L) in the TBR at various liquid flow rates with 3- and 6-mm glass beads.

Liquid flow rate (ml/min)	V_L for 3 mm beads (ml)	V_L for 6 mm beads (ml)
50	24.3	8.1
70	30.4	10.1
90	34.5	14.2
100	40.5	20.3
200	54.7	24.3
300	64.9	30.4
500	82.0	50.4
700	112.0	65.4
800	118.0[a]	73.4
900	123.0[a]	81.4
1000	127.0[a]	90.4

[a] TBR was flooded when gas flow rate was higher than 5.5 sccm

B PRILIMINARY SEMI-CONTINUOUS FERMENTATIONS IN TBR

B Effect of medium replacement and addition of 1X nutrients

B1 Background

The semi-continuous TBR fermentation discussed in this appendix was performed to understand the effect of addition of nutrient (1X) and the medium replacement on semi-continuous fermentations. The results were presented into different phases (A to L) related to changes made in gas and liquid flow rates and pH. To maintain the cell activity in the TBR, either medium was replaced or 1X nutrients were added into the medium when the cell OD_{660} in the medium dropped to 0.3. For the 1X nutrient addition in phases (E, F, G and J), concentrated nutrients were added into the TBR. The volume of the 1X concentrated nutrients was equal to the medium volume removed from the TBR during sampling. In medium replacement phases (H and K), 400 ml of exhausted medium was replaced with an equal amount of fresh medium. The detailed composition of the medium was reported in Appendix G. The detailed materials and methods for semi-continuous fermentations were discussed in Section 5.2. In this preliminary experiment, only 10% (v/v) of inoculum was added in the TBR. The liquid flow rate in this semi-continuous fermentation was maintained at 200 ml/min from 200 h to 1127 h. The total liquid volume in the TBR was increased to 500 ml (V_S) by adding a 500 ml pyrex glass bottle in the recirculation loop to hold the medium. The increased V_S allowed measuring the

change in gas composition at the TBR exit and thus calculating the gas conversion efficiencies at various gas flow rates between 2.93 sccm and 13.8 sccm.

B2 Cell growth, pH and product profiles

B2.1 Cell growth and pH

The cell growth and pH profiles are shown in Figures B1 and B2. No cell activity was observed from 0 to 143 h (Figure B1). In phase A, the gas flow rate was increased at 143 h from 2.3 sccm to 4.6 sccm to check if cells grow when fed more gas. When no cell activity was observed at 199 h, the liquid flow rate was increased from 100 to 200 ml/min in phase B. The cells remained in lag phase during the fisrt 388 h. In phase C, instead of adding fresh medium to replace the medium withdrawn as liquid samples, 50 ml of inoculum was added into the TBR and the gas flow rate was reduced from 4.6 sccm to 2.3 sccm at 388 h. The addition of 50 ml inoculum and lowering gas flow rate helped in starting the fermentation (Figure B1). In phase D, the cell OD_{660} decreased from 0.76 to 0.40 when the pH was maintained at 4.6. However in phase E, the increase in the gas flow rate from 2.93 sccm to 5.50 sccm increased the cell OD_{660} to 0.73 and then decreased to 0.55. In phase F, when 1X nutrients were added the second time to maintain cell activity, no cell growth was observed (Figure B1). The repetitive addition of 1X nutrients might have inhibited cell growth due to high concentration of the added minerals.

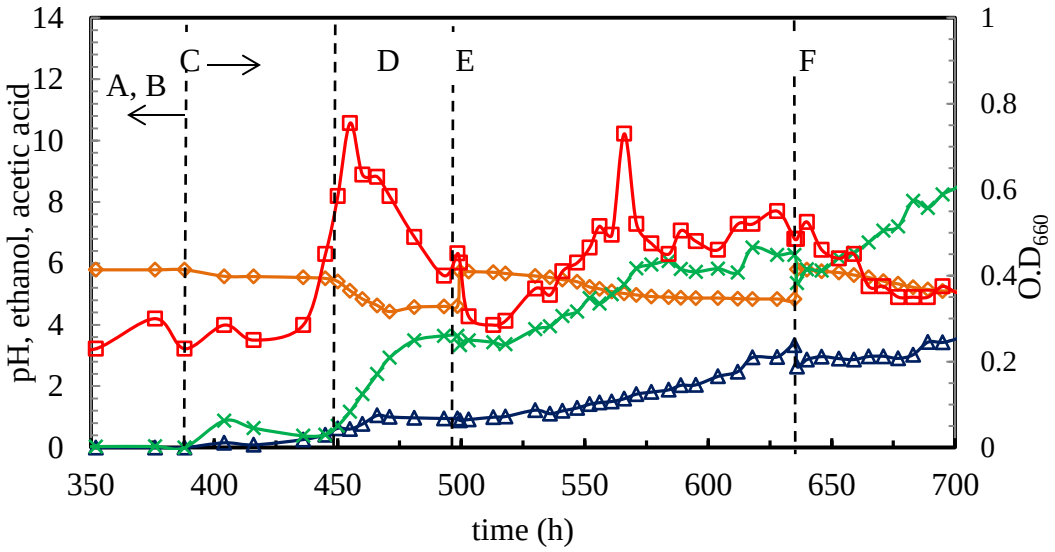

Figure B1 Cell density, pH, ethanol and acetic acid profile from phase C to F in semi-continuous TBR fermentation. ( ) Cell density ( ) pH ( ) Ethanol ( ) Acetic acid; 0 to 350 h resulted in no data due to lag phase; phases (A) changed G from 2.3 sccm to 4.6 sccm at 143 h; (B) changed L from 100 ml/min to 200 ml/min at 199 h; (C) Changed G: 4.6 sccm to 2.93 sccm, added 50 ml inoculum, 388 h; (D) started pH control to maintain pH at 4.6, 466 h; (E) Changed G: 2.93 sccm to 5.5 sccm, added 1X nutrients, adjusted pH to 5.8, 498.5 h; (F) Changed G: 5.5 sccm to 9.2 sccm, added 1X nutrients, adjusted pH to 5.8, 635 h. L:liquid flow rate, G: gas flow rate.

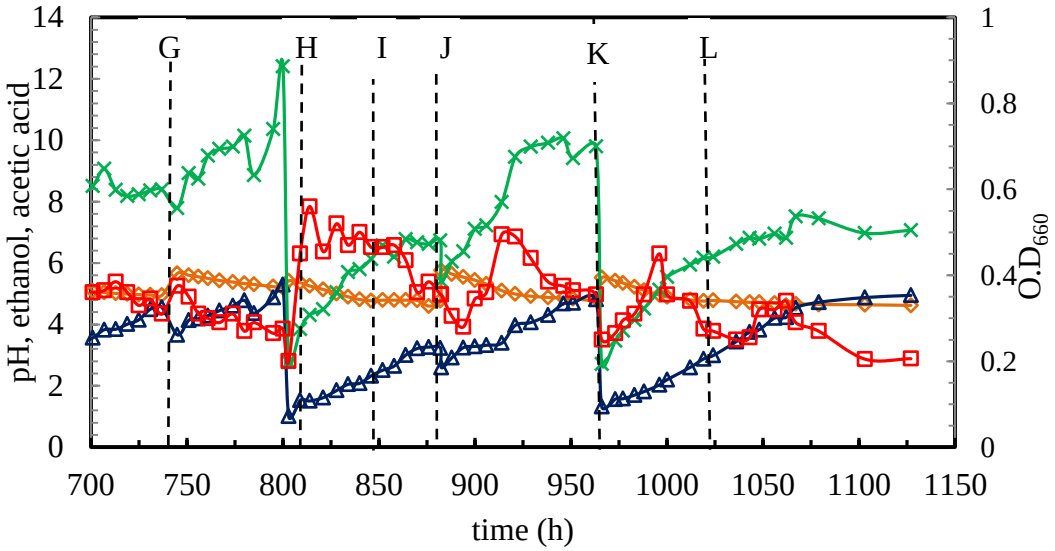

Figure B2 Cell density, pH, ethanol and acetic acid profile from phase G to L in semi-continuous TBR fermentation. ( ) Cell density ( ) pH ( ) Ethanol ( ) Acetic acid. Phases (G) Changed G: 9.2 sccm to 13.8 sccm, added 1X nutrients, adjusted pH to 5.8, 737 h; (H) Replaced exhausted 400 ml medium, 800 h; (I) Controlled pH at 4.6, 846 h; (J**)** Added 1X nutrients, adjusted pH to 5.8, 882.5 h; (K) Replaced exhausted 400 ml medium, 966 h; (L**)** Controlled pH at 4.6, 1019 h. L: liquid flow rate, G: gas flow rate.

Table B1 Kinetic parameters at different operating conditions.

Phases	C to E	E to F	F to G	G to H	H to J	J to K	K to end
Fermentation time(h)	110	137	102	63[a]	82	84	261
Liquid flow rate, ml/min	200	200	200	200	200	200	200
Gas flow rate, sccm	2.93	5.50	9.20	13.80	13.80	13.80	13.80
vvm[a]	0.006	0.01	0.02	0.03	0.03	0.03	0.03
Ethanol yield from CO, %	38.2	71.8	71	34.37[a]	69.41	62.02	81.64
Max. CO conversion (%)	80.95	48.33	21.76	19.75	28.86	26.69	18.47
Max. H2 conversion (%)	74.83	22.47	17.73	12.10	15.35	14.60	12.48
Max. cell $O.D_{660}$	0.76	0.73	0.35	0.35	0.56	0.49	0.45
Acetic acid (g/L)	3.64	2.87	2.59	4.05	2.89	4.39	3.59
Ethanol (g/L)	0.95	2.39	1.92	0.74[a]	2.22	2.21	3.62
CO utilization at 80 h, %	44.78	28.40	16.33	-	15.91	17.33	14.09
H_2 utilization at 80 h, %	30.37	17.66	13.91	-	8.90	11.58	9.68

[a] volume of gas provided per volume of liquid per minute (vvm = gas flow rate/ total liquid volume)

No growth was observed when the 1X nutrients were added again in phases F and G (Figures B1 and B2). Excess minerals and product accumulation could have inhibited cell growth and ruptured the cell wall because of high acidic conditions. The undissociated acetic acid concentration of around 50 mM (i.e., 3g/L) was reported to severely inhibit *C. coskatii* growth (Zahn and Saxena, 2012). *Clostridium butyricum* cease to grow when the undissociated acetic acid concentration was 0.49 g/L at pH 6.5 (Zeng et al., 1994). The undissociated acetic acid concentration that inhibited *Enterobacter aerogenes* growth was 0.19 g/L at pH 5.5 and 6.7 (Zeng et al., 1990). Further, the total acetic acid concentrations were 1.2 g/L and 17.5 g/L at pH 5.5 and pH 6.7, respectively (Zeng et al., 1990). Though the total acid concentrations were different, the undissociated acid concentration was the same at both the pH values (Table B2).

Table B2 Concentrations of undissociated acetic acid that inhibits growth of different bacteria.

Bacteria	Undissociated acetic acid (g/L)	pH	Reference
C. coskatii	3	-	(Zahn and Saxena, 2012)
C. butyricum	0.49	6.5	(Zeng et al., 1994)
Klebsiella oxytoca	0.45	-	(Fond et al., 1985)
E. aerogenes	0.19	5.5 and 6.7	(Zeng et al., 1990)
C. formicoaceticum	0.358	6.45-6.8	(Tang et al., 1989)
C. thermoaceticum	2.4 - 3	-	(Wang and Wang, 1984)

It was reported that the undissociated acid can traverse the cytoplasmic membrane of cells and decrease their internal pH, which results in acidifying cytoplasm and inhibiting cells synthesis (Zeng et al., 1990).

B2.2 Effect of undissociated acid on cell growth

The undissociated acid concentration at the start of each phase when 1X nutrients were added into the TBR is shown in Table B3. Using the Henderson-Hasselbalch equation (Po and Senozan, 2001), the undissociated acid concentrations was calculated as shown below:

According to Henderson–Hasselbalch equation; $pH = pKa + log_{10}\left(\frac{[A^-]}{[HA]}\right)$ (B.1)

$[A^-]$ and [HA] represent the concentrations of dissociated and undissociated acid, respectively.

For Phase E,

pH =4.6; total acid concentration = $[A^-]$+[HA] = 3.6 g/L ➔ $[A^-]$ =3.6-[HA]

pKa of acetic acid =4.75

Substituting these values in Henderson-Hasselbalch equation will give the concentration of the undissociated acid [HA], i.e.,

$$4.6 = 4.75 + log_{10}\left(\frac{3.6-[HA]}{[HA]}\right)$$

$$10^{-0.15} = \frac{3.6-[\mathrm{HA}]}{[\mathrm{HA}]}$$

$$[\mathrm{HA}] = 2.11 \text{ g/L}$$

Table B3 Cell $O.D_{660}$ and undissociated acid concentrations in different phases.

At start of phase	E[a]	F[a]	G[a]	H[b]	H[c]
pH	4.6	4.84	4.95	5.2	5.42
total acid (g/L)	3.6	6.28	8.39	12.40	2.77
undissociated acid (g/L)	2.11	2.82	3.25	3.24	0.49
max. $O.D_{660}$	0.76	0.73	0.35	0.265	0.56

[a] 1X nutrient addition; [b] before medium replacement; [c] after 400 ml of exhausted medium replacement

It can be observed that the total acid concentration and pH were different but the undissociated acid concentrations were similar for phases E and F. In phase E, when the undissociated acid concentration was 2.11 g/L with addition of 1X nutrients, there was a slight growth. In phases G and H, the undissociated acid concentration was 3.25 g/L. However, in phase G, 1X nutrients were added without any measured growth (cell O.D slightly dropped from 0.35 to 0.30). However in phase H, after 400 ml of exhausted medium was replaced with 400 ml fresh medium, the undissociated acid concentration dropped to 0.49 g/L and, cells started growing. The removal of 400 ml exhausted medium and addition of fresh 400 ml medium helped in cell growth by reducing the inhibition caused by undissociated acid and high mineral concentrations.

B2.3 Product profiles

The ethanol and acetic acid profiles are shown in Figures B1 and B2. For phases C to G, the increase in gas flow rate resulted in increase in product concentrations with addition of 1X nutrients. Product formation started from 445 h and reached steady concentrations of 3.64 g/L of acetic acid and 0.94 g/L of ethanol at 498.5 h and 2.93 sscm of gas flow rate. In phase E, the gas flow rate was increased to 5.5 sccm, which resulted in a slow increase in ethanol and acetic acid concentrations to 3.3 g/L of and 6.3 g/L, respectively, at 635 h. In phase F, the gas flow was increased to 9.2 sccm, which resulted in an increase in both ethanol and acetic acid concentrations to 4.6 and 8.4 g/L, respectively, at 737 h. In phase G, the gas flow rate was increased to 13.8 sccm. This resulted in an increase in ethanol and acetic acid concentrations to 5.3 and 12.4 g/L, respectively, at 800 h.

The effects of removal of 400 ml spent medium removal and addition of 400 ml of fresh medium vs addition of1X nutrients were performed in phases from G to L with gas flow rate of 13.8 sccm. In phases H and K, 400 ml of medium was replaced while in phase G and phase J, 1X nutrients were added. The ethanol concentration irrespective of medium replacement or 1X nutrients addition was stable at 4.8 g/L. However, acetic acid concentration dropped from 12.4 to 6.5 g/L when 400 ml of exhausted medium was replacement. At the end of the fermentation of 1127 h, 4.9 g/L of ethanol and 7.1 g/L of acetic acid were produced.

B3 Gas conversion

The CO and H_2 gas conversion efficiencies are shown in Figures B3 and B4. At a constant liquid flow rate of 200 ml/min, the highest gas conversion efficiency was

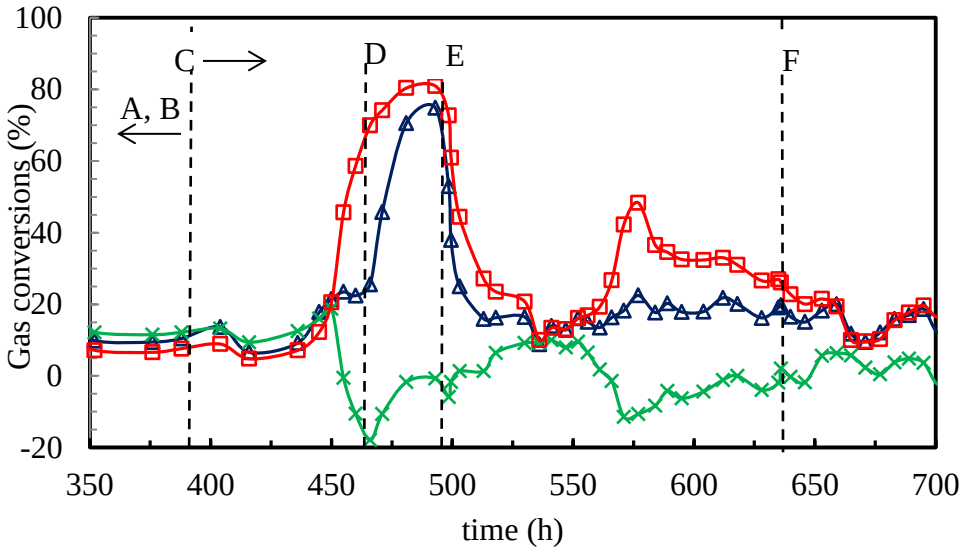

Figure B3 Gas conversions from phases C to F in semi-continuous TBR fermentation ( ) CO ( ) H_2 ( ) CO_2. ; 0 to 350 h resulted in no data due to lag phase; phases (A) changed G from 2.3 sccm to 4.6 sccm at 143 h; (B) changed L from 100 ml/min to 200 ml/min at 199 h; (C) Changed G: 4.6 sccm to 2.93 sccm, added 50 ml inoculum, 388 h; (D) started pH control to maintain pH at 4.6, 466 h; (E) Changed G: 2.93 sccm to 5.5 sccm, added 1X nutrients, adjusted pH to 5.8, 498.5 h; (F) Changed G: 5.5 sccm to 9.2 sccm, added 1X nutrients, adjusted pH to 5.8, 635 h. L : liquid flow rate, G : gas flow rate.

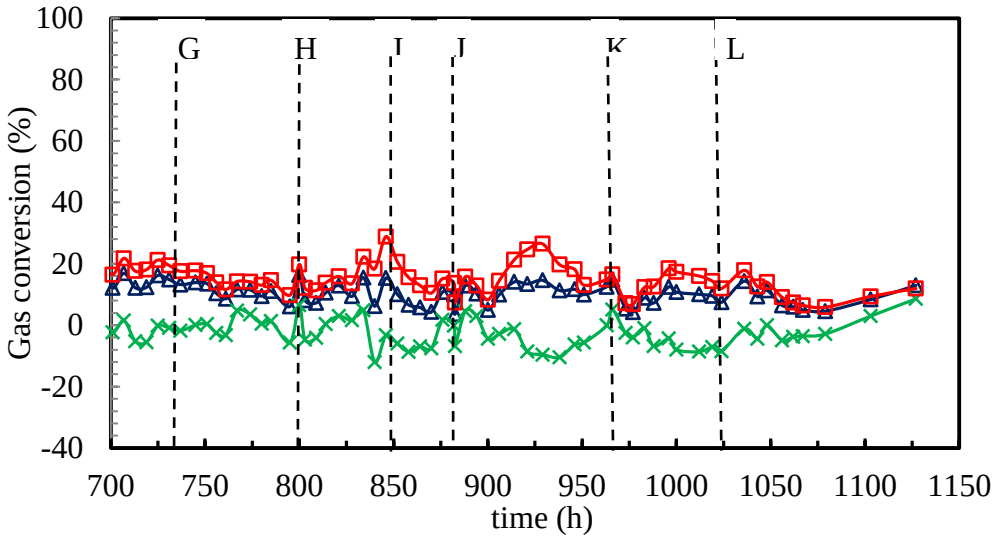

Figure B4 Gas conversions from phases G to L in semi-continuous TBR fermentation ( ) CO ( ) % H_2 ( ) % CO_2. 0 to 350 h resulted in no data due to lag phase; phases (A) changed G from 2.3 sccm to 4.6 sccm at 143 h; (B) changed L from 100 ml/min to 200 ml/min at 199 h; (G). Changed G: 9.2 sccm to 13.8 sccm, added 1X nutrients, adjusted pH to 5.8, 737 h; (H) Replaced 400 ml medium, 800 h; (I) Controlled pH at 4.6, 846 h; (J**)** Added 1X nutrients, adjusted pH to 5.8, 882.5 h; (K) Replaced 400 ml medium, 966 h; (L**)** Controlled pH at 4.6, 1019 h. L: liquid flow rate, G: gas flow rate.

obtained at the lowest gas flow rate i.e., 2.93 sccm. Increasing the gas flow rate decreased the gas conversion efficiency irrespective of whether 1X nutrients were added or 400 ml medium was replaced in the TBR (Figures B3 and B4). A maximum CO and H_2 conversion efficiencies of 81% and 75%, respectively, were obtained at 493 h and 2.93 sccm. In phases E to F, increasing the gas flow rate to 5.5 sccm decreased the CO and H_2 conversion efficiencies to 48% and 22 %, respectively. In phase F, the increase in the gas flow rate to 9.2 sccm decreased the CO and H_2 conversion efficiencies to 22% and 18%, respectively. From phases G to L, the gas flow rate was maintained at 13.8 sccm and the CO and H_2 conversion efficiencies were around 30% and 15%, respectively. Overall from phases G to L, the average conversion efficiency was around 18% CO and 12% H_2. Figure B5 shows the maximum CO and H_2 gas conversion efficiencies obtained with increasing the vvm (volume of gas provided per volume of liquid per minute). It can be observed that increasing the total amount of gas provided (or) the vvm decreased the gas conversion efficiency.

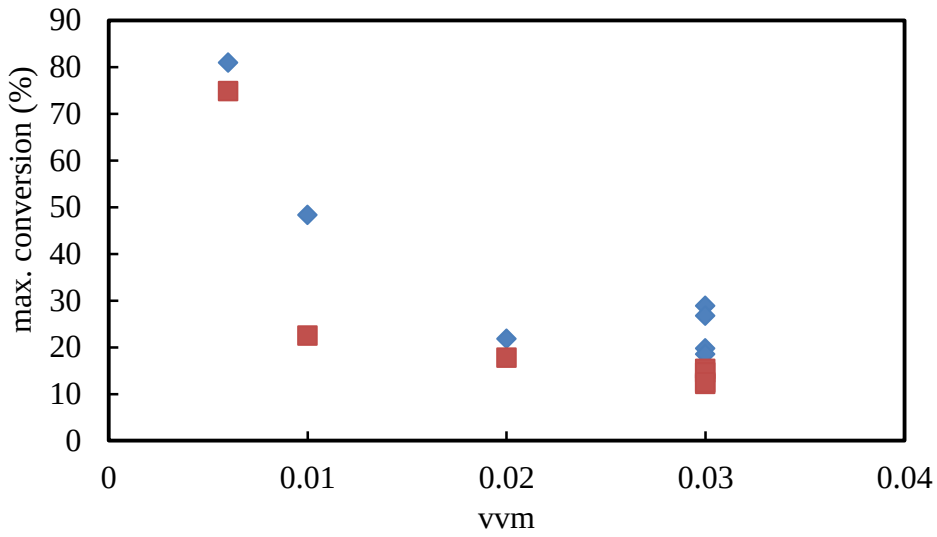

Figure B5 Maximum gas conversions at various vvm in semi-continuous TBR fermentation. (■) CO (◆) H_2 . vvm represents volume of gas supplied per volume of liquid per minute.

B4 Gas uptakes

The gas uptake profiles in mmol/h are shown in Figures B6 and B7. CO gas uptake increased with the increase in the gas flow rate while H_2 uptake decreased due to CO inhibition on hydrogenase. At a gas flow rate of 2.93 sccm, the maximum gas uptake reached were 2.75 mmol/h of CO and 2.22 mmol/h of H_2 at 466 h. At a gas flow rate of 5.5 sccm, CO and H_2 gas uptakes reached 3.1 and 1.1 mmol/h, respectively. Further, increasing the gas flow rate to 13.8 sccm increased CO uptake to 4.7 mmol/h at 828 h. However, H_2 uptake rate was about 1.95 mmol/h at 828 h.

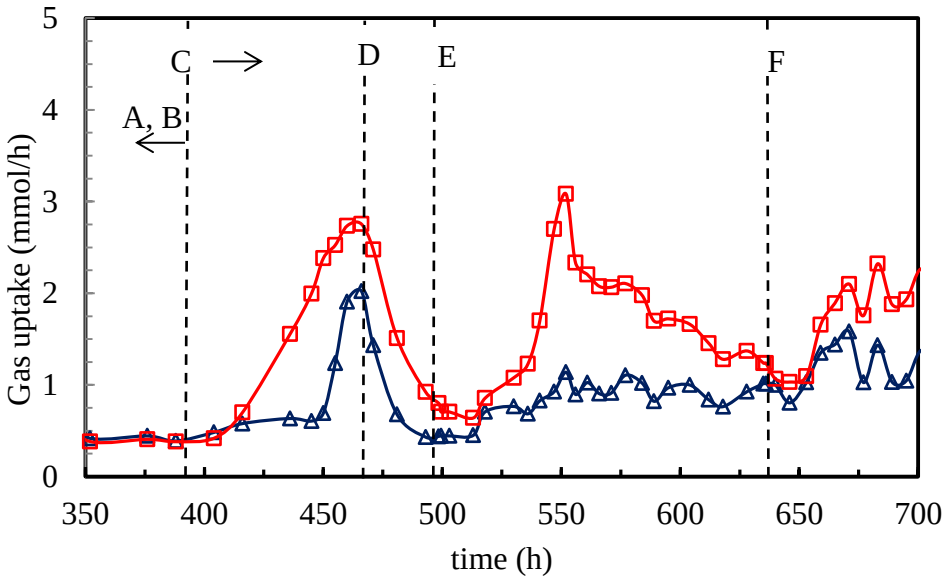

Figure B6 Gas uptake rates from phase C to F in semi-continuous TBR fermentation. ( ) CO ( ) H_2. 0 to 350 h resulted in no data due to lag phase; phases (A) changed G from 2.3 sccm to 4.6 sccm at 143 h; (B) changed L from 100 ml/min to 200 ml/min at 199 h; (C) Changed G: 4.6 sccm to 2.93 sccm, adding 50 ml inoculum, 388 h; (D) started pH control to maintain pH at 4.6, 466 h; (E) Changed G: 2.93 sccm to 5.5 sccm, added 1X nutrients, adjusted pH to 5.8, 498.5 h; (F) Changed G: 5.5 sccm to 9.2 sccm, added 1X nutrients, adjusted pH to 5.8, 635 h. L: liquid flow rate, G: gas flow rate.

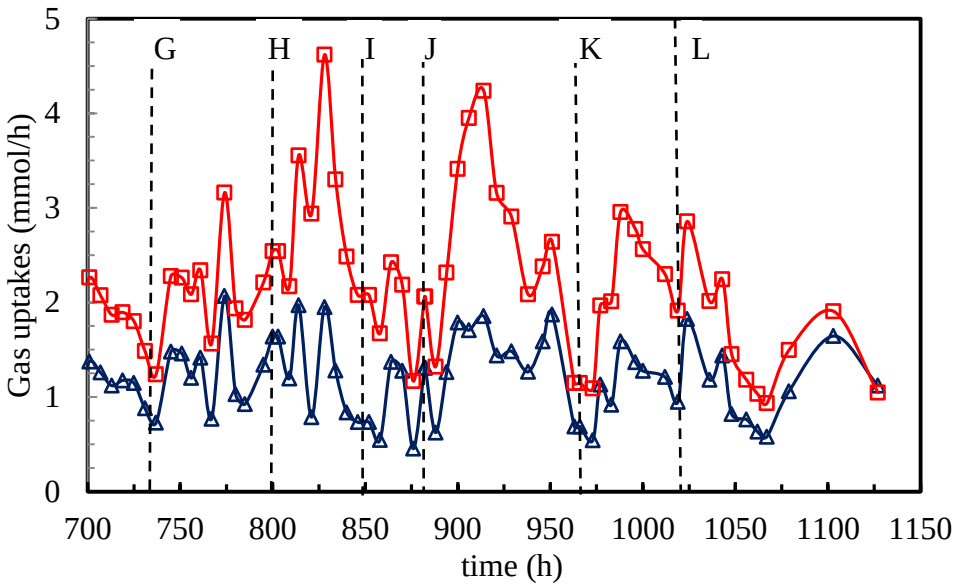

Figure B7 Gas uptake rates from phase G to L in semi-continuous TBR fermentation (—□—) CO (—△—) H_2. Phases (G) Changed G: 9.2 sccm to 13.8 sccm, added 1X nutrients, adjusted pH to 5.8, 737 h; (H) Replaced 400 ml medium, 800 h; (I) Controlled pH at 4.6, 846 h; (J**)** Added 1X nutrients, adjusted pH to 5.8, 882.5 h; (K) Replaced 400 ml medium, 966 h; (L**)** Controlled pH at 4.6, 1019 h. L: liquid flow rate, G: gas flow rate.

B5 ORP

The oxidation reduction potential profile is shown in Figures B8 and B9. The redox potential reading for the first 436 h was constant at around -340 mV indicating that the medium was reduced. Thus, the experiment was not shutdown. In phase D when the cell OD_{660} in the medium was maximum of 0.76, the ORP reduced to a very low value of -530 mV. As the cell OD_{660} in the medium started to drop, the ORP increased to -108 mV at 513 h. An increase in the ORP to around -450 mV was observed after 6 h of 1X nutrients addition or medium replacement. The replenishment of the nutrients increased fermentation and cell activities. However, when the production of acetic acid and ethanol started, the ORP increased to -250 mV. Overall a drop in ORP was associated with increase in cell density in the medium. On the other hand, the increase in ORP was associated with the production of ethanol and acetic acid.

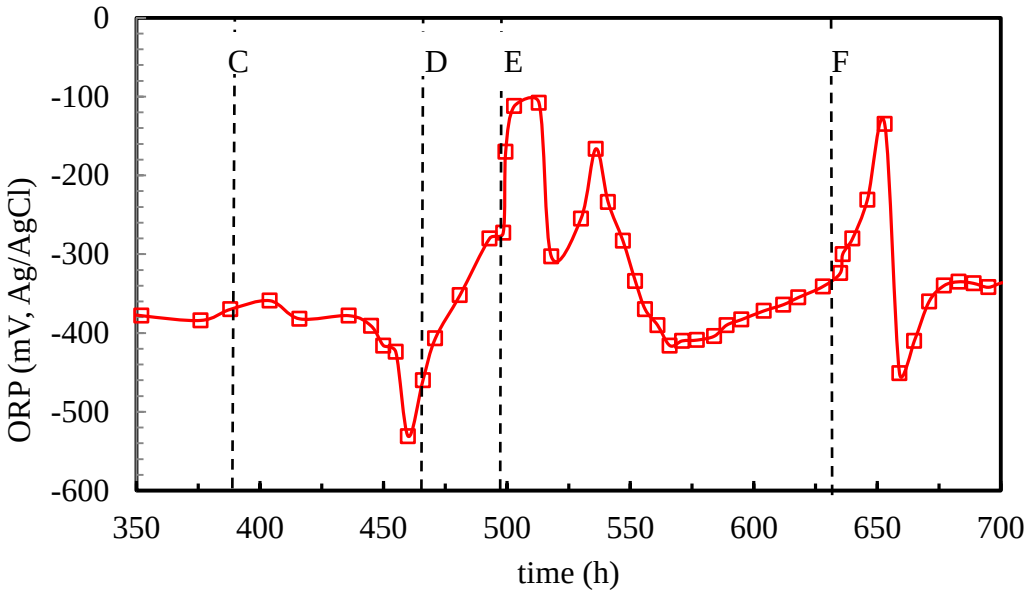

Figure B8 ORP from phases A to F in semi-continuous TBR fermentation. 0 to 350 h resulted in no data due to lag phase; phases (A) changed G from 2.3 sccm to 4.6 sccm at 143 h; (B) changed L from 100 ml/min to 200 ml/min at 199 h; (C) Changed G: 4.6 sccm to 2.93 sccm, added 50 ml inoculum, 388 h; (D) started pH control to maintain pH at 4.6, 466 h; (E) Changed G: 2.93 sccm to 5.5 sccm, added 1X nutrients, adjusted pH to 5.8, 498.5 h; (F) Changed G: 5.5 sccm to 9.2 sccm, added 1X nutrients, adjusted pH to 5.8, 635 h. L: liquid flow rate, G: gas flow rate.

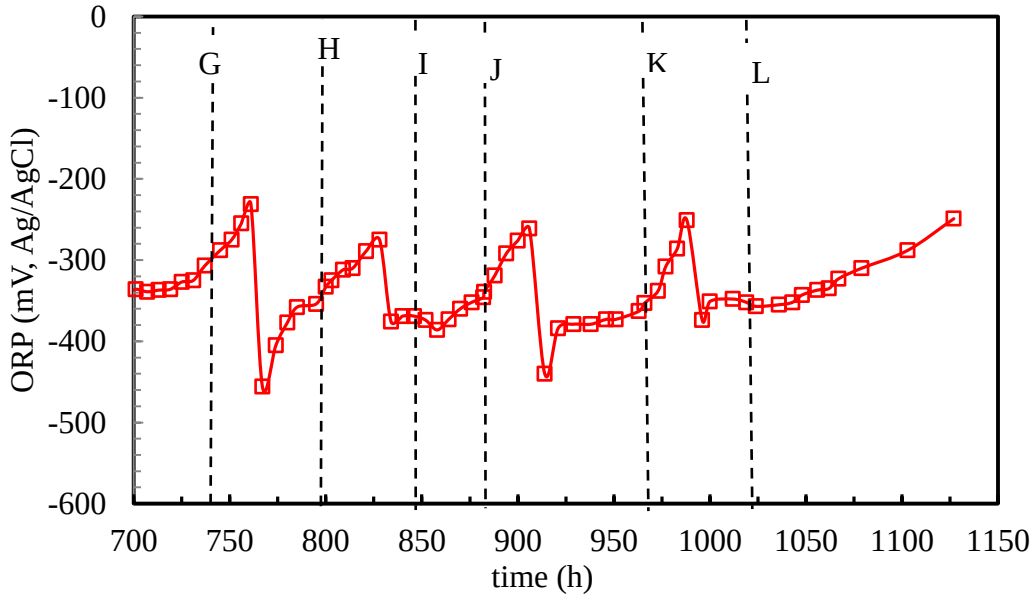

Figure B9 ORP from phases G to H in semi-continuous TBR fermentation; phases (G) Changed G: 9.2 sccm to 13.8 sccm, added 1X nutrients, adjusted pH to 5.8, 737 h; (H) Replaced 400 ml medium, 800 h; (I) Controlled pH at 4.6, 846 h; (J**)** Added 1X nutrients, adjusted pH to 5.8, 882.5 h; (K) Replaced 400 ml medium, 966 h; (L**)** Controlled pH at 4.6, 1019 h. L: liquid flow rate, G: gas flow rate.

B6 Cell mass balance

The glass beads were collected in a clean tub and washed for four times each with 500 ml of DI water to measure the cells formed in the biofilm. Duplicate samples were collected from each wash. A total cell $O.D_{660}$ of 2.3 was measured from the beads wash (Table B4).

Table B4 Cell mass balance from beads and column wash with DI Water.

Samples Description	OD_{660} in 500 ml		
	sample 1	sample 2	average
1^{st} wash of beads with 500 ml DI water	1.575	1.650	1.613
2^{nd} wash of beads with 500 ml DI water	0.115	0.130	0.123
3^{rd} wash of beads with 500 ml of DI water	0.030	0.035	0.033
4^{th} wash of beads with 500 ml of DI water	0.014	0.012	0.013
column wash without beads with 400 ml DI water	0.292	-	-
Medium before removing beads	0.200	-	-
Total cell **OD_{660}** after 1127 h of fermentation	2.270		

B7 Protein analysis

To test the possibility of firm cell attachment on the beads, protein analysis on the washed glass beads was performed using Bradford assay analysis. The protein calibration curve was plotted between OD_{595} and OD_{660} for *C. ragsdalei* cells using DI water as a blank (Figure B10). The 1N NaOH solution used to digest the cells during protein analysis with Bradford reagent and no cells had an OD_{595} of 0.345 with DI water as a blank. Thus, the line did not pass through origin and had an intercept of 0.345.

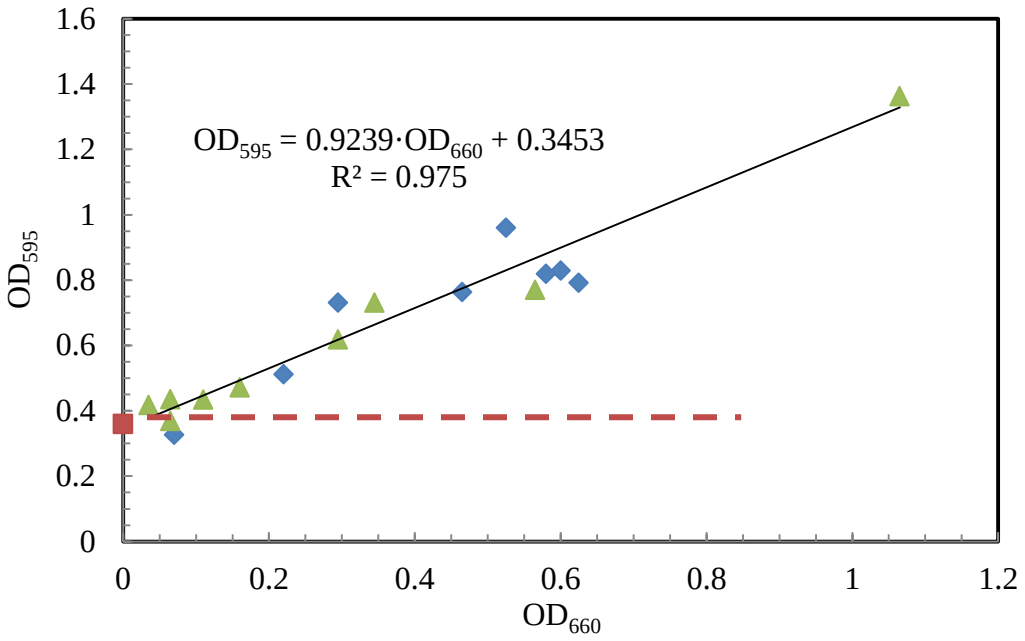

Figure B10 Protein calibration curve.
(◆) Cell mass samples from serum bottle 1 (▲) Cell mass samples from serum bottles 2 (■) NaOH sample reading at OD_{595} without cells.

The protein analysis was performed on three samples of the washed beads used during fermentation and also on control beads which were not used in fermentation (Table B5). After Bradford assay on the control beads without cells, the solution had an OD_{595} of 0.632. To remove the effect of beads and NaOH on OD_{595} measurement and calculate cell OD_{660}, the OD_{595} of the control beads and NaOH solution were subtracted from the OD_{595} values for the sample containing beads and cells. An OD_{660} above zero would indicate a possible cell attachment. Since, the OD_{660} was below zero it was concluded that the there was no cell attachment on the beads.

Table B5 Protein analysis on beads with and without cells after the end of the fermentation.

Sample Description	OD_{595}		
	Sample 1	Sample 2	Average
water blank	0		
Control beads[a]	0.634	0.63	0.632
Beaker 1[b]	0.752	0.904	0.828
Beaker 2[b]	0.847	0.809	0.828
Beaker 3[b]	0.919	0.94	0.930
Average OD_{595} for beads and cells			0.862
Cell OD_{595} on beads[b]			0.230

[a] not used in fermentation; [b]used in fermentation

B8 Conclusions and Recommendations

Major conclusions from this experiment are as follows:

- During 436 h of lag phase, ORP was stable at -340 mV (Ag/AgCl). The low ORP indicated that the medium was reduced without O_2 contamination. Thus, addition of more inoculum at 388 h followed by decreasing the gas flow rate helped in starting the fermentation. Hence, ORP should be used as an indicator of anaerobic conditions in the TBR. Further, the TBR should only be inoculated after a stable ORP is measured for at least 6-8 h prior to the inoculation.
- After 436 h of lag phase, addition of 50 ml more inoculum and use of low gas flow rates helped to overcome inhibition associated with high mass transfer rates in TBR and start the fermentation.
- Increasing the gas flow rates from 2.93 sccm to 13.8 sccm decreased the CO and H_2 gas conversion efficiencies by 60% and 80%, respectively.
- Cell OD_{660} of 2.3 was measured from the cell mass balance performed on the beads after washing with DI water.

- Bradford protein analysis determined that there was no firm attachment of cells on the beads.

Recommendations from this experiment are as follows:

- In order to reduce the lag phase in the future experiments, (i) the inoculum size should be increased to 60% (v/v) and (ii) Fermentation should be started with low gas flow rates to avoid any inhibition on cell activity.
- Instead of addition of 1X nutrients during the experiment, 400 ml of medium will be replaced in the next fermentation to test the effect of operating conditions (gas and liquid flow rates) on the fermentation.

C SEMI-CONTINUOUS FERMENTATION WITH MEDIUM REPLACEMENT AT 0.005 VVM

C1 Background

In this semi-continuous fermentation, the effect of changing liquid flow rates on gas conversion efficiencies, product and cell $OD_{660}$was investigated by keeping the gas flow rate constant at 2.3 sccm (0.005 vvm). The materials and methods are discussed in Section 5.2. In order to reduce the lag phase, the TBR was inoculated with 60% (v/v) inoculum, which resulted in an initial cell $O.D_{660}$ of 0.3. To continue the fermentation and test the effect of different flow rates 400 ml exhausted medium was replaced with fresh medium when the OD_{660} in the liquid medium dropped to 0.3 for runs R1 to R3. For runs R4 to R7, the medium was replenished when the CO conversion efficiency dropped to below 40%. A liquid medium head was maintained at the bottom of the TBR to make sure that the gas does not bypass through the liquid outlet line into the sump headspace in counter-current mode. The liquid flow rates tested were 200, 300, 500 and 700 ml/min.

C2 Cell growth and pH

The cell $O.D_{660}$ and pH profiles are shown in Figures C1 and C2. From the cell $O.D_{660}$ graph, it can be observed that repetitive removal and addition of fresh medium prolonged fermentation (~ 900 h) and resulted in biofilm formation on the beads. Thus, the cell $O.D_{660}$ measured in the liquid medium dropped significantly at every medium change in subsequent runs.

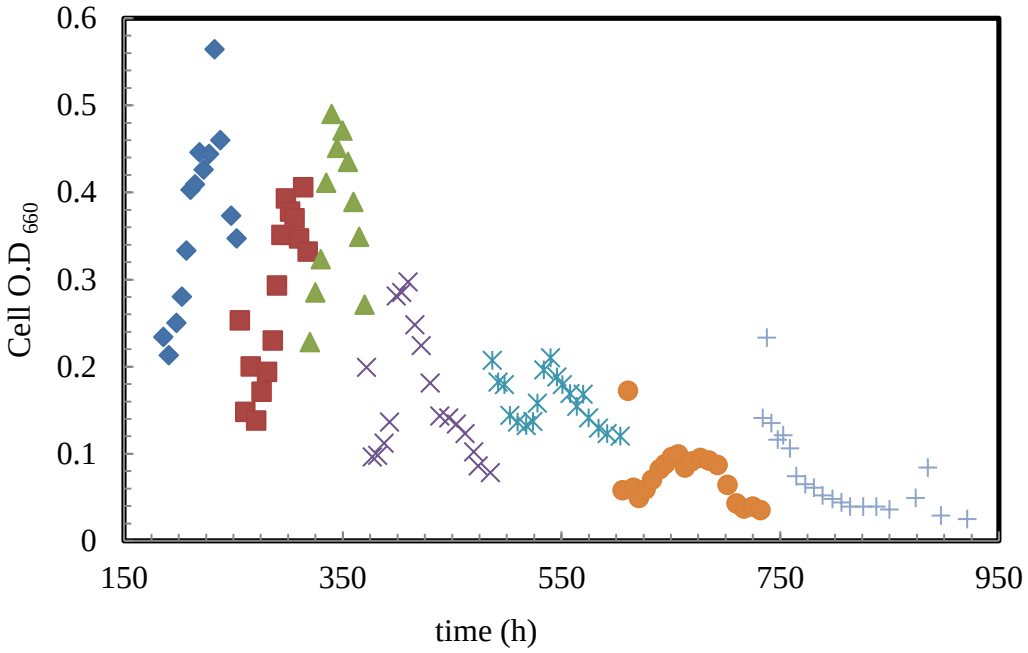

Figure C1 Cell Growth profiles for all runs in semi-continuous TBR fermentation. (◆) R1 (■) R2 (▲) R3 (×) R4 (✳) R5 (●) R6 (+) R7. R1: L = 400-700 ml/min, G = 2.3-2.76 sccm; R2: L = 300 ml/min, G = 2.3 sccm; R3& R7: L = 500 ml/min, G = 2.3 sccm; R4 & R6: L = 200 ml/min, G = 2.3 sccm; R5: L = 700 ml/min, G = 2.3 sccm.

The maximum cell $O.D_{660}$ was achieved when nutrient limitations occurred during fermentation and cells stopped growing. This was clearly evident from the cell $O.D_{660}$ graphs at 500 ml/min liquid flow rate in runs R3 and R7. At the very beginning of this experiment (320 h of fermentation time) when liquid flow rate was 500 ml/min, a clear increase in cell $O.D_{660}$ was observed. However when the liquid flow rate was changed to 500 ml/min at the end of the experiment (730 h of fermentation time) small cell $O.D_{660}$ was observed.

In the initial run R1, a maximum $O.D_{660}$ of 0.56 was observed. The maximum $O.D_{660}$ in subsequent runs dropped to 0.5, 0.3, 0.2, 0.1 in runs R3, R4, R5 and R6. In run R7, the cell $O.D_{660}$ was below 0.1. The sudden increase in the cell $O.D_{660}$ at the beginning

of the runs R5, R6 and R7 are due to the suspension of the cells from packing into the medium when the liquid flow rate was changed.

For all fermentation runs, the pH increased back to 5.8 when the medium was replaced (Figure C2). Further, the pH slowly started to drop as the fermentation progressed and products were formed. Once, the pH dropped to 4.5 it was maintained at this value by the addition of about 1 ml of 2N KOH.

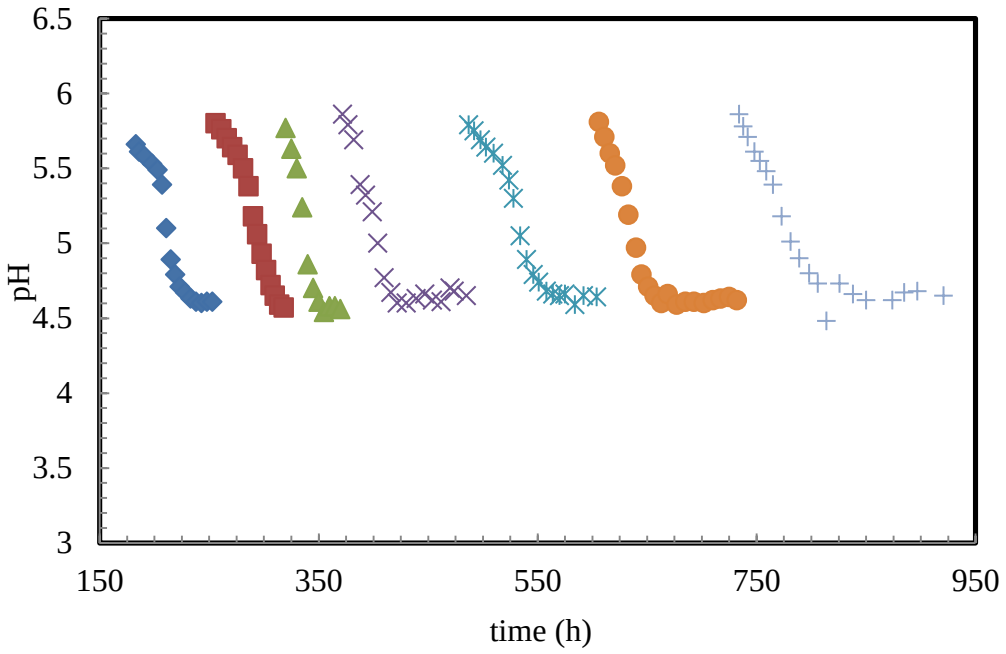

Figure C2 pH profiles for all runs in semi-continuous TBR fermentation. (◆) R1 (■) R2 (▲) R3 (×) R4 (✳) R5 (●) R6 (+) R7. R1: L = 400-700 ml/min, G = 2.3-2.76 sccm; R2: L = 300 ml/min, G = 2.3 sccm; R3& R7: L = 500 ml/min, G = 2.3 sccm; R4 & R6: L = 200 ml/min, G = 2.3 sccm; R5: L = 700 ml/min, G = 2.3 sccm.

C3 Product profiles

Ethanol and acetic acid production profiles are shown in Figures C3 and B4, respectively. The ethanol produced was around 2.4 g/L in run R1. In runs R2 and R3, the ethanol produced was around 1.5 and 1.1 g/L, respectively. Since, the runs were stopped earlier than the previous runs the concentration of ethanol produced was low in these two

runs. For runs R4, R5 and R6, the ethanol produced was between 3.4 to 3.7 g/L. However, ethanol concentrations in runs R2 and R3 were similar at the two liquid flow rates tested. There was no difference in ethanol production in R4 and R5 200 and 700 ml/min. This indicated that the liquid flow rate did not affect product concentrations. The acetic acid produced in run R1 was 3.3 g/L. In runs R2 and R3, 4 g/L of acetic acid was produced. In runs R4, R5and R6, the acetic acid produced slightly increased to 5 g/L. Runs R4 to R6 were performed much longer (i.e., until CO conversion efficiency dropped to below 40%) hence more acid was produced in these runs than in runs R2 and R3. However, overall at different liquid flow rates in runs R2 and R3 or in runs R4 and R5, the amounts of acetic acid produced were similar.

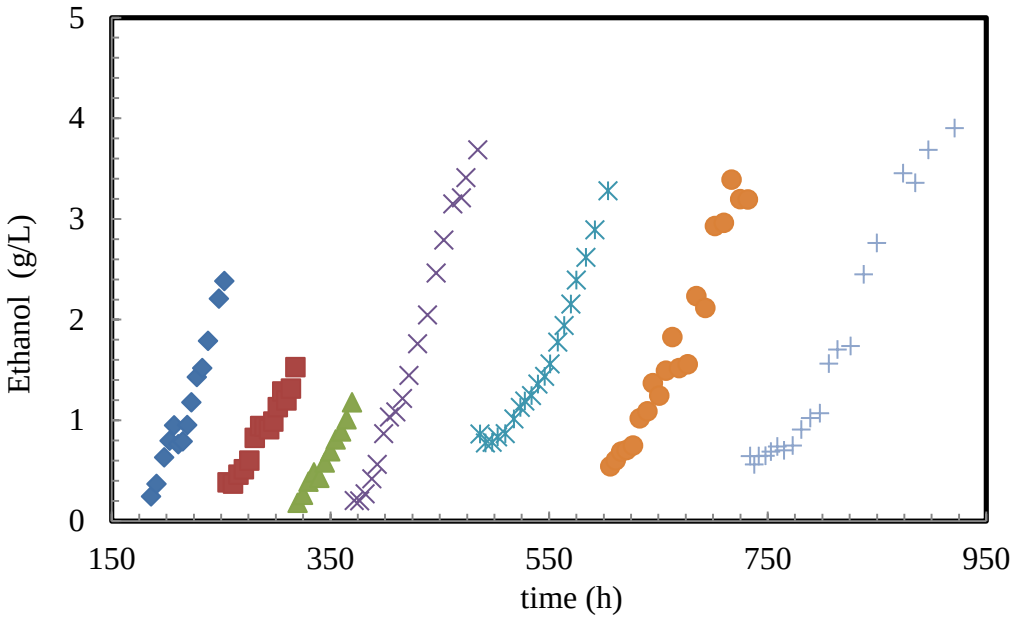

Figure C3 Ethanol profiles for all runs in semi-continuous TBR fermentation. (◆) R1 (■) R2 (▲) R3 (×) R4 (✳) R5 (●) R6 (+) R7. R1: L = 400-700 ml/min, G = 2.3-2.76 sccm; R2: L = 300 ml/min, G = 2.3 sccm; R3& R7: L = 500 ml/min, G = 2.3 sccm; R4 & R6: L = 200 ml/min, G = 2.3 sccm; R5: L = 700 ml/min, G = 2.3 sccm.

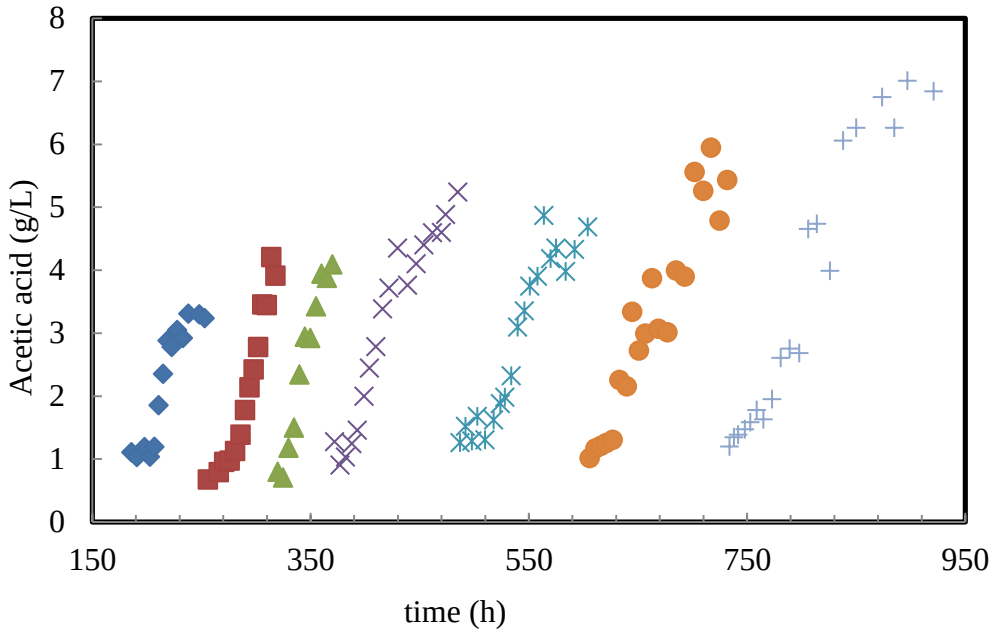

Figure C4 Acetic acid profiles for all runs in semi-continuous TBR fermentation. (◆) R1 (■) R2 (▲) R3 (×) R4 (✳) R5 (●) R6 (+) R7. R1: L = 400-700 ml/min, G = 2.3-2.76 sccm; R2: L = 300 ml/min, G = 2.3 sccm; R3& R7: L = 500 ml/min, G = 2.3 sccm; R4 & R6: L = 200 ml/min, G = 2.3 sccm; R5: L = 700 ml/min, G = 2.3 sccm.

C4 Gas Conversions

CO and H_2 conversion efficiencies are shown in Figures C5 and C6, respectively. The maximum CO and H_2 conversion efficiencies were very similar at different liquid flow rates (200 – 700 ml/min) at 0.005 vvm. The vvm was based on the total liquid volume in the reactor which is 500 ml and was independent of liquid flow rate (i.e., vvm did not change with liquid flow rate). However when the liquid flow rate of 500 ml/min was repeated in the last run R7, CO and H_2 conversion efficiencies were much lower than in run R3. In R3, the medium was changed when the gas conversion efficiencies were as high as 80% CO and 60% H_2. However in run R7, the conversion efficiencies were allowed to drop to as low as 38% CO and 30% H_2 .Thus, it can be concluded that the conditions of cells were different in runs R3 and R7 (i.e., cells were more active in run R3).

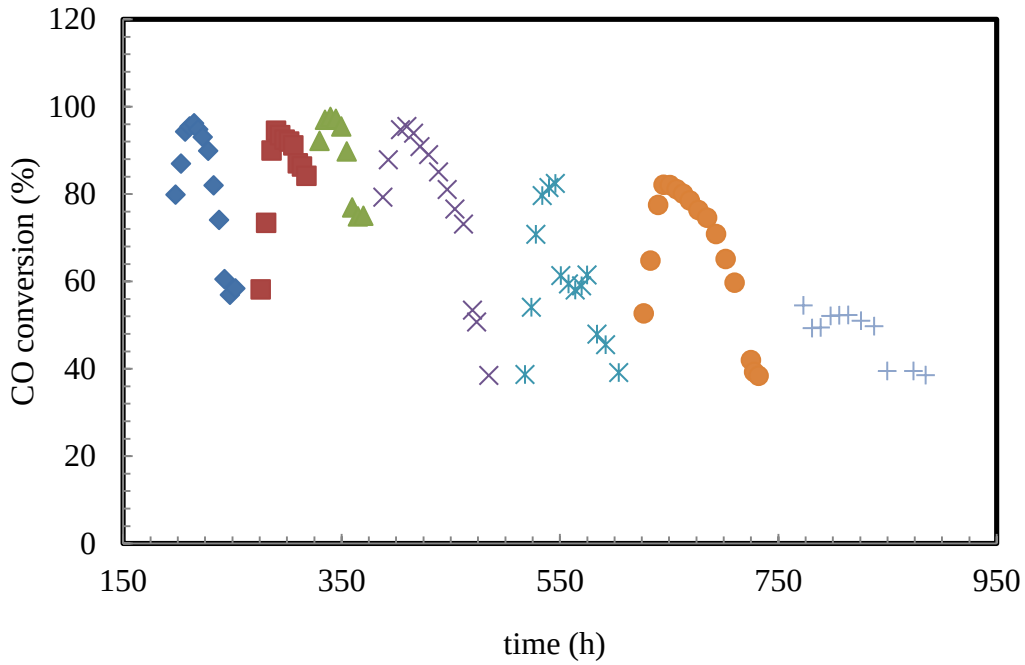

Figure C5 CO conversion for all runs in semi-continuous TBR fermentation. (◆) R1 (■) R2 (▲) R3 (×) R4 (✳) R5 (●) R6 (+) R7. R1: L = 400-700 ml/min, G = 2.3-2.76 sccm; R2: L = 300 ml/min, G = 2.3 sccm; R3& R7: L = 500 ml/min, G = 2.3 sccm; R4 & R6: L = 200 ml/min, G = 2.3 sccm; R5: L = 700 ml/min, G = 2.3 sccm.

The maximum CO conversion efficiency for runs R1 to R4 were about 95 % irrespective of the different liquid flow rates used (Figure C5). In runs R5 and R6, since the medium replacement was performed only when the gas conversions dropped to below 40%, the maximum CO conversion efficiency achieved in these runs dropped to around 82%. In the last run R7, the maximum CO conversion efficiency further dropped to about 55%. In run R7, the liquid flow rate was maintained at 500 ml/min. If proper liquid head was not maintained the gas could have bypassed from the reactor bottom to the sump headspace. This in turn could have resulted in low gas conversions in run R7.

The maximum H_2 conversion efficiencies were between 75 to 89% for runs R1 to R3 (Figure C6). From runs R4 to R6, the maximum H_2 conversion efficiencies obtained

were between 70% and 80%. In the last run R7, the maximum H_2 conversion efficiency was about 55%.

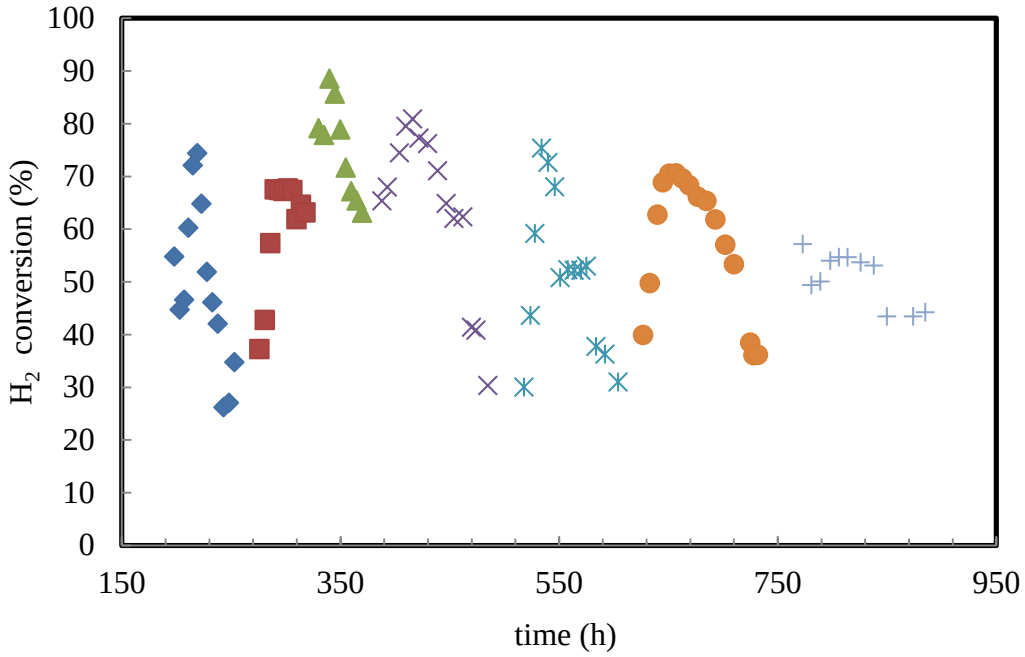

Figure C6 H_2 conversion for all runs in semi-continuous TBR fermentation. (◆) R1 (■) R2 (▲) R3 (×) R4 (✳) R5 (●) R6 (+) R7. R1: L = 400-700 ml/min, G = 2.3-2.76 sccm; R2: L = 300 ml/min, G = 2.3 sccm; R3& R7: L = 500 ml/min, G = 2.3 sccm; R4 & R6: L = 200 ml/min, G = 2.3 sccm; R5: L = 700 ml/min, G = 2.3 sccm.

C5 Gas uptakes

The CO and H_2 gas uptake rate profiles are shown in Figure C7 and C8, respectively. In run R1, a maximum uptake rate of 3 mmol/h of CO and 1.8 mmol/h of H_2 was measured. In runs R2, R3 and R4 at different liquid flow rates, the CO uptake rate was 2.6 mmol/h. In runs R5 and R6 with different liquid flow rates, the maximum CO uptake rates were similar. In run R7, the maximum CO uptake rate dropped to 1.4 mmol/h. However, as described in the Section C4, the drop in uptake rates in run R7 could have been due to gas bypass at the bottom of the TBR. The maximum H_2 uptake rate was 1.4 mmol/h in run R2 and run R6 at 300 ml/min and 200 ml/min, respectively. In

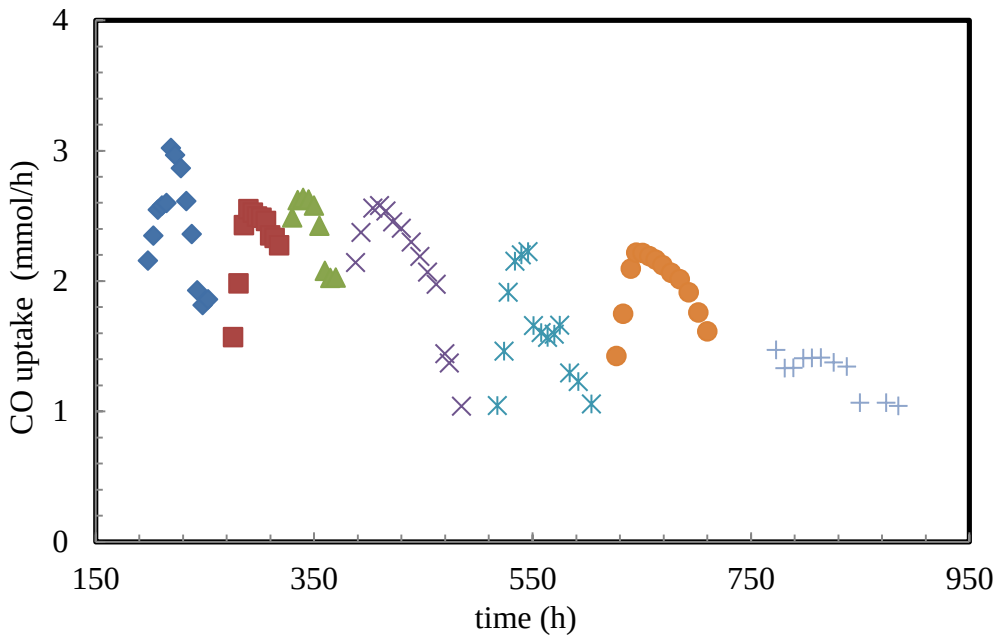

Figure C7 CO uptake rates for all runs in semi-continuous TBR fermentation. (◆) R1 (■) R2 (▲) R3 (×) R4 (✳) R5 (●) R6 (+) R7. R1: L = 400-700 ml/min, G = 2.3-2.76 sccm; R2: L = 300 ml/min, G = 2.3 sccm; R3& R7: L = 500 ml/min, G = 2.3 sccm; R4 & R6: L = 200 ml/min, G = 2.3 sccm; R5: L = 700 ml/min, G = 2.3 sccm.

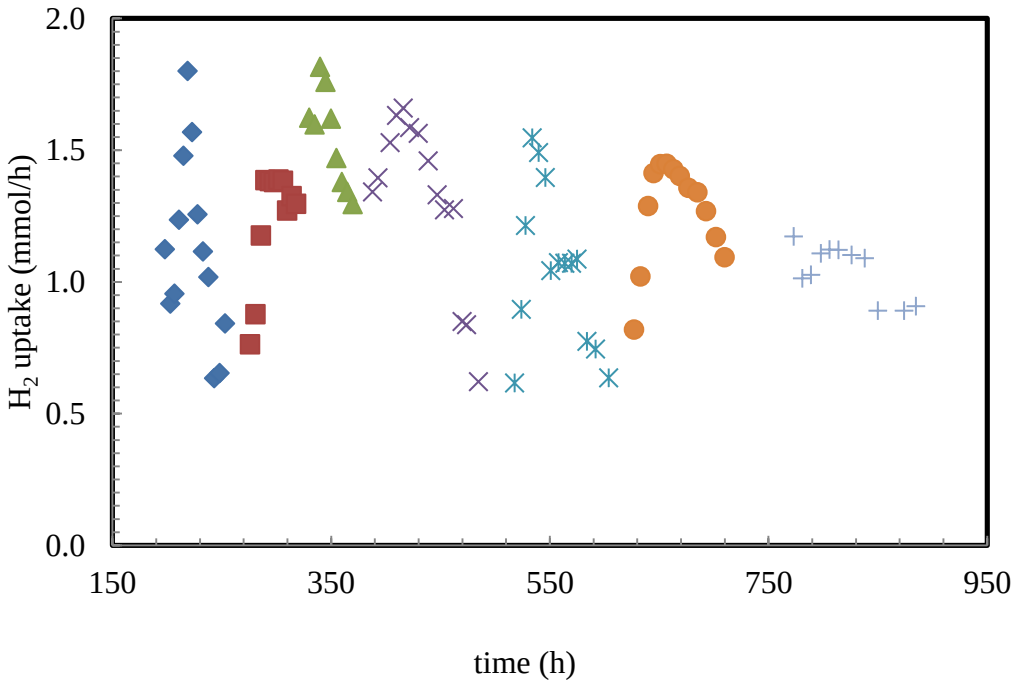

Figure C8 H_2 uptake rates for all runs in semi-continuous TBR fermentation. (◆) R1 (■) R2 (▲) R3 (×) R4 (✳) R5 (●) R6 (+) R7. R1: L = 400-700 ml/min, G = 2.3-2.76 sccm; R2: L = 300 ml/min, G = 2.3 sccm; R3& R7: L = 500 ml/min, G = 2.3 sccm; R4 & R6: L = 200 ml/min, G = 2.3 sccm; R5: L = 700 ml/min, G = 2.3 sccm.

runs R4, R5 and R6, the maximum H_2 uptake rate was similar (about 1.5 mmol/h) at different liquid flow rates.

C6 ORP

The redox potential in the fermentation medium is shown in Figure C9. The medium was very reduced and the redox potential was in the range of -500 mV to -400 mV when fresh medium was added. Further, the medium was very reduced when the cells started to grow. However, as ethanol and acetic acid production started, the ORP started to increase and reached -300 mV to -350 mV. In the last run R 7, the fermentation was performed until the gas conversion efficiency dropped to zero and no further increase in the product concentrations were observed. In run R7, the ORP went up to as high as -41 mV. The increase in ORP was mostly associated with production of ethanol and acetic acid. On the other hand, the decrease in ORP(i.e., very reduced medium) was associated with cell growth.

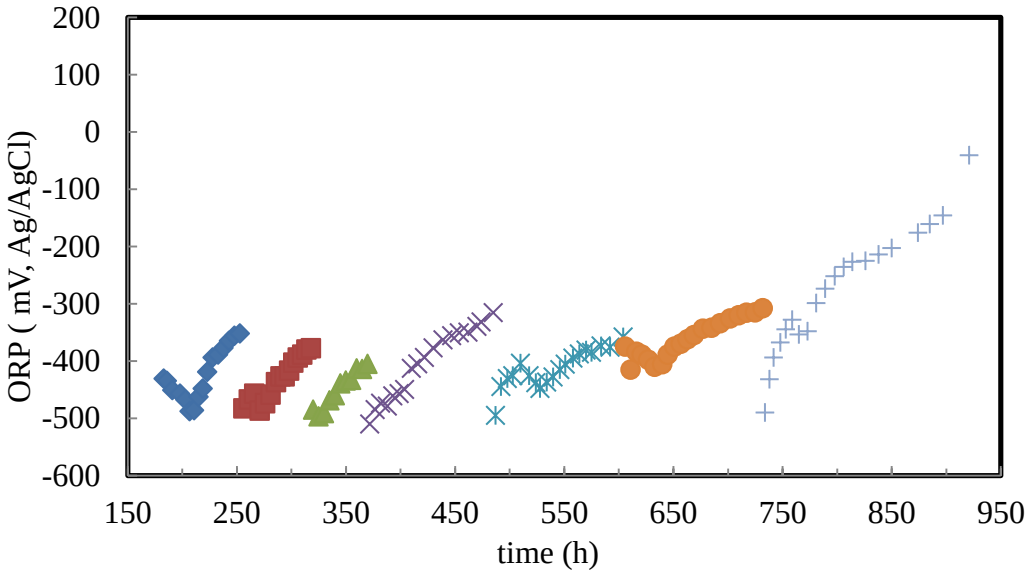

Figure C9 ORP for all runs in semi-continuous TBR fermentation.
(◆) R1 (■) R2 (▲) R3 (×) R4 (✳) R5 (●) R6 (+) R7. R1: L = 400-700 ml/min, G = 2.3-2.76 sccm; R2: L = 300 ml/min, G = 2.3 sccm; R3& R7: L = 500 ml/min, G = 2.3 sccm; R4 & R6: L = 200 ml/min, G = 2.3 sccm; R5: L = 700 ml/min, G = 2.3 sccm.

C7 Cell mass balance

The cell mass balance procedure was similar in Chapter 5, Section 5.2.5. Table C1 shows the cell OD_{660} in the duplicate wash samples. It can be observed that the total cell OD_{660} in the fermentation medium at 921 h was 0.02. However, when the beads were washed with DI water, the cell OD_{660} was 2.35 after 921 h. This indicates that cells were mostly loosely attached on the beads and were easily removed by simple washing of the beads with water. Further protein analysis was done to test if there was any firm attachment of the cells on the beads.

Table C1 Cell mass balance from beads and column wash with DI Water

Samples Description	OD_{660} in 500 ml		
	Sample 1	Sample 2	Average
1st wash of beads with 500 ml DI water	1.739	1.746	1.743
2nd wash of beads with 500 ml DI water	0.371	0.390	0.381
3rd wash of beads with 500 ml of DI water	0.112	0.144	0.128
4th wash of beads with 500 ml of DI water	0.066	0.133	0.099
column wash without beads with 500 ml DI water	0.130	-	-
Medium before removing beads at L: 500 ml/min	0.020	-	-
Total cell OD_{660} after 921 h of fermentation	2.50		

C8 Protein analysis

The protein analysis procedure was similar to the protein analysis in the previous appendix Section B7. From protein analysis shown in Table C2, it was observed that, the cell OD_{660} measured on the beads was 0.001 which is significantly lower than the total cell OD_{660} obtained from the simple wash of the beads from the TBR after fermentation

in Section C5, Table C1. Thus, it can be concluded that there is no firm attachment of the cells on the beads.

Table C2 Protein analysis on beads

Sample Description	OD_{595}		
	Sample 1	Sample 2	Average
water blank	0		
control beads[a]	0.513	0.537	0.525
Beaker 1[b]	0.826	0.889	0.858
Beaker 2[b]	0.86	0.91	0.885
Average OD_{595} for beads and cells			0.871
$O.D_{595}$ with control beads[a]			0.346
$O.D_{660}$ on beads[b]			0.001

[a] not used in fermentation; [b]used in fermentation

C9. Conclusions and Recommendations

Major conclusions are as follows:

- Using cell OD_{660} in the medium as an indicator to replace the medium was not helpful because when the biofilm formation started, the cell OD_{660} in the medium slowly dropped to zero in the subsequent runs from R1 to R7indicating biofilm formation. However, using the drop in the CO conversion efficiency as the indicator of nutrient limitations was helpful in maintaining the same basis for the next run.
- At a gas flow rate of 2.3 sccm, CO and H_2 conversion efficiencies were up to 95 and 90 %, respectively.
- Changing the liquid flow rate had no effect on the fermentation at 0.005 vvm.

- Cell OD_{660} of 2.5 was measured from the cell mass balance performed on the beads by washing with DI water and Bradford protein analysis determined that there was no firm attachment of cells on the beads.

Recommendations from this experiment are as follows:

- In the next experiment, the effect of different liquid flow rates (200, 500 and 700 ml/min) will be tested at 0.01 vvm (i.e., 4.6 sccm gas flow rate).
- Also in the next experiment, the startup inoculum of 60% (v/v) will be used. Additionally, when the CO gas conversion efficiency dropped below 40%, the medium will be replaced.
- Gas analysis will be performed at TBR exit and sump exit to see if appreciable conversions are happening in the sump.

D SEMI-CONTINUOUS FERMENTATION WITH MEDIUM REPLACEMENT AT 0.01 VVM

D1 Background

The semi-continuous fermentation experiment was conducted over a period of 1200 h. In this fermentation, the gas flow rate was 4.6 sccm and liquid flow rates were 200, 500 and 700 ml/min. The materials and methods are discussed in Chapter 5, Section 5.2. In the startup run with 300 ml inoculum and 200 ml fresh medium, the flow rates were set at 4.6 sccm gas and 500 ml/min of liquid flow rate. There was no growth and no gas consumption observed for 46 h. Considering that the gas flow could have been too high resulting in cell inhibition, the TBR was purged with N_2 at 130.5 sccm for 2 h and then the syngas flow was decreased to 2.3 sccm at 48 h. Cells started growing and as the fermentation slowed down and the CO conversion efficiency dropped to about 40% and the medium was replaced. In the subsequent fermentation runs, 400 ml of exhausted medium was replaced with fresh medium when the CO conversions dropped to about 40%.

D2 Cell growth and pH

The cell OD_{660} and pH profiles are shown in Figures D1 and D2, respectively. It was observed that a maximum cell OD_{660} of 0.6 was measured in run R1 at a liquid flow rate of 500 ml/min. The amount of cells suspended in the medium was high in run R1 because of the use of high liquid circulation rate of 500 ml/min at the beginning of the

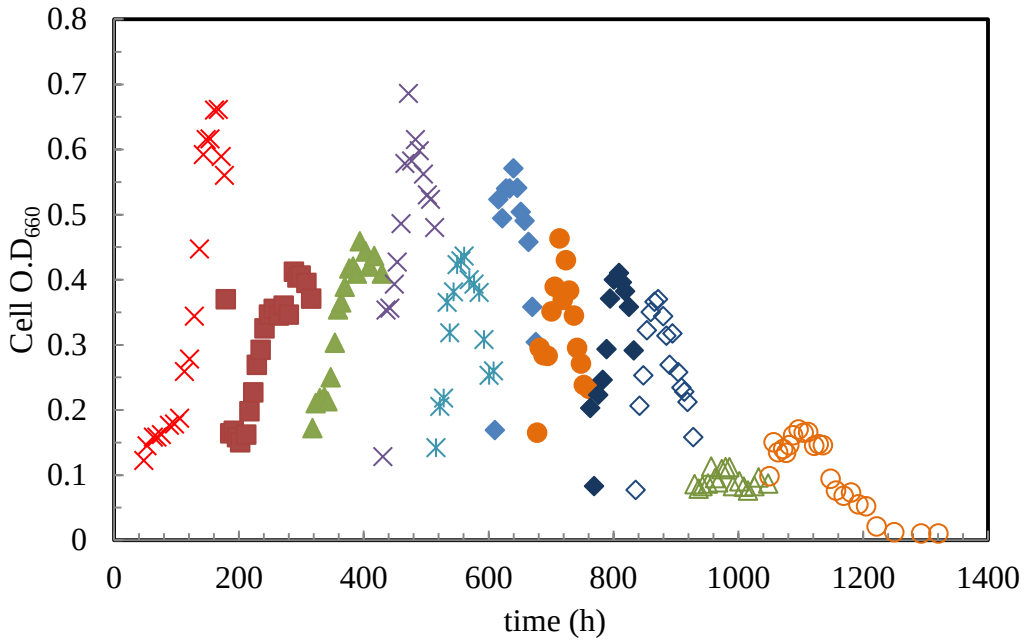

Figure D1 Cell Growth profiles for all runs in semi-continuous TBR fermentation. (×) R1 (■) R2 (▲) R3 (×) R4 (✳) R5 (◆) R6 (●) R7 (◆) R8 (◇) R9 (△) R10 (○) R11. R1: L = 500 ml/min, G = 2.3 sccm; R2: L = 200 ml/min, G = 2.3 sccm; R3 & R5: L = 200 ml/min, G = 4.6 sccm; R4 & R7: L = 500 ml/min, G = 4.6 sccm; R6 &R8: L = 700 ml/min, G = 4.6 sccm; R9: L = 700 ml/min, G = 4.6 sccm, co-current; R10: L = 200 ml/min, G = 4.6 sccm, co-current; R11: L = 500 ml/min, G = 4.6 sccm, co-current.

fermentation. Thus, in order to allow the cells to form biofilm on the packing the liquid flow rate was reduced to 200 ml/min and the gas flow rate was kept stable at 2.3 sccm in run R2. In run R2, the maximum OD_{660} in the liquid medium was 0.4 indicating that there was a possibility of cells attaching to the beads. Again in run R4 when the liquid flow rate was increased to 500 ml/min, the cell OD_{660} was high in the liquid medium indicating possible washout of the loosely attached cells in the packing. In the subsequent runs from R5 to R11, the cells OD_{660} profiles indicate a decrease in maximum cell OD_{660} in the liquid medium. The runs from 700 h to 800 h showed a possibility of biofilm formation because the cell OD_{660} was low in the liquid medium as shown in Figure D1. At the end of the fermentation, the glass beads were collected in a clean tub and then

washed three times each with 500 ml of DI water. Table D1 shows the measured cell OD_{660} of the duplicate samples collected from each wash. The summation of the average of the three washes gave the total cell OD_{660} of 2.4 in the packing after 1321 h of fermentation. This high cell OD_{660} in the packing indicates that cells were loosely attaching to the beads during the fermentation. The cell OD_{660} on the beads in this experiment is consistent with the cell OD_{660} observed in the previous fermentations discussed in Appendix B, Section B6 and Appendix C, Section C7.

Table D1 Cell mass balance from beads and column wash with DI Water.

Samples Description	$O.D_{660}$ in 500 ml		
	sample 1	sample 2	average
1^{st} wash of beads with 500 ml DI water	2.224	2.142	2.183
2^{nd} wash of beads with 500 ml DI water	0.222	0.216	0.219
3^{rd} wash of beads with 500 ml of DI water	0.042	0.036	0.039
Total cell OD_{660} after 1321 h of fermentation	2.44		

The initial pH in all the runs was 5.8. When the cells started to grow acetic acid was produced. This resulted in slow drop in pH. Once, the pH reached around 4.5 it was maintained at pH 4.5 by manually adding about 1 ml of 2 N KOH solution at every sampling. The pH drop was slower in the initial runs at the beginning of the experiment. However, as the fermentation progressed, the drop in the pH was much faster.

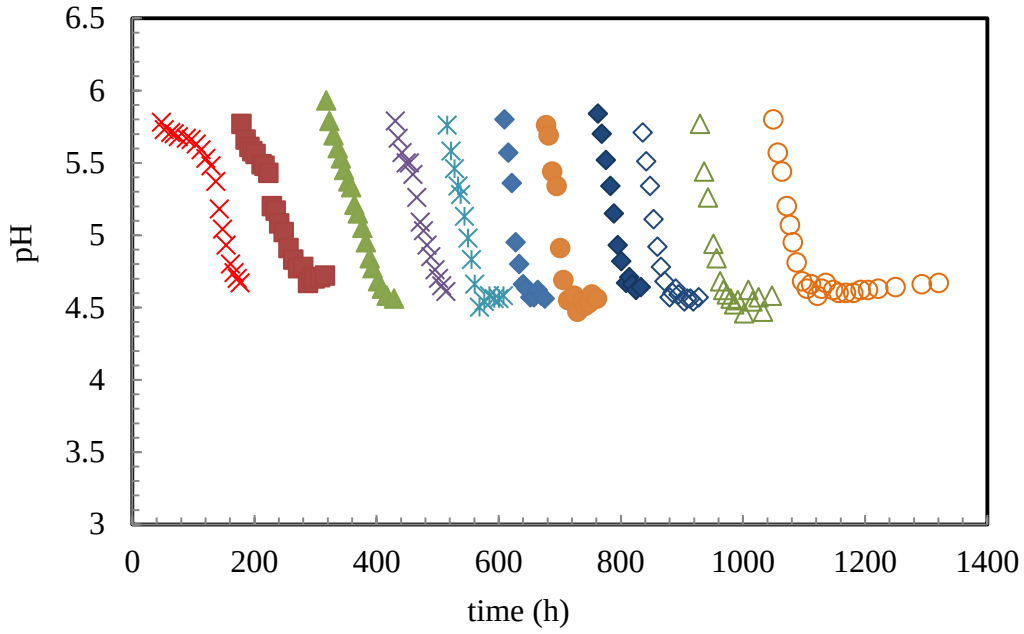

Figure D2 pH profiles for all runs in semi-continuous TBR fermentation. (×) R1 (■) R2 (▲) R3 (×) R4 (✳) R5 (◆) R6 (●) R7 (◆) R8 (◇) R9 (△)R10 (○) R11. R1: L = 500 ml/min, G = 2.3sccm; R2: L = 200 ml/min, G = 2.3 sccm; R3 & R5: L = 200 ml/min, G = 4.6 sccm; R4 & R7: L = 500 ml/min, G = 4.6 sccm; R6 &R8: L = 700 ml/min, G = 4.6 sccm; R9: L = 700 ml/min, G = 4.6 sccm, co-current; R10: L = 200 ml/min, G = 4.6 sccm, co-current; R11: L = 500 ml/min, G = 4.6 sccm, co-current.

D3 Product profiles

The ethanol and acetic acid concentration profiles for runs R1 to R11 had an increasing trend as can be observed from Figures D3 and D4, respectively. The product profiles for the same operating condition varied when the runs were carried out at different times. The ethanol and acetic acid concentrations after 70 h in run R4at liquid flow rate of 500 ml/min were 3.3 and 4.1 g/L, respectively. However after 70 h of run time in run R7 at the same liquid flow rate, the ethanol and acetic acid concentrations were 2.5 and 6.4 g/L, respectively. This difference in ethanol and acetic acid production at the same operating condition was due to biofilm formation. Acetic acid production results in ATP generation and hence is more favored than ethanol production. Thus,

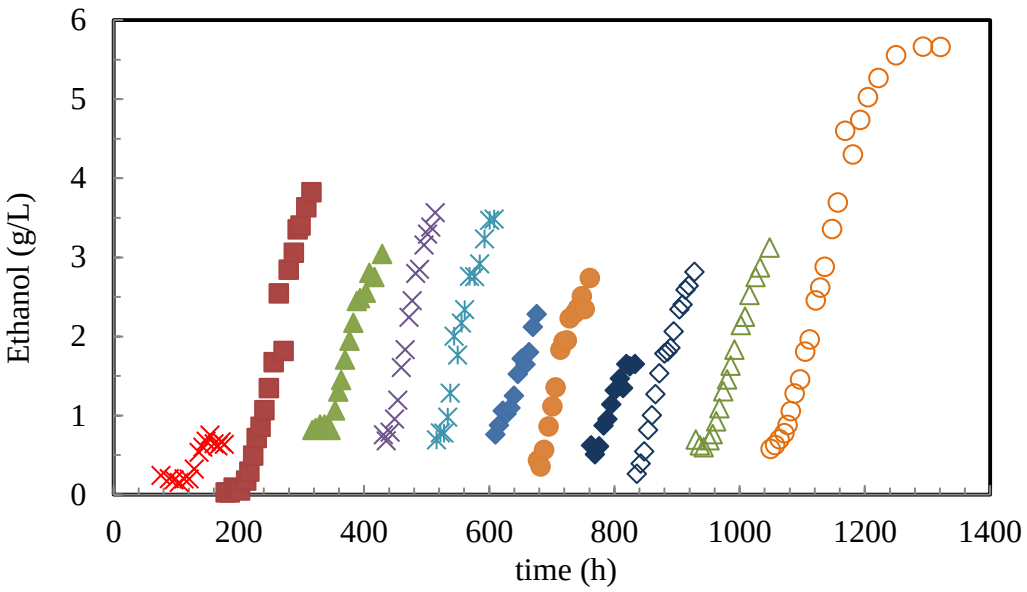

Figure D3 Ethanol profiles for all runs in semi-continuous TBR fermentation. (×) R1 (■) R2 (▲) R3 (×) R4 (✳) R5 (◆) R6 (●) R7 (◆) R8 (◇) R9 (△) R10 (○) R11. R1: L = 500 ml/min, G = 2.3sccm; R2: L = 200 ml/min, G = 2.3 sccm; R3 & R5: L = 200 ml/min, G = 4.6 sccm; R4 & R7: L = 500 ml/min, G = 4.6 sccm; R6 &R8: L = 700 ml/min, G = 4.6 sccm; R9: L = 700 ml/min, G = 4.6 sccm, co-current; R10: L = 200 ml/min, G = 4.6 sccm, co-current; R11: L = 500 ml/min, G = 4.6 sccm, co-current.

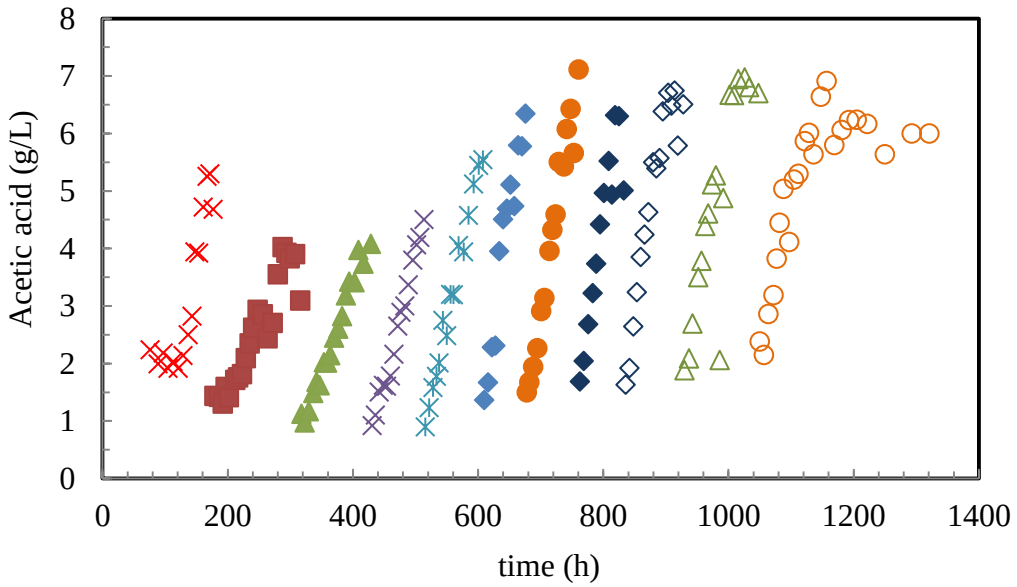

Figure D4 Acetic acid profiles for all runs in semi-continuous TBR fermentation. (×) R1 (■) R2 (▲) R3 (×) R4 (✳) R5 (◆) R6 (●) R7 (◆) R8 (◇) R9 (△) R10 (○) R11. R1: L = 500 ml/min, G = 2.3sccm; R2: L = 200 ml/min, G = 2.3 sccm; R3 & R5: L = 200 ml/min, G = 4.6 sccm; R4 & R7: L = 500 ml/min, G = 4.6 sccm; R6 &R8: L = 700 ml/min, G = 4.6 sccm; R9: L = 700 ml/min, G = 4.6 sccm, co-current; R10: L = 200 ml/min, G = 4.6 sccm, co-current; R11: L = 500 ml/min, G = 4.6 sccm, co-current.

the cell concentration increased in the biofilm more acetic acid was produced. At the end of the fermentation at 1321 h in run R11, 5.7 g/L of ethanol and 5.9 g/L of acetic acid were produced.

D4 Gas Conversions

The CO and H_2 conversion efficiencies are shown in Figures D5 and D6, respectively. The % maximum H_2 gas conversion efficiencies at the same operating condition varied when the runs were carried out at different times. For example, at liquid flow rates of 200 ml/min and 500 ml/min, it can be observed that H_2 gas conversion efficiency was much lower for the first set of runs R3 and R4 conducted at the early stage of the experiment. However, the second set of runs R5 and R7 conducted at a later stage of the experiment showed higher H_2 conversion efficiencies. In the counter-current TBR, the maximum H_2 conversion efficiency was 50% at 500 ml/min in run R7 and 700 ml/min in runs R6 and R8. The maximum H_2 conversion efficiency achieved at 200 ml/min was only 40 % in run R4. A maximum CO conversion efficiency of 85% was obtained at a liquid flow rate of 500 mL/min in run R7. The maximum CO conversion efficiencies at 200 and 700 ml/min were 72% and 68% in run R4 and R6, respectively. The low CO conversion at 700 mL/min in run R8 was due to bypass of part of the gas to the sump from the TBR bottom and not through the 6-mm beads because of liquid head at the bottom of the TBR was very difficult to maintain at this high liquid flow rate.

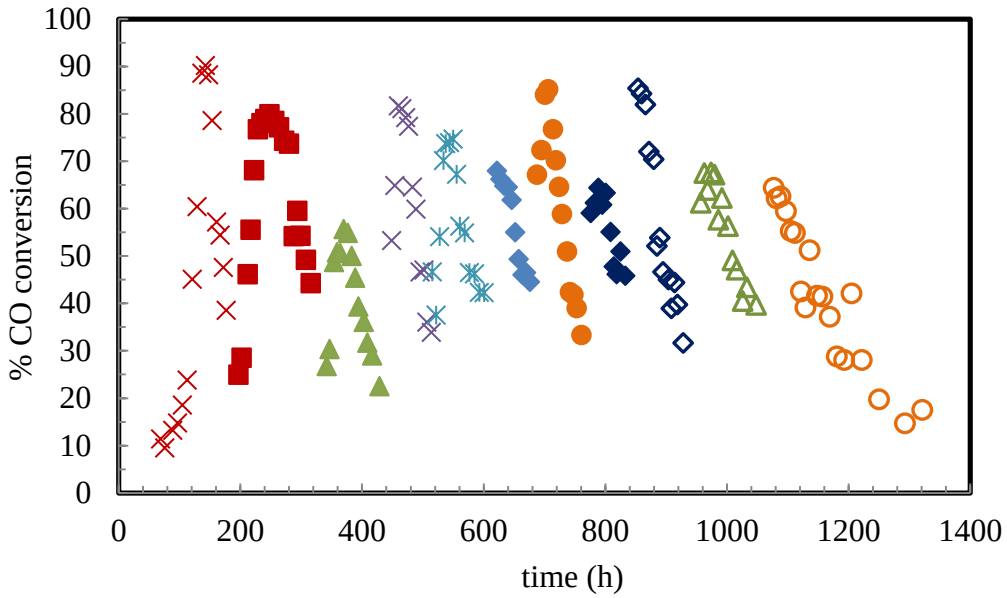

Figure D5 CO conversion for all runs in semi-continuous TBR fermentation. (×) R1 (■) R2 (▲) R3 (×) R4 (✳) R5 (◆) R6 (●) R7 (◆) R8 (◇) R9 (△)R10 (○) R11. R1: L = 500 ml/min, G = 2.3sccm; R2: L = 200 ml/min, G = 2.3 sccm; R3 & R5: L = 200 ml/min, G = 4.6 sccm; R4 & R7: L = 500 ml/min, G = 4.6 sccm; R6 &R8: L = 700 ml/min, G = 4.6 sccm; R9: L = 700 ml/min, G = 4.6 sccm, co-current; R10: L = 200 ml/min, G = 4.6 sccm, co-current; R11: L = 500 ml/min, G = 4.6 sccm, co-current.

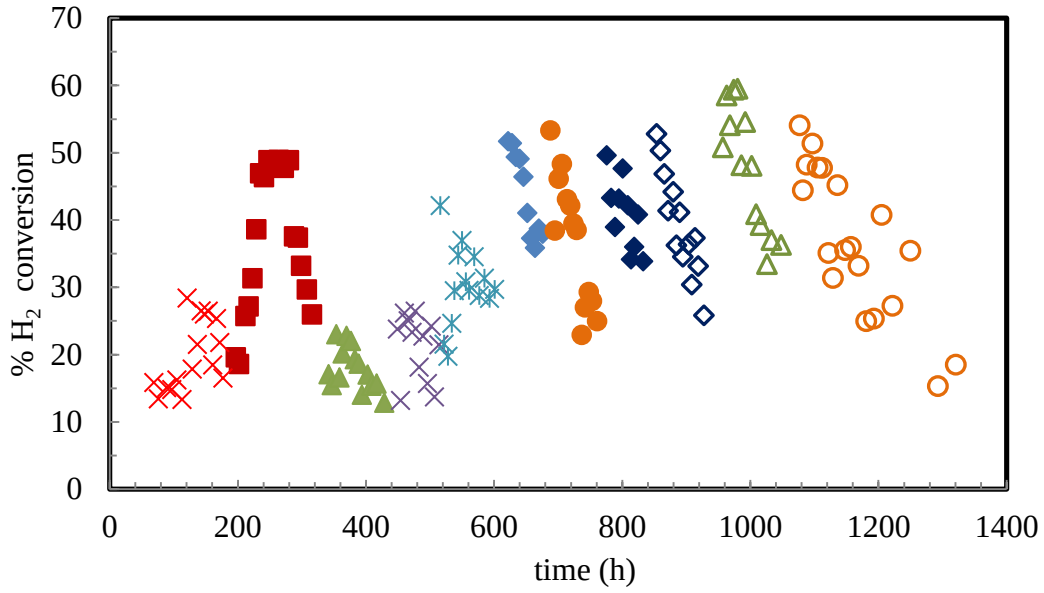

Figure D6 H_2 conversion for all runs in semi-continuous TBR fermentation. (×) R1 (■) R2 (▲) R3 (×) R4 (✳) R5 (◆) R6 (●) R7 (◆) R8 (◇) R9 (△)R10 (○) R11. R1: L = 500 ml/min, G = 2.3sccm; R2: L = 200 ml/min, G = 2.3 sccm; R3 & R5: L = 200 ml/min, G = 4.6 sccm; R4 & R7: L = 500 ml/min, G = 4.6 sccm; R6 &R8: L = 700 ml/min, G = 4.6 sccm; R9: L = 700 ml/min, G = 4.6 sccm, co-current; R10: L = 200 ml/min, G = 4.6 sccm, co-current; R11: L = 500 ml/min, G = 4.6 sccm, co-current.

To reduce the bypass of gas effect, the TBR was operation in co-current mode. In co-current flow, the maximum H_2 conversion efficiency was 60% at 200 ml/min in run R10. The maximum CO conversion efficiency at 700 mL/min was about 85% CO in run R9. However, the maximum CO conversion efficiency was only about 65% at liquid flow rates of 200 and 500 mL/min in runs R11 and R10, respectively. Overall, the CO conversion efficiency was between 56% and 85% for runs R1 to R11 and the H_2 conversion efficiency had an increasing trend with the subsequent runs and then reached a maximum efficiency between 50% and 60% for runs R6 to R11.

D5 Gas uptakes

The CO and H_2 gas uptake rates had increasing trends and reached a maximum and then decreased as the nutrients in the medium were depleted as shown in Figures D7 and D8, respectively. The CO and H_2 gas uptake rates were around 2.2 and 1 mmol/h, respectively at 2.3 sccm gas flow rate in run R2. When the gas flow rate was increased to 4.6 sccm in run R3, the CO uptake rate increased to about 3 mmol/h while the H_2 uptake rate slightly dropped to 0.94 mmol/h. A maximum CO uptake rate of 4.7 mmol/h was obtained in runs R4, R7 and R9 at different liquid flow rates and 4.6 sccm gas flow rate. The H_2 uptake rate had an increasing trend in the subsequent runs and reached a maximum uptake of 2.4 mmol/h in run R10.

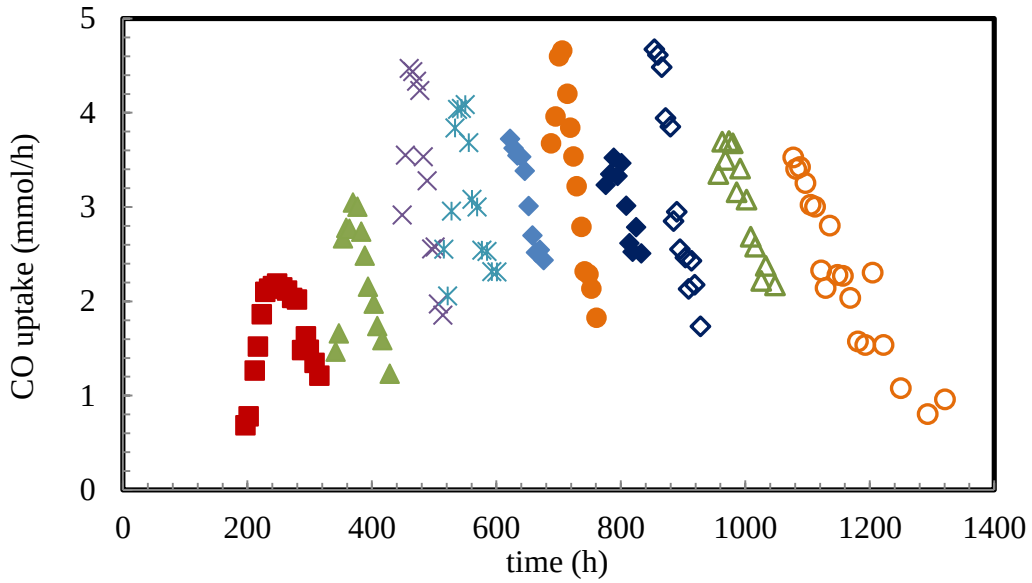

Figure D7 CO uptake rates for all runs in semi-continuous TBR fermentation. (×) R1 (■) R2 (▲) R3 (×) R4 (✳) R5 (◆) R6 (●) R7 (◆) R8 (◇) R9 (△) R10 (○) R11. R1: L = 500 ml/min, G = 2.3sccm; R2: L = 200 ml/min, G = 2.3 sccm; R3 & R5: L = 200 ml/min, G = 4.6 sccm; R4 & R7: L = 500 ml/min, G = 4.6 sccm; R6 &R8: L = 700 ml/min, G = 4.6 sccm; R9: L = 700 ml/min, G = 4.6 sccm, co-current; R10: L = 200 ml/min, G = 4.6 sccm, co-current; R11: L = 500 ml/min, G = 4.6 sccm, co-current.

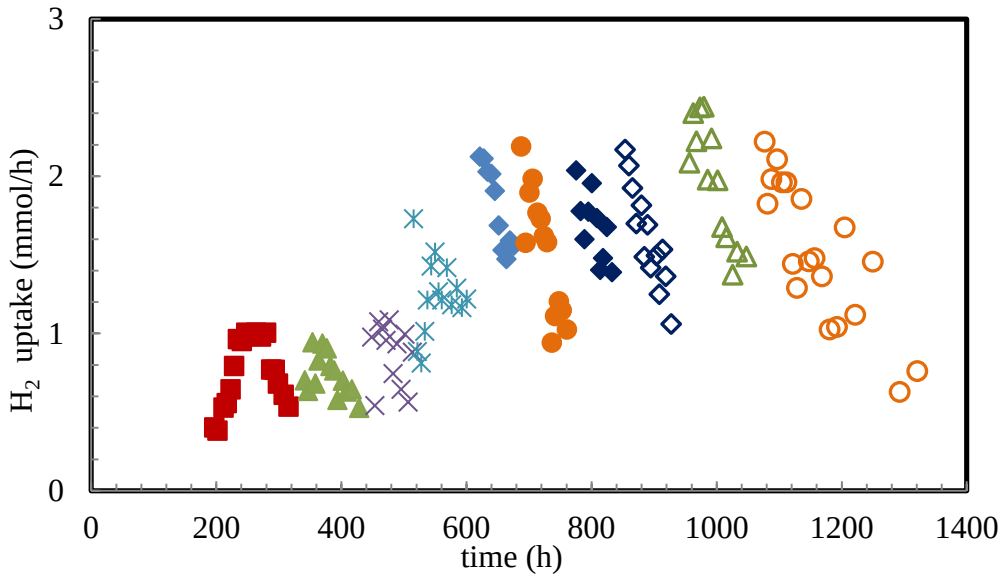

Figure D8 H_2 uptake rates for all runs in semi-continuous TBR fermentation. (×) R1 (■) R2 (▲) R3 (×) R4 (✳) R5 (◆) R6 (●) R7 (◆) R8 (◇) R9 (△) R10 (○) R11. R1: L = 500 ml/min, G = 2.3sccm; R2: L = 200 ml/min, G = 2.3 sccm; R3 & R5: L = 200 ml/min, G = 4.6 sccm; R4 & R7: L = 500 ml/min, G = 4.6 sccm; R6 &R8: L = 700 ml/min, G = 4.6 sccm; R9: L = 700 ml/min, G = 4.6 sccm, co-current; R10: L = 200 ml/min, G = 4.6 sccm, co-current; R11: L = 500 ml/min, G = 4.6 sccm, co-current.

D6 ORP

The ORP profiles are shown in Figure D9. As observed in the previous fermentations, in this experiment the ORP was also very low (-550 mV to -500 mV) immediately after replacing the medium. As the production of ethanol and acetic acid started, the ORP slowly increased to around -400 mV and then to -320 mV. In the last fermentation in run R11, when the fermentation was continued until no gas conversions were observed it reached around -150 mV.

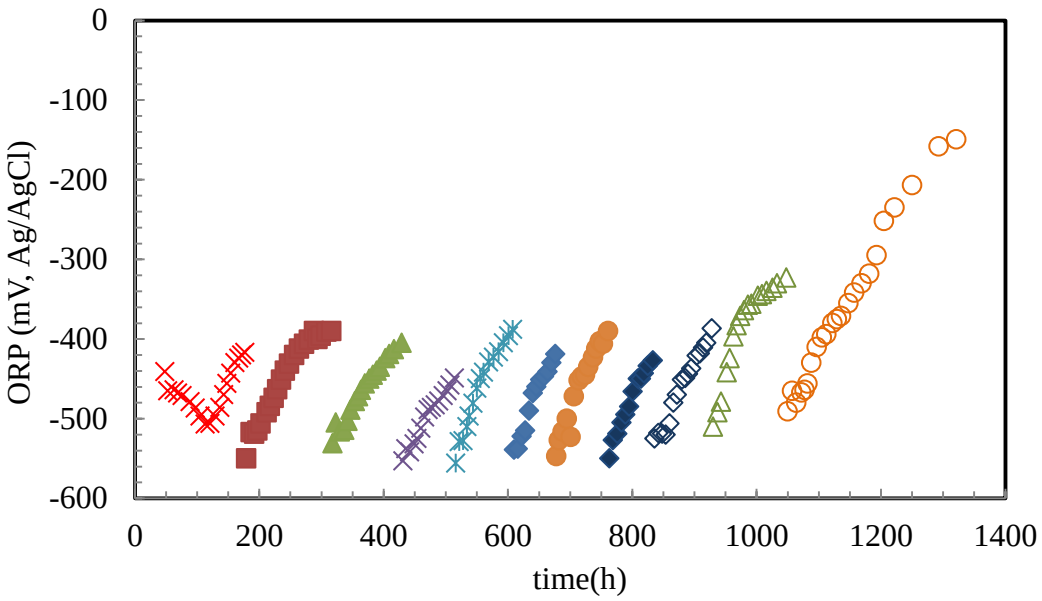

Figure D9 ORP for all runs in semi-continuous TBR fermentation.
(×) R1 (■) R2 (▲) R3 (×) R4 (✳) R5 (◆) R6 (●) R7 (◆) R8 (◇) R9 (△)R10 (○) R11.
R1: L = 500 ml/min, G = 2.3sccm; R2: L = 200 ml/min, G = 2.3 sccm; R3 & R5: L = 200 ml/min, G = 4.6 sccm; R4 & R7: L = 500 ml/min, G = 4.6 sccm; R6 &R8: L = 700 ml/min, G = 4.6 sccm; R9: L = 700 ml/min, G = 4.6 sccm, co-current; R10: L = 200 ml/min, G = 4.6 sccm, co-current; R11: L = 500 ml/min, G = 4.6 sccm, co-current.

D7 Comparison of gas conversions at TBR exit and sump exit

The comparison of CO and H_2 conversion efficiencies between the TBR exit and sump exit for selected fermentation runs is shown in Figures D10 and D11, respectively. In order to confirm that the gas conversion efficiency was occurring in the TBR and not

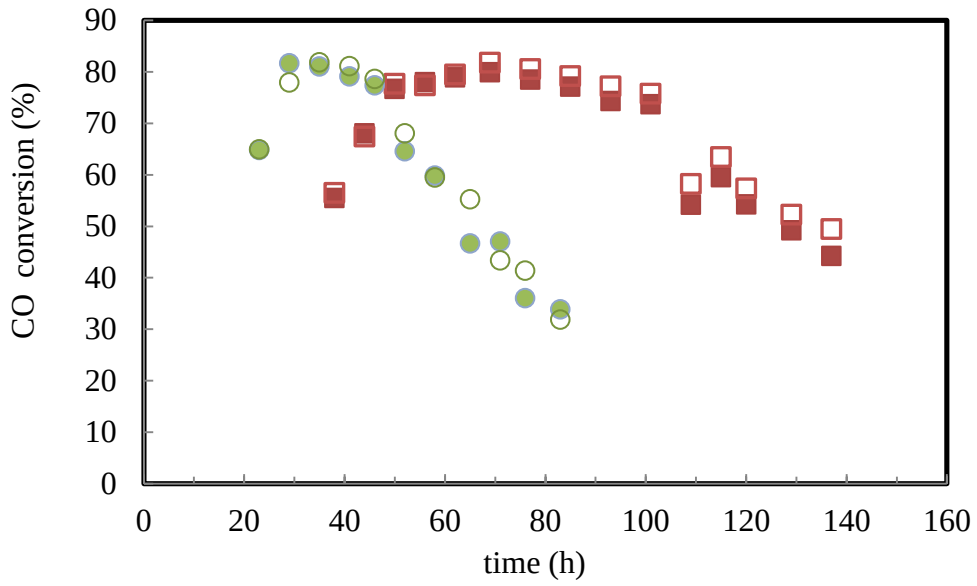

Figure D10 Comparison of CO conversion at TBR exit and sump exit. (■, □) L: 200 ml/min and G: 2.3 sccm (●,○) L = 500 ml/min, G = 4.6 sccm; (◆,◇) L = 200 ml/min, G = 4.6 sccm (▲,△) L = 700 ml/min, G = 4.6 sccm. Solid symbols represent TBR exit and open symbols represents sump exit.

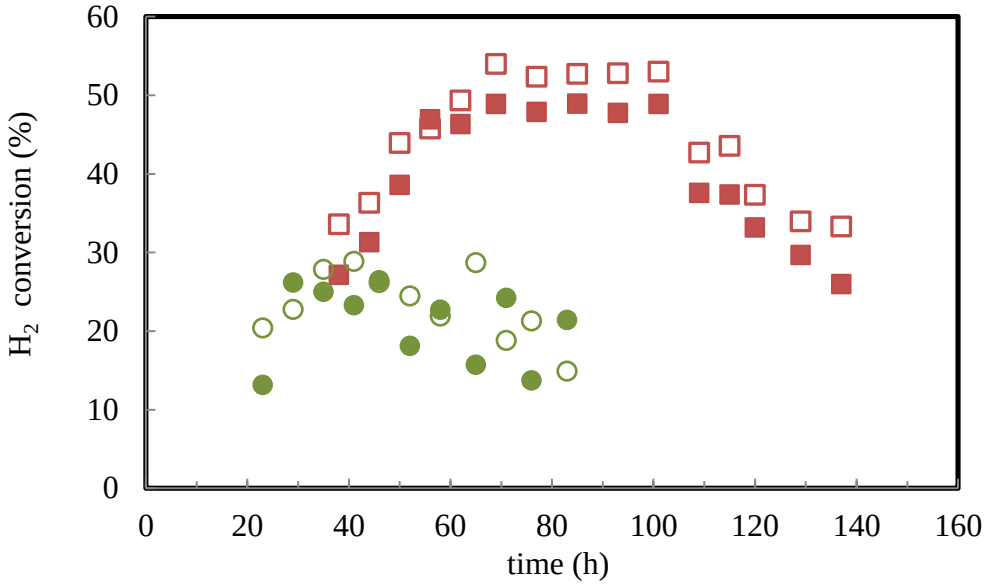

Figure D11 Comparison of H_2 conversion at TBR exit and sump exit. (■, □) L: 200 ml/min and G: 2.3 sccm (●,○) L = 500 ml/min, G = 4.6 sccm; Solid symbols represent TBR exit and open symbols represents sump exit.

in the sump, CO and H_2 gas conversion efficiencies at the TBR exit and the sump exit were compared. The average differences between CO and H_2 conversion efficiencies at

the TBR and sump exits were below 10.7 % and 9.4 %, respectively, indicating that gas conversion occurred mostly inside the TBR and not in the sump.

D8 Conclusions and Recommendations

Major conclusions are as follows:

- The fermentation did not start with an initial gas flow rate of 4.6 sccm. The decreasing in the gas flow rate to 2.3 sccm started the fermentation in TBR. Hence, gas flow rate above 2.3 sccm should not be used during the startup of the fermentation.
- The H_2 conversion efficiency and uptake rate increased by upto 150% from runs R3 to R11 at 4.3 sccm gas flow rate. This phenomenon was not observed in semi-continuous experiment discussed in Appendix C when the gas flow rate was maintained at 2.3 sccm. However, it was not clearly if the liquid flow rate or the biofilm in the packing resulted in the increase in H_2 uptake rate.
- CO conversion efficiencies of upto 85% were achieved at 4.3 sccm gas flow rate.
- Comparison of CO and H_2 conversion efficiencies at TBR and sump exits showed that the gas conversion was high at the TBR exit and no appreciable gas conversion occurred in the sump.

Recommendations are as follows:

- In order to understand if the increase in H_2 conversion efficiency and uptake rate were because of changing the liquid flow rate or from biofilm formation, the next experiment will be performed by keeping the liquid flow rate constant at 200 ml/min and 4.6 sccm gas flow rate until no change in the H_2 conversion and

uptake rate are observed (i.e., cell activity in the TBR reaches a pseudo steady state).

- Similar to this experiment, the startup inoculum of 60% (v/v) will be used. Once, the cell gas conversion drops to about 40 % CO, the medium will be replaced. The effect of liquid flow rate will be tested only after the TBR reaches pseudo steady state.
- The initial TBR startup run will be performed at 200 ml/min and 2.3 sccm in order to allow the cells to adapt slowly. Then in the next run, the gas flow rate will be increased to 4.6 sccm and the liquid flow rate will be kept constant at 200 ml/min.

E RESULTS OF CHAPTER VI SEMICONTINUOUS FERMENTATION RUNS

Figure E1 shows cells attached to the beads in the TBR during semi-continuous fermentation and suspended cells after washing the beads at the end of the fermentation runs in Chapter 5.

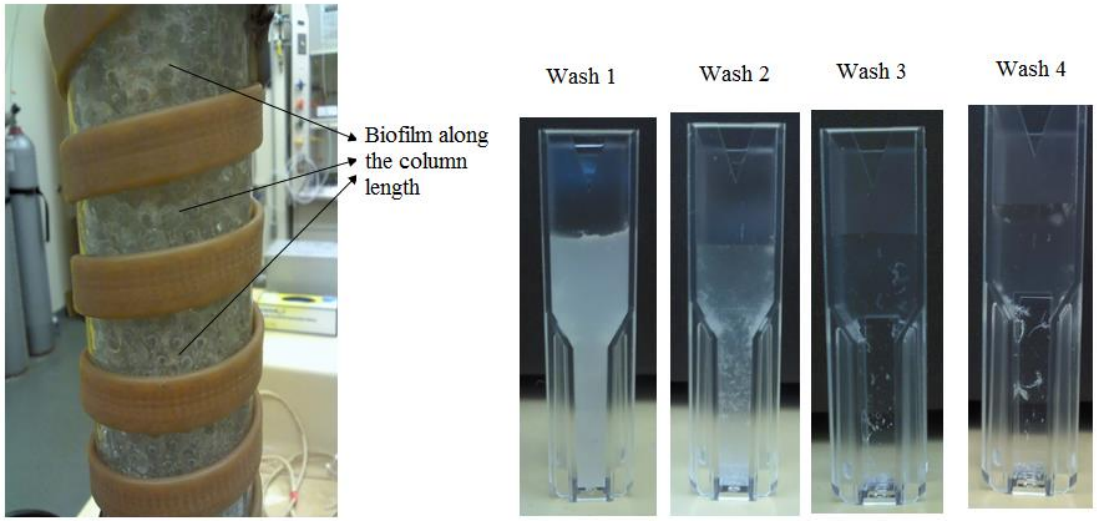

Figure E1 Pictures showing biofilm in the packing and samples from wash1, wash2, wash3 and wash4 of beads from semi-continuous syngas fermentation in TBR using *C. ragsdalei*.

E1 Instantaneous gas uptake profiles

The instantaneous CO and H_2 uptake profiles for selected runs are shown in Figure E1. From the uptake profiles it can be observed that the maximum gas uptake rates were 2.46 mmol/h of CO and 1.26 mmol/h of H_2 at 2.3 sccm of gas flow rate and 200 ml/min of liquid recirculation rate in runs R1 and R2. For run R4 when the gas flow

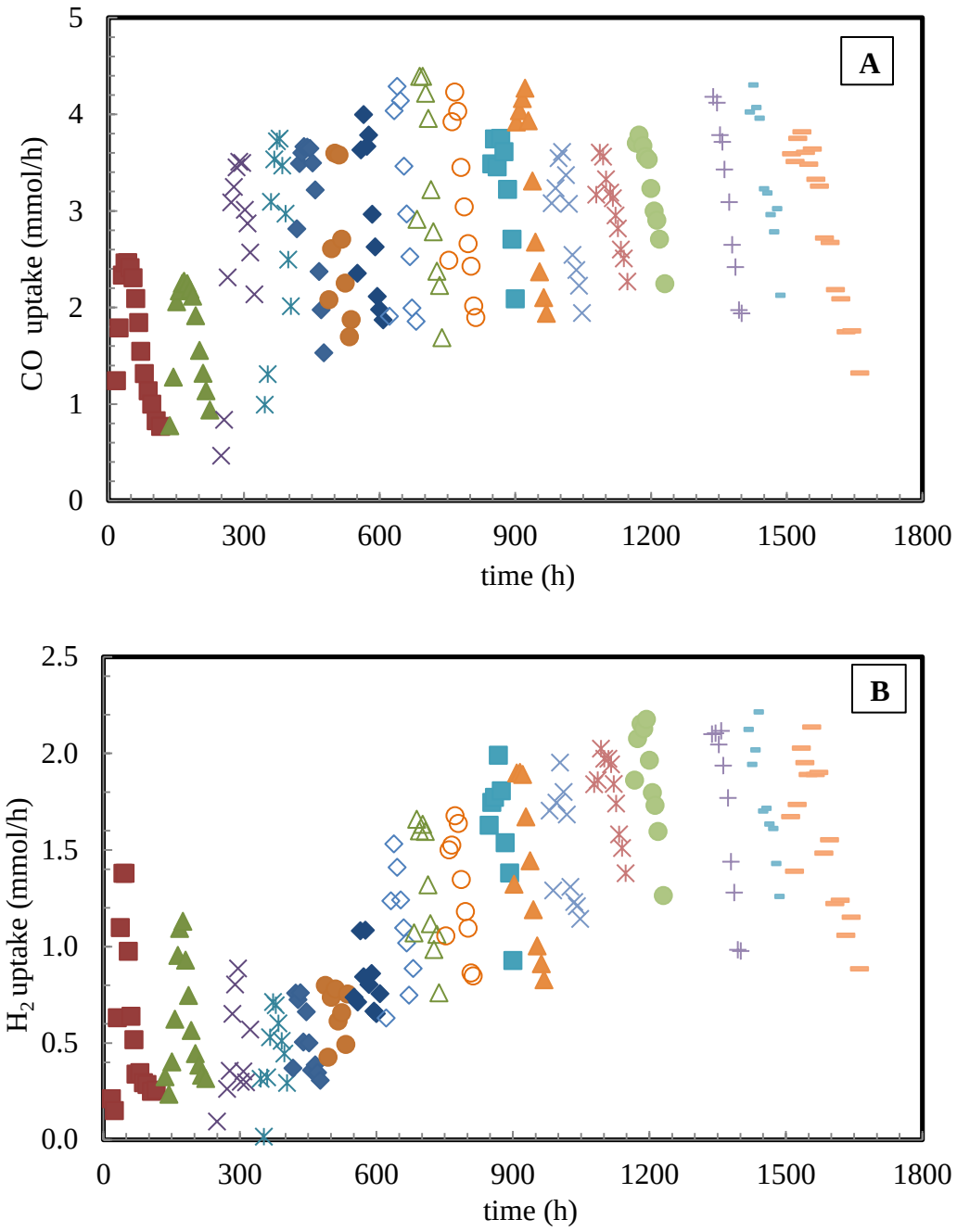

Figure E2 Gas uptake rates profile for all runs in semi-continuous TBR fermentation. (A) CO (B) H_2.

( ) R1 ( ) R2 ( ) R3 ( ) R4 ( ) R5 ( ) R6 ( ) R7 ( ) R8 ( ) R9 ( ) R10 ( ) R11 ( ) R12 ( ) R13 ( ) R14 ( ) R15 ( ) R17 ( ) R18 ( ) R19; R1, R2: L = 200 ml/min, G = 2.3 sccm; R4-R9, R19: L = 200 ml/min, G = 4.6 sccm; R11, R17: L = 500 ml/min, G =4.6 sccm; R14, R15, R18: L = 700 ml/min, G = 4.6 sccm. R1-R15: Counter-current mode; R17-R19: Co-current mode.

rate was increased to 4.6 sccm, the CO uptake increased by 52% and H_2 uptake decreased by 43% (Figure E1). This decrease in H_2 uptake rate is attributed to the availability of high concentrations of CO when the gas flow rate was doubled from 2.3 sccm to 4.6 sccm. From runs R3 to R6 at 4.6 sccm of gas flow rate and 200 ml/min of liquid recirculation rate, the maximum uptake rates of CO and H_2 were 3.63 and 0.79 mmol/h, respectively. However, at the same operating conditions for runs R7 to R10, the maximum gas uptake rates increased by up to 17% for CO and upto to 139% for and H_2. The gas uptake rate data for runs R3 to R10 clearly indicates that the cells activity increased in the subsequent runs (Figure E1) at the same operating condition. At different liquid recirculation rate from runs R10 to R15 in counter-current mode, the variation in the maximum CO and H_2 uptake rates were only upto 15% indicating minor effect of liquid flow rate on instantaneous gas uptake. Also from the Figure E1, it can be observed that the gas uptake in counter-current and co-current were similar.

E2 ORP

The ORP was -485 mV at the beginning of the fermentation indicating that the medium was in a reduced state (Figure E3). As the cells OD_{660} in the medium increased, the ORP further reduced and decreased to -558 mV. However, it started to go positive as cells started producing ethanol. The ORP increased and reached to -405 mV at the end of run R1. However, replacing the exhaust medium decreased the ORP to -543 mV in run R2. This trend was similar for runs from R1 to R19.

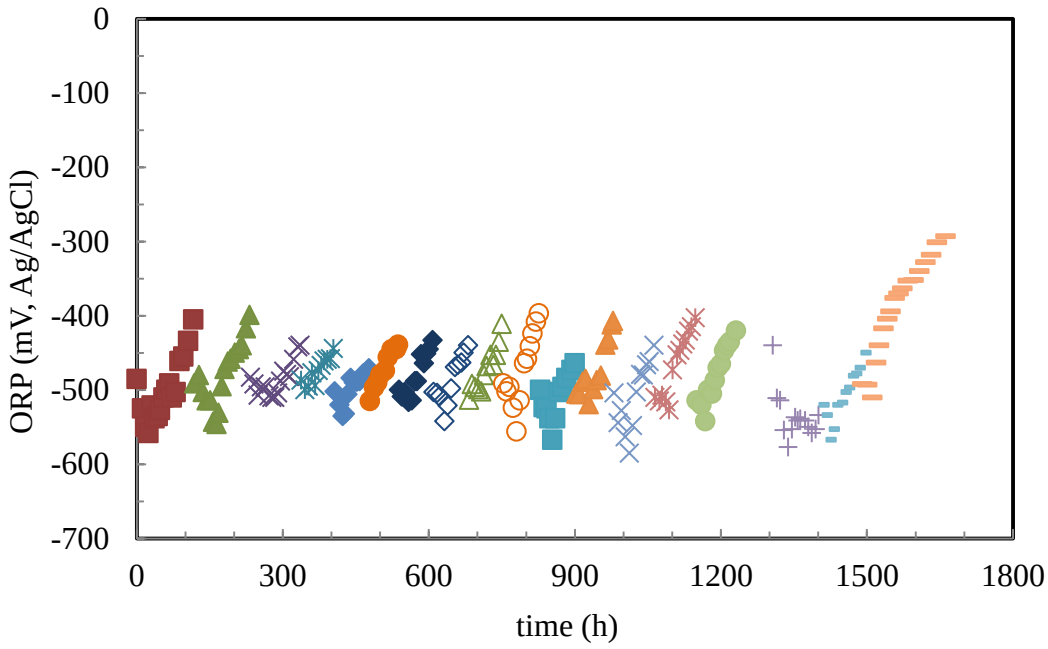

Figure E3 ORP profile for all runs in semi-continuous TBR fermentation. (A) CO (B) H_2.

( ) R1 ( ) R2 ( ) R3 ( ) R4 ( ) R5 ( ) R6 ( ) R7 ( ) R8 ( ) R9 ( ) R10 ( ) R11 ( ) R12 ( ) R13 ( ) R14 ( ) R15 ( ) R17 ( ) R18 ( ) R19; R1, R2: L = 200 ml/min, G = 2.3 sccm; R4-R9, R19: L = 200 ml/min, G = 4.6 sccm; R11, R17: L = 500 ml/min, G =4.6 sccm; R14, R15, R18: L = 700 ml/min, G = 4.6 sccm. R1-R15: Counter-current mode; R17-R19: Co-current mode.

F TBR BIOFILM PICTURES FROM CONTINUOUS FERMENTATION

This appendix contains the trickle-bed reactor pictures taken after 5 months of continuous fermentation reported in Chapter 6. Also included are the microscope pictures of cells taken at 100x magnification from cells collected from the TBR walls, glass beads and product tank.

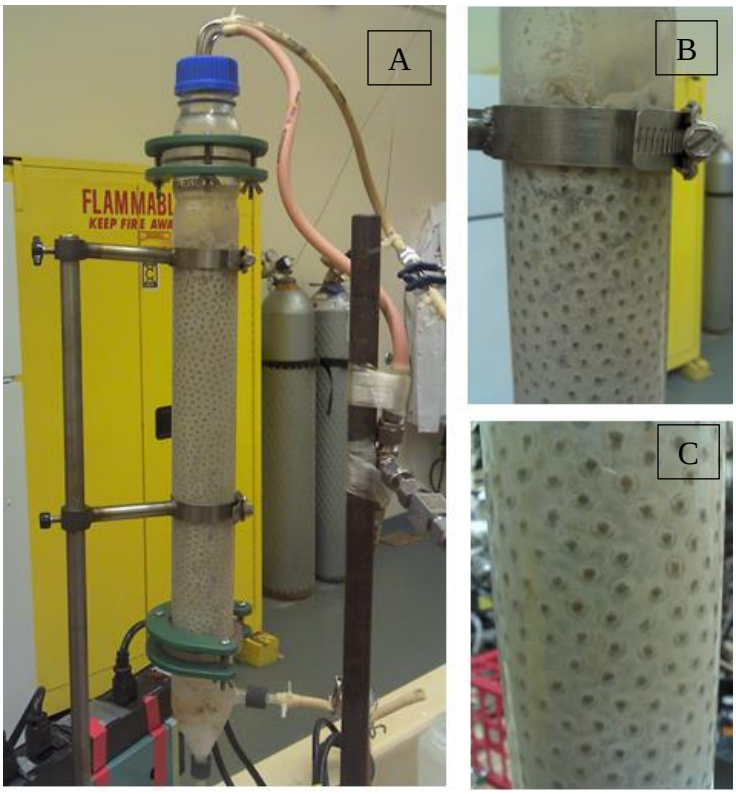

Figure F1 Reactor pictures taken after 5 months of continuous fermentation experiment (A) Reactor with cells attached to the beads (B) Close up of cells in the top section of the packing (C) Close up of cells in the middle of the packing.

Figure F2 TBR pictures taken after 5 months of continuous fermentation experiment (A) Reactor with cells attached to the wall (B) Close up of cells attached to the reactor wall.

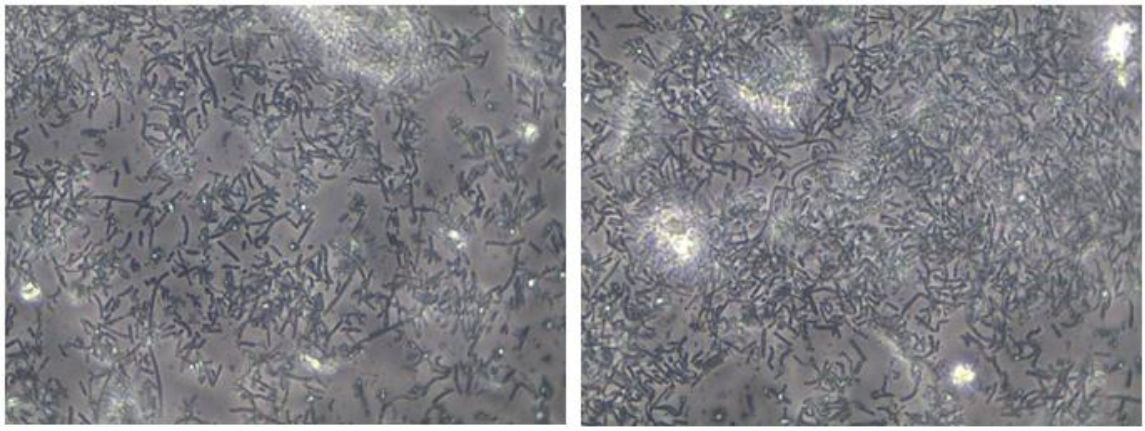

Figure F3 Microscope pictures of cells collected from the TBR wall at 100x magnification.

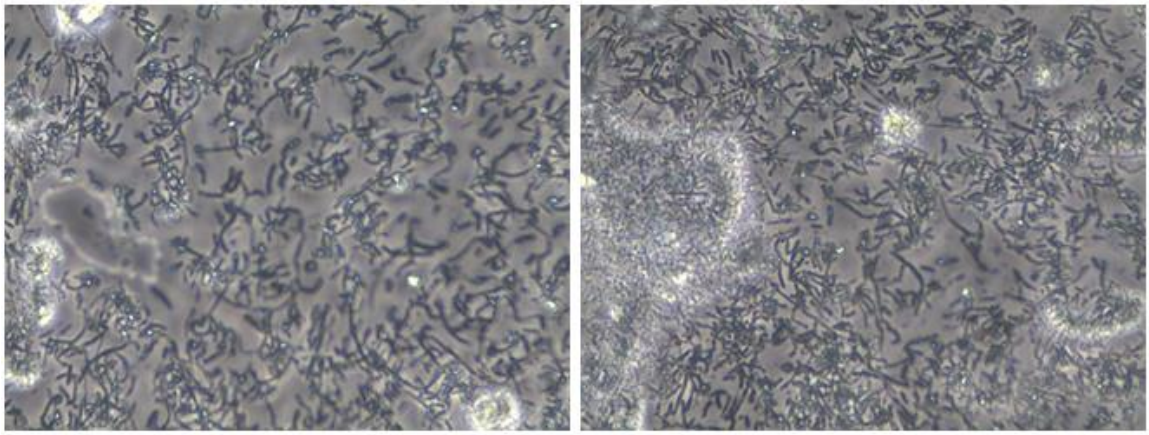

Figure F4 Microscope pictures of cells collected from the glass beads at 100x magnification.

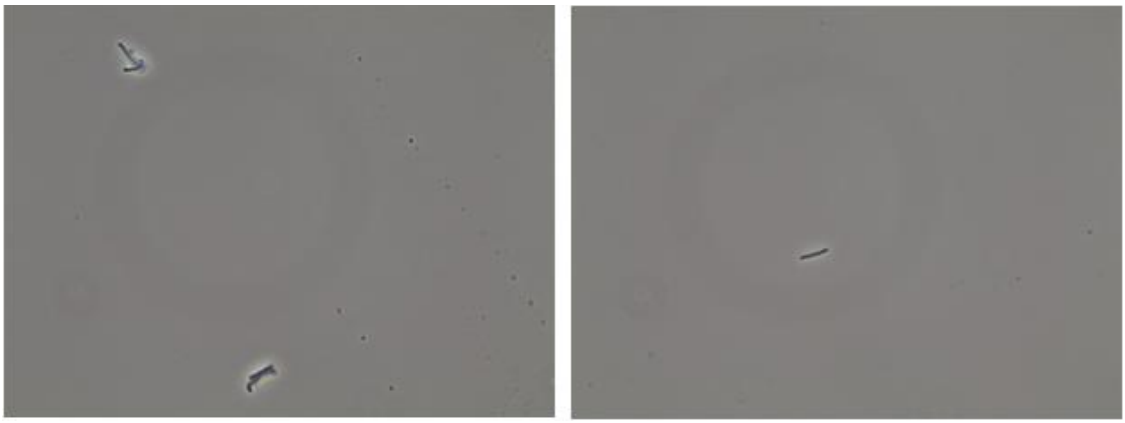

Figure F5 Microscope pictures of cells in the liquid product tank at 100x magnification

F1 ORP

The ORP during the 3200 h of continuous fermentation in the TBR is shown in Figure F6. The ORP was about -550 mV at the beginning of the fermentation. As the pH dropped and the product concentration in the medium increased, the ORP increased and reached to about -400 mV. However, when there was a brief power interruption between 330 h and 350 h, the cell activity decreased and the ORP increased to -150 mV. When the

fermentation was recovered at 450 h, the ORP decreased again and reached to -480 mV. After 450 h, as the pH decreased and product concentrations in the medium increased, the ORP slowly increased. Once, the pH reached 4.6, about 1 ml of 2 N KOH was added to maintain the pH at this value to increase solvent production. Thus, from 700 h to 3200 h irrespective of the dilution rates and the operation mode, the ORP was stable at -300 mV. However, when the TBR was flooded or when the recirculation rate was increased to 500 ml/min intermittently to clear the cell debris, the ORP decrease to -450 mV and then slowly increased back to -300 mV. After 2000 h, the liquid recirculation rate was increased to 500 ml/min at every sampling time for 10 min. Hence, the ORP decreased at every sampling time to about -450 mV and then increased slowly to -300 mV within the next sampling time. Because of this, the ORP profile has a fluctuating trend from 2000 hto 3200 h.

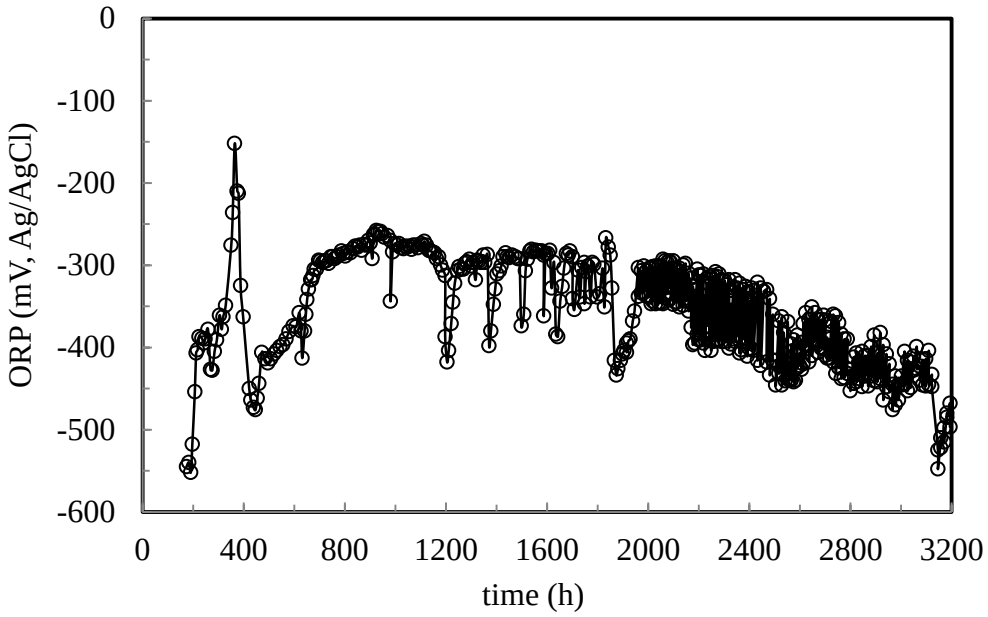

Figure F6 ORP for continuous TBR fermentation.

APPENDIX G

Table G Composition of the standard yeast extract medium for *C. ragsdalei*.

Medium components	Amount per liter
Minerals stock solution	
Sodium chloride (g/L)	-
Ammonium chloride (g/L)	100
Potassium chloride (g/L)	10
Potassium phosphate monobasic (g/L)	10
Magnesium sulfate (g/L)	20
Calcium chloride (g/L)	4
Vitamin stock solution	
Pyridoxine (g/L)	0.01
Thiamine (g/L)	0.005
Riboflavin (g/L)	0.005
Calcium pantothenate(B5) / Pantothenic acid(B5) with Ca (g/L)	0.005
Thioctic acid (g/L)	0.005
p-(4)-Aminobenzoic Acid (g/L)	0.005
Nicotinic acid (g/L)	0.005
Vitamin B12 (g/L)	0.005
Biotin (g/L)	0.002
Folic acid (g/L)	0.002
2-Mercaptoethanesulfonicacid sodium salt (g/L)	0.01
Trace Metal Solution	
Nitrilotriacetic acid (g/L)	2
Manganese sulfate (g/L)	1
Ferrous ammonium sulfate (g/L)	0.8
Cobalt chloride (g/L)	0.2
Zinc sulfate (g/L)	1
Copper chloride (g/L)	-
Nickel chloride (g/L)	0.2
Sodium molybdate (g/L)	0.02
Sodium selenate (g/L)	0.1
Sodium tungstate (g/L)	0.2
Medium composition	
Yeast extract (g/L)	0.5
Morpholinoethanesulfonic acid (g/L)	10
Minerals stock solution (ml/L)	25
Vitamin stock solution (ml/L)	10
Trace Metal Solution (ml/L)	10
4% Cysteine sulfide solution (ml)	10
0.1% Resazurin solution (ml/L)	1

VITA

Mamatha Devarapalli

Candidate for the Degree of

Doctor of Philosophy

Thesis: ANALYSIS OF TRICKLE-BED REACTOR FOR ETHANOL PRODUCTION FROM SYNGAS USING *CLOSTRIDIUM RAGSDALEI*

Major Field: Biosystems Engineering

Biographical:

Education:

Completed the requirements for the Doctor of Philosophy in Biosystems Engineering at Oklahoma State University, Stillwater, Oklahoma in May, 2014.

Completed the requirements for the Master of Science in Chemical Engineering at Oklahoma State University, Stillwater, Oklahoma in 2008.

Completed the requirements for the Bachelor of Science in Chemical Engineering at Jawaharlal Nehru Technological University, Hyderabad, India in 2006.

Experience:
Graduate Research Associate in the Biosystems and Agricultural Engineering, Oklahoma State University, USA, Jul'09– Dec'13.
Research assistant in the School of Chemical Engineering, Oklahoma State University, USA, Aug'07– Dec'08.

Professional Memberships:

Member, BAE Green Student Initiative program	Aug'12–Dec'13
GPSGA representative, BAE Graduate Student Association	Aug'12–Dec'13
Member, American Institute of Chemical Engineers	2008